Star Formation and the Evolution of Massive Galaxies Across Cosmic Time

Jamie Richard Ownsworth

The University of Nottingham

Thesis submitted to the University of Nottingham
for the degree of Doctor of Philosophy

August 2014

"Astronomy? Impossible to understand and madness to investigate"

– Sophocles, c. 420 BC

Supervisor: Prof. Christopher Conselice

Examiners: Dr. Simon Dye
Dr. Sugata Kaviraj

Submitted: 8th August 2014

Examined: 22nd September 2014

Final version: 20th October 2014

Abstract

This thesis investigates the evolution of massive galaxies throughout the last 11 billion years using measured stellar masses and star formation rates. Firstly, we present a study of the resolved star-forming properties of a sample of distant massive ($M > 10^{11} M_{\odot}$) galaxies in the GOODS NICMOS Survey (GNS) within the redshift range $1.5 < z < 3$ in order to measure the spatial location of ongoing star formation (SF). We find that the SFRs present in different regions of a galaxy reflect the already existent stellar mass density, i.e. high density regions have higher SFRs than lower density regions, on average. We find that these massive galaxies fall into three broad classifications of SF distributions. These different SF distributions increase the effective radii to $z = 0$, by $\sim 16 \pm 5\%$, with little change in the Sérsic index (n), with an average $\Delta n = -0.9 \pm 0.9$, after evolution. These results are not in agreement with the observed change in the effective radius and n between $z \sim 2.5$ and $z \sim 0$. We conclude that SF and stellar migration alone cannot account for the observed change in structural parameters for this galaxy population, implying that other mechanisms must additionally be at work to produce the evolution, such as merging.

In Chapter 2, we present a study of the stellar mass growth of the progenitors of local massive galaxies at number densities of $n \leq 1 \times 10^{-4}\,\mathrm{Mpc}^{-3}$ in the redshift range $0.3 < z < 3.0$. We select the progenitors of massive galaxies using two number density selection techniques: a constant number density selection, and one which is adjusted to account for major mergers. We find that the direct progenitors of massive galaxies grow by a factor of four in total stellar mass over this redshift range. On average the stellar mass added via the processes of star formation, major, and minor mergers account for $23 \pm 8\%$, $17 \pm 15\%$ and $35 \pm 14\%$, respectively, of the total galaxy stellar mass at $z = 0.3$. Therefore, $52 \pm 20\%$ of the total stellar mass in massive

galaxies at $z = 0.3$ is created externally to local massive galaxies. We examine the dominance of these processes across this redshift range and find that at $z > 1.5$ SF is the dominant form of stellar mass growth, while at $z < 1.5$ mergers become the dominant form with minor mergers the dominant form of growth at $z < 1.0$. We also explore the implication of these results on other galaxy formation processes such as the cold gas accretion rate of the progenitors of most massive galaxies over the same redshift range. We find that the gas accretion rate decreases with redshift with an average gas accretion rate of $\sim 65\,\mathrm{M_{\odot}yr^{-1}}$ over the redshift range of $1.5 < z < 3.0$.

Finally, we investigate the evolution of the properties of local massive galaxies over the redshift range $0.3 < z < 3.0$. We again select the progenitors of local massive galaxies using a constant number density selection. We find that the average progenitor galaxy appears passive in UVJ colours since at least $z = 3.0$. We examine the UVJ colours and find that the average progenitor of a local massive galaxy has not lived on the blue cloud since $z = 3.0$. The passive fraction of the progenitor population has increased from $56 \pm 7\%$ at $z = 3.0$ to $94 \pm 8\%$ at $z = 0.3$. This result implies that the majority of the progenitors of local massive galaxies have stopped actively star forming by $z = 3.0$. Examining the structural properties of the progenitor galaxies we show that the size evolution of a galaxy sample selected this way is on average lower than the findings of other investigations into the size evolution of massive galaxies which have found that they must grow in size by a factor of $2 - 4$ from redshift 3.0 to the present day. The average n of the progenitor population evolves significantly over the redshift range studied, with the population being dominated by low n objects ($n < 2.5$) at $z > 1.7$ and transitioning to high n objects at $z < 1.7$. Splitting the high and low n objects into SFing and passive samples. We find that $41 \pm 4\%$ of the sample at $z > 2.5$ are passive low n systems, possibly implying that local massive galaxies were passive disk-like systems at early cosmic times.

Acknowledgements

First and foremost I would like to thank Christopher Conselice for his unending support throughout my time here in Nottingham. Thank you for reading countless drafts and helping me fight with referees. I will miss our meetings that don't always stay on the science track and your endless excitement for new plots. I would not have made it this far without you being you. Also I have great respect for Omar Almaini. Thank you for always going the extra mile. More than once you have worked day and night to make sure things turn out OK.

Thank you to my family; Mum, Dad, Lee, Carly and, my Grandparents. Thank you for making me into the person I am today and being there for me all along the way. You have all been there for me in no end of ways and I love you all dearly.

Thanks to my science family; Ruth, Asa, Amanda, Fernando, Sam, Matt, Will, Alice, Ken, Carl, Berta and Dongyao. Thanks to you all for providing the platform on which this thesis is built and being fountains of knowledge. A big thank you goes to Will Hartley for just being amazing in many ways, from knowing the answer to everything to helping drink beer-time dry. Alice, I know 100% that I would not be here today without you. Thank you very much for being the best science big sister that there ever could be. It's not just science though, thank you for befriending the new guy in the department with long hair and a sad man on his hat. The innumerable times we made each other laugh and made science fun made my time here in Nottingham some of the best years of my life. Even though the duo has been split up it will never be truly broken.

I would like to thank the people in the department as a whole for making it a wonderful environment to work in. There are so many people within the department I would like

to thank; Nathan, Emma, Kate and, Kieren, for helping fight latex, IDL or science, many hilarious boozy nights at the JA and many hours of killing terrorists/counter-terrorists. Carl, for being a superstar DJ and committing felicide. Lyndsay, for showing an interest in random plots I show you. Adam, for general banter (BANTER!). And finally Sophie and Cat, for being amazing friends/officemates over the last 4 years and propping each other up so we all make it to the end. We did it! Thank you to you all for this and so much more.

Last but not least, Hannah, thank you for putting up with me over the last few months (or should it be years) though the roller-coaster of emotion that is a PhD. Even though this document is the culmination of my time here in Nottingham it does not reflect the best part, meeting you. So thank you for coming into my life and making it so much brighter.

This thesis is dedicated to all of you.

Publications

Much of the work in this thesis has been presented in several papers. Paper I contains work detailed in Chapter 2 of this thesis and Paper II describes the work presented in Chapters 3 and 4.

I Ownsworth, J. R.; Conselice, C. J.; Mortlock, A; Hartley, W. G.; Buitrago, F.;"Evolution of massive galaxy structural properties and sizes via star formation in the GOODS NICMOS Survey", MNRAS, 426, 764

II Ownsworth, J. R.; Conselice, C. J.; Mortlock, A.; Hartley, W. G.; Almaini, O.; Duncan, K.; Mundy, C. J., "Minor vs Major Mergers: The Stellar Mass Growth of Massive Galaxies from z=3 using Number Density Selection Techniques", MNRAS, Accepted

III Mortlock, A.; Conselice, C. J.; Bluck, A. F. L.; Bauer, A. E.; Grtzbauch, R.; Buitrago, F.; **Ownsworth, J. R.**; "A deep probe of the galaxy stellar mass functions at $z \sim 1-3$ with the GOODS NICMOS Survey", MNRAS, 413, 2845

IV Mortlock, A.; Conselice, C. J.; Hartley, W. G.; **Ownsworth, J. R.**; Lani, C.; Bluck, A. F. L.; Almaini, O.; Duncan, K.; van der Wel, A.; Koekemoer, Anton M.; Dekel, A.; Davé, R.; Ferguson, H. C.; de Mello, D. F.; Newman, J. A.; Faber, S. M.; Grogin, N. A.; Kocevski, D. D.; Lai, K.; "The redshift and mass dependence on the formation of the Hubble sequence at $z > 1$ from CANDELS/UDS", MNRAS, 433, 1185

V Mortlock, A.; Conselice, C. J.; Hartley, W. G.; Duncan, K.; Lani, C.; **Ownsworth, J. R.**; Almaini, O.; van der Wel, A.; Huang, K.; Ashby, M.; Willner, S.; Fontana, A.; Dekel, A.; Koekemoer, A.; Ferguson, H.; Faber, S.; Grogin, N.; Kocevski,

D.; “Deconstructing the Galaxy Stellar Mass Function with UKIDSS and CANDELS: the Impact of Colour, Structure and Environment”, MNRAS , Submitted

VI Duncan, K.; Conselice, C. J.; Mortlock, A.; Hartley, W. G.; Guo, Y.; Ferguson, H.; Davé, R.; Lu, Y.; **Ownsworth, J. R.**; Ashby, M.; Dekel, A.; Dickinson, M.; Faber, S.; Giavalisco, M.; Grogin, N.; Kocevski, D.; Koekemoer, A.; Somerville, R.; White, C.; “The mass evolution of the first galaxies: stellar mass functions and star formation rates at $4 < z < 7$ in the CANDELS GOODS-South field”, MNRAS, Accepted

Contents

List of Figures

List of Tables

Star Formation and the Evolution of Massive Galaxies Across Cosmic Time

Chapter 1

Introduction

The ancient Greeks called them the milky ones, William Herschel called them spiral nebulae but we know them today as galaxies. The study of galaxies as extragalactic objects is less than 100 years old. Galaxies were once considered objects contained within our home galaxy, the Milky Way. In 1925 Edwin Hubble calculated the distance to an irregular nebula in the constellation of Sagittarius using Cepheid stars, a class of variable star first reported by Pigott (1784), and showed that the nebula lay far outside of the Milky Way (Hubble 1925b). Thus he showed that this large nebula was in fact a neighbouring galaxy. From this our view on the Universe was changed drastically. No longer were we living in a Universe populated solely by stars and nebulae, but one where these objects formed into larger individual systems, galaxies. With the discovery that our Galaxy was not unique in its existence, fundamental questions about the Universe needed to be answered, such as how did these objects form and evolve?

1.1 Cosmology and Galaxy Formation

Our Universe is governed by its cosmology. The currently accepted form of cosmology is that the Universe is made up of roughly 71% dark energy, 25% dark matter and 4% baryonic matter (results from Planck space experiment, Ade *et al.* 2013). The largest component of the Universe, dark energy, is thought to be responsible for accelerating the expansion of the Universe but it is not well understood. Dark matter, initially posited by Zwicky (1933), is also not well understood but its effects can be observed

via gravitational lenses and galaxy rotation curves (Rubin, Thonnard & Ford 1978). The baryonic matter that makes up us, planets, stars and galaxies accounts for a small percentage of the total energy budget of the Universe, but this is what we can directly observe.

Although we do not fully understand what the dark components of our Universe consist of we can begin to understand their role in shaping the galaxies we see today. The current paradigm for galaxy formation and evolution is the ΛCDM model. This model incorporates dark energy, Λ, and cold dark matter, CDM. Cold dark matter is dark matter that moves at non relativistic speeds.

In this model of the Universe, galaxies form within larger dark matter haloes that dominate over the total mass and extent of the galaxy. These dark matter haloes begin forming by collapsing under self gravity out the non-uniform dark matter distribution present in the early universe (Peebles 1980). This non-uniform distribution can be seen in the Cosmic Microwave Background (CMB, Figure 1.1). These small seeds of structure build-up their mass over time via merging with other dark matter haloes (Lacey & Cole 1993a). This process is called hierarchical assembly, where the smallest objects form first and build up into more massive objects (White & Rees 1978). Over the last couple of decades computer simulations of this process have shown that this model of the growth of structure produces a universe much like the one we live in (e.g Millennium simulation, Springel *et al.* 2005, Figure 1.2). Along with the build up of the dark matter haloes the baryonic matter is also building at the centre of the haloes under the influence of gravity. The baryonic matter in the form of hydrogen, helium, and few heavier elements cools over time to form molecular clouds within which stars are formed and the first galaxies are created.

1.2 Bimodality of Galaxies

A clear bimodality is seen in the galaxies of the Universe. This indicates that although we understand the basic idea of how stars form into galaxies the individual evolutionary paths are different, and it is important to understand these differences. I explore this bimodality in the following sections.

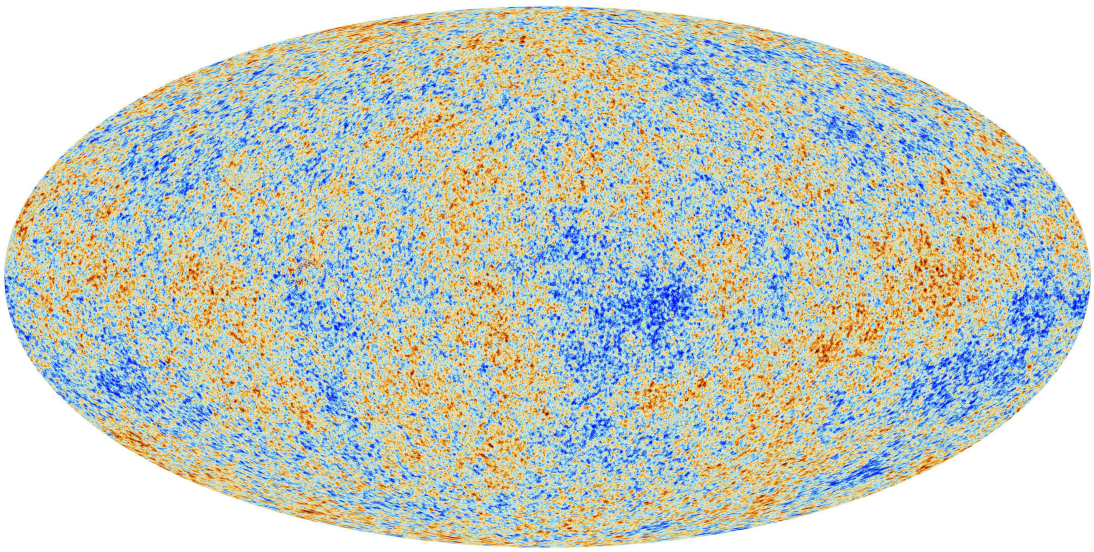

Figure 1.1: The Planck space mission map of the Cosmic Microwave Background (CMB) seen over the full sky. Credit to ESA and the Planck Collaboration *http://www.esa.int/spaceinimages/Images/2013/03/Planck_CMB*

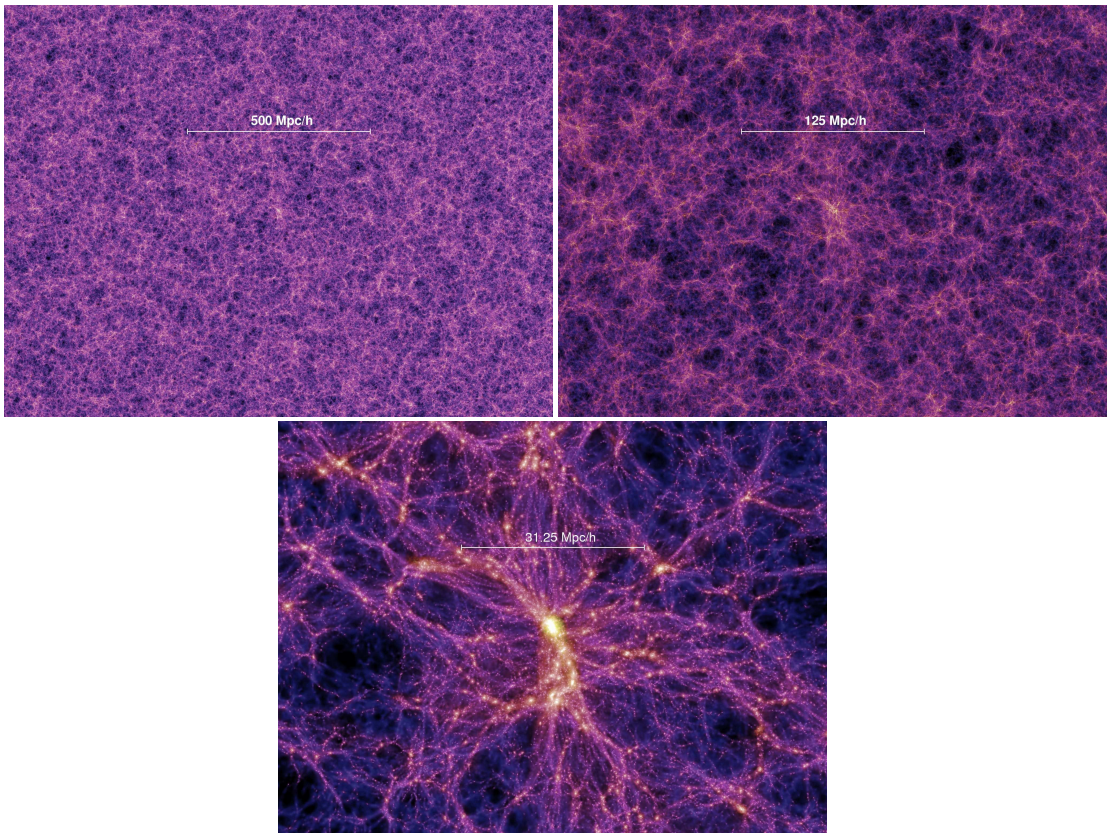

Figure 1.2: Snapshots of the N-body dark matter Millennium simulation (Springel *et al.* 2005). All taken at $z = 0.0$ showing the filamentary structure of the large scale structure of the Universe.

1.2.1 Morphology

Hubble (1925a) visually inspected and classified the shapes of 400 galaxies into his famous ”tuning fork” diagram (Figure 1.3 shows an updated version of the classification scheme). This classification scheme was based on the visual morphology of the galaxies; E corresponding to galaxies that appeared round and featureless, and S corresponding to galaxies that appeared disk like with spiral features. Hubble showed that almost all galaxies in the local Universe fall into these two broad categories.

Galaxy morphologies can also be determined using computational methods. Sérsic (1968) parametrised the general light profile of galaxies where the intensity, I, follows the relation:

$$I(r) = I_{\text{eff}} \times \exp\left(-\kappa\left[\left(\frac{r}{R_{\text{eff}}}\right)^{1/n} - 1\right]\right) \tag{1.1}$$

where R_{eff} is the effective radius, that is that radius that contains half of the galaxy's total light, a proxy for the size of a galaxy; I_{eff} is that intensity at the effective radius; n is the Sérsic index; κ is a function of the Sérsic index that takes the form of $1.992 \times n - 0.3271$. The Sérsic index parameter of this relation indicates the geometrical shape of the light profile and, in general, the morphology. Figure 1.4 shows galaxy light profiles based on a range of Sérsic indices. Studies (e.g. Bell *et al.* 2004, Ravindranath *et al.* 2004, Nair & Abraham 2010, Buitrago *et al.* 2013, Mortlock *et al.* 2013) have shown that galaxies with light profiles best fit by a high Sérsic index, $n > 2.5$ often have an elliptical morphology whereas galaxies best fit by a low Sérsic index, $n < 2.5$, have a disk/spiral morphology.

From Figure 1.3 we notice that by arranging the galaxies in this fashion there is an apparent trend with morphology and galaxy colour, with the round elliptical galaxies having redder colours than the disky spiral galaxies (e.g. Strateva *et al.* 2001, Blanton *et al.* 2003, Wolf, Gray & Meisenheimer 2005). We discuss galaxy colour in the next section.

1.2.2 Galaxy Colour

Galaxy colours are defined as the difference between the magnitude of a galaxy in two wavelength bands. There exists a bimodality in the distribution of galaxy colours in

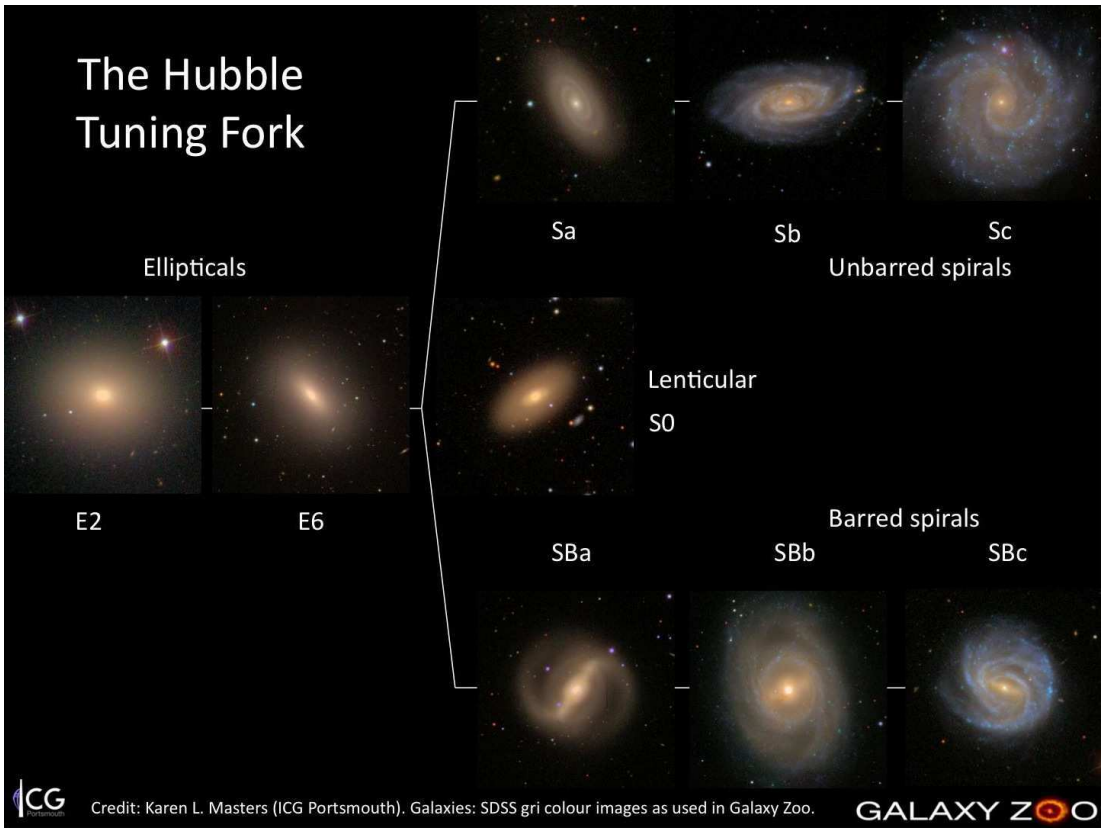

Figure 1.3: The Hubble Tuning fork. The galaxies shown are g, r, i colour composite images from the Sloan Digital Sky Survey (SDSS, York *et al.* 2000) and have been classified by the Galaxy Zoo project (Lintott *et al.* 2008). Credit to Karen L. Masters.

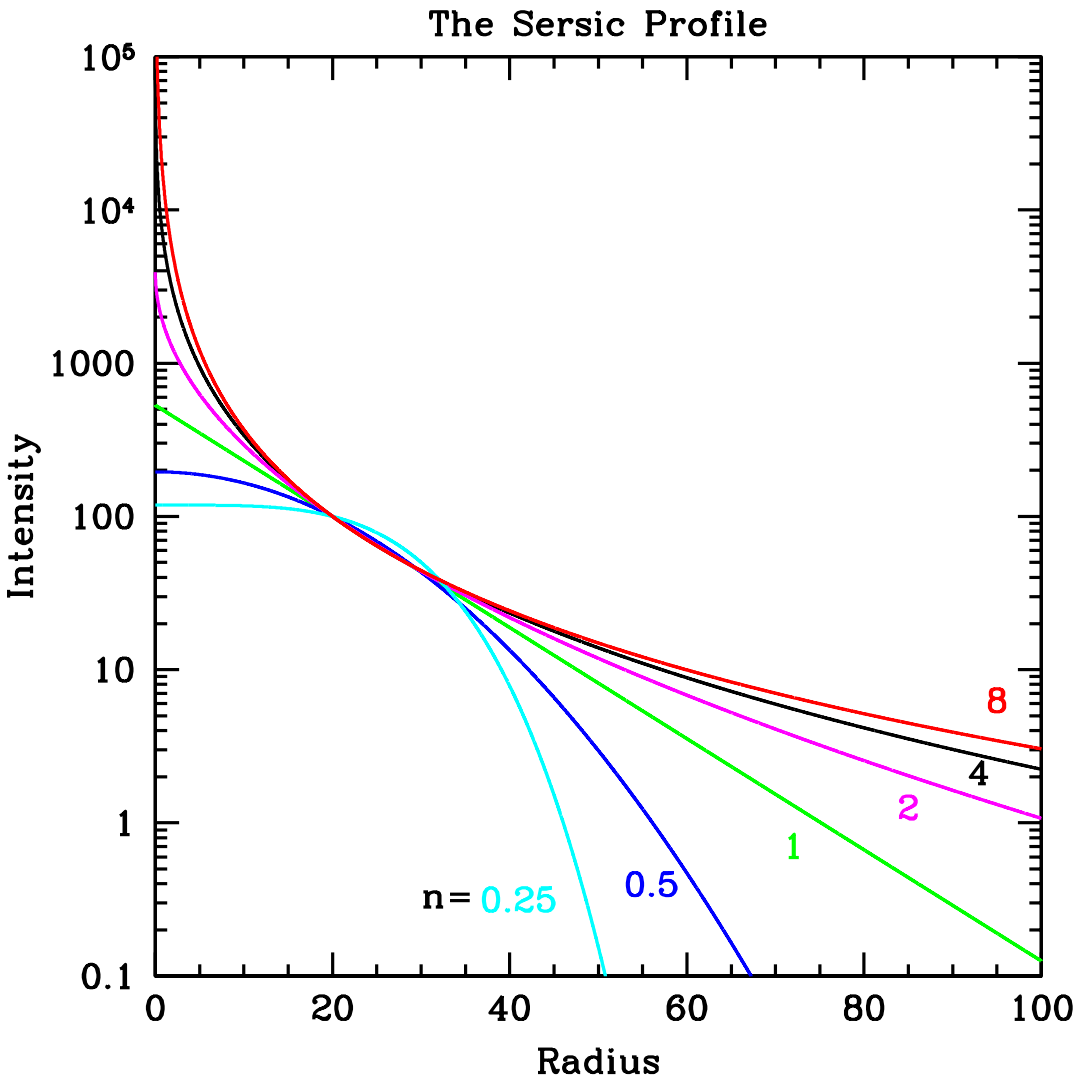

Figure 1.4: The Sérsic profile form given in Equation 1.1, where effective radius and intensity at the effective radius are fixed. http://users.obs.carnegiescience.edu/peng/work/galfit/README.pdf

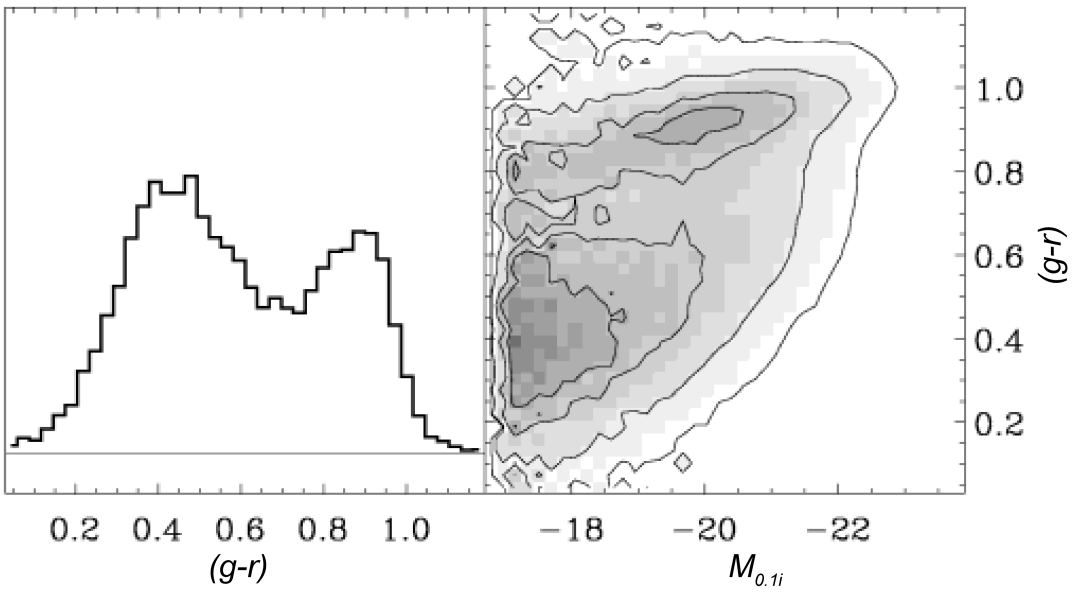

Figure 1.5: Left panel: The histogram of $g - r$ colours of galaxies for the SDSS which shows a clear bimodality. Right panel: The colour magnitude diagram for the same galaxies. Galaxies with red $g - r$ colours appear to have a tight correlation with their magnitude and lie on the so called "red sequence". Galaxies with blue $g - r$ colours lie in a diffuse region called the "blue cloud". Figure adapted from Blanton *et al.* 2003)

the Universe (e.g. Strateva *et al.* 2001, Blanton *et al.* 2003, Kauffmann *et al.* 2003). In the left hand panel of Figure 1.5 we see the bimodal distribution for galaxies within the Sloan Digital Sky Survey (SDSS) in $g - r$ colour. The right hand panel of Figure 1.5 shows how the $g-r$ colour correlates with i band magnitude. Galaxies with red colours follow a tight correlation between colour and magnitude. This is known as the "red sequence". Galaxies with blue colours have a weaker correlation between colour and magnitude and lie in the region known as the "blue cloud". These colours arise from the stellar populations present within the galaxy. Galaxies that appear blue in optical colours host many hot, high mass stars (stellar types O,B). Even though these stars are rare they are brighter than the more numerous cooler, redder, lower mass stars. This gives the galaxy the appearance of a blue colour. As these high mass stars only exist on the stellar main sequence for short, 10s of Myr lifetimes, their presence indicates that there has been recent star formation within the galaxy. If a galaxy ceases to form stars the final generation of high mass stars evolve off the stellar main sequence in relatively short time-scales. This leaves behind the lower mass, cooler stars with redder colours and longer stellar main sequence lifetimes. Therefore, galaxies have redder colours the longer they remain non star forming or quiescent. Therefore, the bimodality in galaxy colour is a gauge of the star forming properties of the galaxy population.

1.3 Star Formation

The rate of ongoing star formation is one of the most fundamental properties of any given galaxy. This property appears to be linked to many of the other attributes a galaxy can possess, such as colour, morphology, and also stellar mass. The star formation rate of a galaxy shows a strong trend with stellar mass, with higher mass galaxies hosting larger amounts of star formation. Galaxies that fall upon this trend are said to be on the star formation main sequence. Non star forming galaxies fall below this trend and galaxies undergoing a large burst of star formation lie above. Figure 1.6 from Daddi *et al.* (2007) shows this trend over a large range of redshifts. Daddi *et al.* (2007) and Noeske *et al.* (2007) also showed that the star formation main sequence undergoes significant evolution with redshift, such that galaxies of equal mass were more highly star forming at earlier cosmic times. This is reflected in the star formation history of

the Universe, shown in Figure 1.7 from Hopkins & Beacom (2006), which also shows that the Universe was more highly star forming at earlier cosmic times. How do we measure the star formation rate (SFR) within a varied population of galaxies and in a consistent manner over cosmic time?

1.3.1 Detecting Star Formation

The past decade has witnessed a wide range of new observational information on star formation thanks to the Galaxy Evolution Explorer, the Spitzer Space Telescope, the Herschel Space Observatory, and the Hubble Space Telescope among others. Calibration of SFR indicators range across the full electromagnetic spectrum, from the Ultraviolet to Radio wavelengths (see Kennicutt 1998a). In the following subsections we describe a few of the SFR indicators for unresolved systems, as this is the type of system this thesis will be focused on. All of these observable quantities depend on the presence of high mass stars ($\mathrm{M_{star}} > 3\mathrm{M_{\odot}}$), as these are a transient population that trace the current SFR. Although lower mass stars are more abundant than high mass stars they cannot be directly measured in these methods. To correct for this issue we need to relate the relative abundances of high to low mass stars using an Initial Mass Function (IMF). Figure 1.8 shows many different IMF models used in various studies. In this thesis I will only be considering the Salpeter (Salpeter 1955) and Chabrier (Chabrier 2003) IMF models.

1.3.1.1 Direct Stellar Light

The youngest stellar populations emit the bulk of their energy in the rest frame UV ($< 0.3\,\mu\mathrm{m}$). This wavelength probes the star formation in galaxies on time-scales of 100s of Myr. However, the UV radiation is highly attenuated by dust in the line of sight. Therefore, in most cases to calculate the correct SFR present in a galaxy the observed UV luminosity requires a correction for energy lost due to dust absorption. For a Chabrier IMF the UV stellar continuum can be converted to a SFR via Kennicutt (1998a) as:

$$SFR_{UV} = 7.7 \times 10^{-44} \nu L_{\nu} \tag{1.2}$$

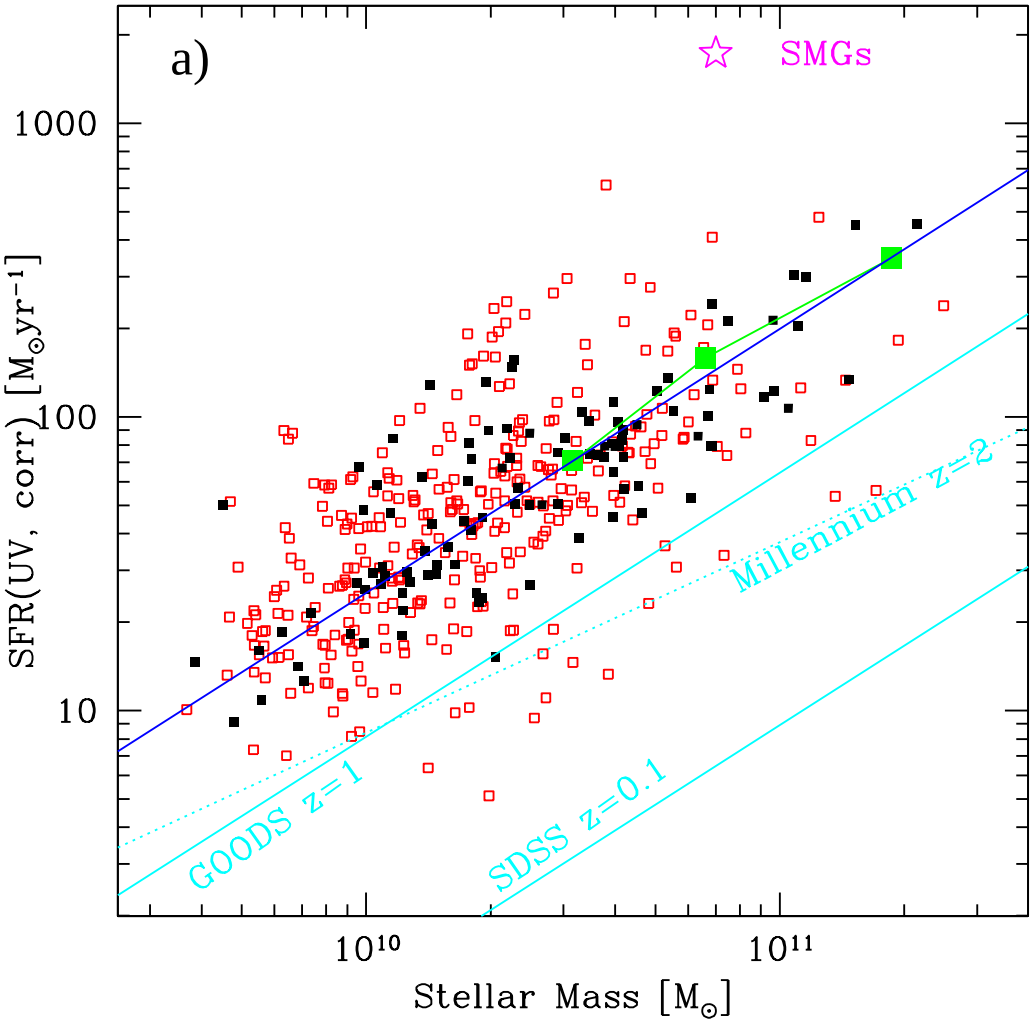

Figure 1.6: The stellar mass-SFR correlation for star forming galaxies over the redshift range of $0.1 < z < 2.0$. The points show star forming galaxies at $z = 2.0$. The dark blue line is the best fit to these galaxies. The cyan solid lines are the $z = 1$ and $z = 0.1$ correlations taken from Elbaz *et al.* (2007). The green squares for the result of the average SFR-mass relation determined from radio stacking of K ¡20.5 galaxies in GOODS-N. Figure from Daddi *et al.* (2007).

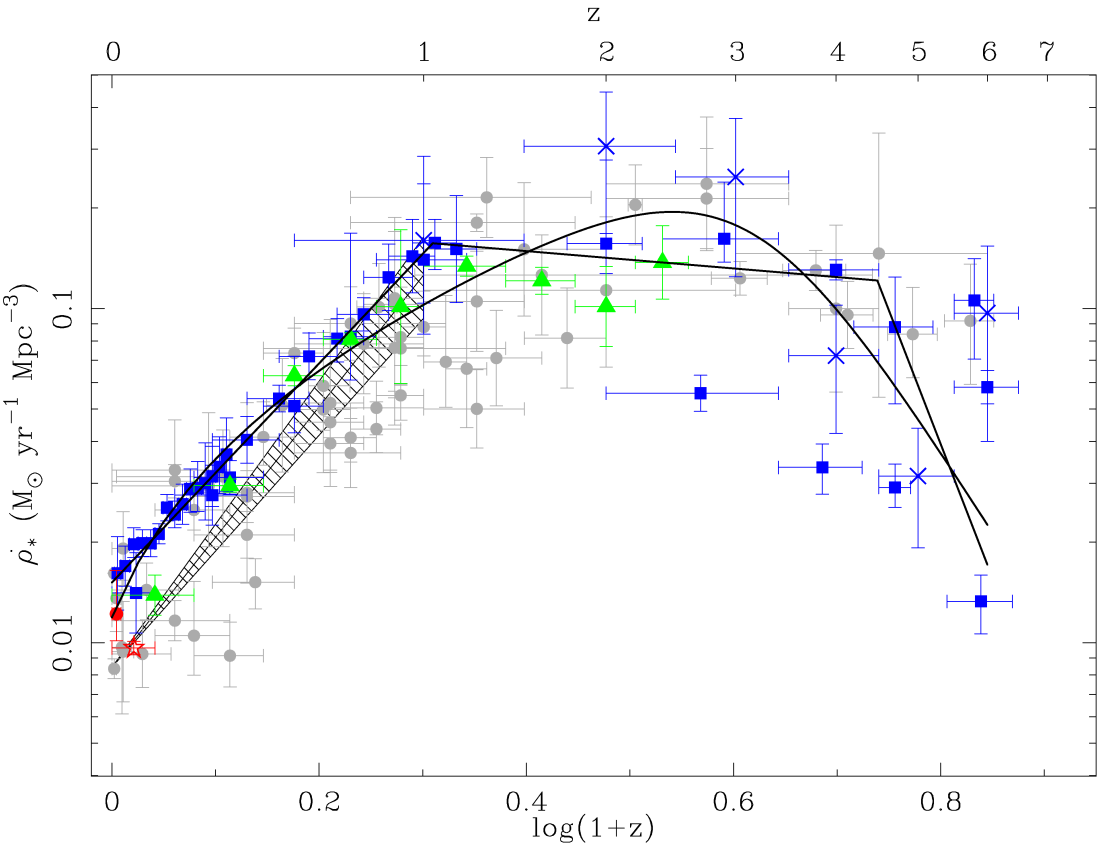

Figure 1.7: The evolution of the star formation density with redshift. This figure shows the peak of the SFR of the Universe at z$\sim$ 2. The Figure is a collection of results from Hopkins & Beacom (2006) and references within.

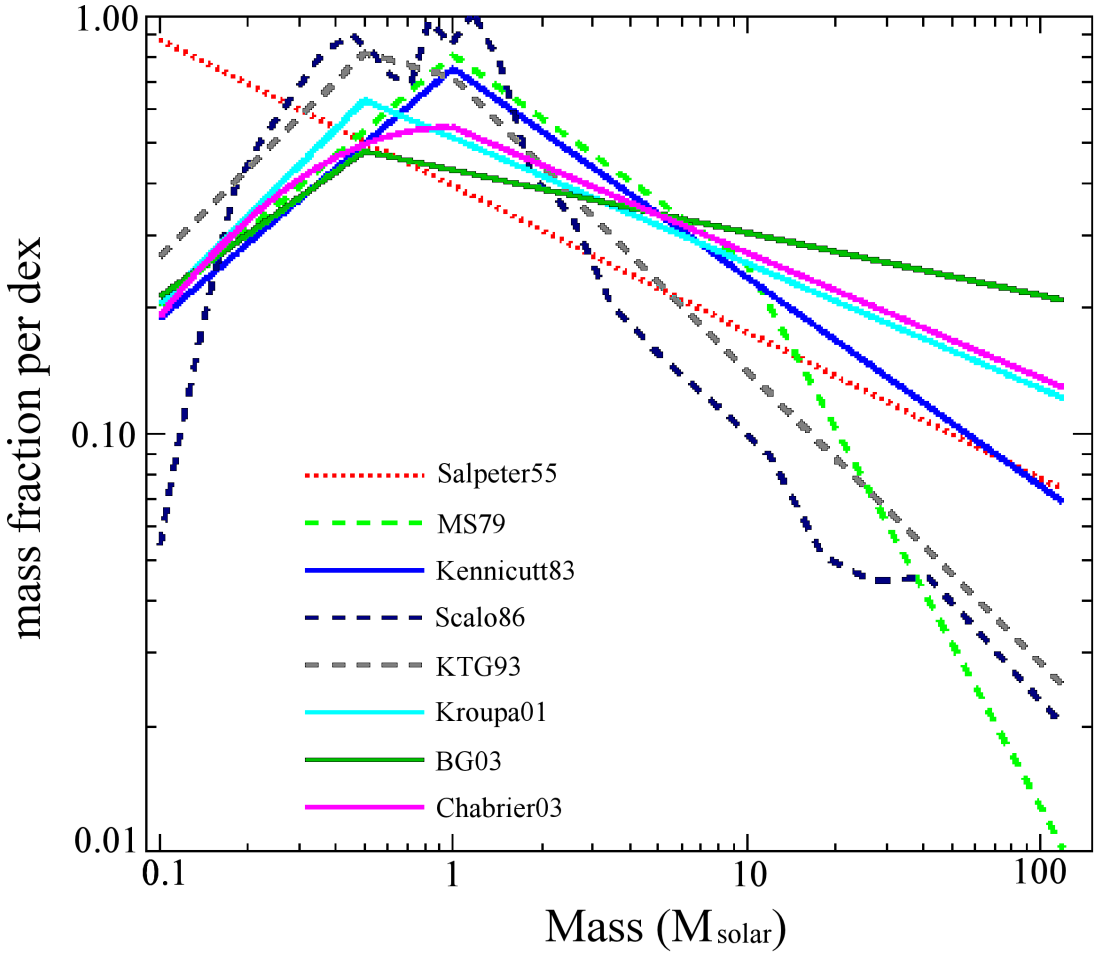

Figure 1.8: A complied diagram of IMF's used in astronomy. Collected from Salpeter (1955) eq. 5; Miller & Scalo (1979) table 7; Kennicutt (1983) section V; Scalo (1986) table; Kroupa, Tout & Gilmore (1993) eq. 13; Kroupa (2001) eq. 2; Baldry & Glazebrook (2003) abstract; Chabrier (2003) table 1. Figure credit to Ivan Baldry

with SFR_{UV} in $\mathrm{M}_{\odot}\mathrm{yr}^{-1}$, ν is the frequency in Hertz, and L_{ν} is the luminoisty in erg/s. Correcting this luminosity for dust is not a trivial matter. Meurer, Heckman & Calzetti (1999) found a correlation between dust attenuation and the shape of the UV continuum for local starburst galaxies. Using these results the unattenuated UV luminosity can be obtained. See Sections $2.2.5$ and $3.2.5.2$ for a full description of this technique.

1.3.1.2 Ionised Gas

The UV flux emitted via the O and B type stars can ionise (with radiation at $< 912\,\text{Å}$) their local neutral hydrogen environments. This then in turn produces the Hydrogen recombination line emissions, including the well known Balmer lines of Hα ($0.6563\,\mu\mathrm{m}$) and Hβ ($0.4861\,\mu\mathrm{m}$). These strong spectral lines can be directly related and converted to the ongoing star formation activity on similar time-scales as SFRs measured from UV luminosities. Using Osterbrock & Ferland (2006) and a Chabrier IMF the strength of the $H\alpha$ line can be converted to a SFR via:

$$SFR_{H\alpha} = 5.5 \times 10^{-54} L_{H\alpha} \tag{1.3}$$

with $SFR_{H\alpha}$ in $\mathrm{M}_{\odot}\mathrm{yr}^{-1}$ and $L_{H\alpha}$ is in erg/s.

1.3.1.3 Dust Processed Stellar Light

As stated before, dust absorbs UV radiation very efficiently then in turn this energy is re-radiated at infra-red (IR) wavelengths ($5 - 1000\,\mu\mathrm{m}$). The thermal IR spectrum of a galaxy will depend on the underlying stellar population i.e. hot young stars will heat the dust to a higher mean temperature than an old stellar population (e.g. Helou 1986). Thus, qualitatively, the dust heated by UV-luminous, young stellar populations will produce an IR SED that is more luminous and peaked at shorter wavelengths ($\sim 60\,\mu\mathrm{m}$) than the dust heated by UV faint, old or low-mass stars ($\sim 100 - 150\,\mu\mathrm{m}$). This is the foundation for using IR emission as a SFR indicator. The full bolometric IR emission can be converted to a SFR using:

$$SFR_{IR,bol} = 2.5 \times 10^{-44} L_{IR,bol} \tag{1.4}$$

with $SFR_{IR,bol}$ in $\mathrm{M}_{\odot}\mathrm{yr}^{-1}$ and $L_{\mathrm{IR,bol}}$ in erg/s. As this method examines the emission of UV heated dust it can be used in conjunction with the UV luminosity methods to form a complete observable SFR measure i.e. $SFR_{\mathrm{UV,uncorr}} + SFR_{\mathrm{IR,bol}} = SFR_{\mathrm{total}}$. With the $SFR_{\mathrm{UV,uncorr}}$ being the SFR derived from the undustcorreced UV luminosity. In the far infra-red there are monochromatic methods for deriving SFRs (e.g $24\,\mu\mathrm{m}$). However, these methods require other properties of the host galaxy to be known to fully calibrate their conversion factors. These properties include; metal abundance (e.g. Marble *et al.* 2010); the presence of polycyclic aromatic hydrocarbons (e.g. Peeters *et al.* 2004) and dust heating from different stellar populations (e.g. Crocker *et al.* 2013).

1.3.1.4 Other Methods

Star formation in galaxies can also be probed via synchrotron radio and X-ray emission. In the case of synchrotron emission, the basic mechanism is the production and acceleration of electrons in supernova explosions. As the rate of supernovae is directly related to the SFR in theory the radio synchrotron luminosity will act as a proxy for the SFR. However, using this method as a proxy is complicated as the synchrotron luminosity is highly affected by the mean electron production per supernova and the galaxy's magnetic field, which are uncertain (e.g. Rybicki & Lightman 2004). There also exists a correlation between a galaxy's IR and radio emission (e.g. Yun, Reddy & Condon 2001). Therefore, since the IR is correlated with both the SFR and radio emission the radio SFR calibration can be derived empirically (e.g. Murphy *et al.* 2011).

A similarly indirect relation exists between SFR and X-ray luminosity. Supernovae and high mass X-ray binaries produced via recent star formation produce a large fraction of the X-ray luminosity of a star forming galaxy. Due to the difficulty of establishing the frequency and intrinsic luminosity of these X-ray sources the SFR again has to be derived empirically (e.g. Mineo, Gilfanov & Sunyaev 2012).

All of the above methods give us insight into the rate new stars are being created. However, a feature of the bimodality of galaxies is that there is a population that contains little to no star formation. This poses the question, why do galaxies stop forming stars?

1.3.2 Quenching Star Formation

The fundamental way to stop forming stars is to remove the cold dense hydrogen gas present within the galactic interstellar medium (ISM). The loss or heating of the ISM can be accomplished by many different processes. The possible mechanisms for quenching the star formation can be divided into two broad categories: internal processes and external processes. Below I briefly outline the quenching processes.

1.3.2.1 Internal Processes

In order to expel or heat a significant amount of gas from a galaxy a large amount of energy is required. Active galactic nuclei (AGN) and supernova are two mechanisms that output huge quantities of energy into their environments.

Many supernovae occurring within a star forming galaxy are able to ionise large regions of gas. This outburst of energy into the surrounding gas also drives outflows that are able to entrain and remove large amounts of gas from a low mass galaxy. We see evidence of this occurring with high velocity gas outflows measured in highly star forming galaxies with young stellar populations (e.g. Bradshaw *et al.* 2013).

AGN have been shown to produce enough energy to remove gas from the most massive galaxies and keep this gas from cooling and falling back onto the host galaxy (e.g. Silk & Rees 1998). Though, how this energy couples to the cold gas is unclear. AGN could drive strong winds in excess of what is observed from supernovae (e.g. Fabian 1999) or shock heat the gas and prevent it from cooling (e.g. Fabian *et al.* 2006). Evidence has been found that both of these processes may be at work. Tremonti, Moustakas & Diamond-Stanic (2007) observed high velocity, possibly AGN driven, outflows from post star-burst galaxies, and Fabian *et al.* (2006) found shocks within the inter-cluster medium of the Perseus cluster caused by radio lobe cavities created by the central AGN.

Recent work on galaxy formation models predict that the dark matter halo in which the galaxy resides can also be responsible for the quenching of star formation (Croton *et al.* 2006, Dekel, Sari & Ceverino 2009, Feldmann *et al.* 2010). These models predict that as the dark matter halo grows in mass its virial temperature increases and the halo

is able to create and maintain a hot gas medium surrounding the galaxy. This hot gas halo shock heats any cold gas infalling onto the system and therefore stops it from forming stars. This so called hot halo model predicts that galaxies residing within high mass dark matter haloes will be starved of cold gas and in turn star formation is halted.

1.3.2.2 External Processes

Over the course of a galaxy's lifetime it can come into contact with external objects and forces that have the ability to remove the cold gas and quench the ongoing star formation. The processes are most prevalent in galaxy cluster environments.

When a star forming gas rich galaxy enters a galaxy cluster environment, it begins to interact with the inter cluster medium (ICM). As the galaxy falls into the cluster the ICM exerts a pressure on to the ISM and, over time removes the cold gas from the system (Gunn & Gott 1972). This is known as ram pressure stripping. Many examples have been observed of galaxies that are undergoing this processes (e.g. Ebeling, Stephenson & Edge 2014 and references within). In large galaxy clusters the ICM is a hot X-ray emitting gas. When a galaxy falls into this environment and becomes embedded in the ICM, the IGM can be heated up and therefore cause cold gas loss by thermal evaporation (Cowie & Songaila 1977).

Galaxy interactions can also cause both an enhancement and a truncation of the SFR. A merger between galaxies can compress the ISM in both galaxies and enhance the SFR's of both galaxies. However, this enhancement may be short lived due to exhausting their cold gas reservoirs maintaining the high SFR (Fujita 1998), an enhancement in the supernova rate or the merger event triggering AGN activity. These processes can heat up and expel the remaining cold gas (e.g. Hopkins *et al.* 2008).

1.4 Massive Galaxies and High Redshift

Hereafter, we will refer to massive galaxies as those with $M_* \geq 10^{11} M_\odot$. Massive galaxies are thought to be formed in the high density peaks of the mass distribution in the early Universe. They are often the most luminous galaxies at all redshifts due

to their large stellar mass component, and therefore observable over a large range of cosmic time. This makes them an excellent probe for investigating galaxy formation. The population of local massive galaxies tend to have elliptical morphologies, high Sérsic indices, large sizes, low star formation rates, live in high density environments, have old stellar ages, and populate the massive end of the tight red sequence (e.g. Bower, Lucey & Ellis 1992, Kauffmann *et al.* 2003, Shen *et al.* 2003, Kauffmann *et al.* 2004, Gallazzi *et al.* 2005, Nelan *et al.* 2005, Baldry *et al.* 2006, Gallazzi *et al.* 2006, Quadri *et al.* 2007 Buitrago *et al.* 2013, Mortlock *et al.* 2013). These galaxies although massive are already in place at early cosmic times (e.g. Mortlock *et al.* 2011), however, they are not the homogeneous population we observe in the local universe.

Massive galaxies at high redshift, $z > 2.0$, have been found to be highly star forming, have low Sérsic indices and smaller sizes (e.g. Daddi *et al.* 2007, Trujillo *et al.* 2006a, Bauer *et al.* 2011, Buitrago *et al.* 2013). How galaxies have transformed over cosmic time is an important open question in modern astrophysics.

1.4.1 Size Evolution

In the local universe there exists a correlation between stellar mass and galaxy size, with the more massive galaxies having larger sizes (e.g. Shen *et al.* 2003). A major finding of recent high redshift studies is that passive massive galaxies at $z > 1.5$ have significantly smaller sizes and are more compact than local passive massive galaxies. This was originally reported by Daddi *et al.* (2005) who showed that massive galaxies at high redshift are a factor of three smaller than local similar mass. Figure 1.9 shows the findings of recent work by van der Wel *et al.* (2014) that explores size evolution over a wide range of galaxy masses over the redshift range of $0 < z < 3$.

Several physical processes have been proposed to explain this strong size evolution within the massive galaxy population at $z < 1.5$. These can be divided into two distinct categories: external or internal processes. External processes that can increase the sizes of galaxies are gas poor (dry) mergers (e.g. Khochfar & Silk 2006, Naab, Johansson & Ostriker 2009) and cold gas flows along cosmic web filaments (e.g. Dekel, Sari & Ceverino 2009, Conselice *et al.* 2013) adding small amounts of stellar mass to the outer regions of massive galaxies. Internal processes that can increase the sizes of

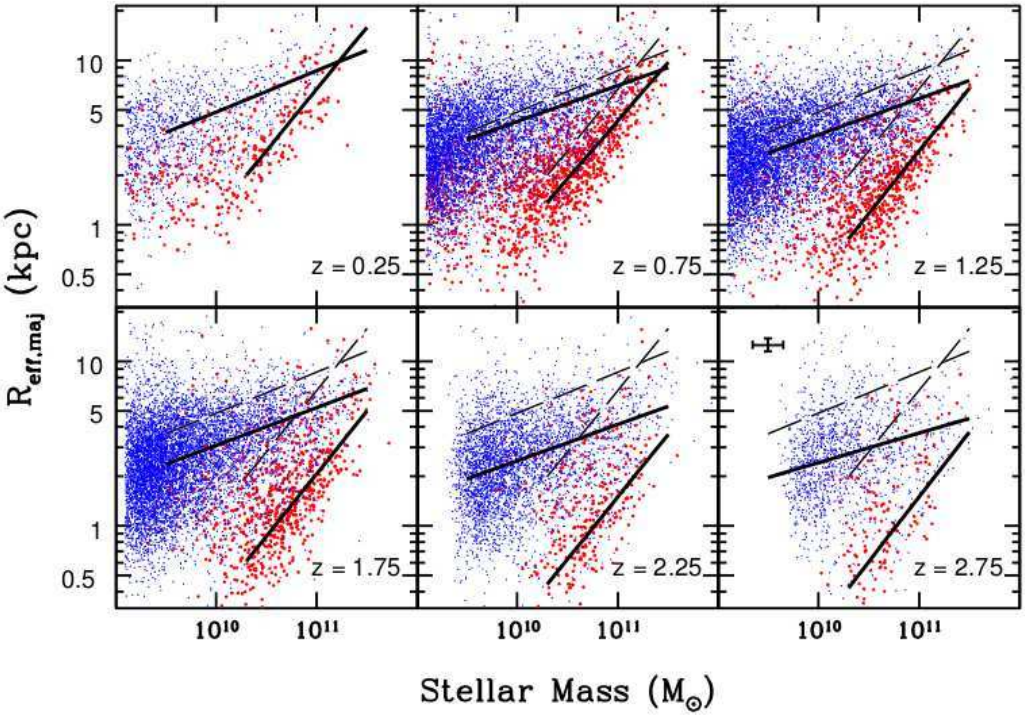

Figure 1.9: The size-stellar mass distribution for star forming and passive galaxies over a range of redshifts. The colour coding represents the early types (red) and late types (blue). The solid lines indicate the best fits to both populations. The dashed line in each plot represent fits to the galaxies in the $z = 0.25$ redshift bin. The strong evolution in galaxy sizes can clearly be seen in both populations. Figure from van der Wel *et al.* (2014)

galaxies are adiabatic expansion resulting from stellar mass loss and strong AGN-fuelled feedback (e.g. Fan *et al.*, 2008, 2010, Hopkins *et al.* 2010, Bluck *et al.* 2011). In the AGN feedback scenario the central AGN engine will remove gas from the central parts of the galaxy, quenching star formation and altering the gravitational potential within the galaxy's inner region. This causes the system to relax and undergo adiabatic expansion resulting in a larger galaxy size.

At the present time there is no clear answer that can fully explain the observed size evolution. Recent works suggest that dry minor mergers could be responsible for this phenomenon, with several works (e.g. Carrasco, Conselice & Trujillo 2010, van Dokkum *et al.* 2010, Bluck *et al.* 2012) finding that the central regions of massive galaxies from $z = 2.2$ do not change but witness the development of "wings" in galaxy light profiles with decreasing redshift. However, the rate that minor merger events occur over a galaxy's lifetime is an unknown, and are there may be other processes contributing to the size evolution.

1.4.2 Stellar Mass Assembly

An important question in galaxy evolution is how do galaxies build and assemble their stellar mass. The stellar mass growth of all galaxies is linked by two fundamental processes: star formation and mergers. By these two processes all galaxies acquire their stellar mass. Star formation and mergers are known to have increasing importance as we look back in time (e.g. Madau *et al.* 1996, Dekel, Sari & Ceverino 2009, Bridge, Carlberg & Sullivan 2010, Bluck *et al.* 2011) but how these processes each contribute to the growth of stellar mass over cosmic time is uncertain.

In the last few decades, much observational effort has been devoted to the dependence of galaxy formation and the assembly of stellar mass. In early studies, Cowie *et al.* (1996) showed that the rest frame K-band luminosity (proxy for stellar mass) of rapidly star forming galaxies declines with redshift. They described this behaviour as "downsizing".

1.4.2.1 Downsizing

Downsizing is a process of galaxy formation where the most massive galaxies finish forming before lower mass objects. The effect of downsizing can be observed in the Universe in multiple ways. Firstly, it was observed by Cowie *et al.* (1996) who showed that the bright end of the galaxy luminosity function shows very little evolution between $0 < z < 1.7$, whereas the faint end shows a significant evolution. This finding suggests that the brightest (i.e. most massive) galaxies have finished building their stellar masses before fainter (lower stellar mass) galaxies. Secondly, it can be seen in the star formation histories of galaxies (e.g. Heavens *et al.* 2004). Several studies have shown that massive galaxies ended their epoch of major star formation before the general galaxy population (e.g Juneau *et al.* 2005, Bundy *et al.* 2006, Daddi *et al.* 2007). See Fontanot *et al.* (2009) for a review of the results of downsizing.

The process of downsizing appears to be at odds with the hierarchical growth scenario where the largest galaxies form last with the "bottom-up" assembly of the dark matter structures in a ΛCDM Universe. However, the two can be reconciled. Even though the massive passive galaxies are assembled at $z > 1$ their host dark matter haloes continue to grow in mass. They grow in mass via mergers with other dark matter haloes, however, the galaxies contained within do not merge on the same time scale. The merger timescale for the most massive haloes are longer than smaller haloes (Binney & Tremaine 1987) and mergers are rare. This would imply that the host galaxies could remain separate after the dark matter haloes have merged. Another possible reconciliation is that the massive galaxies undergo dry gas-less mergers. In conjunction with the hot halo model described previously this would starve a galaxy of fuel for star formation and hence these galaxies will remain "red and dead".

The complete picture of the physical processes that drive downsizing is not clear and if we wish to comprehend this phenomenon we must fully understand the massive galaxy population and its evolution.

1.5 Aims of this Thesis

This thesis will try to answer some of the open questions posed by this introduction. The overarching aim of this thesis is to investigate the evolution of massive galaxies since $z = 3$ to the present day, a period of over 11 billion years.

Our first aim is to attempt to explain the observed size evolution with redshift using the observed distribution of star formation within massive galaxies at high redshift. A process that has not been looked at in detail is the internal star formation distribution present within massive galaxies at high redshift, and whether this can account for the observed structural evolution.

Chapter 2 is a study of the evolution of the structure and size of massive galaxies via star formation from $z = 3$ to the present day. This uses data from the GOODS NICMOS Survey (GNS). In this chapter we also investigate the effect stellar migration has on the evolution of the light profiles of massive galaxies.

In Chapter 3, we investigate the stellar mass growth of massive galaxies over the redshift range of $0.3 < z < 3.0$ in the UKIDSS Ultra Deep Survey (UDS). Using new number density selection techniques we can trace the progenitors of today's massive galaxies and explore their stellar mass growth. Using their observed star formation and major merger histories we can attempt to determine by which processes these galaxies assemble their mass and at what epochs. In this chapter, we also explore the implications on these results on the cold gas accretion histories.

In Chapter 4, we further investigate the evolution of the progenitors of today's massive galaxies in the UDS. Using our knowledge of the direct progenitors of massive galaxies we examine the evolution of their colours, passivity, stellar ages, star formation histories, structural parameters and their locations on the colour-magnitude diagram.

All of the above chapters are then concluded in Chapter 5.

Chapter 2

Evolution of Massive Galaxy Structural Properties and Sizes via Star Formation In the GOODS NICMOS Survey

2.1 Introduction

One of the least understood aspects of galaxy evolution is the star formation rates in galaxies and, how these vary across individual galaxies, and influence galaxy properties. A key way to address galaxy evolution directly is to understand how the nearby galaxy population was put into place and evolved from higher redshift galaxies, which we can now observe in near complete mass-selected samples up to $z = 3$ (e.g. Daddi *et al.* 2007; Conselice *et al.* 2011). One major finding of high redshift studies is that massive galaxies $(M_* > 10^{11} M_\odot)$ have significantly smaller effective radii than low redshift galaxies of similar mass (e.g. Daddi *et al.* 2005; Trujillo *et al.*, 2006a,b, 2007; Trujillo, Ferreras & de La Rosa, 2011; Buitrago *et al.*, 2008; Cimatti *et al.* 2008; van Dokkum *et al.*, 2008, 2010; Franx *et al.* 2008 ; van der Wel *et al.* 2008; Damjanov *et al.* 2009; Carrasco, Conselice & Trujillo 2010; Newman *et al.* 2010; Szomoru *et al.* 2011; Weinzirl *et al.* 2011).

Several physical processes have been proposed to explain this strong size evolution within the massive galaxy population at $z < 2$. These can be divided into two distinct categories, external processes such as gas poor (dry) mergers (e.g. Khochfar & Silk 2006; Naab, Johansson & Ostriker 2009) and cold gas flows along cosmic web filaments (e.g. Dekel, Sari & Ceverino 2009; Conselice *et al.* 2013) as a means for puffing up the stellar components of these massive galaxies, or internal processes such as adiabatic expansion resulting from stellar mass loss and strong AGN-fuelled feedback (e.g. Fan *et al.*, 2008, 2010; Hopkins *et al.* 2010; Bluck *et al.* 2011). One process that has not been looked at in detail is the internal star formation distribution present within massive galaxies at high redshift, and whether this can account for the observed structural evolution. This can now be examined due to high resolution data from the GOODS NICMOS Survey taken with the ACS and NICMOS-3 instruments on the Hubble Space Telescope (Conselice *et al.* 2011).

We know that galaxies evolve significantly in stellar mass from observational studies showing that half of the stellar mass of present day galaxies is already in place by $z \sim 1$ (e.g. Brinchmann & Ellis 2000; Drory *et al.* 2004; Bundy *et al.* 2006; Pérez-González *et al.* 2008a; Mortlock *et al.* 2011). The most massive galaxies $(M_* > 10^{11} M_\odot)$ appear on average to have red rest-frame colours which we expect to see for galaxies dominated by old stellar populations (Saracco *et al.* 2005; Labbé *et al.* 2006; Conselice *et al.* 2007; Grützbauch *et al.* 2011). However, Bauer *et al.* (2011) show that $\sim 80\%$ of these massive red galaxies likely harbour dusty star formation. This star formation over cosmic time could contribute large amounts of stellar mass to massive galaxies, and depending on where this mass is created could affect their observable structural properties as they evolve.

In the merger scenario, estimates for the total number of major mergers experienced by a massive galaxy on average since $z = 3$ is $N_m = 1.7 \pm 0.5$ (Bluck *et al.* 2009). We explore this more thoroughly in Chapter 3. This would imply an average stellar mass increase of, at best, a factor of two due to major mergers. However over the same period of time the effective radius of massive galaxies has increased on average by a factor of three for disk-like galaxies, and a factor of five for spheroid-like galaxies, effectively building up stellar mass in the outer regions of galaxies (see e.g.

Buitrago *et al.*, 2008; Trujillo *et al.* 2007; Carrasco, Conselice & Trujillo 2010; van Dokkum *et al.* 2010). This additional stellar mass could arise from star formation already present at high redshift within these outer regions.

To date studies have only looked at the total star formation rates of these galaxies as a whole (e.g. Pérez-González *et al.* 2008a; Cava *et al.* 2010; van Dokkum *et al.* 2010; Bauer *et al.* 2011; Grützbauch *et al.* 2011; Hilton *et al.* 2012), but have not examined the locations of the star formation within these galaxies. Thus, we combine the observed stellar mass profiles with the observed star formation profiles of high redshift massive galaxies in order to measure the effect stellar mass added via star formation over ~ 10 Gyr has on different spatial regions, and to the total stellar mass profile. We also ascertain whether this star formation can account for the observed size evolution.

Along with size evolution within the massive galaxy population there is also a change in overall morphology. The present day universe is populated by massive galaxies with early-type morphologies (e.g. Baldry *et al.* 2004, Conselice 2006b). At earlier epochs, $z > 1.5$, observational studies have found that the massive galaxy population is dominated by galaxies with late-type morphologies (e.g. Buitrago *et al.* 2013; Cameron *et al.* 2011; van der Wel *et al.* 2011; Weinzirl *et al.* 2011). This morphological shift can be seen via a change in Sérsic index from low values, $n \lesssim 2.5$ denoting a possible late-type morphology, to high values, $n \gtrsim 2.5$ denoting a possible early-type morphology. In the hierarchical model of galaxy evolution there are many methods that can drive morphological evolution. These methods include in situ star formation producing disk-like systems (e.g. Dekel, Sari & Ceverino 2009; Oser *et al.* 2010; Ricciardelli *et al.* 2010; Wuyts *et al.* 2010; Bournaud *et al.* 2011), and/or mergers with satellite galaxies producing a more spheroid-like system (e.g. Khochfar & Silk 2006; Hopkins *et al.* 2009; Feldmann *et al.* 2010; Oser *et al.* 2010). We therefore also investigate how in situ star formation over cosmic time changes the Sérsic index of the massive galaxies, and ascertain whether this process can account for the observed morphological changes.

This chapter is set out as follows: Section 2.2 discusses the GOODS NICMOS Survey, the galaxy sample, and how the data used in this chapter was obtained. Section 2.3.1

examines the stellar mass radial density distributions of the massive galaxies. Section 2.3.2 describes how the stellar mass density added via star formation is calculated. In Section 2.3.3 we examine the evolved galaxy profiles. Section 2.4.1 presents the findings of how the structure and size of the massive galaxies is altered by star formation. In Section 2.4.2 we introduce a simple stellar migration model to the stellar mass added by star formation in order to gauge the effect this has on structures and sizes. Section 2.5 and 2.6 contain the discussion and summary of our findings, respectively. Throughout this chapter we assume $\Omega_M = 0.3$, $\Omega_\Lambda = 0.7$ and $H_0 = 70$ km s^{-1} Mpc^{-1}. AB magnitudes and a Salpeter IMF are used throughout.

2.2 Data and Analysis

In this section we describe the survey we use in this study, the GOODS NICMOS Survey (GNS), as well as the measurements of photometric redshifts, stellar masses, rest-frame colours and star formation rates for our galaxies.

2.2.1 The GOODS NICMOS Survey

The data we use in this chapter is obtained through the GNS. The GNS is a 180 orbit Hubble Space Telescope survey consisting of 60 single pointings with the NICMOS-3 near-infrared camera, with an imaging depth of three orbits per pointing (Conselice *et al.* 2011).

These pointings were optimised to contain the maximum number of massive galaxies $(M > 10^{11} M_\odot)$ in the redshift range $1.7 < z < 3$, identified in the two GOODS fields by their optical-to-infrared colours (see Conselice *et al.* 2011). The survey covers a total area of about 45 arcmin^2 with a pixel scale of ~ 0.1 arcsec/pixel, corresponding to ∼0.9 kpc at the redshift range of interest $(1.5 < z < 3)$. The target selection, survey characteristics and data reduction are fully described in Conselice *et al.* (2011). Other analyses of the GNS data set can be found in Buitrago *et al.* (2008), Bauer *et al.* (2011), Bluck *et al.* (2011), Grützbauch *et al.* (2011) and Mortlock *et al.* (2011).

The GNS has a 5σ limiting magnitude of $H_{AB} = 26.8$, which is significantly deeper

than ground based near-infrared imaging of the GOODS fields carried out with e.g. ISAAC on the VLT, which reaches a 5σ depth of $H_{AB} = 24.5$ (Retzlaff *et al.* 2010). Sources were extracted from the NICMOS H_{160}-band image and matched to the optical HST-ACS bands B,V,i and z, which are available down to a AB limiting magnitude of $B = 28.2$. The matching is done within a radius of 2 arcsec, however the average separation between optical and H_{160}-band coordinates is much better with $\sim 0.28 \pm 0.4$ arcsec, roughly corresponding to the NICMOS resolution (see also Bauer *et al.* 2011).

The photometric catalogue covering the B$vizH$ bands comprises 8298 galaxies, and is used to compute photometric redshifts, rest-frame colours and stellar masses described in the following sections (see also Conselice *et al.* 2011 for more details). Along with this, each galaxy has imaging data in the Bviz ACS bands (Giavalisco *et al.* 2004).

Within our NICMOS fields is a total of 81 galaxies with stellar masses larger than $10^{11} M_{\odot}$ with photometric and spectroscopic redshifts in the range $1.5 < z < 3$. This H_{160}-band sample of massive galaxies is reduced to 52 due to optical band non--detections where we are unable to calculate accurate ultraviolet (UV) dust extinction corrections (Bauer *et al.* 2011). The sample is further reduced to 45 galaxies due to removing those galaxies with Sérsic fits to the H_{160} light profiles with high uncertainties or profiles that cannot be constrained (see §2.3.1 and Buitrago *et al.* 2008). We examine the UV surface brightness profiles of the excluded galaxies in the bands they were detected in, and found them to be consistent with the profiles of the remaining galaxies. Figure 2.2 shows the z_{850} and H_{160} band images of the 45 galaxies used in this study.

2.2.2 Redshifts

Where possible, we use spectroscopic redshifts published in the literature for our GNS galaxies, otherwise we use photometric redshifts. Spectroscopic redshifts of sources in the GOODS-N field were compiled by Barger, Cowie & Wang (2008), whereas the GOOD-S field spectroscopic redshifts are taken from the FIREWORKS compilation (Wuyts *et al.* 2008). In the full GNS sample, there are 537 spectroscopic redshifts for sources in GOODS-N and 369 in GOODS-S. In the massive galaxy sample used in this chapter there are however only six galaxies with spectroscopic redshifts.

Photometric redshifts are therefore crucial for this study. These photo-zs were obtained by fitting template spectra to the B$vizH$ photometric data points using the HYPERZ code (Bolzonella, Miralles & Pelló 2000). The method is described in more detail in Grützbauch *et al.* (2011). The synthetic spectra used by HYPERZ are constructed with the Bruzual $\&$ Charlot evolutionary code (Bruzual A. & Charlot 1993) representing roughly the different morphological types of galaxies found in the local universe. Five template spectra are used corresponding to the spectral types of E, Sa, Sc and Im, as well as a single starburst scenario. The reddening law is taken from Calzetti *et al.* (2000). HYPERZ computes the most likely redshift solution in the parameter space of age, metallicity and reddening. The best fit redshift and corresponding probability are then output together with the best fit parameters of spectral type, age, metallicity, A_v and secondary solutions.

To assess the reliability of our photometric redshifts we compare them to available spectroscopic redshifts in the GOODS fields. We matched the two catalogues to our photometric catalogue with a matching radius of 2 arcsec, obtaining 906 secure spectroscopic redshifts. Figure 2.1 shows the matched sources. The reliability of photometric redshifts measures we use is defined by $\Delta z/(1+z) \equiv (z_{spec}-z_{photo})/(1+z_{spec})$. In the following we compare the median offset from the one-to-one relationship between photometric and spectroscopic redshifts, $\langle \Delta z/(1+z) \rangle$, and the RMS scatter around this relation, $\sigma_{\Delta z/(1+z)} = 0.061$. We then investigate the performance of HYPERZ at different redshifts, at low redshift $(z < 1.5)$ and at $1.5 \leq z \leq 3$, which is the redshift range of the galaxy sample we use. For the high redshift complete sample we obtain an average offset $\langle \Delta z/(1+z) \rangle = 0.06$ and a RMS of $\sigma_{\Delta z/(1+z)} = 0.1$, with a fraction of catastrophic outliers of 20%, where catastrophic outliers are defined as galaxies with $|\Delta z/(1+z)| > 0.3$, which corresponds to ~ 3 times the RMS scatter. This error has been folded into the results.

2.2.3 Stellar Masses and e-folding Star formation Timescales

Stellar masses and rest-frame colours of our sample are determined from multicolour stellar population fitting techniques using the same catalogue of five broad band data

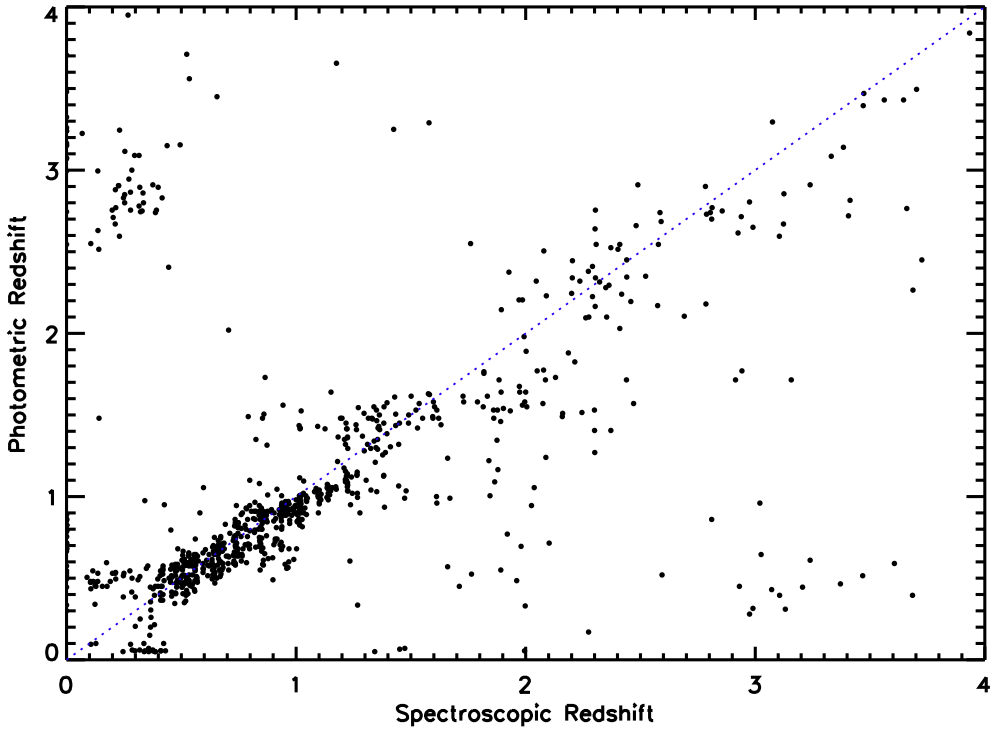

Figure 2.1: Matched photometric redshifts versus spectroscopic for the GNS (906 galaxies). The dispersion, $\Delta z/(1+z)$, and catastrophic outlier fraction are 0.06 and 20% for galaxies within the redshift range of study ($1.5 < z < 3.0$).

points used to determine photometric redshifts for all GNS galaxies. A detailed description of how stellar masses and rest-frame $(U - B)$ colours are derived can be found in Bundy *et al.* (2006), Conselice *et al.* (2011) and Grützbauch *et al.* (2011), and is summarised in the following.

To calculate the stellar masses and colours of galaxies a grid of model spectral energy distributions (SEDs) are constructed from Bruzual & Charlot (2003) stellar population synthesis models, assuming a Salpeter initial mass function, varying star formation history, age, metallicity and dust extinction. The star formation history is characterised by an exponentially declining model of the form

$$SFR(t) = SFR_0 \times e^{-t/\tau}. \tag{2.1}$$

The parameters in Equation 2.1 are varied over a wide range of values within the ranges; $\tau = 0.01$ to 10 Gyr - with values (all in Gyr): 0.01 0.025 0.05 0.08 0.1 0.12 0.65 1.21 1.37 1.73 1.99 2.52 2.71 2.84 2.99 3.09 3.34 3.7 4.23 4.33 4.45 4.69 5.16 5.23 5.47 5.68 5.83 6.21 6.61 6.95 7.03 7.27 7.37 7.95 8.38 8.76 8.80 8.94 9.57 9.80 9.88, and the time since the onset of star formation ranging from $t = 0$ to 10 Gyr, with a condition that ages are not older than the universe itself at the redshift of observation. The dust content is parametrised by the V-band optical depth with values $\tau_V = 0.0, 0.5, 1, 2$ and the metallicity ranges from 0.0001 to 0.05 (Bruzual & Charlot 2003).

The magnitudes obtained from the model SEDs are fit to the observed photometric data of each galaxy using a Bayesian approach. A grid of models is constructed from the parameters defined above and the H-band $M_*/L_{\rm H}$, minimum χ^2 and the probability that each model accurately describes a given galaxies is calculated at each grid point. The corresponding stellar mass is then determined by scaling the $M_*/L_{\rm H}$ ratios to the H-band luminosity based on the total H-band magnitude and redshift of the observed galaxy. The probabilities are then summed across the grid and binned my model stellar mass, yielding a stellar mass probability distribution for each galaxy. We use the peak of the distribution as the best estimate, and the uncertainty is the width. The final error, as a result of the models used, lie within the range of 0.2 to 0.3 dex.

We use negative τ models in this chapter to fit our stellar masses, although other forms of the star formation history are included later in the chapter when considering the addition of stellar mass, including constant star formation rate measures, and an exploration of possible forms of the star formation history, including those which are maximal and would exceed the observed stellar mass density evolution (§2.5.4.1). While there is some evidence that the star formation history actually increases from $z = 8$ to $z = 3$ (e.g., Papovich *et al.* 2011), there is also evidence that at redshifts lower than this, and particularly for high mass galaxies, that the star formation rate is starting to decline (e.g., Conselice *et al.* 2007, 2011). We investigate this in detail by examining our sample at a constant co-moving number density, as Papovich *et al.* (2011) does, and seeing how our star formation rate changes for the same co-moving density. Doing this, we find that the star formation declines over our epoch using this method, although the star formation history at redshifts $z > 3$ is more complicated than this. However, this does show that our values of τ that we use here are mimicking the form of the empirical star formation history.

It is possible that the stellar masses are an over estimate due to the poor treatment of the TP-AGB phase in a star's life and due to the effect of strong emission lines contaminating the broadband photometry. The effects of the TP-AGB phase are less important at the rest frame wavelengths used in this study, especially in the infrared H_{160} band. Using newer models by Bruzual & Charlot (2007) which have an improved treatment of the TP-AGB phase we find that this lowers the stellar masses of the massive galaxy sample by < 0.07 dex. This effect from the new models is smaller than the stellar mass error, and the effects of cosmic variance, and is therefore negligible. Table 2.1 contains the full list of values for all variables used in this study.

2.2.4 Star Formation Rates

The star formation rates (SFRs) used in this chapter are measured from rest-frame UV luminosities, using the methods described in Bauer *et al.* (2011). The rest-frame UV provides a direct measurement of ongoing SFR, since the UV luminosity is directly related to the presence of young and short-lived stellar populations produced by recent star formation. However, UV light can be contaminated from older stellar populations

(e.g. Helium core burning stars) and is very susceptible to dust extinction and a careful dust-correction has to be applied. The correction we use here is based on the rest-frame UV slope. We briefly describe the method in the following.

We determine the $SFR_{UV,uncorrected}$ from the observed optical ACS z_{850}-band flux density (with a 5 σ limit of 27.5 in the AB system) spanning wavelengths of 2125 - 3400Å for $z = 1.5$ - 3 galaxies. After applying an SED based k-correction using the IDL KCORRECT package (Blanton & Roweis 2007, v4.2) this corresponds to a rest frame wavelength of 2800Å. This is done by using the full SEDs of these galaxies. The result of this is a k-correction at rest-frame UV wavelengths ~ 2800Å which we use throughout this chapter.

To measure the SFR we first derive the UV luminosity of the massive galaxies, then use the Kennicutt (1998a) conversion from 2800Å luminosity to SFR assuming a Salpeter IMF:

$$SFR_{UV}(M_{\odot}\mathrm{yr}^{-1}) = 1.4 \times 10^{-28} L_{2800}(\mathrm{ergs\,s^{-1}\,Hz^{-1}}) \tag{2.2}$$

Before dust extinction is taken into account we find a limiting $SFR_{UV,obs} = 0.3 \pm 0.1 M_{\odot}\mathrm{yr}^{-1}$ at $z = 1.5$, and a limiting $SFR_{UV,obs} = 1.0 \pm 0.3 M_{\odot}\mathrm{yr}^{-1}$ at $z = 3$. The errors quoted here take into account photometric errors and the conversion from a luminosity. The error for individual SFRs are around 30%. This error is dominated by the uncertainty on the measurement of the UV slope (β) and the conversion to a dust correction.

We compare our total integrated SFR for each galaxy in this sample to the same sample used in Bauer *et al.* (2011) which included both SED determined and UV SFR. We find on average that our total SFRs are slightly higher due to the use of a larger aperture but within the quoted error.

Several studies (e.g. Bauer *et al.* 2011; Reddy *et al.* 2012) have found that when comparing the IR derived SFRs plus UV derived SFRs (SFR_{IR+UV}) against dust corrected UV SFRs ($SFR_{UV,corr}$) that the SFR_{IR+UV} is on average a factor of 3 larger than $SFR_{UV,corr}$. This overestimation has been seen in other studies looking at luminous galaxies (e.g. Papovich *et al.* 2007). Results from the Herschel Space Telescope (e.g.

Elbaz *et al.* 2010; Nordon *et al.* 2010; Hilton *et al.* 2012) suggest that at $z > 1.5$, the 24 μm flux may overestimate the true SFR due to a rise in the strength of polycyclic aromatic hydrocarbon (PAH) features, changes in the SEDs, or AGN contamination.

Recent work on the same sample of massive galaxies used in this chapter by Hilton *et al.* (2012) using Herschel Space Telescope data and new fitting methods of the same sample of massive galaxies found that the scatter of these results can be reduced to $< 1\sigma$ between the IR+UV and UV corrected SFRs by taking into account new templates in the FIR that account for these issues. We however are unfortunately forced to only use the $SFR_{UV,corr}$ in this chapter since the *Spitzer* IR 24μm and *Herschel* images are not resolved.

2.2.5 Dust Corrections

To obtain reliable star formation rates in the rest-frame ultraviolet, we need to account for the obscuration due to dust along the line of sight. Meurer, Heckman & Calzetti (1999) found a correlation between attenuation due to dust and the rest-frame UV slope, β, for a sample of local starburst galaxies (where $F_\lambda \sim \lambda^\beta$). More recent studies of local galaxies using the *Galaxy Evolution Explorer* (GALEX) near-ultraviolet band show that the UV slope from the local starburst relation can be used to recover the dust attenuation of moderately luminous galaxies at $z \sim 2$ (Buat *et al.* 2005; Seibert *et al.* 2005; Reddy *et al.* 2010).

A method for determining dust extinction uses the reddening parameter extracted from the best-fitting SED template as described in §2.2.3. We fit sets of template stellar population synthesis models to derive the stellar masses (Grützbauch *et al.* 2011; Conselice *et al.* 2011). This method has some limitations when using it to correct for dust as this approach assumes that the UV slope is due to dust reddening instead of other sources, such as evolved stellar populations (Grützbauch *et al.* 2011).

We apply a method for determining a UV dust attenuation, A_{2800}, in terms of the UV slope. The UV slope is determined using an SED-fitting procedure described in Bauer *et al.* (2011). To summarise, we fit an SED to the multi-wavelength observations from optical-to-infrared. The SEDs obtained for all sources in the GOODS fields were fit

with stellar population synthesis models. The best fitting templates were then used to obtain a synthetic estimate of the UV emission at 1600Å and 2800Å. From the model-derived UV luminosities at 1600Å and 2800Å we calculate the spectral slope, β. The Calzetti *et al.* (2000) law is then used to derive A_{2800} from the UV spectral slope, which we apply to the UV-derived star formation rates. Using this method we find an average extinction value of $A_{2800} = 3.2 \pm 1.0$ magnitudes for our sample.

Bauer *et al.* (2011) find in a comparison between an SED determined, and an observationally derived A_{2800}, that the values obtained from these two methods are in relatively good agreement for $M_* > 10^{11} M_\odot$ across the whole redshift range with an average offset of $\delta A_{2800} = 0.86$. This corresponds to a $\sim 27\%$ error in the average dust attenuation and this is folded into the following results.

2.3 Stellar Mass Density Profiles

2.3.1 Stellar Mass Radial Density Distributions

We construct our sample galaxy's stellar mass density distributions by examining the distribution of the H_{160}, rest-frame optical light profiles for our sample (for $1.5 < z < 3$ this corresponds to rest $\lambda = 640 - 400$nm). We base this determination on the Sérsic fits to the light distribution. A detailed description of how the Sérsic indices were measured can be found in Buitrago *et al.* (2008) and is summarised in the following.

The Sérsic profiles were measured using GALFIT (Peng *et al.*, 2002; Peng, 2010). GALFIT uses $r^{1/n}$ 2D models of the form (Sérsic 1968):

$$\Sigma(r) = \Sigma_e \times \exp(-\mathrm{b_n}[(\mathrm{R}/\mathrm{R_e})^{1/\mathrm{n}} - 1]) \tag{2.3}$$

where R_e is the effective radius of the galaxy, Σ_e is the surface brightness at R_e, n is the Sérsic index and $b_n = 1.9992n - 0.3271$. This model is convolved with the Point Spread Function (PSF) of the images, and GALFIT determines the best fit by comparing the convolved model with the observed galaxy surface brightness distribution using

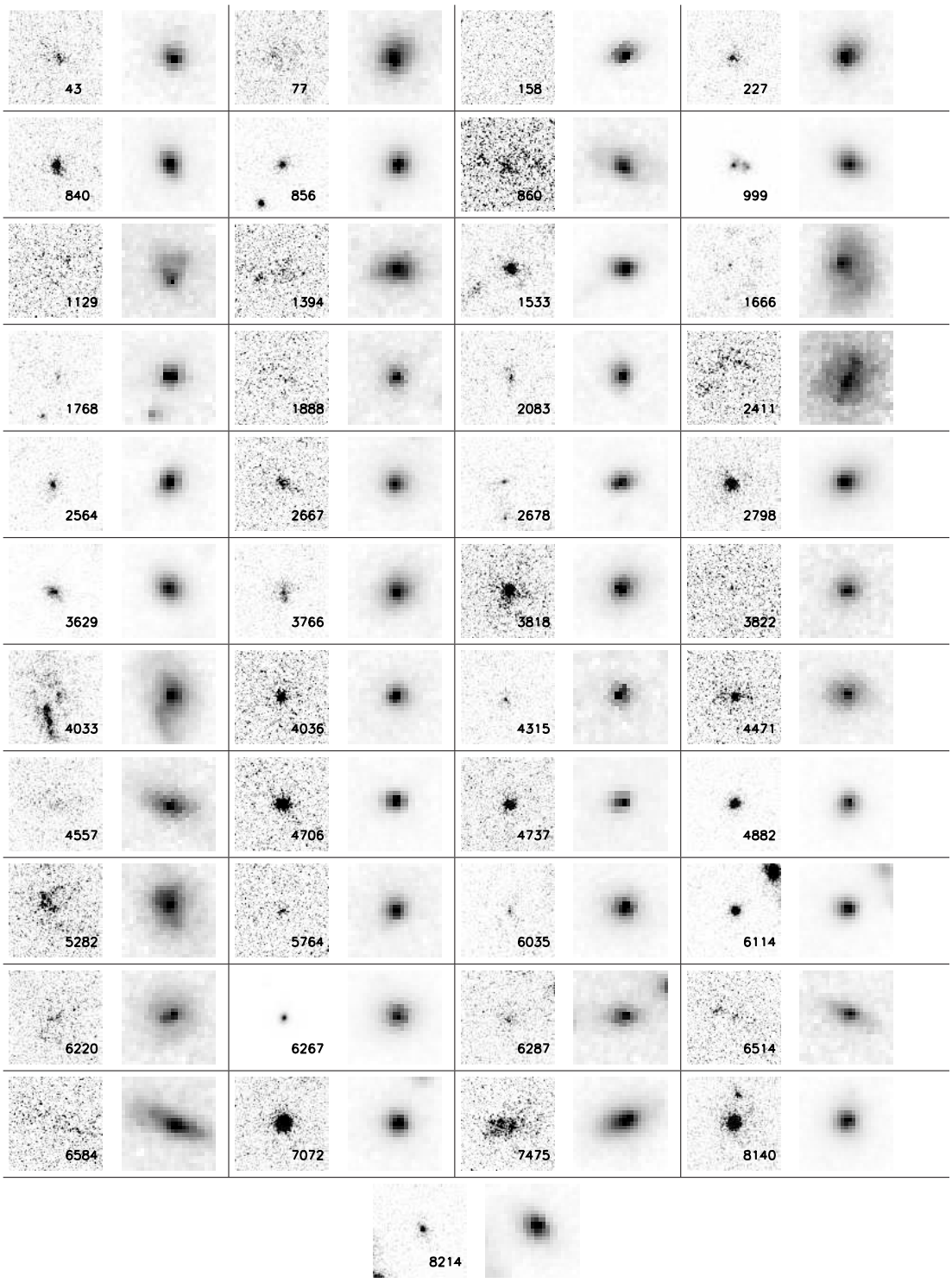

Figure 2.2: Images in the z_{850} band (left) and H_{160} band (right) of the 45 massive galaxies in this study. The ID number of each galaxy is shown in the lower right hand corner of the z_{850} band image with the corresponding image of the same region in the H_{160} band to the right. All images are 2.5 by 2.5 arcsecond cutouts for galaxies between $1.5 < z < 3$ centred on the H_{160} band detection. The properties of each galaxy are listed in Table 2.1.

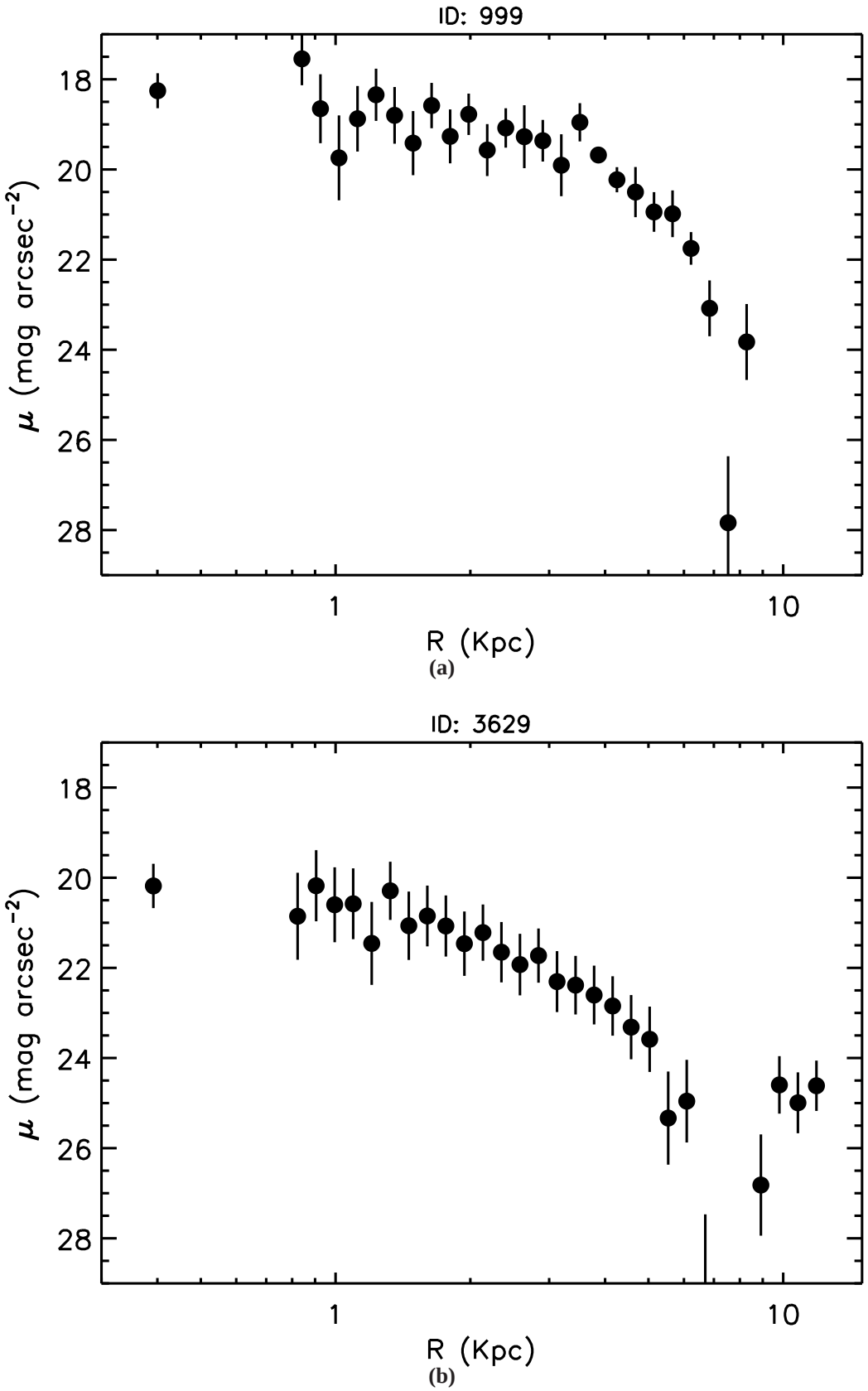

Figure 2.3: Example rest frame UV surface brightness profiles from ACS z_{850}-band imaging. (a) Galaxy ID: 999, Initial stellar mass: $1.5 \times 10^{11} M_{\odot}$, Rest frame optical effective radius: 2.0kpc, Rest frame optical Sérsic index:$n = 1.42$, SF growth classification: Inner SF growth. (b) Galaxy ID: 3629, Stellar mass: $2.6 \times 10^{11} M_{\odot}$, Rest frame optical effective radius: 1.8kpc, Rest frame optical Sérsic index:$n = 1.26$, SF growth classification: Non-significant SF growth.

a Levenberg-Marquardt algorithm to minimise the χ^2 of the fit. We use single Sérsic models to compare our size estimations with previous work. Neighbouring galaxies are masked out before the fitting, and in the case of overlapping isophotes the objects are fit simultaneously. Due to variations of the shape of the NICMOS-3 PSF in our images, we select five non- saturated bright stars to sample the PSF within our imaging and with which to gauge the accuracy of the parameter measurements. The structural parameters of each galaxy are measured five times for each unique star. The uncertainty (1σ) on the structural parameters due to changes in the PSF is $\sim 15\%$ for the effective radius r_e, and $\sim 20\%$ for the Sérsic index n. We then remove galaxies from our galaxy sample that are not well constrained after Sérsic profile fitting i.e. Galaxies with high uncertainties in n or R_e or have $n < 0.2$. Objects with $n < 0.2$ have been removed as these objects have non physical profiles and also have not reached the Chi^2 global minima due to the fitting constraints and are therefore unreliable.

A concern when measuring sizes and Sérsic indices at high redshift is surface brightness dimming which in principal could bias our measured sizes. Previous studies have examined this issue, and have conducted many simulations in order to check the importance of surface brightness dimming in HST observations (e.g. Trujillo *et al.*, 2006a, 2007; Buitrago *et al.* 2013). In Appendix A of Buitrago *et al.* (2013) one can find the descriptions of the extensive simulations conducted in order to asses the reliability of the galaxy structural parameters within GNS. The median observable characteristics of our massive galaxies ($H_{AB} = 22.5$, n$\sim$2, r$_e$ $\sim$2 kpc) allow us to retrieve their structural properties without any significant bias. However it is worth noting that, for individual galaxies, the parameters are not as well constrained for galaxies which display higher Sérsic indices.

Using the total stellar mass for the galaxies and the H-band light (see §2.2.3) we equate the total stellar mass to the total rest-frame optical light received from the individual galaxies. We then convert the H_{160}-band Sérsic profile to a stellar mass profile. The total initial stellar mass defined by:

$$M_* = \rho_e \int_0^{R_{\rm max}} \exp(-{\rm b_n}[({\rm R}/{\rm R_e})^{1/{\rm n}} - 1]) 2\pi {\rm R dR} \tag{2.4}$$

The radius within which the total stellar mass is contained, $R_{\rm max}$, is taken to be 20kpc in all cases. $R_{\rm max}$ is chosen to be 20kpc as it is approximately 8 times the average effective radius and will encompass more than 99.9% of the total flux. The effective radius, R_e and Sérsic index, n, come from the H_{160}-band Sérsic profile as described in this section. From this, the stellar mass density at the effective radius ρ_e is calculated, and the full stellar mass density profile is constructed via:

$$\rho_{observed}(R) = \rho_e \times \exp(-\mathrm{b_n}[(\mathrm{R}/\mathrm{R_e})^{1/\mathrm{n}} - 1]) \tag{2.5}$$

with the implicit assumption that the mass to light ratio is constant over the galaxy, as used in other works studying surface brightness profiles (e.g. Szomoru *et al.* 2011).

2.3.2 Stellar Mass Density Added Via Star Formation

We measure star formation profiles for our sample using the IRAF program *ellipse* by fitting a series of isophotal ellipses to the z_{850}-band data with the H_{160}-band determined centre of the massive galaxies. This isophotal fitting returns the z_{850}-band flux binned in a series of increasing radii. This is then converted to a dust corrected star-formation rate in each radius bin via the procedure described in §2.2.5. Examples of such surface brightness profiles are shown in Figure 2.3.

The total galaxy magnitudes obtained from this isophotal fitting are checked against a previous catalogue of the z_{850}-band magnitudes for these galaxies in Bauer *et al.* (2011) measured with SExtractor (Bertin & Arnouts 1996), and are found to be consistent.

In order to measure how this star formation affects the $z = 0$ mass density of the galaxy we simulate the amount of stellar mass added via star formation in each radius bin by assuming that the same global star formation history we use in §2.2.3 applies through to $z = 0$. We also apply several other star formation histories that these galaxies could experience such as constant SFR to $z = 0$, constant SFR to $z = 1.5$ and variations on the derived tau model. These are discussed in §2.5.4.2. We find very similar results as discussed below for the tau models.

ID	SF Class	SFR_0	z	Mass	A_{2800}	R_e	n	$\tau\ (yr)$
43	OG	126.7±34.2	1.79	11.0±0.4	3.8±1.0	1.8±0.3	2.5±0.8	6.5×10^8
77	NG	173.8±46.9	2.33	11.1±0.2	3.5±0.9	3.2±0.1	1.4±0.1	1.2×10^8
158	NG	28.8±7.8	1.84	11.2±0.4	2.0±0.5	1.4±0.3	2.0±2.0	6.5×10^8
227	NG	23.1±6.2	2.48	11.2±0.3	0.8±0.2	2.1±0.1	2.1±0.1	1.2×10^8
840	NG	87.8±23.7	2.31	11.1±0.3	2.4±0.6	1.6±0.2	2.3±0.5	1.2×10^8
856	NG	257.8±69.6	2.32	11.2±0.2	2.6±0.7	1.7±0.1	3.7±0.3	1.2×10^8
860	OG	367.0±81.0	1.79	11.2±0.3	3.9±1.1	3.8±0.3	3.5±0.6	6.5×10^8
999	IG	672.6±181.6	1.58	11.2±0.4	4.0±1.1	2.0±0.1	1.4±0.3	1.4×10^9
1129	NG	464.7±125.5	2.61	11.3±0.4	5.0±1.3	3.1±0.1	0.2±0.1	1.2×10^8
1394	NG	208.4±56.3	2.29	11.5±0.3	3.5±0.9	3.3±0.1	1.1±0.1	1.2×10^8
1533	NG	97.4±26.3	2.45	11.6±0.3	1.8±0.5	1.3±0.1	0.9±0.5	6.5×10^8
1666	NG	244.5±66.0	*1.76	11.9±0.4	4.7±1.3	6.2±0.1	0.6±0.1	1.2×10^8
1768	NG	314.7±85.0	2.22	11.4±0.3	3.6±1.0	1.4±0.1	2.1±0.6	1.2×10^8
1888	NG	133.4±36.0	2.75	11.2±0.4	3.5±0.9	2.0±0.5	5.0±1.2	1.2×10^8
2083	NG	160.6±43.4	2.31	11.1±0.4	3.5±0.9	1.2±0.2	1.3±0.6	1.2×10^8
2411	OG	241.7±65.3	2.09	11.0±0.3	3.8±1.0	5.2±0.1	0.6±0.1	6.5×10^8
2564	NG	127.8±34.5	2.10	11.1±0.3	3.5±0.9	1.4±0.1	1.8±0.3	1.2×10^8
2667	OG	284.8±76.9	1.79	11.2±0.4	3.5±0.9	2.0±0.1	3.5±0.9	6.5×10^8
2678	NG	51.8±14.0	2.30	11.1±0.3	1.2±0.3	1.4±0.1	0.8±0.1	1.2×10^8
2798	NG	196.2±53.0	1.72	11.6±0.3	3.5±0.9	4.5±0.6	4.6±0.2	6.5×10^8
3629	NG	140.6±37.0	2.17	11.4±0.2	2.5±0.7	1.8±0.2	1.3±0.2	6.5×10^8
3766	NG	76.0±20.5	1.87	11.2±0.2	2.2±0.6	2.8±0.1	1.9±0.3	1.4×10^9
3818	NG	255.9±69.1	1.82	11.5±0.4	3.5±0.9	3.7±0.4	5.1±1.3	6.5×10^8
3822	NG	115.3±31.1	2.41	11.1±0.5	3.5±0.9	1.9±0.1	2.1±0.5	1.2×10^8
4033	OG	81.5±22.0	1.72	11.2±0.3	1.0±0.3	6.1±0.8	1.2±0.1	1.7×10^9
4036	OG	134.3±36.3	1.72	11.0±0.3	3.5±0.9	1.7±0.4	7.5±2.0	6.5×10^8
4315	NG	231.1±62.4	2.85	11.0±0.4	4.0±1.1	0.9±0.5	1.8±1.3	1.2×10^8
4471	OG	401.0±108.3	*2.29	11.2±0.4	3.5±0.9	2.8±0.1	1.4±0.1	6.5×10^8
4557	NG	232.6±62.8	2.09	11.3±0.4	3.1±0.8	4.6±0.1	1.4±0.1	1.2×10^8
4706	NG	236.2±63.8	*2.35	11.1±0.2	3.4±0.9	0.9±0.1	1.7±1.2	1.2×10^8
4737	NG	34.4±9.2	2.52	11.0±0.3	1.3±0.4	1.1±0.3	3.3±3.7	1.2×10^8
4882	IG	448.4±121.1	1.67	11.1±0.3	4.2±1.1	1.2±0.1	2.2±0.2	6.5×10^8
5282	IG	276.8±74.7	1.64	11.0±0.3	3.5±0.9	4.9±0.1	1.1±0.1	2.7×10^9
5764	NG	170.2±41.6	2.54	11.5±0.3	3.5±0.9	1.7±0.1	2.9±0.4	1.2×10^8
6035	NG	208.6±56.3	1.60	11.3±0.4	3.5±0.9	2.0±0.1	4.2±0.6	6.5×10^8
6114	NG	108.0±29.2	1.96	11.3±0.3	2.5±0.7	1.5±0.6	0.3±0.3	6.5×10^8
6220	IG	558.3±150.7	1.71	11.0±0.4	5.1±1.4	3.8±0.1	1.5±0.1	6.5×10^8
6267	OG	136.2±36.8	*1.54	11.4±0.2	1.6±0.4	2.3±0.1	2.3±0.5	1.7×10^9
6287	NG	102.9±27.8	1.84	11.0±0.4	3.5±0.9	2.5±0.1	2.4±0.4	6.5×10^8
6514	NG	199.6±53.9	2.49	11.2±0.3	3.2±0.9	2.7±0.2	2.5±0.1	1.2×10^8
6584	NG	180.4±48.7	1.62	11.2±0.3	3.5±0.9	6.2±0.1	1.1±0.1	1.2×10^8
7072	OG	101.0±27.3	1.74	11.1±0.2	1.9±0.5	1.4±0.1	2.3±0.4	1.4×10^9
7475	OG	377.9±102.0	*1.61	11.2±0.3	3.5±0.9	4.9±0.2	2.1±0.2	6.5×10^8
8140	OG	319.6±86.3	*1.90	11.4±0.4	3.0±0.8	1.8±0.1	2.7±0.5	6.5×10^8
8214	OG	817.0±220.6	2.05	11.3±0.2	3.8±1.0	1.6±0.1	1.7±0.2	6.5×10^8

Table 2.1: (col. 1) ID number of the galaxy; (col.2) The classification of the galaxy based on the location of the star formation (see §3.3); Non-significant star formation growth (NG), outer star formation growth (OG) and inner star formation growth (IG) ; (col.3) Total observed UV star formation rate in solar masses per year ; (col. 4) Best redshift of the object, spectroscopic redshifts are denoted by * ; (col. 5) Stellar Mass with error in units of $\log_{10} M_\odot$ calculated from multi colour stellar population fitting techniques ; (col. 6) A_{2800} Dust correction and error in magnitudes, determined from UV slope fitting ; (col. 7) Effective radius and error in units of kpc from Sérsic $r^{1/n}$ 2D models fits of the H_{160} band data using GALFIT. ; (col. 8) Sérsic index and error from Sérsic $r^{1/n}$ 2D models fits of the H_{160} band data using GALFIT. ; (col. 9) e-folding star formation time in years calculated from multi-colour stellar population fitting techniques (see §2.2.3).

The exponentially declining model of star formation uses the observed dust-corrected rest-frame UV star formation as the initial rate, SFR_0, and the values of the e-folding time, τ, which we obtained from the M_* fitting (see §2.2.3). To obtain the total amount of stellar mass added via star formation, $M_{\rm SF}$, we integrate Equation 2.1 over time from the total look back time derived from the redshift of the galaxy, ranging from ~ 9.7 Gyr at $z = 1.7$ to ~ 11.5 Gyr at $z = 3$ to the present day. We experimented with evolving the massive galaxies only until $z = 1$ but found very similar results as the evolution to $z = 0$ as the majority of the evolution in both size and structural properties of these massive galaxies seems to occur within the first ~ 2 Gyr of our simulation.

In Figure 2.4 we show the change in the total stellar mass of each of the galaxies within our sample as measured through the SFR. We find that the total stellar mass on average increases by $91 \pm 22\%$ via this modelled star formation. The evolved total stellar masses of our galaxies do not exceed constraints placed upon the observed total stellar mass evolution from other studies (e.g. Cole *et al.* 2001; Bell *et al.* 2003; Conselice *et al.* 2007; Brammer *et al.* 2011; Mortlock *et al.* 2011). Brammer *et al.* (2011) show that the total stellar mass growth for massive galaxies from $z \sim 2$ to 0 is of the order of 100%. We see that there is an anticorrelation between the original stellar mass and the evolved stellar mass, with some of the lower mass galaxies increasing substantially in stellar mass, while the higher mass galaxies have a much smaller change in mass over cosmic time. This is a sign of galaxy downsizing (e.g. Cowie *et al.* 1996; Bundy *et al.* 2006), such that the most massive galaxies are less affected by star formation at $z < 3$ than the lower mass galaxies.

This total stellar mass added via star formation is converted to a stellar mass projected density via, $\rho_{\rm SR} = M_{\rm SF}/A_{\rm an}$, were $A_{\rm an}$ is the area of the annulus the star formation is contained within. From this we construct a new stellar mass profile by including the stellar mass added via star formation to the original profile via:

$$M_*(R,t) = M_*(R,t=0) + SFR_0(R) \int_0^t e^{-t/\tau} dt \tag{2.6}$$

where $M_*(R,t=0)$ is the initial stellar mass at radius R, $SFR_0(R)$ is the observed initial SFR at the same radius and $M_*(R,t)$ is the stellar mass at radius R after time t.

We consider other cases of star formation histories in §2.5.4.

2.3.3 Profiles

In this section we examine the profiles of the stellar mass density distributions at high redshift, the stellar mass density added via star formation, and for the combination of the two - an evolved stellar mass density profile for each of the 45 massive galaxies in our sample. The evolved profiles are then fit with a new Sérsic profile. The Sérsic profiles for the evolved stellar mass profiles are obtained by the best fitting Sérsic (1968) function to the new profile,

$$\rho(R) = \rho_e \times \exp(-\mathrm{b_n}[(\mathrm{R}/\mathrm{R_e})^{1/\mathrm{n}} - 1]) \tag{2.7}$$

We find that the galaxies in our sample can be classified into three distinct groups based on the location of star formation regions and the effect they have on our sample galaxy's evolved stellar mass density profile.

To examine the results we first divide the galaxies into two regions. An inner region, at $R \leq$ 1kpc with an observed initial stellar mass density in the inner region, $\rho_{\mathrm{observed,inner}}$ and a stellar mass density added via star formation in the inner region, $\rho_{\mathrm{SF,inner}}$. An outer region, $R >$ 1kpc with a observed stellar mass density, $\rho_{\mathrm{observed,outer}}$ and a stellar mass density added via star formation in the outer region, $\rho_{\mathrm{SF,outer}}$. We chose 1kpc as the boundary for our inner region based on stellar surface brightness comparisons at high and low redshifts (e.g. Hopkins *et al.* 2009; Carrasco, Conselice & Trujillo 2010; Szomoru *et al.* 2011). We discuss the three types below.

Non-significant Star Formation Growth (NG) : This category is for galaxies in which the stellar mass density added via star formation is smaller than the galaxy's initial stellar mass density present over both the inner and outer regions. $\rho_{\mathrm{observed,inner}} > \rho_{\mathrm{SF,inner}}$ and $\rho_{\mathrm{observed,outer}} > \rho_{\mathrm{SF,outer}}$.

Outer Star Formation Growth (OG) : In this category the stellar mass density added via star formation is greater than the initial stellar mass density present in the outer region, but the initial stellar mass density in the inner region is greater than the stellar mass density added via star formation; $\rho_{\mathrm{observed,inner}} > \rho_{\mathrm{SF,inner}}$ but $\rho_{\mathrm{observed,outer}} < \rho_{\mathrm{SF,outer}}$

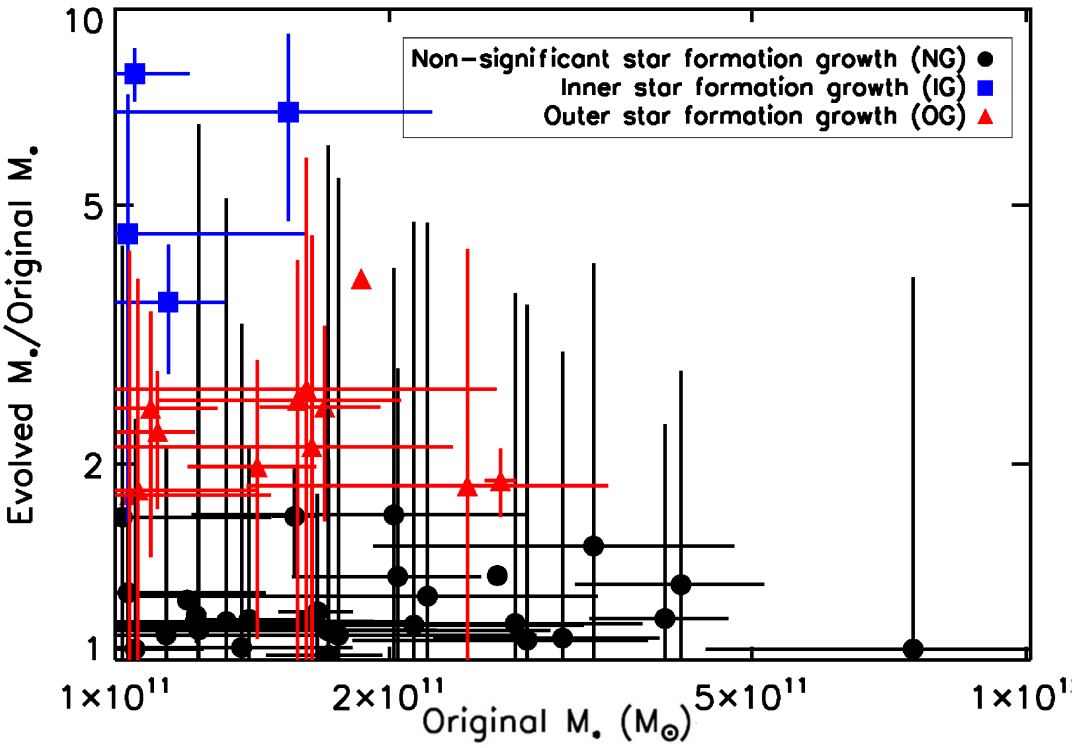

Figure 2.4: Total stellar mass before ($\mathrm{Original\,M_*}$) and after evolution ($\mathrm{Evolved\,M_*}$) from the derived tau model of star formation evolution. The black circles represent the non-significant star formation growth galaxies. The blue squares represent the inner star formation growth galaxies. The red triangles represent the outer star formation growth galaxies (see §2.3.3).

Type	No. of galaxies	% of sample
Non-significant SF Growth (NG)	29	$64.4^{+4.5}_{-33.3}$
Inner SF Growth (IG)	4	$8.9^{+2.2}_{-2.2}$
Outer SF Growth (OG)	12	$26.7^{+31.1}_{-2.3}$

Table 2.2: Evolved massive galaxies using the derived tau model of SF evolution separated into the three classifications. Insignificant Star Formation Growth (NG), Inner Star Formation Growth (IG), Outer Star Formation Growth (OG). We see that nearly half of the sample resides in the NG class with a significant fraction in the OG class.

Inner Star Formation Growth (IG) : This category is for galaxies in which the stellar mass added via star formation is greater over both regions than the initial stellar mass density present, $\rho_{\rm observed,inner} < \rho_{\rm SF,inner}$ and $\rho_{\rm observed,outer} < \rho_{\rm SF,outer}$

In Figure 2.5 we show examples of the three different galaxies classes and in Table 2.2 we list the numbers of each class we have in our sample.

2.4 Results

The profiles for the stellar mass already in place at high redshift (§2.3.1) and the stellar mass added via star formation (§2.3.2) are combined to give an evolved modelled stellar mass density profile of the galaxy after evolving for ~ 10 Gyr from $z \simeq 2.5$ until the present day. Using the new stellar mass density profiles we fit a new Sérsic profile of the same form as Equation 2.5 to examine how the stellar mass added via star formation would change the structure and sizes of our massive galaxies over time.

2.4.1 Stellar Mass

Figure 2.4 shows the growth in total stellar mass for all of the galaxies within our sample. As stated before the average growth for the sample is $91 \pm 22\%$. The evolved total stellar masses of our sample of galaxies does not exceed constraints placed upon the observed total stellar mass evolution from other studies (e.g. Conselice *et al.* 2007; Brammer *et al.* 2011; Mortlock *et al.* 2011). This represents the maximal stellar mass increase, negating the effects of supernova and other types of feedback that would impede star formation and reduce the total amount of stellar mass created. From this figure we can also see that there is a clear divide between the three classes of galaxies

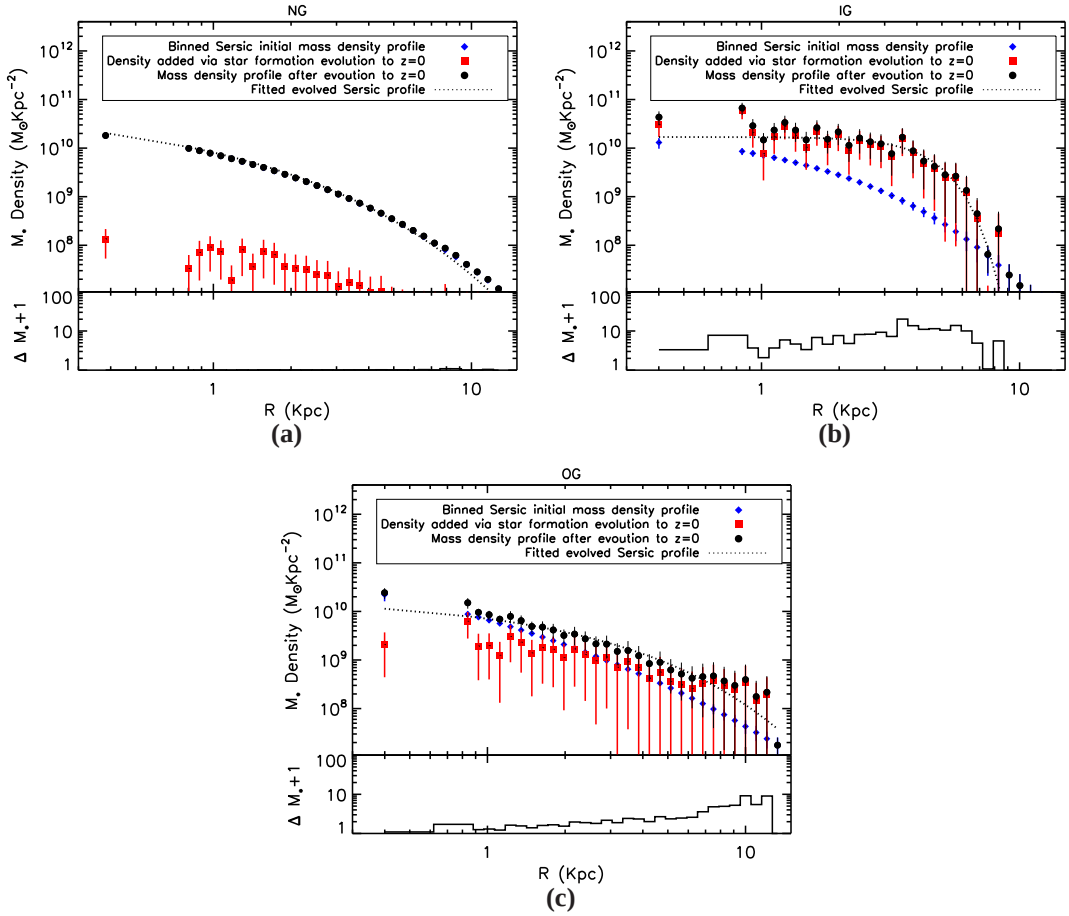

Figure 2.5: Example of the three star formation growth classifications. a)Non-significant star formation growth (NG) b)Inner star formation growth (IG) c) Outer star formation growth (OG). The blue diamonds represent the observed stellar mass density present at high redshift based on the H_{160}-band Sérsic profile. The red squares represent the stellar mass density added via star formation to $z = 0$. The black circles represent the combined (evolved) profiles of both the stellar mass density present at high redshift and the stellar mass density added via star formation to $z = 0$. The black dotted line is the best fit Sérsic profile to the evolved stellar mass density profile. The sub-plot shows the change in the stellar mass density profile, ΔM, from the stellar mass density present at high redshift compared (blue diamonds) to the evolved stellar mass density profile (black circles).

in our sample (see §2.3.3). The NG class galaxies have the smallest change in total stellar mass of $22 \pm 34\%$, and do not come close to doubling in stellar mass. The IG class has the largest change in stellar mass of $474 \pm 89\%$, and lie exclusively in the top region of the figure. The OG class of galaxies in this sample have an intermediate mass change of $129 \pm 90\%$. This is a clear segregation in stellar mass build up via star formation between the three classes based upon the star formation locations, showing that the three different classes also have differing specific star formation rates, with IG galaxies having the highest and NG having the lowest. This divide is also present in all of the other models of SF we applied to this sample.

2.4.2 Structure and Size Evolution

We find from the Sérsic fits to the evolved profiles that the average change in n over the whole massive galaxy sample is such that the Sérsic index goes slightly down, $n_{\rm evolved} - n_{\rm original} = \Delta n = -0.9 \pm 0.9$. This is consistent with a small change with the profile shape over time.

In Figure 2.6a we show that the change in Sérsic index n differs for the three profile classifications. The NG galaxies lie nearly completely along the 1:1 line, denoting a small change from the observed to the evolved n, $\Delta n = -0.6 \pm 0.1$. This is expected as these galaxies are classified as having a small amount of stellar mass density added via star formation compared to the observed stellar mass density. However, we note that the NG galaxies with a high original n do not fall upon the 1:1 line, and have a lower n after evolution due to small amounts of star formation in the outer regions.

Also, we find that all of the OG and IG galaxies lie below the 1:1 line. This reveals that these galaxies have a lowered n value after star formation evolution. Over the whole OG class there is a change of $\Delta n = -1.6 \pm 0.4$, and $\Delta n = -1.1 \pm 0.3$ for the IG class. The result is expected for the OG class as these are defined as galaxies where there is a disparity in the amounts of star formation between the two regions, inner and outer. This disparity results in the outer regions of the galaxy increasing in stellar mass density, while the inner region does not.

The small changes in Sérsic n after star formation evolution shows that the star forma-

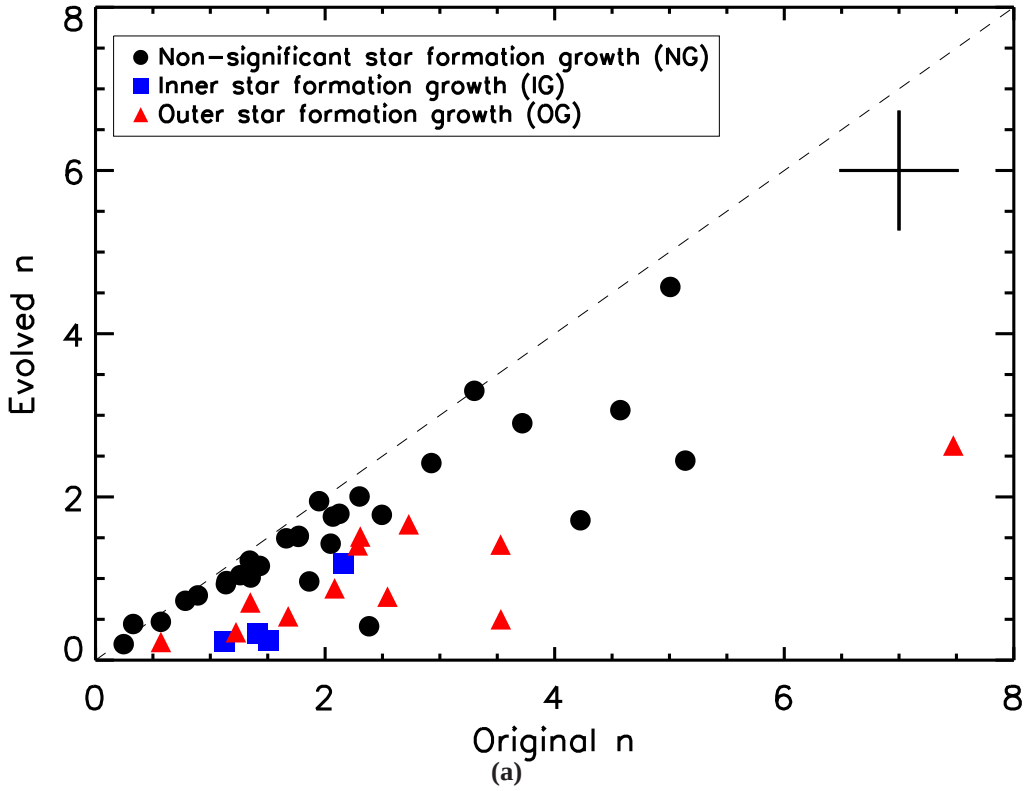

(a)

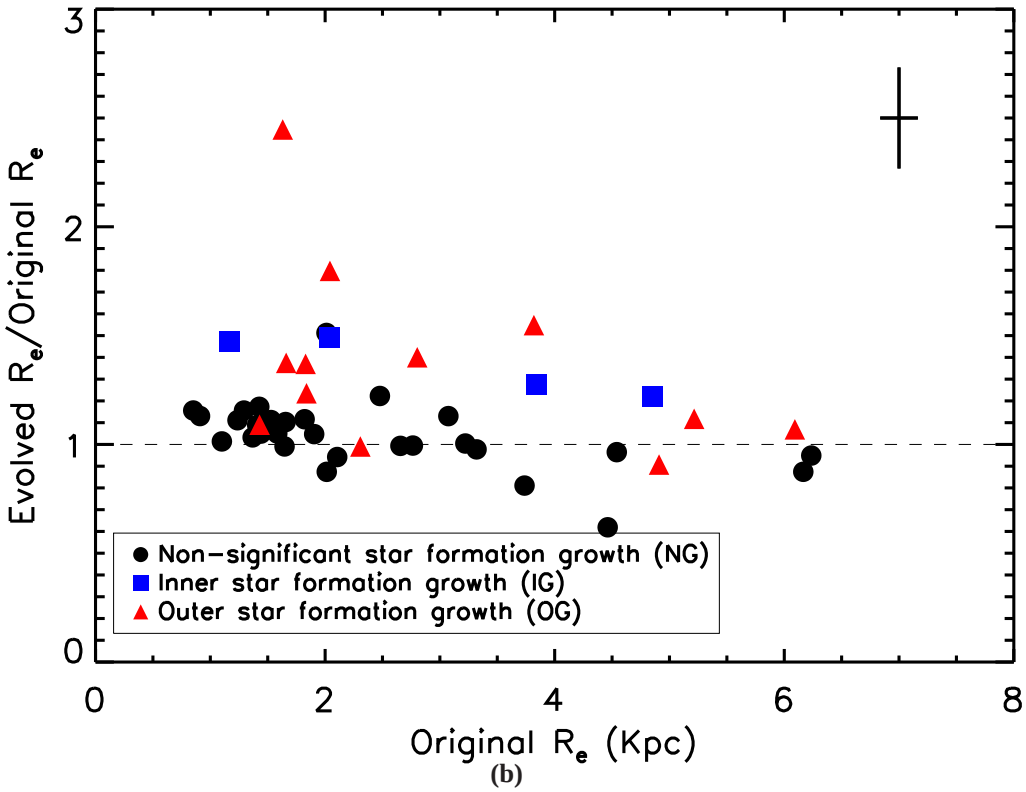

(b)

Figure 2.6: The evolution of the Sérsic index (a), and the effective radius (b) via star formation to $z = 0$. The black circles denote galaxies classified as NG. The red triangles denote galaxies classified as OG and the blue squares denote galaxies classified as IG (see §2.3.3). The dashed line in both cases shows a $1:1$ relation. The typical error bars are shown in the top right hand corner.

tion density within these galaxies largely follows the underlying stellar mass density profile. In the case of IG galaxies where the stellar mass added via star formation dominates over the entire galaxy, the initial stellar mass density profile is almost completely negligible after evolution but the new profile retains the same general shape.

The effective radius, R_e, for our entire sample increases by $16 \pm 5\%$ averaged over the entire sample after our simulation. Separating the galaxies into our different classifications we find that the NG class has a very minor increase in size of $4 \pm 3\%$. We find the OG class has an increase in R_e of $37 \pm 12\%$. This increase in the effective radius is due to the addition of stellar mass in the outer regions of these galaxies. The IG class has an increase in R_e of $36 \pm 16\%$. This small increase is most likely related to the non-changing n we find for this class.

Figure 2.6b shows the evolution of the effective radius before and after star formation evolution. We find that galaxies in the NG class all lie close to their original effective radius with the other two classes having a larger change. We also see that the massive galaxies with smaller original effective radii have a larger growth in size after star formation evolution compared to systems with larger original effective radii.

2.4.3 Stellar Migration

We show above that the star formation within the massive galaxies is not sufficient to produce a large growth in effective radius. We now investigate stellar migration as a method that may also be at work.

Recent theoretical work suggests that it may be common for stars to migrate radically across significant distances within spiral galaxies (Sellwood & Binney 2002, Roškar *et al.* 2008). These works showed that stellar migration happens via processes in the spiral arms of disk galaxies. However, we cannot reliably distinguish disk-like galaxies in our sample using a Sérsic index cut at $n = 2.5$ because we cannot rule out that some of the galaxies with $n > 2.5$ do not have spiral like features (e.g. Buitrago *et al.* 2013). Therefore we add into our evolution models a simple stellar migration model to all the galaxies in the sample in order to gauge the effect this would have on the size and structural changes of the evolved galaxy profiles.

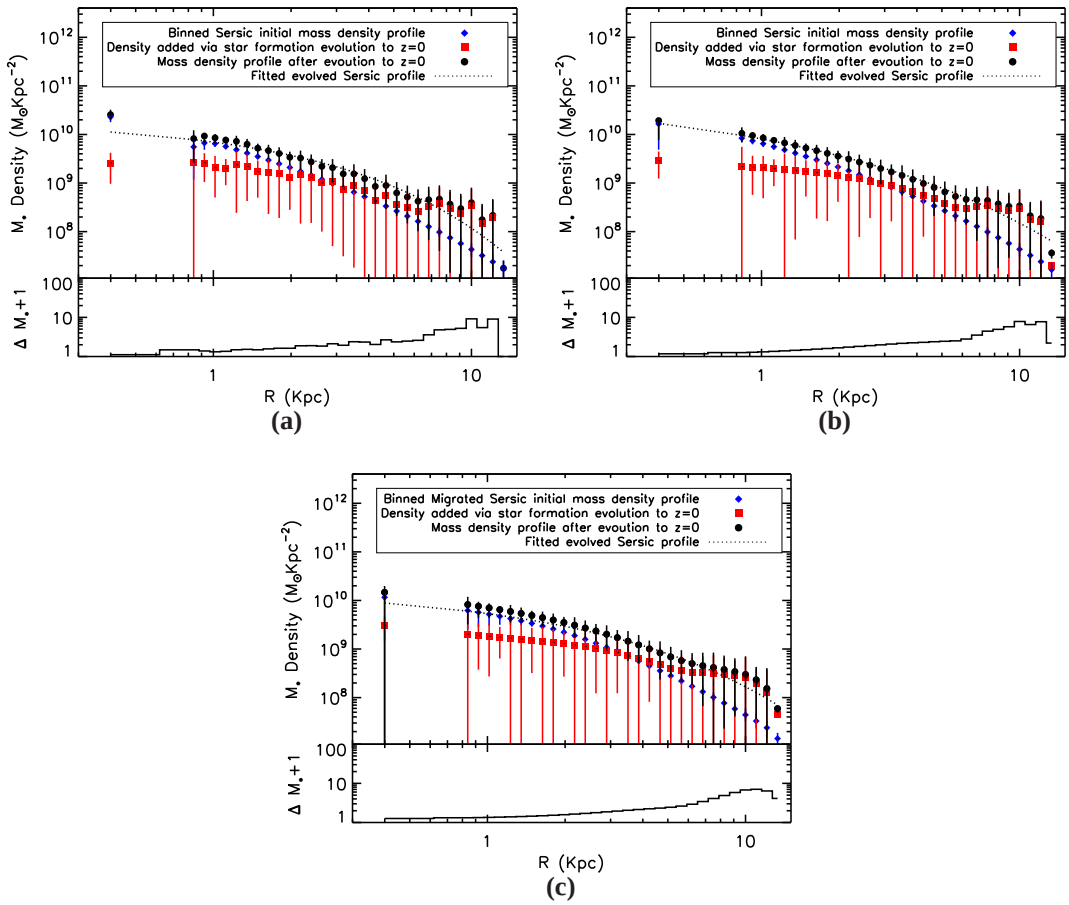

Figure 2.7: Example of the effect of the stellar migration models on one example galaxy density profiles with increasing Gaussian widths of σ = (a)0.1kpc, (b) 0.5kpc, (c) 1.0kpc. The non-migration profile can be seen in Figure 2.4 (c) which is the galaxy we use in this example. The sub-plot shows the change in the stellar mass density profile from the stellar mass density present at high redshift compared to the evolved stellar mass density profile.

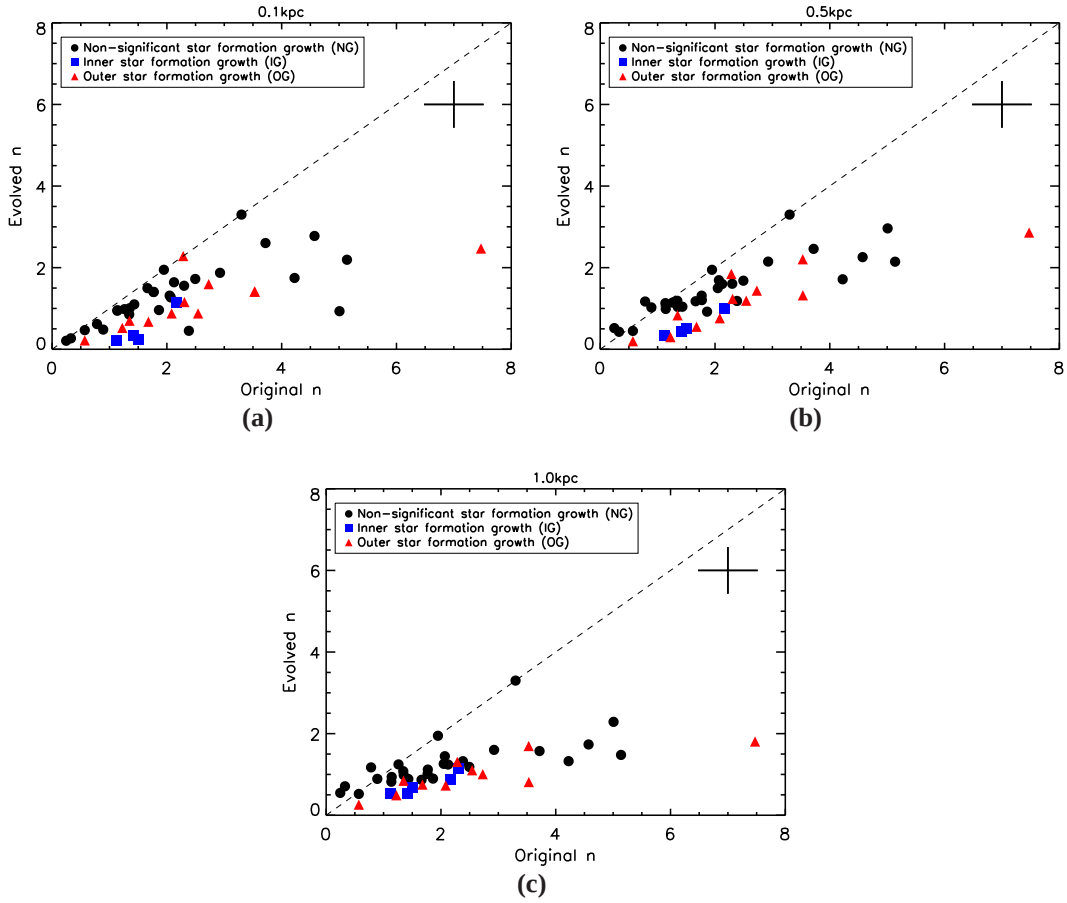

Figure 2.8: The evolution of the Sérsic index with due to various stellar migration models, the Gaussian form for stellar migration is shown in Equation 2.8. The values of σ used are (a) 0.1kpc, (b) 0.5kpc (c) 1.0kpc. The black circles denote galaxies classified as NG. The red triangles denote galaxies classified as OG and the blue squares denote galaxies classified as IG. The typical error bars are shown in the top right hand corner.

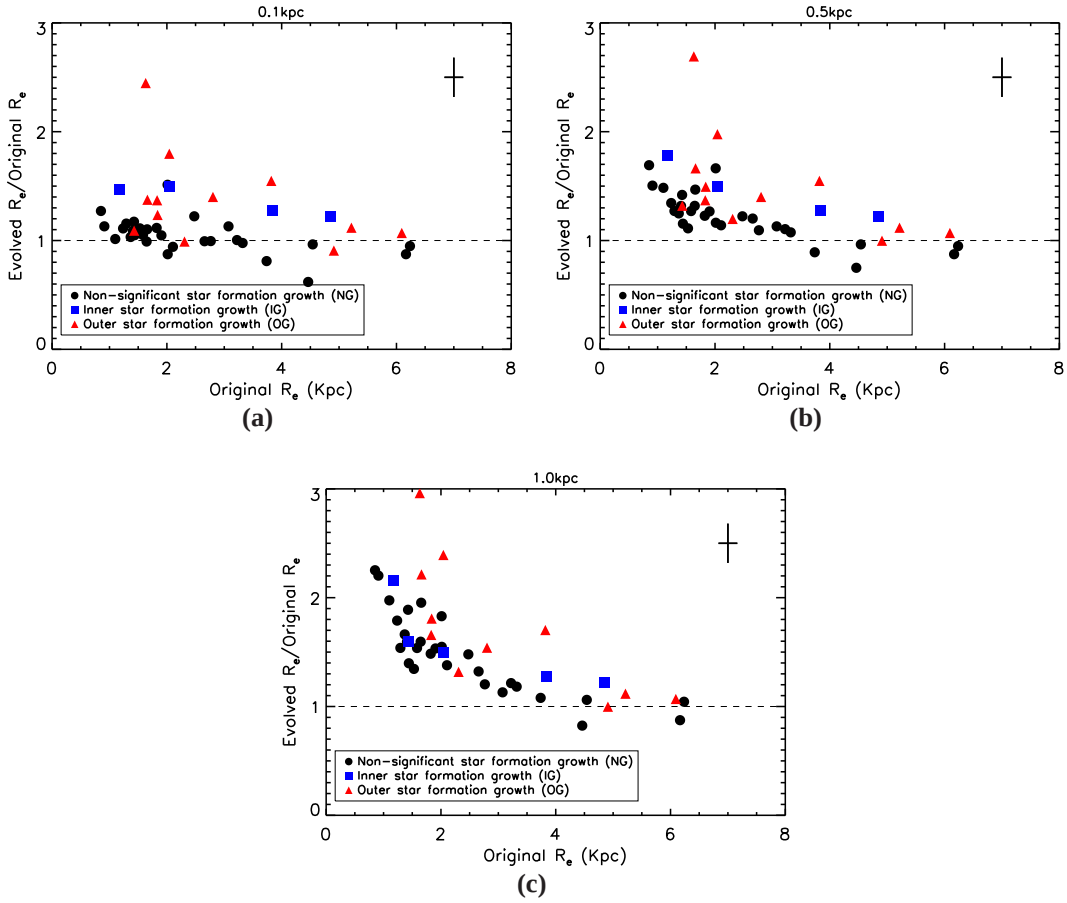

Figure 2.9: The evolution of the effective radius due to various stellar migration models, the Gaussian form for stellar migration is shown in Equation 2.8. The values of σ used are (a) 0.1kpc, (b) 0.5kpc (c) 1.0kpc. The black circles denote galaxies classified as having non-significant star formation growth (NG). The red triangles denote galaxies classified as having outer star formation growth (OG) and the blue squares denote galaxies classified as having inner star formation growth (IG). The typical error bars are shown in the top right hand corner.

In order to simulate this effect on the galaxies in this sample we apply a Gaussian distribution function centred on each individual radial bin across each galaxy in the sample. This distributes the total stellar mass (the stellar mass added via star formation and the in situ stellar mass) across the galaxy according to the summed Gaussian distribution:

$$M_{*,\mathrm{mig}}(R,t) = \sum_{i=R_{\mathrm{min}}}^{R_{\mathrm{max}}} M_*(i,t)\frac{1}{\sigma\sqrt{2\pi}}e^{-\frac{(R-i)^2}{2\sigma^2}} \tag{2.8}$$

where $M_*(i,t)$ is the total stellar mass at radius i and at time t from Equation 2.6 and σ is the width of the Gaussian distribution. The R_{min} and R_{max} are the total range of the galaxy radial distribution.This is motivated by the work of Roškar *et al.* (2011). They show that the stellar migration within a spiral galaxy can approximated by a Gaussian distribution. Their work also showed that with increasing formation radius the peak of the migration distribution becomes increasingly offset from the formation radius. However, this offset in the distribution only affects stars formed at radii greater than 10kpc. As all of the objects in this study have sizes much smaller the effect of this offset will be negligible to this work and is therefore not included. Simulations from Roškar *et al.* (2011) showed that the radial migration of stars in a Milky Way type disk can change by several kpc over the lifetime of the galaxy. To simulate this with some scatter we run a series of different widths to represent a wide range of migrations with, $0.01\mathrm{kpc} < \sigma < 1.0\mathrm{kpc}$. The new stellar mass distribution is then fit with a new Sérsic profile. Figure 2.7 shows the effect of increasing levels of stellar migration upon one galaxy at different levels.

As expected, we find that larger levels of migration have an increasing stronger effect on the effective radius. The maximal effect on the radius of the galaxy is for the largest width Gaussian we applied, $1.0\mathrm{kpc}$. This level of migration is of the same order as the effective radii for the galaxies in our sample. Therefore to test maximal size growth we use a 1.0kpc migration from this point on. It is quite possible that stellar migration may happen on a larger scale and we experimented with wider Gaussian distributions but found that we could no longer accurately simulate the galaxy evolution due to losing stellar mass outside the confines of the simulation. From the $1.0\mathrm{kpc}$ Gaussian we find the effective radius grows by $54 \pm 19\%$ of the original effective radius. This represents

an evolved effective radius ~ 3.4 times larger than with just the star formation evolution alone. The effect of this migration on the Sérsic indices on average is consistent with a small change, with $\Delta n = -1.1 \pm 1.3$, similar to the non migration case. This is similar to the insignificant change in n we found in the profiles without the stellar migration.

In Figure 2.8 we show how the Sérsic index changes using different stellar migration models. When this is applied to our different galaxy classes we find that the NG galaxies have a increased effective radius of $48 \pm 7\%$ over the initial effective radius.

The IG galaxies show an increase in the effective radius of $55 \pm 15\%$. Compared to the increased radii from star formation alone this is a ~ 1.5 times larger result. OG galaxies have an effective radius the largest increase with migration of $71 \pm 18\%$. This increase in effective radius is ~ 1.9 times larger than the non-migration case for the OG class of galaxies in this sample. This is likely due to these galaxies producing more stellar mass in the outer regions than the other classes by definition, and therefore having a larger amount of stellar mass already at large radii to move during migration.

In Figure 2.9 we show how the effective radius changes due to the addition of the star formation and stellar migration. The galaxy classes that have the highest star formation rates are affected the most by stellar migration due to having more new stellar mass to migrate, with the non-changing, non-significant star formation galaxies lying close to the non-changing line and the outer and inner star formation growth galaxies lying above.

2.5 Discussion

2.5.1 Size Evolution

As stated previously, recent studies over the last few years have found evidence for a dramatic size evolution of massive galaxies over the past 10 billion years (e.g Daddi *et al.* 2005; Trujillo *et al.* 2007; van Dokkum *et al.* 2010; Buitrago *et al.* 2008). Current estimates for this growth in the effective radius argue that massive galaxies may grow in size on average up to a factor of 3 for disk-like galaxies, while for spheroid-like

objects this evolution reaches even a factor of 5 since $z = 3$ (Buitrago *et al.* 2008).

In this chapter we have shown that the effective radius of massive galaxies is altered by the star formation present, growing on average by $16 \pm 5\%$ from $z = 3$ to $z = 0$. This value is only $\sim 3 - 5\%$ of the total increase in the size of massive galaxies from observational studies (e.g. Buitrago *et al.* 2008). This indicates that the star formation has a very minor contribution to the observable overall size evolution at $z < 3$.

When we apply a simple model of stellar migration to the new stellar mass created via star formation to the present day we find that the size of these massive galaxies is influenced to a greater extent. The effective radius increases by $54 \pm 19\%$. This increase would represent $11 - 18\%$ of the total size evolution that massive galaxies undergo between $z > 1$ and 0. This result shows that the effects of stellar mass added via star formation, and any subsequent stellar migration, plays a minor role in massive galaxy size evolution and only contributes roughly a tenth of the total size growth needed to explain the observed size evolution. This implies that other evolution mechanisms must also be at work to produce the remaining $\sim 80\%$ of the observed size growth over cosmic time. From also examining the total size growth in the other models of evolution (see §2.5.4.1) we also find that the maximal size increase we can obtain can only produce $\sim 54\%$ of the total observed size growth.

Recent studies have found that minor and major mergers have a large influence on the size evolution of massive galaxies. These mergers could explain the majority of the remaining $\sim 80\%$ of the observed size growth unaccounted for by the SF via increasing the total stellar mass of the galaxies (Bluck *et al.* 2011). Our results are consistent with this view that something other than SF produces the change in the sizes of massive galaxies.

2.5.2 Structural Properties

Recent studies have shown that the massive galaxy population at $z \geq 1.5$ is dominated by disk like galaxy morphologies with $n < 2$ (e.g., Weinzirl *et al.* 2011; Buitrago *et al.* 2013;). This is in contrast to the local universe where the massive galaxy population is almost entirely dominated by spheroids (e.g. Baldry *et al.* 2004; Conselice 2006b).

This transformation is also seen through changes in the Sérsic index of these galaxies from a low value of n at $z > 1$ to a high value of n at $z < 1$.

In this study we show that due to the star formation present within the massive galaxies at $z > 1.5$ the Sérsic index has an insignificant change over cosmic time, $\Delta n = -0.9 \pm 0.9$. When we introduce the effects of stellar migration to the mass added via star formation the change in Sérsic index is again negligible over cosmic time with, $\Delta n = -1.1 \pm 1.3$. In the other methods of SF evolution we find that the change in n is very similar. This implies that with both star formation and stellar migration the change to the Sérsic index is minimal. Also, this does not agree with observations of the general increase of n over time. Therefore SF alone cannot account for the observed morphological change which appear to show that n is increasing over time (e.g Buitrago *et al.* 2013).

2.5.3 Spatial Location of Star Formation

In this study we find that the structural properties of our massive galaxies remain largely unchanged after evolution via star formation. This unchanging n shows that the location and magnitude of star formation within massive galaxies largely follows the observed initial stellar mass density profile. This is most pronounced in the case of the inner growth (IG) galaxies. In this class of galaxy the observed stellar mass profile is much smaller than the stellar mass profile added via star formation. Therefore, for this class of galaxy to retain its original Sérsic index the stellar mass produced via star formation over evolution to the present day would have to be produced in amounts which largely reflect the already present stellar density i.e. high density regions would have a higher star formation rates than lower density regions. This was also seen in other ways in Trujillo *et al.* (2007), Buitrago *et al.* (2008) and (Cassata *et al.*, 2010, 2011).

The measured $\sim 16\%$ growth of the effective radii of our massive galaxies due to star formation alone, without any stellar migration, reveals that there is star formation located in the outer regions of our massive galaxies. This is most pronounced in the OG galaxies by definition. In these galaxies the surface stellar mass density of the inner region remains roughly constant over star formation evolution with the outer regions

increasing in stellar mass density. Thus in our simulated star formation evolution the observed high redshift galaxy would become surrounded by an envelope of new stellar material over time. With the addition of stellar migration this effect becomes more pronounced with newly created stellar mass migrating outwards. Recent work examining the stellar mass density profiles of high redshift, $z > 2$, and low redshift, $z = 0$, massive galaxies has shown that the density in the core region of low redshift galaxies is comparable to the density of the compact high redshift galaxies (Hopkins *et al.* 2009; van Dokkum *et al.* 2010; Carrasco, Conselice & Trujillo 2010). The compact high redshift galaxies have become surrounded by an envelope of lower density material from $z > 2$ to 0. This is similar to what we find in the OG class of galaxies.

The models that we use in this study do not account for any new gas that can be accreted at later times, at $z < 1.5$, and at early times at $z > 3$ where we also do not observe our sample. This new gas and possible new star formation is likely to have a different radial distribution from the current in situ gas, with most of the new gas being at larger radii (Kereš *et al.* 2005; Dekel, Sari & Ceverino 2009). Therefore the distribution of star formation that we observe at high redshift is mostly likely the result of previous events of gas accretion (see Conselice *et al.* 2013). However, not all the gas accreted may convert into stars immediately, and this gas may remain in the outer portions of these galaxies and may form into stars at an epoch later than our observations at $z < 1.5$, which in principle may increase the sizes of these systems at a later time, or alter their Sérsic indices.

2.5.4 Model Limitations

In this study we have taken a snapshot of our massive galaxy sample over 2 Gyr in time, and derived the resulting evolution based on a derived star formation model. Thus we do not take into account any post-observation star formation events in our basic model. However this is likely a fair assumption due to observations of the majority of massive galaxies at $z < 1.4$ having old stellar populations and red colours (e.g. McCarthy *et al.* 2004; Daddi *et al.* 2005; Saracco *et al.* 2005; Bundy *et al.* 2006; Labbé *et al.* 2006; Conselice *et al.* 2007; Mortlock *et al.* 2011; Grützbauch *et al.* 2011). This would imply that the SF we observe at $z > 1.5$ is the last major burst of SF in massive

galaxies. The effect of new star formation events would increase the total amount of stellar mass added to the host galaxy. The galaxy's structural properties and size could also be affected by these events, depending on the location and magnitude of this star formation as discussed in the previous section.

Conversely, we also do not take into account any feedback mechanisms that would negatively affect star formation rates. Examples of such processes are AGN and supernovae feedback. Massive galaxies can spend up to 1/3 of their lifetimes in an AGN phase (Hickox *et al.* 2009; Bluck *et al.* 2011). This phase introduces energy into the interstellar gas and can expel it from the host galaxy (Schawinski *et al.* 2006), or heat it such that it cannot cool. Also ongoing star formation results in the creation of many high mass stars which can lose mass during evolution and subsequently die in supernovae, thereby lowering the total stellar mass of the galaxy. When many supernovae are present in a short time the created shock waves introduce vast amounts of energy into interstellar gas. The gas can then can be heated or ejected from the host galaxy (e.g. Bertone, De Lucia & Thomas 2007). The result of these feedback mechanisms would be a reduction of the star formation rate, and the total stellar mass within the galaxy would be lower. This decreased amount of stellar mass added via SF would also result in the stellar mass added via star formation having a decreased effect on the total size growth and morphological change.

We also use a very simple model to describe the stellar migration that is limited to the extent of the z_{850} band profiles. This means that we can not accurately measure how large values of stellar migration would affect the sizes and structural properties of our massive galaxies. However even though we cannot accurately measure the Sérsic index or the effective radius of the simulated galaxies with larger values of the stellar migration, we find that the stellar mass begins to be distributed evenly over all radii, with increasing amounts of stellar mass lost outside the confines of the simulation. The amount of stellar mass added via star formation moved by migration is constant for each galaxy but is distributed over wider areas for larger values of stellar migration. This results in the stellar mass density added via star formation to individual regions of the massive galaxies dropping to increasingly smaller values. This implies that with larger values of stellar migration, the stellar mass density added via star forma-

tion would have an increasingly smaller effect on the total stellar mass density profile. Therefore even if larger values of stellar migration could be simulated in this study the change in Sérsic index and effective radius after star formation evolution and migration would be negligible.

Stellar migration has also been found, in simulations, to be most affected by spiral arms in galaxies (Roškar *et al.* 2011). 73% of the sample of massive galaxies have a low Sérsic index, $n < 2.5$, implying a disk-like morphology. Within these galaxies we may assume therefore that stellar migration via disk features may take place, but this is far from certain. A few of the galaxies in our sample have a high Sérsic index, $n > 2.5$, implying an early-type morphology, and within these galaxies stellar migration is less understood. This does not imply that stellar migration does not take place in these galaxies but it must occur by other processes than those involving disks. Also, as stated in §2.4.3 we cannot reliably distinguish disk-like galaxies in our sample using a Sérsic index cut because we cannot rule out that some of the galaxies with $n > 2.5$ do not have spiral like features (e.g. Buitrago *et al.* 2013; Mortlock *et al.* 2013).

2.5.4.1 Evolutionary models

In this chapter we extrapolate the star formation evolution using an exponentially declining star formation model based on SED derived τ values. This value can be uncertain so we explore different models of evolution that the star formation could follow down to $z = 0$. Firstly we do not investigate an exponentially increasing SFR evolution model because previous studies (e.g. Papovich *et al.* 2011) show that galaxies at $z < 3$ are not well described by this SF history. Therefore we investigate the SF evolution models of: constant SFR to $z = 0$, constant SFR to $z = 1.5$, maximum valid tau and minimum valid tau.

- Constant SFR_0 to $z = 0$: This model of evolution assumes that the massive galaxies we observe at $z > 1.5$ have a very large reservoir of gas and can continue the observed SFR over the next 10Gyr. This evolutionary method produces galaxies in the local universe with very high star formation rates compared to the galaxies we observe (e.g. Conselice *et al.* 2007). This combined with the fact

that over the course of their evolution these galaxies will have accumulated significant amounts of stellar mass with the average massive galaxy in this sample increasing its total stellar mass by $\sim 1500\%$. This large amount of stellar mass added to the galaxies increases the value of R_e by $80 \pm 20\%$. This is an increase of a factor of 5 over the derived tau model in effective radius growth, but still only $16 - 27\%$ of the observed size evolution. This model of evolution is highly unlikely due to the many features of this model that we do not observe in the local universe, such as very large stellar mass growth leading to very massive galaxies with stellar masses over $10^{13} M_{\odot}$ (e.g. Brammer *et al.* 2011; Conselice *et al.* 2011; Mortlock *et al.* 2011, all find that the stellar mass growth at the massive end of the luminosity function is on the order of 200% from $z > 1.5$ to 0) and very high star formation rates of 100's of solar masses per year.

- Constant SFR_0 to $z = 1.5$: This model of SF evolution is based on the observation that the majority of massive galaxies at $z < 1.4$ have old stellar populations and red colours (e.g. Conselice *et al.* 2007: Mortlock *et al.* 2011, Grützbauch *et al.* 2011). This would imply that these galaxies have turned off their SF before $z = 1.5$. To model this we employed a constant observed SFR until $z = 1.5$ at which point the SFR is reduced to 0. In this evolution scenario the total stellar mass of the massive galaxies is increased by $126 \pm 20\%$. The effective radii in this model are increased on average by $37 \pm 19\%$. This is a factor of ~ 2.5 larger than the increase from the derived tau model. This is still insignificant compared to the total observed size increase. This model has a very similar effect on the change in n, $\Delta n = -1.1 \pm 1.1$, as the derived tau model.

- Maximum valid tau to $z = 0$: In this model of evolution we use the largest value of tau derived for our galaxy sample, $\tau = 2.71 \times 10^9 \mathrm{yr}$. We apply this exponentially declining rate to all the galaxies in the sample. In this scenario we obtain a large average increase in total stellar mass of the sample of $377 \pm 172\%$. The change in the effective radii of this model is on average $R_e = 57 \pm 33\%$ a factor of ~ 3.8 larger than the derived tau model of evolution. This increase in effective radius is still only $\sim 11 - 19\%$ of the observed size evolution. The change in n for this model, $\Delta n = -1.5 \pm 1.7$ is similar to change for the derived

tau model.

- Minimum valid tau to $z = 0$: This model is similar to the previous model, except that the minimum valid tau, $\tau = 1.2 \times 10^{8}\mathrm{yr}$, is used to extrapolate the SF. This would give the shortest time scale that the SF would occur. In this model the average galaxy in the sample increases its stellar mass by only $\sim 17\%$. This very small increase in mass is accompanied by an equally small change in R_e, average $\Delta R_e = 3 \pm 1\%$, and n, $\Delta n = -0.4 \pm 0.6$.

From this investigation of different models of SF evolution to $z = 0$ we find that the value in the increase of the effective radii of the massive galaxies can at no point fully explain the total observed size increase. The valid models of SF evolution that we applied can only produce a factor of ~ 3.8 times larger than the size increased we obtained from using the derived tau model at maximum. The change in Sérsic index in all the models are within the error consistent with the answer obtained from the derived tau model used in this chapter.

2.5.4.2 Dust Gradients

In this chapter we assume that the dust obscuration is constant across the radius of individual galaxies. From studies of local and distant studies this may not be the case. Colour gradients in the local universe have been shown to correspond to age and dust gradients (e.g. Boquien *et al.* 2011; Smith *et al.* 2012).

We apply a dust gradient to our sample of massive galaxies that allows the attenuation due to dust to vary within the given error across each galaxy. This is done in two ways. A positive dust gradient with higher attenuation towards the outer regions of the galaxy, and a negative dust gradient with higher dust attenuation towards the central regions of the galaxy.

In the positive gradient case we find that the average increase in the effective radius was $68 \pm 36\%$ larger than the original measured effective radius. This is a factor of ~ 4.5 larger change than the growth in R_e we obtain from using a radially constant dust correction. From this gradient the change in n is largely the same as before but

with a much larger scatter, $\Delta n = -0.9 \pm 2.0$. The positive gradient could contribute a maximum of $\sim 23\%$ to the $300 - 500\%$ size growth.

In the negative gradient case we find that the average increase in R_e is minimal, $\Delta R_e = 7 \pm 3\%$. This small increase in the effective radius is accompanied by a change in n that is very similar to most other cases, $\Delta n = -1.0 \pm 1.0$. This negative gradient case would seem to produce a very small increase in the effective radii of our sample and only contribute a maximum of $\sim 2\%$ to the total observed size growth.

Neither of the gradient cases that we applied to the sample are able to fully explain the observed size growth or observed change in Sérsic index.

2.6 Summary

We investigate the resolved star formation properties of a sample of 45 massive galaxies ($M_* > 10^{11} M_\odot$) within a redshift range of $1.5 \leq z \leq 3$ detected in the GOODS NICMOS Survey, a HST H_{160}-band imaging survey. We derive the star formation rate as a function of radius using rest frame UV data from deep z_{850} ACS imaging. The star formation present at high redshift is then extrapolated to $z = 0$, and we examine the stellar mass produced in individual regions within each galaxy. We also construct new stellar mass profiles of the in situ stellar mass at high redshift from Sérsic fits to rest-frame optical, H_{160}-band, data. We combine the two stellar mass profiles to produce an evolved stellar mass profile.

We then fit a new Sérsic profile to the evolved profile, from which we examine what effect the resulting stellar mass distribution added via star formation has on the structure and size of each individual galaxy. In summary:

- We find three different profiles of star formation within the massive galaxies in this sample, Non-significant Star Formation Growth (NG), Outer Star Formation Growth (OG) and Inner Star Formation Growth (IG) (see §2.3.3). With most of this sample of massive galaxies falling in to NG class using the derived tau model of evolution.

- We find that the star formation we observe at high redshift, and its effects on

galaxy sizes, is not large enough to fully explain the observed size evolution of effective radius of $\sim 300 - 500\%$. Star formation alone can only produce an increase in effective radius on the order of $\sim 16\%$ over the whole sample. This value can vary as much as a factor of 4.5 by using different evolution mechanisms but is always insufficient to fully explain the observations.

- We find that over the whole sample of massive galaxies the stellar mass added via star formation has a slight effect on the Sérsic index of the evolved galaxy profile such that they decrease. This indicates that the star formation within these galaxies follows the same radial distribution as the original stellar mass profile. This also implies that star formation evolution has a minimal effect on structural evolution between $z \sim 3$ and the present day.

- The increase in effective radius can be enhanced by adding in the effects of stellar migration to the stellar mass created via star formation. This increases the total effective radius growth to $\sim 55\%$, which is still however much smaller than the total observed size increase.

We conclude that due to the lack of sufficient size growth and Sérsic evolution by star formation and stellar migration other mechanisms must contribute a large proportion to account for the observed structural evolution from $z > 1$ to the present day. Recent studies by Bluck *et al.* 2011) have found that minor and major mergers have a large influence on the size of massive galaxies possibly contributing the remaining 80% of size growth needed to explain the observed trends. Large surveys such as CANDELS and future telescopes such as JWST and E-ELT will provide the quality of data that is required to explore the star formation locations of lower mass galaxies and probe resolved star formation at higher redshifts for similarly massive galaxies.

Chapter 3

Minor vs Major Mergers: The Stellar Mass Growth of Massive Galaxies from z=3 using Number Density Selection Techniques

3.1 Introduction

The main process by which galaxies acquire their stellar mass and gas is still an open question in galaxy formation. We know from galaxy stellar mass functions that galaxies increase in stellar mass over time (e.g. Cole *et al.* 2001, Pérez-González *et al.* 2008b, Ilbert *et al.* 2010, Mortlock *et al.* 2011, Muzzin *et al.* 2013). We also know that there are at least two primary processes via which galaxies can increase their stellar mass; star formation and merging of pre-existing galaxies. However, it has been very difficult to disentangle these two processes primarily as it is challenging to link descendants and progenitors of galaxies at different redshifts.

A common solution for linking galaxies at different redshifts is to examine galaxies at a fixed stellar mass. This is however only truly effective at selecting galaxies that have undergone passive evolution over the examined redshift range, e.g. luminous red galaxies (e.g. Wake *et al.* 2006) assuming there are no mergers. However the general

population of galaxies at high redshift are not passively evolving but show signs of recent large amounts of star formation (e.g. Daddi *et al.* 2007, Bauer *et al.* 2011, Ownsworth *et al.* 2012 , van Dokkum *et al.* 2013) and mergers (e.g. Conselice 2006b, Bluck *et al.* 2009, 2012).

Recent studies (e.g. van Dokkum *et al.* 2010, Papovich *et al.* 2011, Conselice *et al.* 2013, Marchesini *et al.* 2014, Lundgren *et al.* 2014) introduced a new approach to help solve this problem by tracing galaxies at a constant number density. This approach assumes that the relative number density of the most massive galaxies does not evolve i.e. they undergo very few mergers with galaxies of similar stellar mass over the redshift range studied. This technique has been used to examine the evolution of a number of galaxy properties e.g. star formation histories at $z > 3$ (Papovich *et al.* 2011, Salmon et al. in prep), as well as structural parameters and stellar mass (van Dokkum *et al.* 2010, Patel *et al.* 2013, Conselice *et al.* 2013). Semi-analytical methods have shown the constant number density selection to be a considerable improvement in tracking the evolution of an individual galaxy population over $0 < z < 3$ compared to previous mass selection techniques (Leja, van Dokkum & Franx 2013).

Using a constant number density selection to trace galaxy population however does have its limitations. For example, Behroozi *et al.* (2013) and Leja, van Dokkum & Franx (2013) find that a constant number density selection in semi-analytical models over the redshift range of $z = 0$ to $z = 3.0$ could only reproduce the median stellar mass growth of descendants of the most massive galaxies to within 40% of the "true" value in the model. This offset can be reduced to 12% when this number density is adjusted for the galaxies destroyed via mergers. In practice however, we are just now starting to measure the merger history with any accuracy. To make further progress with tracing galaxy populations through time the number density selection must be adjusted at each redshift to account for major mergers that occur within this population.

Mergers are of course important in themselves, as in the hierarchical picture of galaxy formation massive objects form by the merging together of smaller objects. As such, galaxies will be undergoing mergers at all redshifts. Over a wide range of redshifts ($0 < z < 3$) close pair and morphological methods find a positive evolution of the major merger fraction with redshift (e.g. Bluck *et al.* 2009, 2012, Bridge, Carlberg &

Sullivan 2010). From a theoretical perspective, in the Λ Cold Dark Matter paradigm dark matter halos form from the bottom up, with larger halos created at later times (e.g. Lacey & Cole 1993b, Springel *et al.* 2005). As galaxies lie inside these haloes they trace the underlying dark matter distribution, and therefore we expect these to undergo hierarchical growth as well. However, it has been shown that some massive galaxies exist and have old stellar populations in place at high redshifts (e.g.McCarthy *et al.* 2004, Daddi *et al.* 2005, Bauer *et al.* 2011, Mortlock *et al.* 2011, Hartley *et al.* 2013). This implies that these galaxies must undergo rapid evolution at early times in the universe, or that some distant mergers are 'dry'.

Galaxy formation is likely driven, at least in part, by mergers. But there are other processes that account for the build up of stellar mass, most especially the star formation rate. The peak in the volume averaged star formation rate for all galaxies in the Universe occurs in the redshift range of $1.5 < z < 2.5$ (e.g. Madau *et al.* 1996, Hopkins & Beacom 2006, Tresse *et al.* 2007, Wilkins, Trentham & Hopkins 2008, Behroozi, Wechsler & Conroy 2013). Within this epoch, the star formation rate in typical galaxies is an order of magnitude higher than in the local universe (e.g. Reddy & Steidel 2009). Studies of massive galaxies show a similar trend whereby at high redshift they experience high star formation rates (SFRs) that decrease towards lower redshifts (e.g. Daddi *et al.* 2007, van Dokkum *et al.* 2010, Bauer *et al.* 2011 Ownsworth *et al.* 2012). However, the SFRs of the most massive galaxies in the Universe peaks earlier than the total galaxy population at around $z \sim 3$ (Papovich *et al.* 2011). This reveals that the galaxy population is experiencing the effects of downsizing, wherein the most massive galaxies shut off their star formation before lower mass objects.

There also exists a tight correlation and a low scatter between SFRs and stellar mass over a large range of redshifts for star forming galaxies (Daddi *et al.* 2007, Noeske *et al.* 2007, Pannella *et al.* 2009, Magdis *et al.* 2010). These studies suggest that massive galaxies at high redshift sustain high levels of star formation for extended amounts of time. The high star formation rates (SFRs) experienced by massive galaxies are fuelled by the large cold gas fraction found in galaxies at high redshift compared to low redshift (e.g. Tacconi *et al.* 2010). The high levels of star formation in massive galaxies would however exhaust these gas reservoirs on very short time scales, ~ 500Myr

(Conselice *et al.* 2013). Therefore it can be inferred that the difference between the integrated SFR and the total stellar mass must correspond to the stellar mass acquired via mergers over $0.3 < z < 3.0$.

We present a study of the stellar mass growth of the progenitors of local massive galaxies at a number density of $n < 1 \times 10^{-4}\,\mathrm{Mpc}^{-3}$ in the redshift range $0.3 < z < 3.0$ by examining all of their processes. We indirectly measure the minor merger rates of the progenitors of local massive galaxies at early cosmic times using a major merger adjusted number density technique. From this we measure the relative contributions of star formation, major, and minor merger to the total stellar mass growth of these progenitor galaxies. This will help us understand how and when the most massive galaxies in the universe assembled their stellar mass.

The chapter is set out as follows: §3.2 discusses the Ultra Deep Survey and how the data used in this chapter was obtained including the redshifts, stellar masses and star formation rates. §3.3 discusses the galaxy number density selection methods. §3.4.1 presents the results of the stellar mass growth of the progenitors of massive galaxies from $z = 3.0$. §3.4.2 presents the star formation history of the progenitors of massive galaxies from the two selection methods. In §3.4.3 we calculate the contribution of minor mergers to the total stellar mass growth. §3.4.4 examines the contributions of all stellar mass growth processes over the redshift range of $0.3 < z < 3.0$. In §3.4.5 we use the results from this chapter to examine the implications for the cold gas accretion rate from the intergalactic medium of the progenitors of local massive galaxies. Finally §3.5 summarises our findings.

Throughout this chapter we assume $\Omega_M = 0.3$, $\Omega_\lambda = 0.7$ and $H_0 = 70$ km s^{-1} Mpc^{-1}. AB magnitudes and a Chabrier IMF are used throughout.

3.2 Data and Analysis

3.2.1 The UDS

This work is based on the 8th data release (DR8) of the Ultra Deep Survey (UDS; Almaini *et al* in prep.), which is the deepest of the UKIRT (United Kingdom Infra-Red

Telescope) Infra-Red Deep Sky Survey (UKIDSS; Lawrence *et al.* 2007) projects. The UDS covers 0.77 deg^2 in J, H, K and the limiting magnitudes (AB), within an aperture of 2 arcsec and at a 5σ level, are 24.9, 24.2, 24.6 in J, H, K respectively. It is the deepest infra-red survey ever undertaken over such an area. It benefits from an array of ancillary multi-wavelength data: U-band data from CFHT Megacam (Foucoud et al. in prep); B,V, R, i′ and z′ -band data from the Subaru-XMM Deep Survey (SXDS; Furusawa *et al.* 2008); infrared data from the Spitzer Legacy Program (SpUDS, PI: Dunlop). All of these are fundamental for the computation of accurate photometric redshifts, stellar masses and rest-frame magnitudes. The galaxy catalogue employed in this work is K-band selected and contains approximately 96000 galaxies. This survey reaches a depth of K_{AB}=24.4, which was determined from simulations and guarantees a 99% completeness level. See Hartley *et al.* (2013) for more details.

The depth and wavelength of the UDS allows us to study the distant Universe with fewer biases against red and dusty galaxies, which could otherwise be completely missed in ultraviolet and optical surveys.

3.2.2 Redshifts

Photometric redshifts are determined by fitting template spectra to photometry from the following bands: U, B, V, R, i′, z′, J, H, K, 3.6μm and 4.5μm, with a K-band apparent magnitude prior. The package employed for the template fitting was EAZY (Brammer, van Dokkum & Coppi, 2008). The template fitting makes use of the standard six EAZY templates and an extra one, a combination of the bluest EAZY template with a small amount SMC-like extinction (Prevot *et al.*, 1984). Furthermore, $\sim$1500 spectroscopic redshifts from the UDSz programme (an ESO Large Programme; PI Almaini) are also used to train the fitting procedure. Following the comparison to spectroscopic redshifts from the UDSz programme, and $\sim$4000 archival spectroscopic redshifts, and the removal of obvious AGN and catastrophic outliers ($\delta z/(1+z) > 0.15$), the dispersion between the photometric and the spectroscopic redshifts is measured as $\delta z/(1+z) \sim 0.031$ (Hartley *et al.* 2013).

3.2.3 Stellar Masses & SED fitting

The stellar masses and rest-frame colours of our sample are measured using a multi-colour stellar population fitting technique. For a full description see Mortlock *et al.* (2013) and Hartley *et al.* (2013). Synthetic spectral energy distributions (SEDs) constructed are from the stellar populations models of Bruzual & Charlot (2003) to the U, B, V, R, i′, z′, J, H, K bands and IRAC Channels 1 and 2, assuming a Chabrier initial mass function. The star formation history is characterised by an exponentially declining model with various ages, metallicity and dust content of the form

$$SFR(t) = SFR_0 \times \exp(-\mathrm{t}/\tau) \tag{3.1}$$

where τ ranges between 0.01 and 13.7 Gyr and the age of the onset of star formation ranges from 0.001 to 13.7 Gyr. Templates that are older than the age of the Universe at the redshift of the galaxy being fit are excluded. The metallicity ranges from 0.0001 to 0.1 solar, and the dust content is parametrised, following Charlot & Fall (2000), by τ_v, the effective V-band optical depth. τ_v ranges from 0.0 to 2.5 with a constant inter-stellar medium fraction of 0.3. The Charlot & Fall (2000) dust model dust attenuation is proportional to $\lambda^{-0.7}$ the normalization of the curve is lowered typically by a factor of 3 after 10^7 yr to account for the dispersal of the birth clouds. To fit the SEDs they are first scaled in the observed frame to the K-band magnitude of the galaxy. Then they are fit to each scaled model template in the grid of SEDs to the measured photometry of each individual galaxy. The calculated χ^2 values for each template are used to select the best fitting template, obtaining a corresponding stellar mass and rest-frame luminosities. Hartley *et al.* (2013), following the method from Pozzetti *et al.* (2010), found the 95% mass completeness limit of $\log(\mathrm{M_{lim}}) = 8.27{+}0.81\mathrm{z}{-}0.07\mathrm{z}^2$. Galaxies that fall below M_{lim} are not used in the subsequent analysis.

3.2.4 Galaxy Structural Parameters

The structural parameters are measured on ground based UDS K-band images using GALAPAGOS (Galaxy Analysis over Large Area: Parameter Assessment by GALFITing Objects from SExtractor; Barden *et al.* 2012). This program uses SExtractor and GALFIT to fit Sérsic light profiles (Sérsic 1968) to objects in the UDS field. A

Sérsic light profile is given by the following equation:

$$\Sigma(R) = \Sigma_e \times \exp\left(-\mathrm{b_n}\left[\left(\frac{\mathrm{R}}{\mathrm{R_e}}\right)^{1/\mathrm{n}} - 1\right]\right) \tag{3.2}$$

Where $\Sigma(R)$ is the surface brightness as a function of the radius, R; Σ_e is the surface brightness at the effective radius, R_e; n is the Sérsic index and b_n is a function dependent on the Sérsic index. The sizes (effective radius) are calibrated with galaxy sizes derived from the UDS area from the Hubble Space Telescope (HST) Cosmic Assembly Near-infrared Deep Extragalactic Legacy Survey (CANDELS) (Grogin *et al.* 2011, Koekemoer *et al.* 2011) by van der Wel *et al.* (2012). For a full description of this method see Lani *et al.* (2013). Lani *et al.* (2013) show that the ground based size measurements are reliable for galaxies with $K < 22$ in the UDS. In Sections 3.4.5 and 3.4.6 galaxies that fall below $K < 22$ are not used in the subsequent analysis.

3.2.5 Star Formation Rates

We determine the star formation rates within galaxies over the redshift range $0.3 < z < 3$. Determining the star formation activity at these redshifts is however not trivial. Infra-red observations are useful indicators of dust heating due to star formation, but the Spitzer Space Telescope observations are not deep enough to accurately detect a full mass selected sample of galaxies as only a small number ($\sim 10\%$) of the whole sample are detected at $24\mu m$ above a flux limit of 300μJy (Conselice *et al.* 2013, Hilton *et al.* 2012).

The SED fitting procedure described in §3.2.3 also cannot be used to retrieve a value for the $24\mu m$ flux for our sample due to the lack of constraints from photometric data points in this part of the spectrum. However the photometric bands used in the SED fitting correspond to the rest-frame UV, optical and near infra-red wavelengths over the redshift range of this survey and therefore this part of the spectrum is well constrained. This enables us to use the dust corrected rest frame UV as an indicator of the star formation rate of these galaxies.

3.2.5.1 UV SFRs

The rest-frame UV light traces the presence of young and short-lived stellar populations produced by recent star formation. The star formation rates can be calculated from scaling factors applied to the luminosities. These scaling factors are dependent on the assumed IMF (Kennicutt 1983). However, UV light is very susceptible to dust extinction and a careful dust correction has to be applied. The correction we use here is based on the rest frame UV slope as explained in the following section.

The raw 2800Å NUV star formation rates ($SFR_{2800,\mathrm{SED}}$) used in this chapter are obtained from the rest-frame near UV luminosities measured from the best fit SED model found in the stellar mass fitting. We determine the dust-uncorrected SFRs, $SFR_{2800,\mathrm{SED,uncorr}}$, for $z = 0.5 - 3$ galaxies from applying the *Galaxy Evolution Explorer* (GALEX) NUV filter to the best fit individual galaxy SED.

To measure the SFR we first derive the UV luminosity of the galaxies in our sample, then use the Kennicutt (1998a) conversion from 2800Å luminosity to SFR assuming a Chabrier IMF:

$$SFR_{UV}(\mathrm{M_{\odot}yr^{-1}}) = 8.24 \times 10^{-29} L_{2800}(\mathrm{ergs\ s^{-1}\,Hz^{-1}}) \tag{3.3}$$

This however does not account for dust obscuration which can significantly influence the measured SFR.

3.2.5.2 Dust Corrections

To obtain reliable star formation rates in the rest-frame ultraviolet, we need to account for the obscuration due to dust along the line of sight. From the SED fitting in §3.2.3, we obtain the best fitting value of the dust content of individual galaxies from a course binning of dust values that are allowed to take values up to $\tau_{\mathrm{v}} = 5$. However, to derive accurate SFR's from the UV luminosity a more precise value of the dust content is required. We therefore calculated the UV dust attenuation value from a different method based on the shape of the UV region of a galaxy's spectrum. Meurer, Heckman & Calzetti (1999) found a correlation between attenuation due to dust and the rest-

frame UV slope, β, for a sample of local starburst galaxies

$$f_\lambda \sim \lambda^\beta \tag{3.4}$$

where f_λ is the flux density per wavelength interval and λ is the central rest wavelength. Using the ten UV windows defined by Calzetti, Kinney & Storchi-Bergmann (1994) we measure β values from the best fitting SED template. This can be done as the redshift range we examine has well calibrated UV SED fits due to many of the input photometric bands lying in the UV part of the spectrum. This β value is then converted to a UV dust correction using the Fischera & Dopita (2005) (FD05) dust model.

However, recent work by Wijesinghe *et al.* (2010, 2012) on local galaxies using the GALEX probe has shown that a FD05 dust model with the 2200Å feature removed is a better correction to the general population of galaxies than the Calzetti (2001) dust model, which is mainly applied to only highly star forming systems. We note that at the wavelength range we examine in this chapter there is very little difference in the dust correction given by the two models.

Using the Meurer, Heckman & Calzetti (1999) description of the attenuation, and converting it to attenuation at 2800Å using the FD05 dust model, we derive the equation:

$$A_{2800} = 1.67\beta + 3.71 \tag{3.5}$$

One caveat in correcting for the dust extinction in this way is that the β parameter is also affected by the age of the stellar population. A galaxy with an old and passive stellar population will, in the UV part of the spectrum, look very similar to a very highly dust extincted young and star forming galaxy population. This is a problem that can cause massive galaxies to artificially appear to have a very high dust content and thus high star formation rates.

This problem can be corrected via selecting out the galaxies that are passive via other methods. For these galaxies we can assume the β parameter will be driven by the old stellar populations, not dust attenuation. The selection we use is based on the U, V and J Bessel band rest frame luminosities. These were used by Williams *et al.* (2009) to select evolved stellar populations from those with recent star formation at $z < 2$. This technique is also used in Hartley *et al.* (2013) to extend the passive galaxy selection out to higher redshifts. The selection criteria for passive galaxies are as follows:

$$U - V > 0.88 \times V - J + 0.69 (z < 0.5) \tag{3.6}$$

$$U - V > 0.88 \times V - J + 0.59 (0.5 < z < 1.0) \tag{3.7}$$

$$U - V > 0.88 \times V - J + 0.49 (z > 1.0) \tag{3.8}$$

with $U - V > 1.3$ and $V - J < 1.6$ in all cases. The objects that are selected via this method are assigned to a passive category of galaxies. The dust correction derived from the β parameter therefore is not used when calculating the SFR for these systems.

To determine the dust content of passive galaxies we refer to recent studies from the Herschel space mission. Bourne *et al.* (2012) show from stacking that star forming and passive galaxies have similar dust masses. This possibly indicates that both populations have a similar average UV dust correction. Therefore within a given redshift bin we use the average dust attenuation from star forming galaxies with similar stellar masses as the dust attenuation for passive galaxies. However if we assume these galaxies contain no dust and therefore require no dust correction, then the star formation rates for the passive galaxies are on average a factor of ~ 3 lower than the average dust corrected star formation rates. The effect of changing the dust correction is discussed in sections 3.4.2, 3.4.3 and 3.4.4, but this does not significantly affect the conclusions of this chapter. The true dust correction may lie between these two corrections we apply here, implying that the two sets of SFRs for passive galaxies we present are upper and lower bounds.

Although these criteria efficiently select galaxies with old stellar populations, there is a possibility that the sample could still be contaminated by dusty star forming galaxies, edge on disks or AGN. We minimise this contamination by using the wealth of multi-wavelength data that is available in the UDS field. We cross match our sample with surveys on the UDS field taken at X-ray and radio wavelengths.

For the X-ray we use data from the Subaru/XMM-Newton Deep Survey (Ueda *et al.* 2008) which covers the UDS field over the energy range of 0.5 keV to 10 keV. For the radio we use Simpson *et al.* (2006) which utilises VLA 1.4 GHz data. We remove any galaxies that have either a detection in the X-ray or radio to clean this sample of AGN. This data will only effectively select out AGN at $z \lesssim 1$ due to the limits of these

surveys, and will only be able to select the most radio loud and very active AGN at higher redshifts.

Furthermore the $24\mu\mathrm{m}$ data from the SpUDS provides a way to identify red objects that harbour dust-enshrouded star formation. Therefore any objects with a $24\mu\mathrm{m}$ detection (300μJy, 15σ) are assumed to be dusty star forming objects. Any galaxy shown to be passive via the UVJ selection criteria, but which has a $24\mu\mathrm{m}$ source associated with it will be reassigned to the star forming population and have a full UV dust correction applied. In total $\sim 2\%$ of objects selected via the UVJ criteria were reassigned to the star-forming sample through this method.

Figure 3.1 shows SFR versus the stellar mass for all galaxies in the UDS galaxy sample separated into redshift bins. The black points show galaxies that have been classified as passive via the UVJ selection criteria, and blue points show the remaining star forming galaxies. The dotted lines show the stellar mass limits corresponding to the number density selection described in the following section derived from the integrated stellar mass functions of the different galaxy selections. The dashed lines show relations between the SFR and stellar mass of star forming galaxies found by Daddi *et al.* (2007) at $1.4 < z < 2.5$, Whitaker *et al.* (2012b) at $0 < z < 2.5$ and Bauer *et al.* (2011) at $1.5 < z < 3.0$. Our SFR_{2800} are in good agreement with these relations.

3.3 Sample Selection

In this study we use two selection methods, a constant and a merger adjusted galaxy number density selection. The constant galaxy number density selection uses the number density of the most massive galaxies in the local universe to select the direct progenitors of the most massive galaxies at higher redshifts. The merger adjusted galaxy number density selection is a relatively new method that incorporates the measured major merger rate of massive galaxies over the redshift range studied. This method selects all of the progenitors of the most massive galaxies, and all major merger progenitor galaxies. This selection method allows us to disentangle between the stellar mass growth of major and minor mergers. In the following sections we describe these two selection methods.

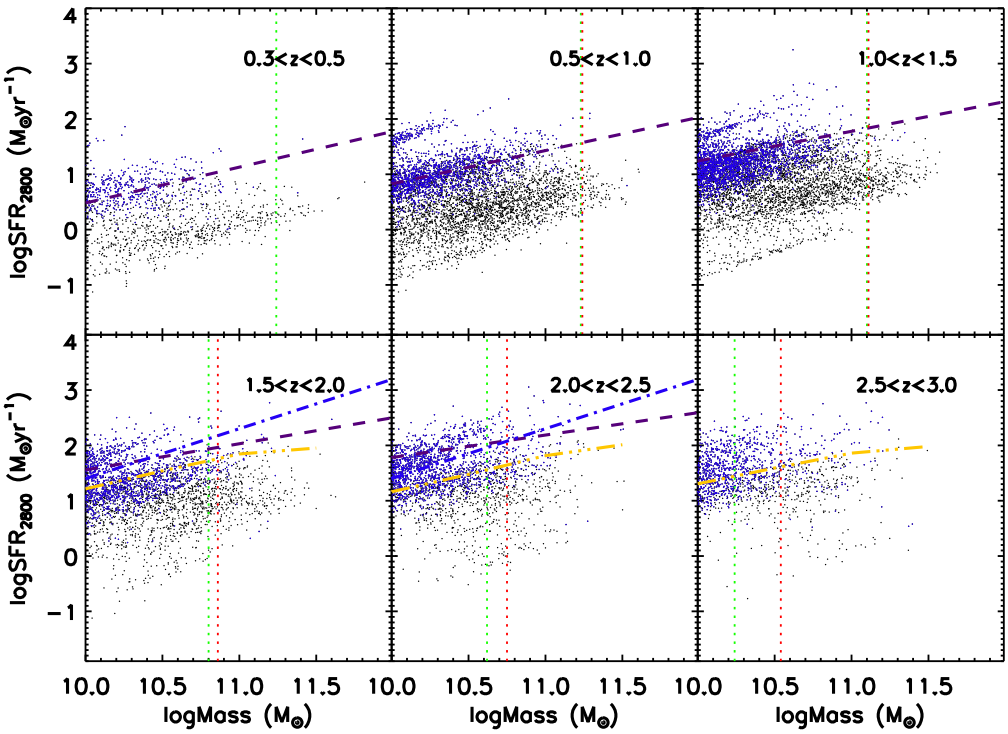

Figure 3.1: The dust corrected UV star formation rates for all galaxies in the UDS sample as a function of stellar mass. The black points show individual galaxies in the total UDS galaxy catalogue that have been classified as passive using the UVJ criteria described in §3.5.2. The blue points show individual star forming galaxies in the UDS galaxy catalogue. The red and green dotted vertical lines show the stellar mass limits given in Table 3.1 and 3.3 denoting the stellar mass limits of the constant number density (red) and major merger adjusted number density (green) selections. The blue dot dashed line is the relation found in Daddi et al. (2007) denoting the relation between the total stellar mass and star formation rate for star forming galaxies between $1.4 < z < 2.5$. The purple dashed line is the SFR stellar mass relation from Whitaker et al. (2012) using IR+UV SFRS. The yellow treble dot dashed line is the SFR stellar mass relation from Bauer et al. (2011).

3.3.1 Constant Galaxy Number Density (C-GaND)

A few studies to date have examined galaxy formation and evolution using galaxy number density as a method of selecting galaxies over a large redshift range (e.g. van Dokkum *et al.* 2010, Papovich *et al.* 2011, Conselice *et al.* 2013). Several studies have shown that this method of selecting galaxies has several advantages. In the absence of major mergers, or extreme changes of star formation, the number density of galaxies above a given density threshold is invariant with time. These galaxies will grow in stellar mass through star formation and minor mergers, but their number density will stay constant.

In principle, selecting galaxies at a constant number density directly tracks the progenitors and descendants of massive galaxies at all redshifts. A study by Leja, van Dokkum & Franx (2013) showed that this technique is robust at linking descendant and progenitor galaxies over cosmic time when applied to semi-analytic models that trace individual galaxies evolving over the last eleven billion years.

In this study we select and compare galaxies at constant co-moving number density values of $n = 5 \times 10^{-4}\,\mathrm{Mpc}^{-3}$, $n = 1 \times 10^{-4}\,\mathrm{Mpc}^{-3}$, and $n = 0.4 \times 10^{-4}\,\mathrm{Mpc}^{-3}$ at redshifts $0.3 < z < 3$. We chose these number densities as a trade-off between having a robust number of galaxies in the analysis at each redshift, and retaining a mass complete sample at the highest redshifts. This number density range is comparable to number densities used in other similar studies (e.g. Papovich *et al.* 2011 Conselice *et al.* 2013).

We select our sample based on the integrated mass functions of the UDS field over the redshift range of $z = 0.3$ to 3.0 from Mortlock et al (2014, in prep). Table 3.1 shows the Schechter function fitted parameters. Figure 3.2 (a) shows the integrated mass functions from Mortlock et al. (2014, in prep) and the lower stellar mass limits for the constant number density selection. The values for the limits are listed in Table 3.2. The arrows in the top left hand corner of Figure 3.2 show how the galaxy stellar mass functions will change due to the two processes of stellar mass growth explored in this chapter. Figure 3.3 shows, in green, the galaxies selected via this selection compared to the whole galaxy sample over the redshift range in this study.

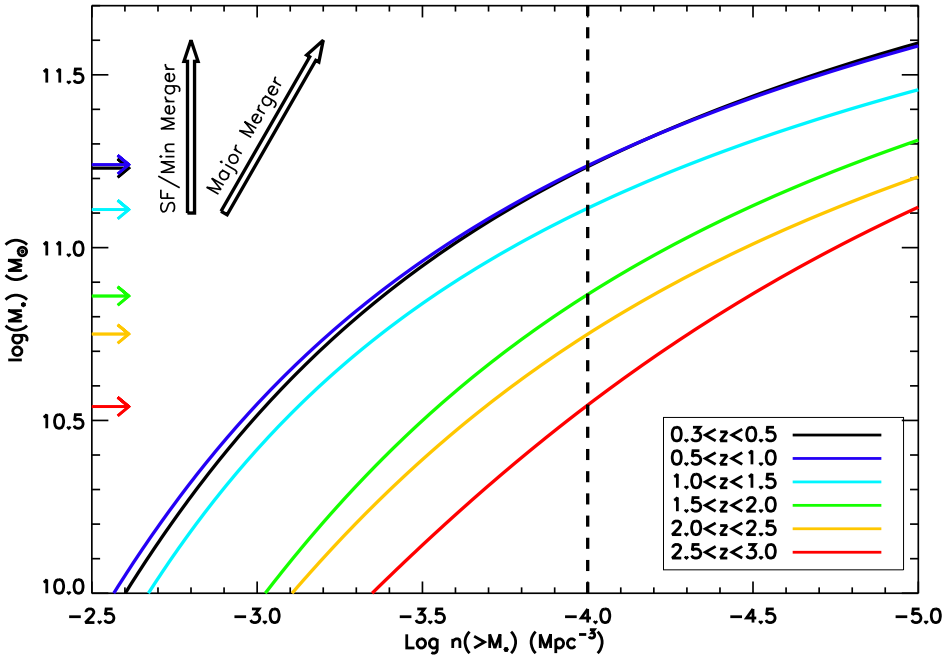

(a)

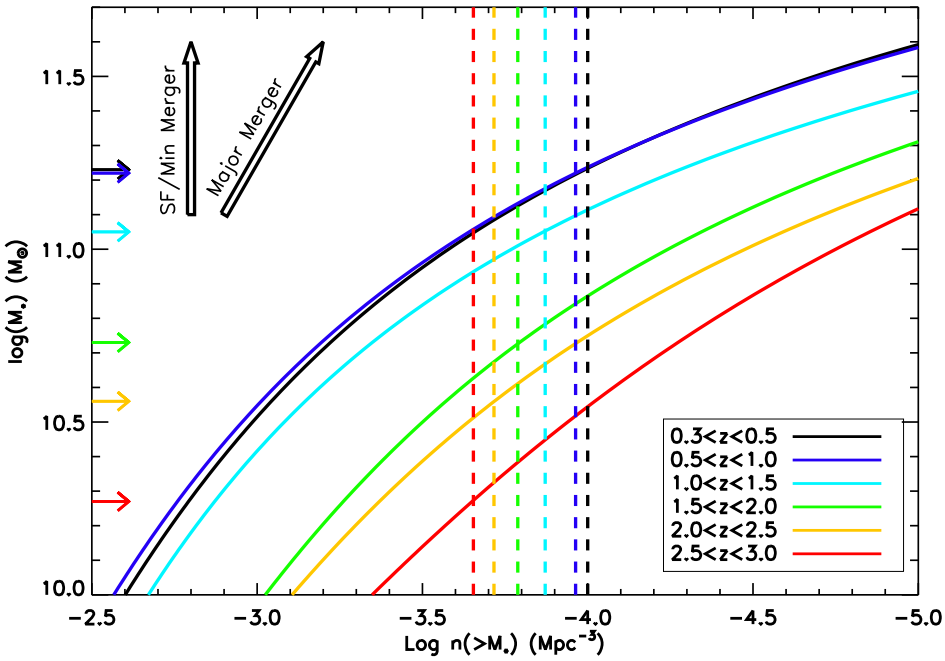

(b)

Figure 3.2: The integrated stellar mass functions from $z = 0.3$ to $z = 3$ from Mortlock et al. (2014, in prep). These integrated stellar mass functions gives us the co-moving number density of all galaxies more massive than a given stellar mass. The large open black arrows indicate the expected evolution due to star formation, minor mergers and major mergers. (a) We compare galaxies at a constant number density by selecting galaxies at each redshift at limits of $n(> M_*) = 1 \times 10^{-4}\mathrm{Mpc}^{-3}$. The black dashed vertical line denotes the constant number density of $1 \times 10^{-4}\mathrm{Mpc}^{-3}$. The coloured arrows indicate the values of M_* that correspond to this number density for each integrated stellar mass fraction. (b) The galaxy selection using an evolving number density based on the major merger rate from Bluck et al. (2012). by selecting galaxies at each redshift such that $n(> M_*)$ equals the values for each redshift given in Table 3.3. The coloured dashed lines denote the number density selection for each redshift. The coloured arrows indicate the values M_* that correspond to this number density for each integrated stellar mass function.

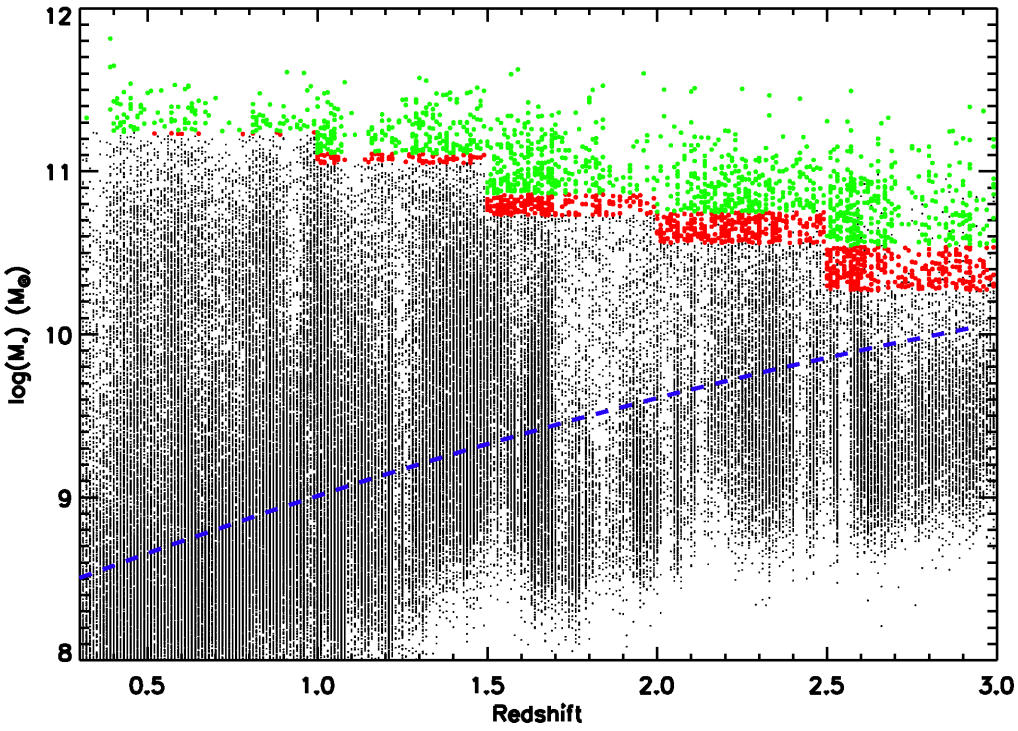

Figure 3.3: Stellar mass versus photometric redshift for the UDS galaxy parent sample. The blue dashed line is a second order polynomial fit to the 95% mass completeness limit at that redshift (Hartley et al. 2013). The green points indicate the galaxies selected via the constant number density selection, and the red and green points combined show the galaxies statistically selected via the evolving number density selection.

Table 3.1: Stellar mass function Schechter function fitted parameters from Mortlock et al (2014, in prep).

z	$\log(\mathrm{M}_*)(\mathrm{M}_\odot)$	$\Phi^*(\times 10^{-4})$	α
$0.3-0.5$	11.2 ± 0.1	7 ± 3	-1.4 ± 0.1
$0.5-1.0$	11.1 ± 0.1	8 ± 3	-1.3 ± 0.1
$1.0-1.5$	11.0 ± 0.1	8 ± 2	-1.3 ± 0.1
$1.5-2.0$	11.0 ± 0.1	2 ± 2	-1.5 ± 0.2
$2.0-2.5$	11.0 ± 0.1	2 ± 2	-1.5 ± 0.2
$2.5-3.0$	11.1 ± 0.4	1 ± 1	-1.8 ± 0.2

Table 3.2: C-GaND stellar mass limits for a constant number density selected sample taken from the integrated mass functions shown in Figure 2.2 from Mortlock et al (2014, in prep).

z	$\log \mathrm{n}(<\mathrm{M}_\odot)(\mathrm{Mpc}^{-3})$	Stellar Mass limit ($\log\mathrm{M}_\odot$)
$0.3-0.5$	-4.00	11.24 ± 0.07
$0.5-1.0$	-4.00	11.24 ± 0.04
$1.0-1.5$	-4.00	11.11 ± 0.04
$1.5-2.0$	-4.00	10.86 ± 0.05
$2.0-2.5$	-4.00	10.75 ± 0.07
$2.5-3.0$	-4.00	10.54 ± 0.09

3.3.2 Merger Adjusted Galaxy Number Density (M-GaND)

Many studies to date have investigated the average number of major mergers (1:4 mass ratio or greater) a massive galaxy experiences over cosmic time (e.g. Bluck *et al.* 2009, Bundy *et al.* 2009, de Ravel *et al.* 2011, López-Sanjuan *et al.* 2012, Xu *et al.* 2012, Ruiz, Trujillo & Mármol-Queraltó 2013). Figure 3.4 shows the observed pair fractions in the literature that investigated the major merger rates of massive galaxies using similar methods. Using these merger fractions we can adjust the number density selection to study the contribution of major mergers to the total stellar mass growth. Using both the C-GaND and M-GaND selections we can separate the stellar mass growth due to major mergers, star formation and indirectly minor mergers from the total stellar mass growth. We do this using a number density selection that changes due to the rate of major mergers that are occurring between redshift bins. From the best fitting power law to the data shown in Figure 3.4 we quantify the fraction of major merger events as:

$$f_m = (0.009\pm0.002)(1+z)^{2.9\pm0.2} \tag{3.9}$$

where $f_{\rm m}$ is the fraction of major merger events at redshift z. This relation is derived using galaxies with stellar masses greater than $\log(\mathrm{M}) > 11.0$ at all redshifts. Bluck *et al.* (2012) shows that the merger fraction relation with redshift does not change over the stellar mass range of interest in this chapter.

In previous works the merger fraction has been converted into a galaxy merger fraction, f_{gm}. The galaxy merger fraction measures the fraction of galaxies in a population undergoing a merger, The merger fraction measures the fraction of merger events within a galaxy population. Using the galaxy merger fraction is appropriate when examining the merger rates within a population. Using Mortlock *et al.* (2011) we calculate that galaxies below the C-GaND stellar mass limits which are large enough to constitute a 1:4 stellar mass merger ratio are five times more numerous than galaxies larger than the C-GaND stellar mass limits. Thus we calculate the number of major mergers using f_m.

From this we calculate the average time between mergers that a galaxy experiences at a given redshift, Γ, as:

$$\Gamma = \tau_{\rm m}/f_{\rm m} \tag{3.10}$$

where $\tau_{\rm m}$ is a merger time-scale for for galaxy close pairs. We adopt a time-scale over which merging is occurring for galaxy close pairs in a 1:4 or less mass ratio of $\tau_{\rm m} = 0.4 \pm 0.2$ Gyr derived from simulation results of Lotz *et al.* (2008). We use the Γ value to calculate the average number of mergers between redshift bins using the equation:

$$N_{\rm m} = \int_{t_1}^{t_2} \frac{dt}{\Gamma(z)} = \int_{z_1}^{z_2} \frac{1}{\Gamma(z)} \frac{t_H}{(1+z)} \frac{dz}{E(z)} \tag{3.11}$$

where z_1 and z_2 are the redshift limits of interest, t_H is the Hubble time and $E(z) = [\Omega_{\rm M}(1+z)^3 + \Omega_k(1+z)^2 + \Omega_\Lambda]^{-1/2} = H(z)^{-1}$. Calculating this from $z = 3.0$ to $z = 0.3$ we obtain $N_{\rm m} = 1.2 \pm 0.5$ as the average number of major mergers that the galaxies selected via the C-GaND selection will undergo. The error on $N_{\rm m}$ is derived from Monte Carlo techniques incorporating the error on $\tau_{\rm m}$ and $f_{\rm m}$. N-body simulations from Wetzel *et al.* (2008) suggest that pair fraction methods may overestimate the number of true major mergers, as massive galaxies pairs may have high relative velocities. However, also in Wetzel *et al.* (2008) they find that pair fraction can underestimate the number of true major mergers due to pairs at higher separations may also

merge. If these are true, it suggests that the error on our merger fractions and merger time-scales may be underestimated.

Using Equation 3.11 we calculate the average number of major mergers in each redshift bin. We then compute the major merger adjusted number density via the equation:

$$n_{z(1)} = n_{z(0)} * (1.0 + N_{\mathrm{m,z(0-1)}}) \tag{3.12}$$

where $n_{z(0)}$ is the co-moving number density of the massive galaxies at redshift $z(0)$. The value $n_{z(1)}$ is the number density of the progenitors of the galaxies at redshift $z(0)$ at $z(1)$, where $z(1) > z(0)$. $N_{\mathrm{m,z(0-1)}}$ is the average number of major mergers the progenitor galaxies will experience between $z(1)$ and $z(0)$. Using this we find that the number density of all the major merger progenitors of local massive galaxies increases with look-back time by a factor of 2.2 ± 0.5 by redshift $z = 3.0$. The exact values of the evolving number densities can be found in Table 3.3. Figure 3.2 (b) shows the integrated galaxy mass functions and lower limit stellar mass cuts based on the evolving number density. Figure 3.3 furthermore plots the galaxies selected via this method in green and red compared to the total UDS galaxy population. Figure 3.5 shows the mean number of progenitor galaxies at each redshift.

Using a major merger adjusted number density selection method we in theory obtain close to a complete sample of the major progenitors of local massive galaxies, including the less massive galaxies that have merged during a major merger event with the direct central progenitors over the redshift range $0.3 < z < 3.0$. This selection method also allows us to examine and disentangle the contributions to the total stellar mass growth from major and minor mergers. We achieve this by examining how the stellar mass density of the M-GaND sample evolves with redshift compared to the C-GaND sample. The stellar mass density of the M-GaND sample contains both the stellar mass of the progenitors of local massive galaxies and the stellar mass of the total major merger progenitors. When examining other properties of massive galaxies, e.g. size, across a large redshift range methods that select only the direct progenitors of the local massive galaxies are appropriate.

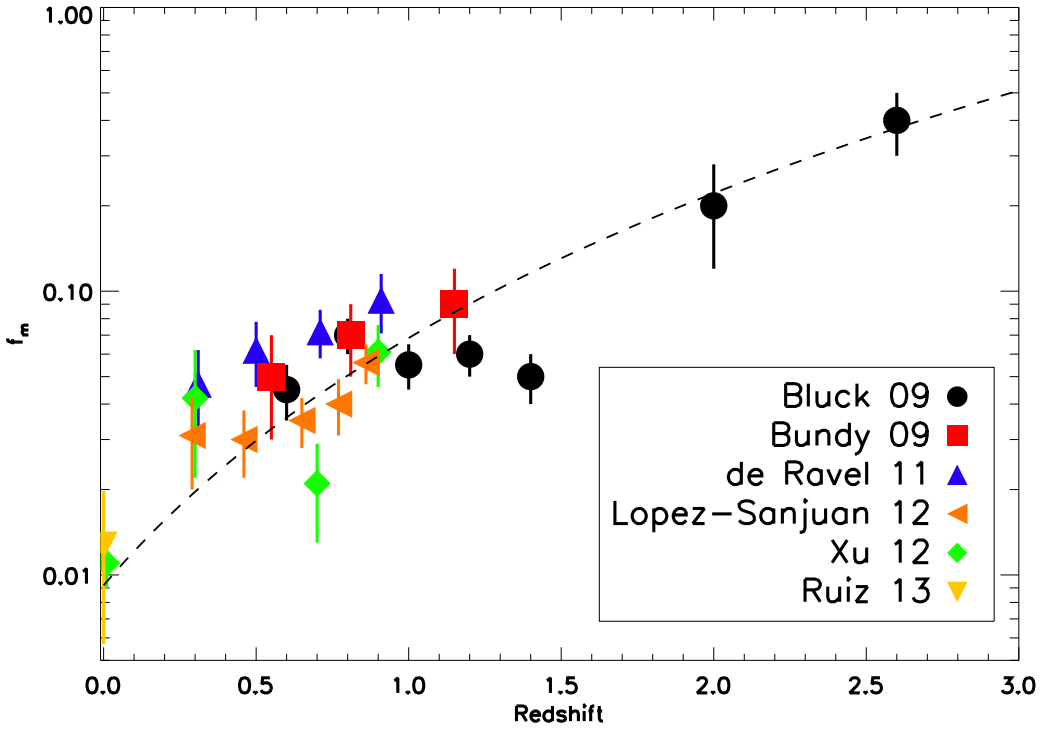

Figure 3.4: Observed galaxy pair fractions in the literature. Bluck *et al.* (2009) calculate the merger fraction down to a stellar mass ratio of 1:4 for galaxies with $\log(\mathrm{M}_*) > 11.0$ using close pairs within 30kpc. Bundy *et al.* (2009) calculate the merger fraction down to a stellar mass ratio of 1:4 for galaxies with $\log(\mathrm{M}_*) > 11.0$ using close pairs within 20kpc. de Ravel *et al.* (2011) calculate the merger fraction of galaxies with $\log(\mathrm{M}_*) > 11.0$ using close pairs within 30kpc and $\Delta B < 1.5$. López-Sanjuan *et al.* (2012) calculate the merger fraction down to a stellar mass ratio of 1:4 for galaxies with $\log(\mathrm{M}_*) > 11$ using close pairs within 30kpc. Xu *et al.* (2012) calculate the merger fraction down to a stellar mass ratio of 1:3 of galaxies with $\log(\mathrm{M}_*) > 10.6$ using close pairs within 20kpc. Ruiz, Trujillo & Mármol-Queraltó (2013) calculate the merger fraction down to a stellar mass ratio of 1:5 for galaxies with $\log(\mathrm{M}_*) > 11.3$ using close pairs within 100kpc. The Ruiz, Trujillo & Mármol-Queraltó (2013) point has been modified to compensate for the large close pair search radius. The dashed line is the best fit to all points with the form $\mathrm{f_m} = \mathrm{A} \times (1+\mathrm{z})^{\mathrm{B}}$ with $A = 0.009 \pm 0.002$ and $B = 2.9 \pm 0.2$.

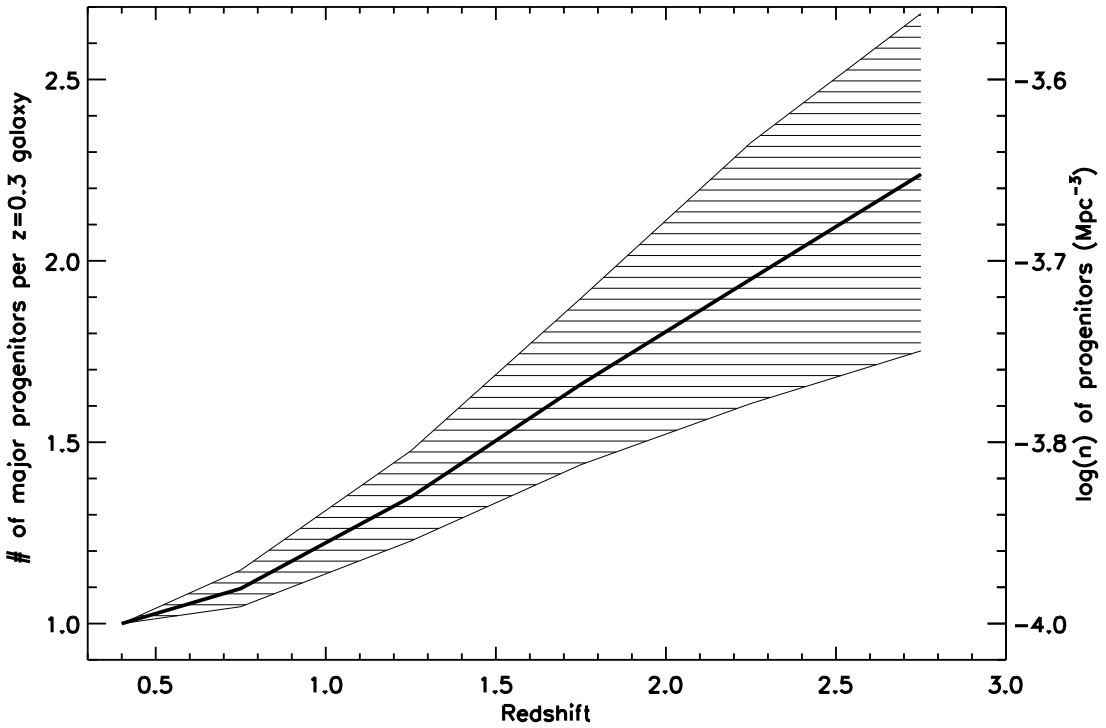

Figure 3.5: The mean number of major merger progenitor galaxies against redshift for galaxies with $n = 1 \times 10^{-4}\mathrm{Mpc}^{-3}$ at $z = 0.3$. The solid black line is derived from equation 3.12. The black hashed area shows the 1 sigma uncertainty on this relation. The y axis on the right hand side shows how the number density of the major merger progenitors evolves with this relation.

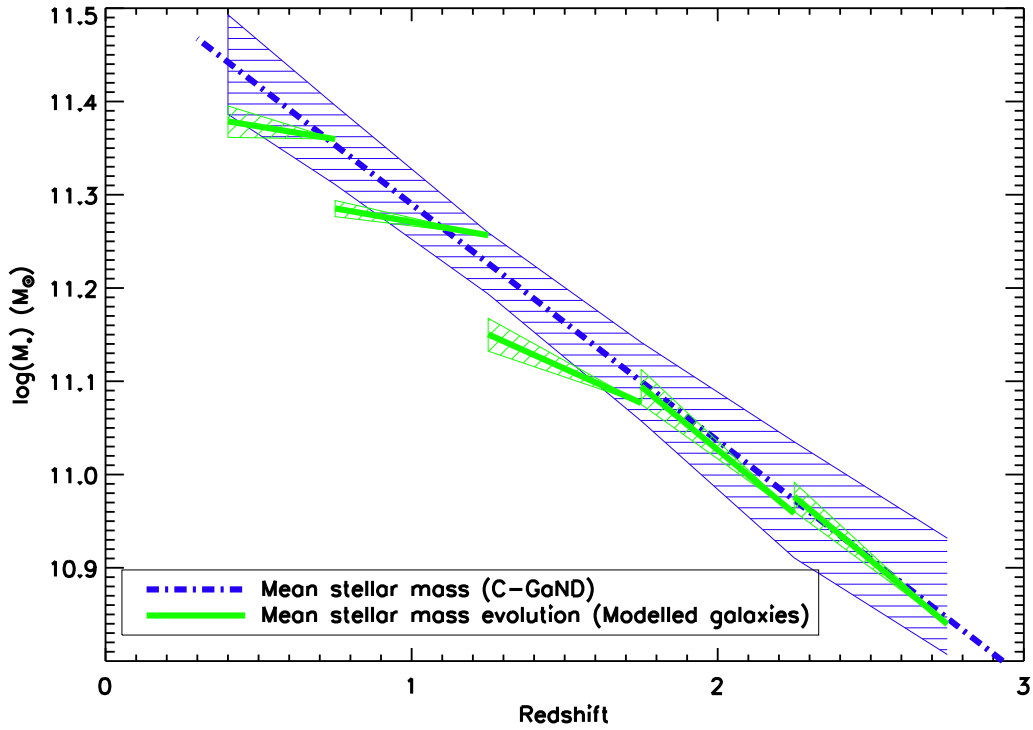

Figure 3.6: The mean stellar mass evolution of the modelled galaxies. Figure shows how well star formation and major mergers within a given galaxy population is able to account for the change in stellar mass. The blue dot dash line shows the best fit to the evolution of the mean stellar mass of the C-GaND selected sample with $n = 1 \times 10^{-4}\mathrm{Mpc}^{-3}$. The blue hashed region shows the 1 sigma uncertainty on this relation. See Section 3.4.1 for more details. The green solid lines show the evolution of the mean stellar mass of the galaxies with modelled stellar mass growth. The green hashed regions show the standard error on the mean of these results. The stellar mass growth modelling is described in Section 3.3.2.

3.3.3 Limitations of the Method

One caveat of selecting galaxies using cuts in stellar mass is contamination from lower mass galaxies entering the sample at lower redshifts or galaxies dropping out due to quenching. This arises due to galaxies below the stellar mass selection limit growing in stellar mass between redshift bins via star formation and mergers. We model this contamination using our knowledge of star formation rates and major merger rates. The stellar mass of each individual galaxy is evolved to the next lowest redshift bin by modelling the star formation histories and major mergers. The stellar mass added via star formation is modelled by integrating the fitted declining τ model derived from SED fitting for each individual galaxy. The stellar mass added via major mergers is modelled by assigning each galaxy a probability that it will undergo a major merger between redshift bins with a merger ratio between 1:1 and 1:4 with the likelihood of each merger ratio defined by the galaxy stellar mass function. The probability of a major merger is then converted to a number of merger events within a redshift bin by using a Monte Carlo technique.

Adding together these two stellar mass evolution processes we calculate the evolved stellar mass for each galaxy. We do not take into account the effect of minor mergers as we do not fully understand the full influence these events have on the stellar mass growth. Figure 3.6 shows how the mean stellar mass of the galaxies we evolve compares to the evolution of the C-GaND sample. We find that at high redshifts the modelling appears to more accurately trace the stellar mass evolution of the C-GaND population than at lower redshifts. This could be due to a higher importance of minor mergers at lower redshifts. From this modelling we find that the number density selection techniques used here has between a $20 - 30\%$ contamination rate per redshift bin. However the contamination is, on average, three times lower than a constant mass selection technique. We also note that the galaxies with the highest probability of contaminating the sample arise from galaxies within 0.15 dex below the stellar mass limits.

When using a merger adjusted number density selection, the exact stellar mass of the smaller galaxy within a major merger is unknown as it could be any galaxy within the mass ratio of 1:4. The selection we use here to construct the M-GaND sample provides

Table 3.3: M-GaND stellar mass limits for the evolving number density sample taken from the integrated mass functions shown in Figure 2.2 from Mortlock et al (2014, in prep). Starting at log(n)$= -4.0$ in the $z = 0.3 - 0.5$ redshift bin.

z	$\log \mathrm{n}(< \mathrm{M}_{\odot})$	Stellar Mass limit ($\log \mathrm{M}_{\odot}$)
$0.3 - 0.5$	-4.00	11.24 ± 0.07
$0.5 - 1.0$	-3.96 ± 0.01	11.22 ± 0.04
$1.0 - 1.5$	-3.87 ± 0.02	11.05 ± 0.05
$1.5 - 2.0$	-3.78 ± 0.03	10.73 ± 0.05
$2.0 - 2.5$	-3.72 ± 0.04	10.56 ± 0.09
$2.5 - 3.0$	-3.65 ± 0.05	10.27 ± 0.10

a hard upper limit on the amount of stellar mass that can be assembled via major mergers. This is because we select the most massive galaxies that fall below the C-GaND selection limit at each redshift. However, constructing the M-GaND sample this way does result in an apparently sequential merger process i.e., less massive satellites merge first. This is counter to recent findings (e.g. López-Sanjuan *et al.* 2012, Xu *et al.* 2012). The stellar mass accretion rates calculated by this work are derived from the total stellar mass densities of both samples, the exact sequence of mergers therefore does not affect the results.

3.4 Results

3.4.1 Stellar Mass Growth

Figure 3.7 shows the evolving mean stellar mass per progenitor for both the C-GaND and M-GaND selected galaxies as a function of redshift and look back time. This represents for the M-GaND sample the total stellar mass that has already been created, but is in disparate objects. Figure 3.5 shows the mean number of disparate objects per $z = 0.3$ galaxy at this redshift. The blue squares show the C-GaND selected sample with $n = 1 \times 10^{-4} \mathrm{Mpc}^{-3}$ and the black circles show the M-GaND selected sample starting at $z = 0.3$ with $n = 1 \times 10^{-4} \mathrm{Mpc}^{-3}$. The blue dot dashed line shows the best simple linear fit to the C-GaND data with the form:

$$M_{*}(z) = 11.56 \pm 0.13 - (0.26 \pm 0.03)z \tag{3.13}$$

The hashed area denotes the 1 sigma errors on this fit. The fit to the C-GaND implies that the direct progenitors of local massive galaxies with stellar masses of $\sim 4 \times 10^{11}\mathrm{M}_{\odot}$ assembled $75 \pm 9\%$ of their stellar mass at $0.3 < z < 3.0$. This is consistent with stellar mass growth rates found in other number density studies (e.g., Lundgren *et al.* 2014, Marchesini *et al.* 2014)

3.4.2 Star formation history of massive galaxies from $\mathbf{z = 3}$ to 0.3

Using the average SFRs of the two galaxy populations we investigate the average star formation history of the massive galaxies over the range $0.3 < z < 3.0$. Figure 3.8 shows the evolution of the dust corrected average SFR of the C-GaND and M-GaND galaxy populations. We observe that there is very little difference in the mean SFRs of the two samples, and there is a smooth decrease in the SFR from $z = 3$ to 0.3. This decline can be fit by an exponentially declining model of the form:

$$SFR(t) = SFR_0 \times \exp(-\mathrm{t}/\tau) \tag{3.14}$$

with $\tau = 2.3 \pm 0.6$ Gyr for the C-GaND sample and $\tau = 2.3 \pm 0.6$ Gyr for the M-GaND sample. This in contrast to the SFRs of massive galaxies at $z \gtrsim 3$ which appear to be best fit with an increasing SFR model peaking at $z \simeq 3.0$ (e.g. Papovich *et al.* 2011). We compare the star formation history for both galaxy samples to the star formation histories obtained for the same galaxies derived from SED fitting (see §3.2.3). We find that the average star formation history from SED fitting, $\tau_{SED} = 2.3 \pm 0.9$ Gyr, is very similar but with a larger error. We also examine how the star formation history of a population of galaxies varies as a function of the galaxy number density.

We examine the star formation histories within a range of number densities from $n = 5 \times 10^{-4}\mathrm{Mpc}^{-3}$ to $4 \times 10^{-5}\mathrm{Mpc}^{-3}$. We observe a slight change in the τ values within the number density selected samples. The C-GaND selection has τ ranging from 2.4 ± 0.5 Gyr at $n = 5 \times 10^{-4}\mathrm{Mpc}^{-3}$ to 2.2 ± 0.5 Gyr at $n = 0.4 \times 10^{-4}\mathrm{Mpc}^{-3}$. The M-GaND sample cannot be examined over the same range due to the galaxy sample dropping below the mass completeness limits at number densities lower than $n = 1 \times 10^{-4}\mathrm{Mpc}^{-3}$. Therefore we examine it over a smaller range in number density from the studied $n = 1 \times 10^{-4}\mathrm{Mpc}^{-3}$ to $0.4 \times 10^{-4}\mathrm{Mpc}^{-3}$. The value for τ obtained from

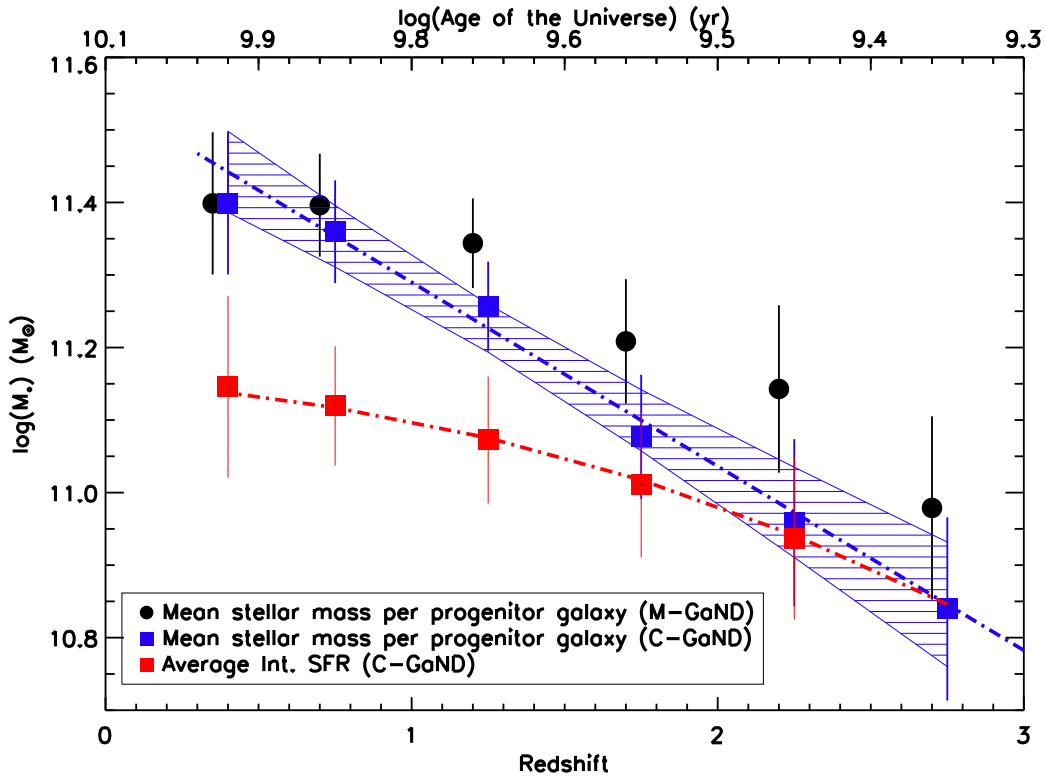

Figure 3.7: The mean stellar mass of galaxies per progenitor selected using the two number density selections as a function of redshift. The blue squares denote galaxies selected via the constant galaxy number density selection, and the black circles denote the major merger adjusted number density selected galaxies. This represents for the M-GaND sample the total stellar mass that has already been created, but is in disparate objects. The blue dot dashed line shows the best simple linear fit to the C-GaND data with the blue hashed region showing the 1 sigma uncertainty. The error bars are derived from Monte Carlo analyses incorporating the errors on stellar masses, redshift and number density. The red squares show the integrated SFR of the C-GaND sample. This is calculated from the average galaxy SFR in each redshift bin and incorporates stellar mass loss due to stellar evolution derived from BC03 Chabrier model with sub-solar metallicity. The integrated SFRs are best fit by a power law shown in Equation 3.16.

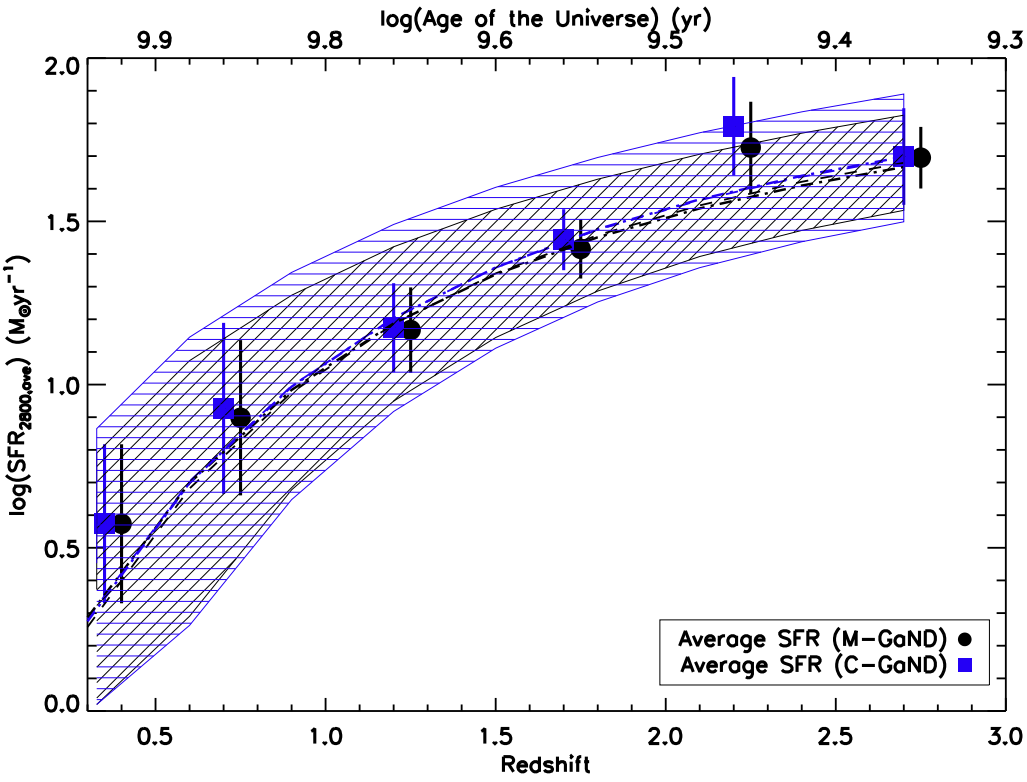

Figure 3.8: The average SFR of galaxies selected at a constant number density of $n = 1 \times 10^{-4}\mathrm{Mpc}^{-3}$ (Blue squares) and galaxies selected using the major merger corrected number density as a function of redshift (Black circles). The SFRs are derived from the dust corrected UV luminosities. The average SFRs are fit with an exponentially declining model star formation history from $z = 3.0$ to 0.3. The blue and black dotted lines show the best fits to each data set. The average SFRs are fit with an exponentially declining model star formation history from $z = 3.0$ to 0.3.

the best fit to the SFRs at $n = 0.4 \times 10^{-4}\mathrm{Mpc}^{-3}$, is $\tau = 2.3 \pm 0.6$ Gyr, showing the same trend as the C-GaND sample. We also fit this relation excluding the point at $z = 3.0$ as it appears that galaxies possibly depart from the exponentially declining model of SF at this redshift (Papovich *et al.* 2011). We find that even with excluding this redshift bin we recover essentially the same result.

From Section 3.2.5.2 if we assume zero dust correction for passive galaxies the star formation history for the $n = 1 \times 10^{-4}\mathrm{Mpc}^{-3}$ C-GaND sample changes to $\tau_{nodust} = 1.7 \pm 0.7$ Gyr, within the error of the full dust correction sample. This is also a hard lower limit on the star formation history due to the dust correction applied.

Using the average SFRs of the C-GaND sample we examine the stellar mass contribution of the SFR to the direct progenitors of massive galaxies over time. We study this directly by integrating the average SFRs from $0.3 < z < 3.0$ to obtain a total stellar mass added via SF. As the time scales involved within this integration are much larger than the main sequence lifetimes of high mass stars we need to consider the effect of the loss in stellar mass that will occur due to stellar evolution.

To do this we used Bruzual & Charlot (2003) stellar population models with varying metallicity from $1/50$th solar, to solar, to estimate the fraction of the stellar mass created via SF that will be lost between integration steps.

We do this by integrating the average star formation history in each redshift bin to yield the stellar mass added via star formation between each redshift interval. We then model the added stellar mass within each redshift bin as a zero age single stellar population and evolve it with time accordingly with the Bruzual & Charlot (2003) stellar population model. The fraction of stellar mass that is lost due to stellar evolution, dictated by the stellar population model, is removed from the added stellar mass. As an example, these models show that after 1 Gyr of stellar evolution for a $1/2$ solar metallicity system, $\sim 35\%$ of the stellar mass produced at t$= 0$ has been lost due to stellar evolution processes.

In the previous sections we examine the average total stellar mass growth of the selected massive galaxy populations seen in Figure 3.7. Also in Figure 3.7 we plot the integrated SFR of the C-GaND sample against redshift. From $z = 3.0$ the integrated SFR is fitted using a power law of the form:

$$\log(M_{\rm SFR}(z)) = a - b * (1+z)^c \tag{3.15}$$

We find the best fit to all the free parameters for the $n = 1 \times 10^{-4}\mathrm{Mpc}^{-3}$ C-GaND sample is: $a = 11.2 \pm 0.1, b = 2 \pm 1 \times 10^{-2}$ and $c = 3 \pm 1$. We find that between $1.5 < z < 3.0$ the stellar mass produced via the integrated SF can account for a large fraction, $\sim 60\%$, of the total stellar mass growth over this redshift range. This implies that SF is the dominant stellar mass growth process at these redshifts, and consequently the stellar mass growth from mergers must be smaller in comparison at $1.5 < z < 3.0$.

At lower redshifts, $0.3 < z < 1.5$, the SF only accounts for ~ 0.1 dex of stellar mass growth, wherein at the same redshift the total stellar mass grows by ~ 0.5 dex. Using the results of this stellar mass build up in the C-GaND sample we calculate the stellar mass added to the progenitor galaxies via all mergers across the redshift range $0.3 < z < 3.0$. The total mass deficit between the total stellar mass and the integrated SFR at $z = 0.3$ is $\Delta M_* = (1.3 \pm 0.6) \times 10^{11}\mathrm{M}_\odot$. As the integrated SFR at low redshift cannot account for the total stellar mass growth, mergers must be taking over as the dominant process of formation for the progenitors of local massive galaxies at $z = 1.5$. In the next section we use these results, plus the results from the M-GaND selected galaxies to calculate the stellar mass added via minor mergers.

3.4.3 Galaxy Formation From Minor Mergers

As discussed before in §3.1 the main two methods for increasing a galaxy's stellar mass are star formation and mergers. Therefore the growth of the stellar mass density (ρ_*) of a number density selected sample can be written as:

$$\rho_*(z_0) = \rho_*(z_1) + \int_{z_0}^{z_1} \rho_{\rm SFR}(z)\,\mathrm{d}z + \int_{z_0}^{z_1} \rho_{\rm m}(z)\,\mathrm{d}z \tag{3.16}$$

where $\rho_*(z_0)$ and $\rho_*(z_1)$ is the stellar mass density of the sample at different redshifts, where $z_1 > z_0$, and $\rho_{\rm SFR}(z)$ is the star formation rate density of the sample corrected for stellar evolution. This is integrated over the redshift range of interest to give a total stellar mass density added via star formation between $z_0 - z_1$. The value $\rho_m(z)$ is the stellar mass of all galaxy mergers, both major and minor mergers, per unit volume of

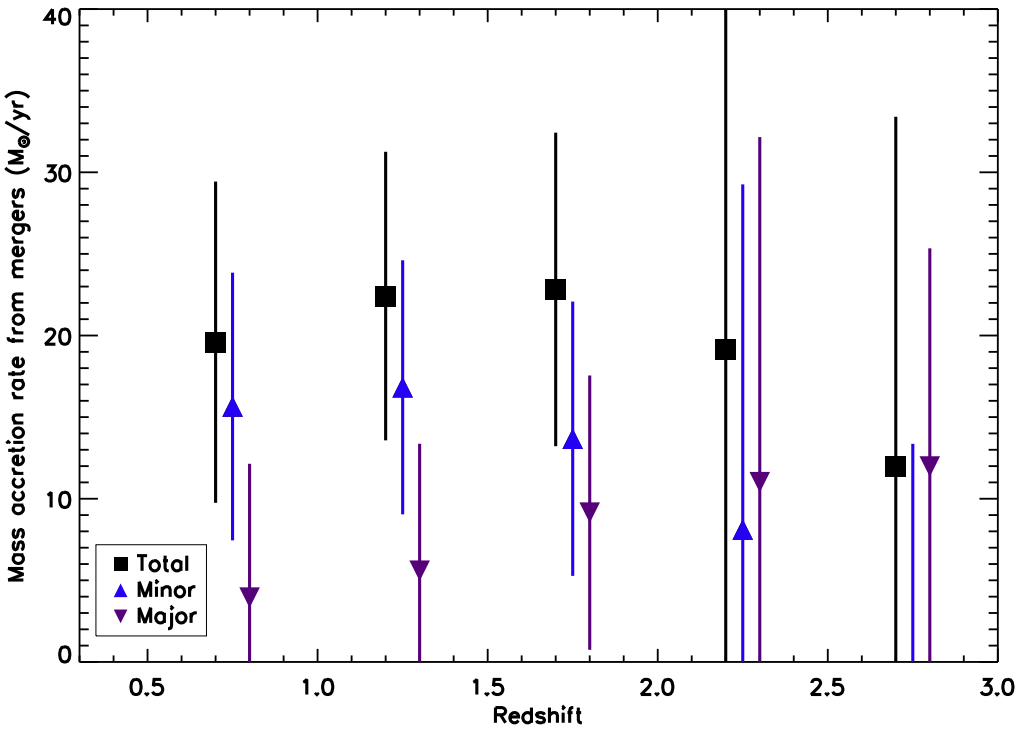

Figure 3.9: The total, minor and major merger accretion rate as a function of redshift in units of $M_{\odot}yr^{-1}$. This is calculated from the deficit between the integrated SFR and the observed mass growth shown in Figure 3.7. The errors are calculated from Monte Carlo analyses incorporating the errors on the redshift, total stellar mass and the star formation rate. The black squares show the total merger rate, the blue upward pointing triangles show the minor merger rate and the purple downward pointing triangles show the major merger rate.

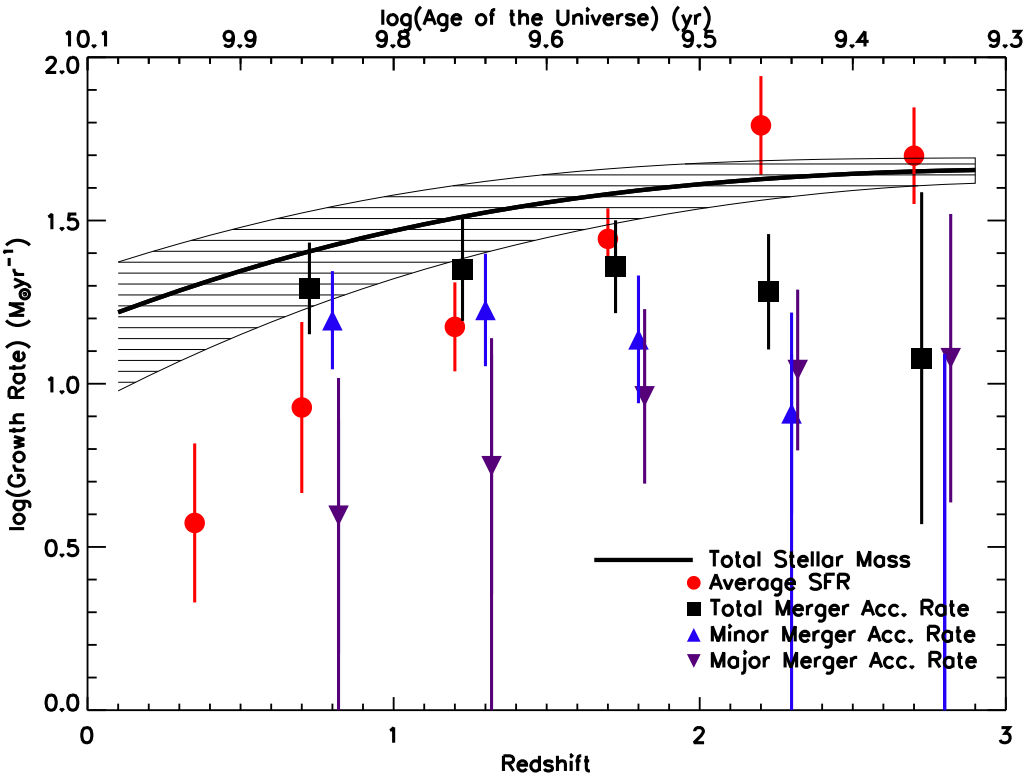

Figure 3.10: Growth rate of the number density selected galaxies as a function of redshift. The total growth rate is derived from the total stellar mass evolution shown in Figure 3.7. The black solid line shows the total stellar mass growth rate of the C-GaND sample. The hashed region around the line show the 1 σ uncertainty of the stellar mass growth rates derived from our Monte Carlo analysis. The red circles show the average SFR of the C-GaND sample. The black squares show the calculated total merger rate for the C-GaND sample. The blue upward pointing triangles show the minor merger rate and the purple downward pointing triangles show the major merger rate. See §3.4.3 for full details on how these are derived. All error bars in this figure are derived from Monte Carlo analysis incorporating the errors of stellar masses, redshifts, selection criteria and SFRs.

the sample, which can also be integrated over the redshift range to yield a total stellar mass density added via mergers.

As we are selecting galaxies above a number density threshold, the total stellar mass density added via mergers cannot be due to mergers within the selected population. Within the M-GaND selection the stellar mass of all major mergers that are likely to happen between $0.3 < z < 3.0$ are already contained within the sample. Therefore stellar mass density increase from the M-GaND sample must be added from galaxies at higher number densities, or rather lower galaxy stellar mass (minor mergers).

The three variables $\rho_*(z = 0.3)$, $\rho_*(z = 3.0)$ and $\rho_{\rm SFR}(z)$ are known from the previous sections in this study (see §3.4.1 and §3.4.2 respectively). From this we calculate, using a rearranged Equation 3.16, that the total stellar mass density added via mergers over the redshift range $z = 0.3 - 3.0$ for the two samples are:

$$\int_{0.3}^{3.0} \rho_{\rm m,C-GaND}(z)\,{\rm d}z = 13.9 \pm 2.4 \times 10^6\,{\rm M_\odot Mpc^{-3}} \tag{3.17}$$

$$\int_{0.3}^{3.0} \rho_{\rm m,M-GaND}(z)\,{\rm d}z = 10.2 \pm 2.3 \times 10^6\,{\rm M_\odot Mpc^{-3}} \tag{3.18}$$

The C-GaND selection result gives the total stellar mass density added via all mergers, and M-GaND selection result gives the total stellar mass density added via only minor mergers due to the selection encompassing all major merger progenitors. Therefore we can write these values as:

$$\int_{0.3}^{3.0} \rho_{\rm m,total}(z)\,{\rm d}z = \int_{0.3}^{3.0} \rho_{\rm m,C-GaND}(z)\,{\rm d}z \tag{3.19}$$

$$\int_{0.3}^{3.0} \rho_{\rm m,minor}(z)\,{\rm d}z = \int_{0.3}^{3.0} \rho_{\rm m,M-GaND}(z)\,{\rm d}z \tag{3.20}$$

From these values we also calculate the total stellar mass density added via major mergers to the C-GaND sample using the follow equation:

$$\int \rho_{\rm m,major}(z)\,{\rm d}z = \int \rho_{\rm m,total}(z)\,{\rm d}z - \int \rho_{\rm m,minor}(z)\,{\rm d}z \tag{3.21}$$

$$\int_{0.3}^{3.0} \rho_{\rm m,major}(z)\,{\rm d}z = 3.7 \pm 3.3 \times 10^6\,{\rm M_\odot Mpc^{-3}} \tag{3.22}$$

If we assume that the total merger rate has been constant over this redshift range this equates to an average change in the stellar mass density due to major mergers

of $\rho_{\rm m,major} = 4.6 \pm 4.1 \times 10^{-4} {\rm M}_{\odot} {\rm Mpc}^{-3} {\rm yr}^{-1}$, and an average change in the stellar mass density due to minor merger of $\rho_{\rm m,minor} = 12.9 \pm 2.9 \times 10^{-4} {\rm M}_{\odot} {\rm Mpc}^{-3} {\rm yr}^{-1}$ over $0.3 < z < 3.0$. Factoring in the number density of these objects implies that the total stellar mass accretion rate per galaxy from major mergers is $5 \pm 4\,{\rm M}_{\odot} {\rm yr}^{-1}$ and the total stellar mass accretion rate per galaxy from minor mergers is $13 \pm 3\,{\rm M}_{\odot} {\rm yr}^{-1}$. The large uncertainties on these results are due in the uncertainty on the minor merger rate at high redshifts. This can be improved by better knowledge of the major merger rates and stellar mass functions. However it is clear from observations that the major merger rate is not constant across this redshift range but it not yet clear from observations if the minor merger rate changes with redshift (e.g. Bluck *et al.* 2012). We also note that the definition in terms of stellar mass for what is classified as a major and a minor merger changes with redshift.

The results of Bluck *et al.* (2012), López-Sanjuan *et al.* (2012), Xu *et al.* (2012), suggest that the average satellite in a major merger is 0.5 times the central galaxy stellar mass. Therefore, an alternative estimate for the expected increase in stellar mass density due to major mergers is approximately $1.5 \times N_m \times \rho_{m,C-GaND}$. When applying this method we obtain a stellar mass density increase due to major mergers of $5.6 \pm 1.0 \times 10^{6} {\rm M}_{\odot} {\rm Mpc}^{-3}$, which is broadly consistent with method of choice for this work.

In the previous section we studied the difference in the integrated SFR and observed stellar mass growth of massive galaxies as a function of time. In this section we calculate the stellar mass deficit between the two relations and deduce the total stellar mass accreted over $0.3 < z < 3.0$ via mergers for the C-GaND sample, $\Delta M_* = M_{m,total} = 1.4 \pm 0.6 \times 10^{11} {\rm M}_{\odot}$. Therefore $50 \pm 20\%$ of the stellar mass of a massive galaxy at $z = 0.3$ is accreted via merger accretion events since $z = 3.0$. Dividing this figure into minor and major merger events, $34 \pm 14\%$ of the total stellar mass of a massive galaxy at $z = 0.3$ is accreted from minor merger events and $17 \pm 15\%$ is accreted from major merger events. If we examine each redshift bin individually we can measure how the stellar mass accretion rate has changed due to various processes across the redshift range of this study.

In Figure 3.9 we show the calculated minor merger stellar mass accretion rate from

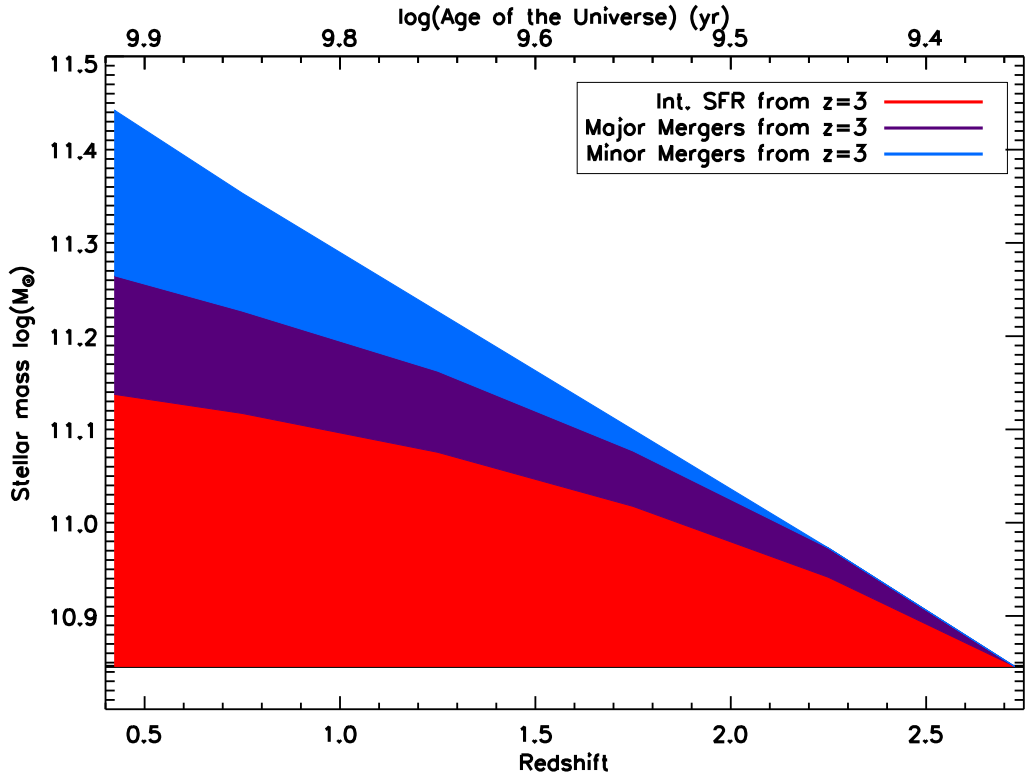

(a)

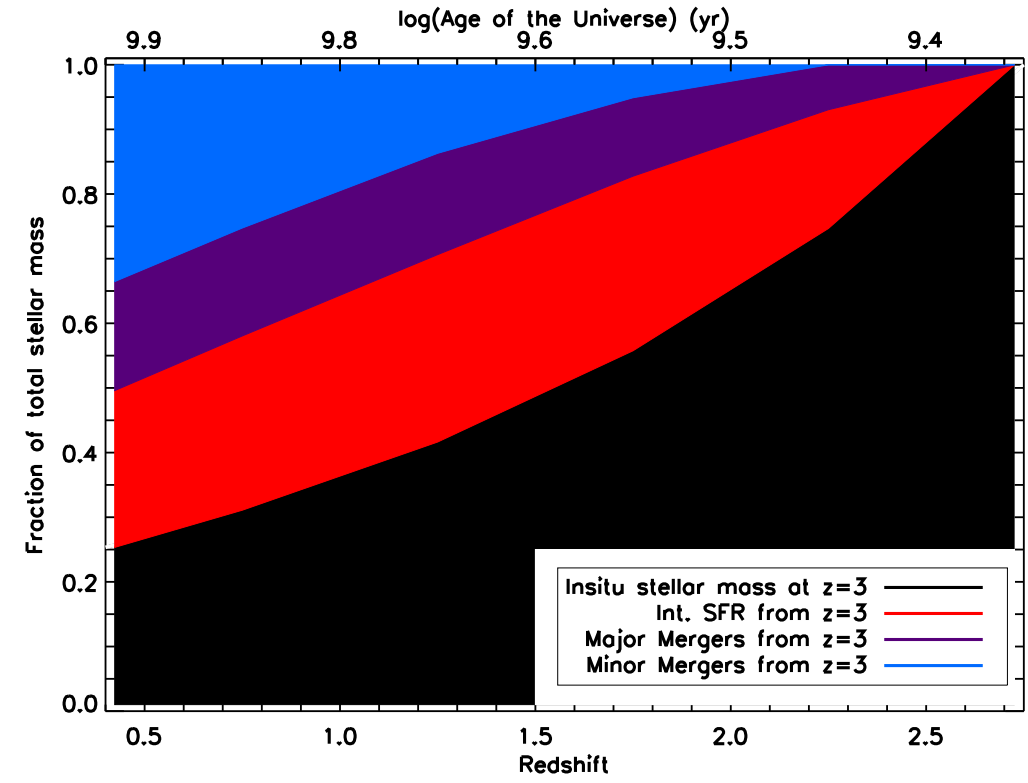

(b)

Figure 3.11: The fraction of the total stellar mass created via SF since $z = 3$ (red) and the stellar mass accreted from major mergers since $z = 3$ (purple) and the stellar mass accreted from minor mergers since $z = 3$ (blue) for the direct progenitors of local $\log \mathrm{M}_* > 11.24$ massive galaxies corresponding to $\log \mathrm{n} = -4.0$ (C-GaND selected sample). (a) shows the total stellar mass growth and (b) shows the growth as a fraction of the total stellar mass at each redshift including the in-situ stellar mass at $z = 3.0$ (black). Uncertainties on the fractions are shown in Figure 3.12.

the stellar mass density equations above applied to each redshift bin. Figure 3.10 shows the calculated minor merger rate compared to the SFR and stellar mass growth rate. As before the total merger rate is derived from the C-GaND sample, and the minor merger rate from the M-GaND sample. The two highest redshift bins have large uncertainties due to the SFR dominating at these redshifts. This does not rule out mergers at high redshift, but the effect caused via mergers must be small compared to the SFR at the same redshift. By examining the major mergers we find that the major merger accretion rate decreases towards lower redshifts. In Figure 3.10 we also find that the major merger rate in all of our redshift bins is lower than the SFR, therefore this implies that the major merger rate is at no point the dominant form of stellar mass growth between $0.3 < z < 3.0$.

The minor merger rate however increases towards lower redshifts. In the highest redshift bins the minor merger rate is within the error consistent with zero but this again is due to the stellar mass added via the SFR being more significant at these times. Unlike the major merger rate in Figure 3.10 we see that the minor merger rate does become larger than the SFR at around $z = 1.0$. Consequently the minor merger rate alone is the dominant form of stellar mass growth in the progenitors of local massive galaxies at $z < 1$.

3.4.4 Relative contributions to the stellar mass

We compare the different stellar mass growth rates in massive galaxies for both selection criteria in Figure 3.10. The total stellar mass growth rate for the C-GaND sample is derived from the best fit to the total stellar mass growth shown in Figure 3.7. We see that the total stellar mass growth rate for massive galaxies has been declining since $z = 3.0$. The blue points show the calculated minor merger rate as shown in Figure 3.9.

We convert the values of the SFR, major and minor merger rates into the total amount of stellar mass created via these processes as a function of redshift shown in Figure 3.11. In Figure 3.11 (a) we see the contribution of the three processes to the total stellar mass growth since $z = 3.0$. Figure 3.11 (b) shows the fractional contributions of in-situ stellar mass at $z = 3.0$ (black), Integrated SFR (red), major mergers (purple)

and minor mergers (blue) to the total stellar mass as a function of redshift. Figure 3.12 shows the errors on the fraction contributions derived from Monte Carlo analysis.

At our lowest redshift ($z = 0.3$) the in-situ stellar mass at $z = 3.0$ accounts for only $25 \pm 2\%$ of the total galaxy stellar mass. The stellar mass added via star formation accounts for $24 \pm 10\%$, and hence $51 \pm 20\%$ of the total galaxy stellar mass has been accreted via minor and major mergers. Therefore half of the stellar mass in local massive galaxies is not created within the galaxy, but has formed in other galaxies and has later been accreted. This is assuming that the cold gas that fuels the ongoing SFR originates from within the host progenitor galaxy, however this cold gas could also be accreted from the merger events or from the intergalactic medium, which we investigate in the next section. Within the mass obtained through mergers, $17 \pm 15\%$ of the total stellar mass has been accreted via major mergers, and the remaining $34 \pm 14\%$ via minor mergers. This implies that all three processes contribute approximately equal amounts of stellar mass to the total stellar mass of local massive galaxies from $z = 3$ to 0.3. Our work would seem to be in agreement with recent work by Lee & Yi (2013) that showed, using merger tree simulations, that the most massive galaxies can obtain up to 70% of their low redshift total stellar mass from mergers and accretion events. van Dokkum *et al.* (2010) using a different constant number density technique than used in this chapter show that 40% of the total stellar mass of massive galaxies ($\log(\mathrm{M}_*) > 11.45$) at z=0 was added through mergers and 10% through star formation between $0 < z < 2$. Over the same redshift range this work finds that $\sim 41\%$ of the total stellar mass of massive galaxies is added via all mergers and $\sim 16\%$ is added via star formation. Conversely to the study, previous works (e.g. López-Sanjuan *et al.* 2012 Ferreras *et al.* 2013 Ruiz, Trujillo & Mármol-Queraltó 2013) have suggested that major mergers may play a more prominent role with up to $\sim 60\%$ of a massive galaxies stellar mass growth at $z < 2$ arising from major merger events.

If we assume that galaxies selected as passive via the UVJ selection technique have no dust correction to their SFRs (see §3.2.5) these results change slightly. The fraction of stellar mass created via star formation decreases to $14 \pm 10\%$, A factor of two smaller but within the errors quoted. Therefore the fraction of stellar mass accreted via all mergers increases to $61 \pm 15\%$ this breaks down to $41 \pm 10\%$ via minor mergers and

$20 \pm 10\%$ via major mergers. The major merger fraction increases due to the objects within the M-GaND sample being less affected by the change in dust correction.

3.4.5 Implications for gas accretion

In this section we use our measured evolution in the total stellar mass, SFR and mergers to predict the evolution in the total cold gas mass in the progenitors of local massive galaxies. We derive the cold gas mass surface density by using the global Schmidt--Kennicutt relation calibrated for nearby star forming galaxies. The relation takes the form of:

$$\Sigma_{SFR} = 1.7 \pm 0.5 \times 10^{-4} \left(\frac{\Sigma_{\rm gas}}{1\,{\rm M}_{\odot}{\rm pc}^{-2}} \right)^{1.4\pm0.15} {\rm M}_{\odot}{\rm yr}^{-1}{\rm kpc}^{-2} \tag{3.23}$$

where Σ_{SFR} is the surface density of star formation, and $\Sigma_{\rm gas}$ is the surface density of cold gas (Schmidt 1959, Kennicutt 1998b). We calculate the star formation surface density for each galaxy based on the effective radius, R_e, obtained from GALFIT fitting Sérsic light profiles to the UDS K-band images (see §3.2.4). At high redshift Ownsworth *et al.* (2012) showed that the rest frame optical light profile is a good tracer for the profile of SF within massive galaxies. Using half of the measured SFR and effective radius we obtain the gas mass surface density using a rearranged form of Equation 3.23, to obtain the surface density of cold gas. From the surface density of cold gas we calculate the total cold gas masses contained within these galaxies assuming a spherical geometry.

We can then express how the cold gas mass changes over time as:

$$M_{\rm g}(t) = M_{\rm g}(0) + M_{\rm g,M}(t) + M_{\rm g,A}(t) - \int M_{SFR} + M_{\rm g,recy.} \tag{3.24}$$

This is similar to Conselice *et al.* (2013), where we have an expression for the total gas mass of the galaxy at t=t, $M_{\rm g}(t)$, in terms of the total gas mass of the galaxy at t=0, $M_{\rm g}(0)$, the total gas mass accreted onto the galaxy via galaxy mergers from $t = t_0$ to $t = t_f$, $M_{\rm g,M}(t)$, the total amount of gas accreted onto the galaxy from the intergalactic medium i.e. with no corresponding increase in stellar mass from $t = t_0$ to $t = t_f$, $M_{\rm g,A}(t)$, as well as the amount of gas that is converted within the galaxy into stars, $-\int M_{SFR}$, and the amount of stellar mass that is returned to the interstellar medium via stellar evolution, $M_{\rm g,recy}$.

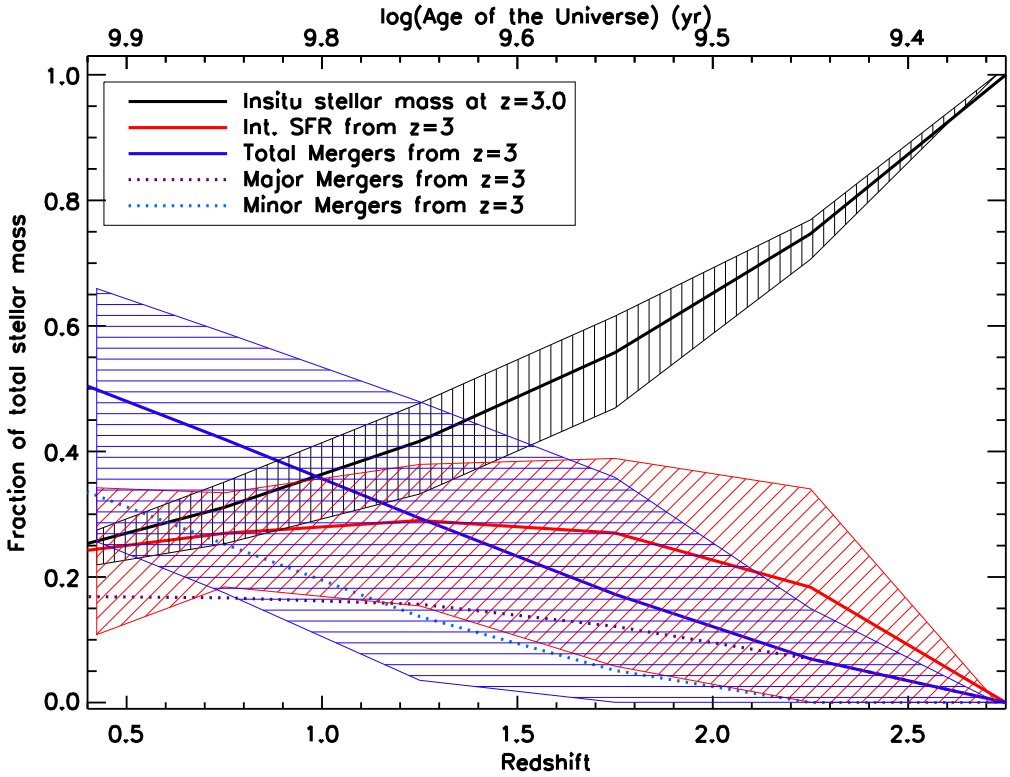

Figure 3.12: Errors on the fractional contributions to the total stellar mass derived from a Monte Carlo analysis. The stellar mass created via SF since $z = 3.0$ (red), the total stellar mass accreted via all mergers since $z = 3.0$ (blue) and the in-situ stellar mass at $z = 3.0$ (black). The thin dotted lines show the fractional contribution of the major mergers (purple) and minor mergers (blue).

As we do not know the SFR of the galaxies that constitute the minor mergers we cannot calculate the exact total cold gas mass added via minor mergers for these systems. Utilising other studies, Conselice *et al.* (2013) calculated the average stellar mass to cold gas mass ratio of all galaxies from $M_* = 10^{10.8}\mathrm{M}_\odot$ down to $M_* = 10^{9.5}\mathrm{M}_\odot$ as $f_\mathrm{g} = 1.03$. Using this information we calculate cold gas accretion needed across the redshift range $0.3 < z < 3.0$. We also know that cold gas can be ejected from the galaxy in winds from stellar or AGN sources. We account for the stellar outflows by assuming that the gas outflow rate is proportional to the SFR (e.g. Erb 2008,Weiner *et al.* 2009, Bradshaw *et al.* 2013). Therefore we add an extra term to Equation 3.25 of $M_\mathrm{g,outflow}$ which we set equal to M_{SFR}. Therefore we modify Equation 3.24 to account for this, and rearrange for $M_\mathrm{g,A}(t)$:

$$M_\mathrm{g,A}(t) = M_\mathrm{g}(t) - M_\mathrm{g}(0) - M_\mathrm{g,M}(t) + 2 \times \int M_{SFR} - M_\mathrm{g,recy} \tag{3.25}$$

Figure 3.13 shows how the derived cold gas accretion rate changes with redshift. We see that the cold gas accretion rate has been in decline since $z = 2.5$. At $z = 2.5$ the progenitors of massive galaxies were accretion cold gas with an average rate of $97 \pm 49\,\mathrm{M}_\odot\mathrm{yr}^{-1}$. From $z = 2.0$ the cold gas accretion rate has undergone a decline to lower redshift ($z = 0.3$). In fact at $z = 0.3$ massive galaxies in the C-GaND sample appear to have begun to have a negative gas accretion rate, $M_\mathrm{g,A}(z = 0.3) = -4 \pm 15\,\mathrm{M}_\odot\mathrm{yr}^{-1}$. This is consistent with zero cold gas accretion, however negative cold gas accretion rates could occur due to processes actively expelling gas from the host galaxy such as AGN.

We compare this work with Conselice *et al.* (2013) which also constrained the cold gas accretion rate within the redshift range of $1.5 < z < 3.0$. They found that within the redshift range of $1.5 < z < 3.0$ massive galaxies ($\log(\mathrm{M}_*) > 11.0\mathrm{M}_\odot$) have an average cold gas accretion rate of $96 \pm 26\,\mathrm{M}_\odot\mathrm{yr}^{-1}$. In the same redshift range we find that the progenitors of the local massive galaxies have an average cold gas accretion rate of $66 \pm 32\,\mathrm{M}_\odot\mathrm{yr}^{-1}$. When we take into account the differences between the two works such as IMF and method of calculated SFR the two figures quoted are in agreement. We also examined different methods of calculating the cold gas outflow rate from massive galaxies (e.g. Weiner *et al.* 2009) and found that the cold gas accretion rate derived using these methods are within the error of the method used

here.

3.5 Summary

In this chapter we investigate the role of star formation as well as major and minor mergers in relation to the total stellar mass growth of a constant number density selected galaxy sample within the redshift range of $0.3 < z < 3.0$. We use data from the UKIDSS UDS DR8, a deep near infra-red survey covering ~ 1 square degree. We derive UV star formation rates for all the galaxies within this redshift range using SED fitted rest frame UV photometry accounting for dust and old stellar populations.

We select the sample of massive galaxies using two number density methods; a constant number density selection (C-GaND) and a major merger adjusted number density selection (M-GaND). The major merger adjusted number density selection uses a selection that changes with time due to the rate of major mergers that occur over the redshift range studied. This selection traces the direct progenitor galaxies and the less massive galaxies that will merge with the direct progenitor galaxies at higher redshift. We use these selections to examine the average stellar mass growth of the progenitors of the most massive galaxies from $z = 3.0$ to $z = 0.3$ and disentangle the contributions of different processes of stellar mass growth.

First we test the contamination of selecting progenitor galaxies using number density techniques using knowledge of the major merger rates and star formation histories. Contamination arises from lower mass galaxies entering the sample at lower redshifts via extreme star formation or high mass galaxies quenching and undergoing mergers. We find that the average contamination rate per redshift bin is $20 - 30\%$. We find that number density techniques are a factor of 3 better at tracing progenitor than using a constant stellar mass selection technique. Our major results are:

- Local massive galaxies, with $\log \mathrm{M}_* > 11.24\,\mathrm{M}_\odot$, assemble $75 \pm 9\%$ of their $z = 0.3$ total stellar mass between $0.3 < z < 3.0$.
- Stellar mass created in star formation over the redshift range of $0.3 < z < 3.0$ comprises $24 \pm 8\%$ of the total stellar mass of massive galaxies at $z = 0.3$.

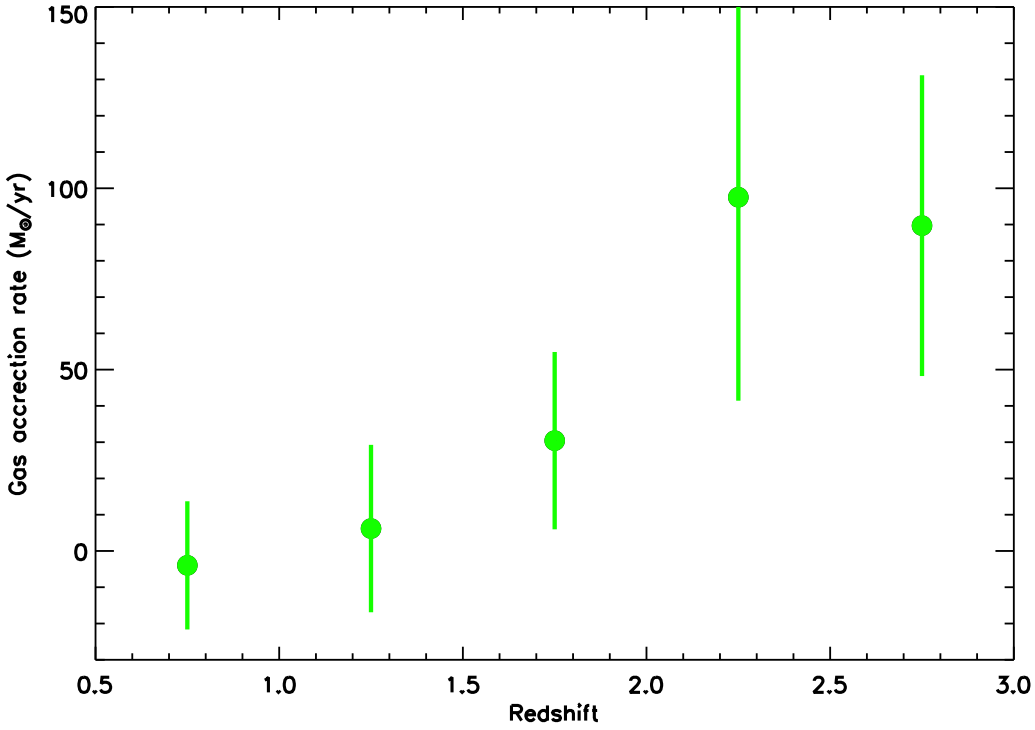

Figure 3.13: Cold gas accretion rate from the intergalactic medium of the C-GaND galaxy sample. Error bars denote the 1 sigma error on the cold gas accretion rate derived from Monte Carlo methods.

Examining the stellar mass contribution from total mergers between $0.3 < z < 3.0$ we find that the stellar mass added via mergers comprises $51 \pm 20\%$ of the total stellar mass of massive galaxies at $z = 0.3$. We also find that the star formation history of the direct progenitors of the massive galaxies at $z = 0.3$ can be defined by a declining τ model with $\tau = 2.4 \pm 0.6\,\mathrm{Gyr}^{-1}$.

- Star formation is the dominant process of stellar mass growth with the progenitor galaxies at $z > 1.5$.
- Total mergers (major and minor mergers combined) take over as the dominant process of stellar mass growth at $z < 1.5$.

Using the M-GaND galaxy sample we separate the contributions of major and minor mergers to the total stellar mass growth.

- We find that the minor merger rate of the progenitors of massive galaxies has been increasing with time since $z = 3.0$ down to $z = 0.3$.
- Minor mergers become the dominant form of stellar mass growth in the progenitor galaxies at $z \leq 1.0$.
- The contribution from all minor mergers between $0.3 < z < 3.0$ is $34 \pm 14\%$ of the $z = 0.3$ total galaxy stellar mass. All major mergers between $0.3 < z < 3.0$ contribute $17 \pm 15\%$ of the $z = 0.3$ total galaxy stellar mass.
- Major mergers are not the dominant form of stellar mass growth in the progenitor galaxies at any time between $0.3 < z < 3.0$.

Using the merger rate, SFR and stellar mass growth information we also investigate the cold gas accretion rate between $0.3 < z < 3.0$. We use the global Schmidt-Kennicutt relation combined with work from Conselice *et al.* (2013) to calculate the cold gas mass content of the progenitor galaxies at each redshift.

- We find that the cold gas accretion rate of the progenitor galaxies at $z = 3.0$ is $97 \pm 49\,\mathrm{M}_{\odot}\mathrm{yr}^{-1}$.
- This cold gas accretion rate decreases with redshift until $z = 0.3$.

To further this work large surveys such as the HSC survey and future telescopes such as JWST, E-ELT and Euclid will provide better constrained stellar mass functions that are required to explore these trends to a much higher precision.

Chapter 4

The Evolution of the Progenitors of Local Massive Galaxies

4.1 Introduction

In the local Universe, the most massive galaxies ($M_* > 10^{11.24} M_{\mathrm{M}_\odot}$) are a nearly homogeneous population. They have early-type morphologies, red rest-frame optical colours and low star formation rates (Bower, Lucey & Ellis 1992, Kauffmann *et al.* 2003, Gallazzi *et al.* 2005, Baldry *et al.* 2006, Conselice 2006b, Grützbauch *et al.* 2011, Ownsworth *et al.* 2012, Mortlock *et al.* 2013). How have massive galaxies evolved over cosmic time to become this population?

Over the last few decades there has been much research into the evolution of massive galaxies. These studies have shown that the more massive the galaxy is today, the earlier its star formation must have started and subsided (e.g. Renzini 2006, van Dokkum *et al.* 2010). This is often related to the process of "Downsizing", in which the largest objects seem to be in place and stop star forming first in an apparently anti-hierarchical manner. In the introduction to this thesis we talk about the ways this process can be reconciled with the ΛCDM, including longer merger time scales for massive dark matter haloes and the hot halo model of strangling a massive galaxy of star formation fuel.

At high redshift, massive galaxies have been observed to be unlike their present day

counterparts. The population displays evidence of being dominated by low Sérsic index, and having high star formation rates (e.g. Daddi *et al.* 2007, Buitrago *et al.* 2013, Mortlock *et al.* 2013).

Various theoretical galaxy evolution models (e.g. Faber *et al.* 2007) have suggested the the formation of the local massive red sequence galaxies involves early mass assembly and star formation, with the progenitors living on the blue cloud. This early assembly is followed by quenching and dry merging which migrates the progenitors onto the red sequence and grows them in size into the massive galaxies we see today.

However, many other studies that investigate the stellar mass functions of red sequence galaxies from $z = 1$ to the present day show that the massive galaxies have not significantly grown in stellar mass over this time (e.g. Cowie *et al.* 1996, Cimatti *et al.* 2008). Recent measurements of the stellar mass function of galaxies out to $z = 4$ (e.g. Muzzin *et al.* 2013, Duncan *et al.* 2014) show evidence that massive galaxies exist at very early cosmic times and their number densities evolve very little in the following 4Gyr from $z = 4$ to $z = 1$.

Although the stellar mass function of galaxies provides a way to measure the abundance of a population and its overall growth as a function of time, it does not tell us how individual galaxies have assembled and evolved. Ultimately, we would like to be able to connect local massive "red and dead" galaxies to their progenitors at early cosmic times and examine how they evolved and changed. Many studies have examined the properties of massive galaxies out into the distant universe using various selection methods, However now using number density selection techniques we can select a more complete and clean sample of the progenitors of local massive galaxies. With this selection we can examine the evolutionary paths local massive galaxies have travelled to become the homogeneous population we see today. With number density selection methods we can begin to answer the questions of: Do massive galaxies form in extreme star formation episodes in the early universe? At what cosmic epoch to they stop forming stars? Do they evolve from the blue cloud to the red sequence? How has their structure changed from high redshift?

Recent work has begun to investigate the evolution of the properties of massive galaxies using number density techniques (e.g. Papovich *et al.* 2011, Patel *et al.* 2013,

Marchesini *et al.* 2014).Marchesini *et al.* (2014) showed using number density selections the progenitors of ultra massive galaxies (log(M_*)¿11.8) appear to have red $U-V$ colours and host large amounts of star formation (sSFR$> 10^{-}10\,yr^{-1}$) at $z > 3$. Therefore they find that the progenitors of ultra massive galaxies, including the star forming objects, have never lived on the blue star-forming cloud in the last 11.4Gyr of cosmic history. Thus suggesting an alternative path for the formation of massive galaxies than proposed by Faber *et al.* (2007). However, is this true for lower stellar mass objects?

In this chapter we investigate the evolution with cosmic time of the progenitors of local massive ($\log(\mathrm{M}_*) > 11.24$) galaxies from $z = 3$. The progenitors are selected using a constant number density technique. The evolution of the progenitor population is examined as a function of redshift. We investigate the evolution of their colours, stellar masses, star formation rates, passivity and structural parameters over the redshift range of $0.3 < z < 3.0$.

Throughout this paper we assume $\Omega_M = 0.3$, $\Omega_\lambda = 0.7$ and $H_0 = 70$ km s^{-1} Mpc^{-1}. AB magnitudes and a Chabrier IMF are used throughout.

4.2 Data and Analysis

4.2.1 The UDS

This work is based on the 8th data release (DR8) of the Ultra Deep Survey (UDS; Almaini et al in prep.), which is the deepest of the UKIRT (United Kingdom Infra-Red Telescope) Infra-Red Deep Sky Survey (UKIDSS; Lawrence *et al.* (2007)) projects. In this chapter we use the photometric redshifts and stellar masses, colours, star formation rates and structural parameters derived from ground based UDS data as described in Section 3.2 in the previous chapter.

4.3 Selection

4.3.1 Constant Galaxy Number Density

We define our galaxy sample in the same way as in the previous chapter, using a constant galaxy number density selection (C-GaND). In this study we select and compare galaxies at constant co-moving number density values of $n = 1 \times 10^{-4}\,\mathrm{Mpc}^{-3}$, at redshifts $0.3 < z < 3$. We then select our sample based on the integrated mass functions of the UDS field over the redshift range of $z = 0.3$ to 3.0 from Mortlock et al (2014, in prep). Using this selection technique we obtain a sample of the progenitors of the local massive galaxies in which we can study the evolution of a variety of properties across 11 billion years.

4.4 Results

4.4.1 Colour Evolution

The rest-frame $U - V$ vs $V - J$ diagram is a powerful tool to separate quiescent and star forming galaxies. It has become commonly used due to its ability to distinguish between truly quiescent objects and dust reddened systems (e.g. Williams *et al.* 2009). Figure 4.1 shows the UVJ diagram for the constant number density selected sample in different redshift bins. The red box region plotted in Figure 4.1 is from Williams *et al.* (2009) and denotes the passive galaxy selection (see Section 3.2.5.2 for full UVJ selection details). Red points show galaxies that are selected as passive and blue points show galaxies that are selected as star forming. The large cross in each redshift plot denotes the median value for the whole progenitor population within each redshift bin. The greyscale shows the total population selected above the 95% stellar mass completeness limit stated in section 3.2 in the previous chapter. Many alternative methods exist to separate a galaxy population into star forming and passive objects using broad-band photometry e.g. g-r colour (Bell *et al.* 2003), u-r colour (Baldry *et al.* 2004), U-B colour (Peng 2010) and BzK colours (Daddi *et al.* 2004) see Taylor *et al.* (2014) for a comparison of these techniques. We use UVJ colour selection in this chapter to

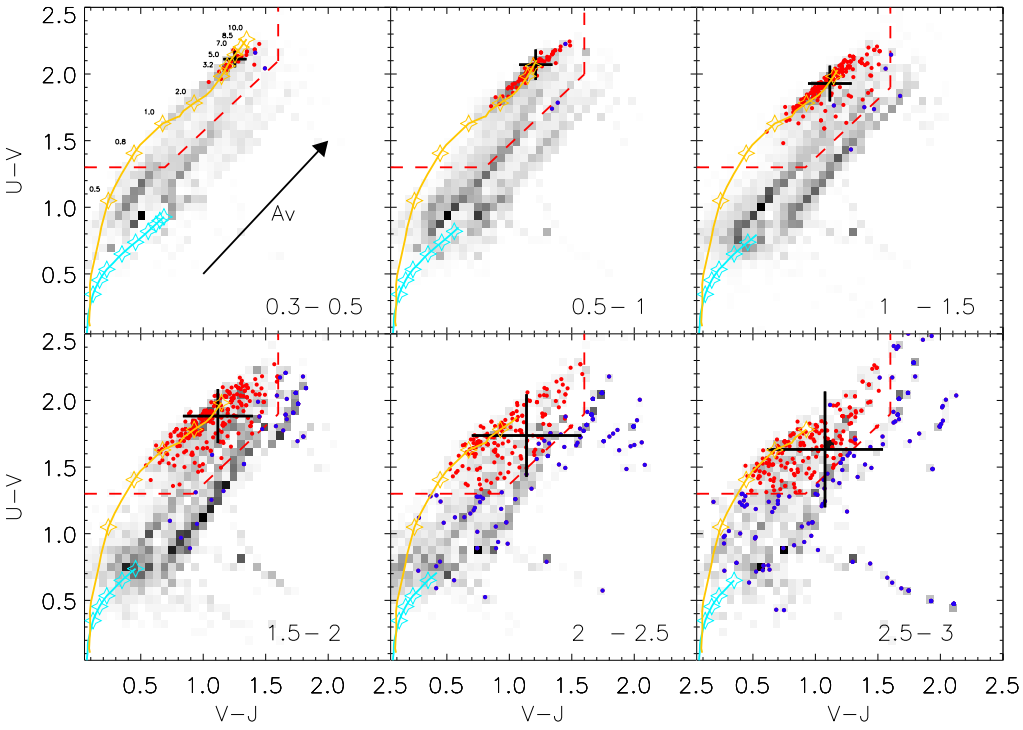

Figure 4.1: Rest frame $U-V$ versus $V-J$ diagram in redshift bins between $z=0.3$ and $z=3.0$ of the C-GaND selected sample with $n=1\times10^{-4}\mathrm{Mpc}^{-3}$. Red dashed line denotes UVJ passive selection. Red circles show the progenitors of massive galaxies that are selected as passive via the UVJ method. Blue circles show the progenitors of massive galaxies that are selected as star forming via the UVJ method and $24\mu m$ criteria (see Section 3.2.5.2). The black cross shows the median colour and standard deviation for the progenitor sample in each redshift bin. Greyscale shows total population selected above the 95% completeness limit within each redshift bin (see Figure 3.3). The colour evolution tracks from Bruzual & Charlot (2003) SSP models are also shown. The light blue line shows a constant star formation history with no dust and the yellow line shows an exponentially declining star formation history with $\tau=0.1\,\mathrm{Gyr}$. The open stars represent that model colours at the specified ages, given in Gyr. The colour evolution tracks are plotted up to the age of the Universe in each redshift bin.

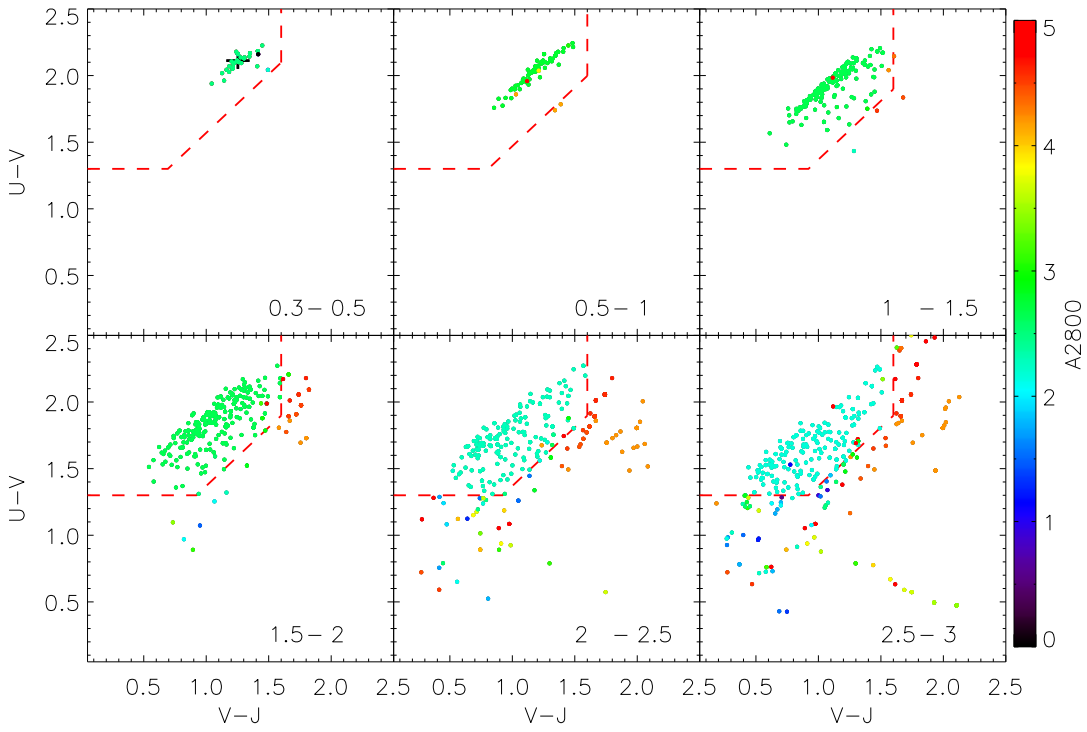

Figure 4.2: Similar to Figure 4.1 Rest frame $U-V$ versus $V-J$ diagram in redshift bins between $z=0.3$ and $z=3.0$ of the C-GaND selected sample with $n=1\times10^{-4}\mathrm{Mpc}^{-3}$. Coloured circles show the progenitors of massive galaxies with the colour representing the UV dust attenuation as shown by the colour bar on the right hand side.

compare to previous work.

Within the lowest redshift bin the massive galaxy population constitutes a homogeneous population with extremely red $U-V$ colours with very little scatter. Moving to higher redshifts the scatter increases and the population becomes more diverse in both $U-V$ and $V-J$ colours. However, as this population diversifies towards higher redshifts we find that the median UVJ colour remains at all redshifts within the passive region. This indicates that the average progenitor of local massive galaxies have had red rest frame colours since $z=3$. Examining the individual systems we find that the fraction of galaxies classified as passive via the UVJ selection alone decreases from $100\pm4\%$ at $z<0.5$ to $55\pm8\%$ at $z>2.5$. This is slightly converse to the findings of Marchesini *et al.* (2014), who find that the progenitors of the local ultra-massive galaxies (with $\log(\mathrm{M}_*/\mathrm{M}_\odot)=11.8$) have blue average rest frame colours and only $\sim17\%$ are selected as passive at $z>2.5$.

Also in Figure 4.1 we have plotted the evolutionary tracks for the two colours from Bruzual & Charlot (2003) single stellar population models. The light blue line is a constant star formation history with no dust (CSFH) and the yellow is an exponentially declining star formation history (DSFH) with $\tau=0.1\,\mathrm{Gyr}$ and zero dust attenuation. From these models we find that at $z<0.5$ the progenitors of local massive galaxies harbour old (ages older than 5 Gyr) stellar populations. Examining the progenitors at higher redshifts, the median UVJ colours within the error is always consistent with the DSFH showing that a large fraction of this population is passively evolving. If we consider the effect of dust the average age of the stellar populations would decrease with increasing dust attenuation. As we move to higher redshift the CSFH evolution track with zero dust does not accurately trace the whole star forming population therefore this clearly indicates that the star forming progenitors contain significant amounts of dust.

In Figure 4.2 we examine the dust extinction properties of the progenitor galaxy sample. In Figure 4.2 the progenitor galaxies are colour coded to represent their dust extinction at $2800\,\text{Å}$ (A2800) measured from the UV slope. The uniformity of the passive objects in Figure 4.2 arises from the method we used to derived the dust correction for these objects (see section 3.2.5.2). Of the objects that are selected as star forming

systems we find that at $z > 1.5$ there is a wide population of objects from dust poor objects lying towards the bottom left hand corner to highly dust attenuated systems lying towards the top right hand corner as expected for UVJ colour selection. The total star forming population at $z > 1.5$ has an average $2800(\text{Å})$ dust correction of 3.7 mag.

Of the dust poor objects we see a marked evolution over the redshift range of $1.5 < z < 3.0$, with these systems being abundant at $z < 2.5$, with $28 \pm 4\%$ of star forming galaxies with $V - J < 1.0$, and decreasing towards $z = 1.5$, where only $6 \pm 2\%$ of star forming galaxies have $V - J < 1.0$. We also find that a small population, $10 \pm 4\%$, of the star forming progenitors show rest-frame $U - V$ colours redder than the quiescent progenitors and at $z > 2.5$ these objects span a wide range of rest frame colour values. Examining the UV slope derived dust corrections for the star forming population we find that the fraction of highly dust attenuated systems increases with redshift, similar to the result before. $5 \pm 3\%$ of the star forming population at $z = 3$ have $A_{2800} > 5$ mag increasing to 14 ± 4 at $z = 1.5$. This is accompanied by a decrease in the low dust attenuated systems, with $12 \pm 3\%$ of the star forming population with $A_{2800} < 2$ mag at $z = 3$ decreasing to $2 \pm 2\%$ at $z = 1.5$. This suggests that the star forming progenitors at this redshift contain a wide range of dust and star formation properties unlike their low redshift descendants (see also Whitaker *et al.* 2012a, Kaviraj *et al.* 2013). We explore this in more detail in relation to the stellar mass of these systems.

4.4.2 Evolution in Colour vs Stellar Mass

As highlighted in the previous section, the progenitors of local massive galaxies at low redshift have similar colours, typical of quiescent and old stellar populations. As we look towards higher redshifts, some of the progenitors become star forming. We find that some of the star forming progenitors exhibit a wide range of $U - V$ colours. We examine this result in a different way in Figure 4.3 using the $U - V$ rest frame colour versus stellar mass. Figure 4.3 shows the star forming and quiescent samples selected in the same way as in Figure 4.1. The red dashed line shows the 95% stellar mass completeness limit within each redshift interval. The blue points show the star forming progenitors with the median of this population represented by the black plus

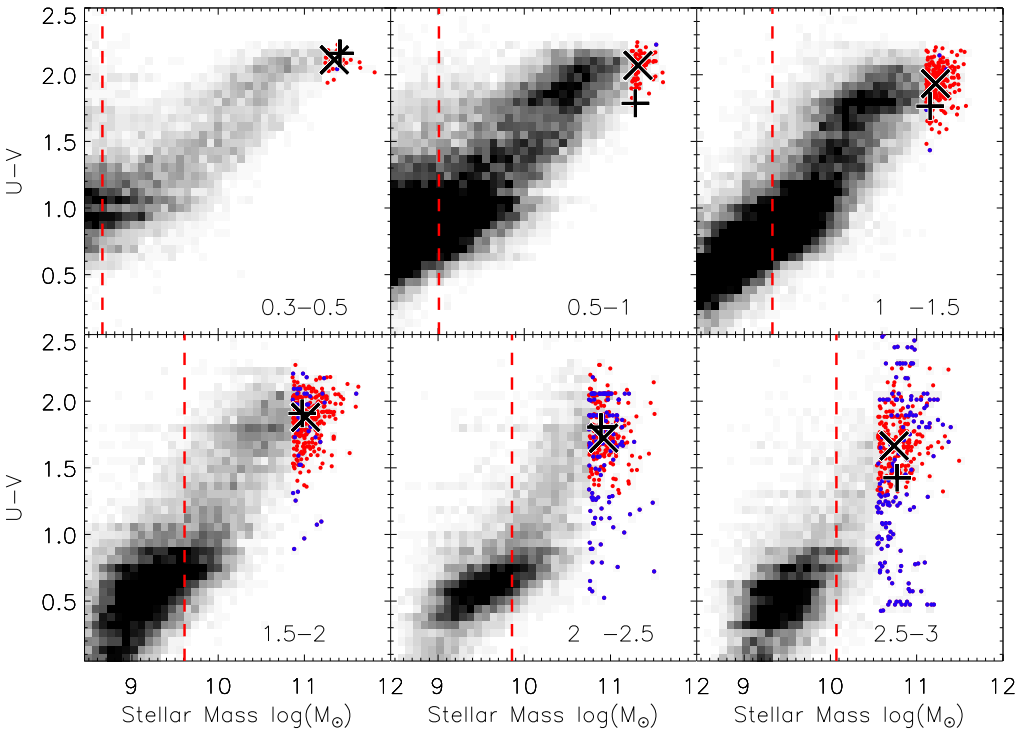

Figure 4.3: Stellar mass versus rest frame $U-V$ colour for all galaxies selected via the C-GaND selected sample with $n = 1 \times 10^{-4}\mathrm{Mpc}^{-3}$. The red circles show the progenitors of massive galaxies that are selected as passive via the UVJ method. The blue circles show the progenitors of massive galaxies that are selected as star forming via the UVJ method. The black "X" shows the median $U-V$ colour for the passive population and the black plus sign shows the median $U-V$ colour for the star forming population. The greyscale shows the whole UDS galaxy sample within each redshift bin. The red dashed line shows the 95% stellar mass completeness limit.

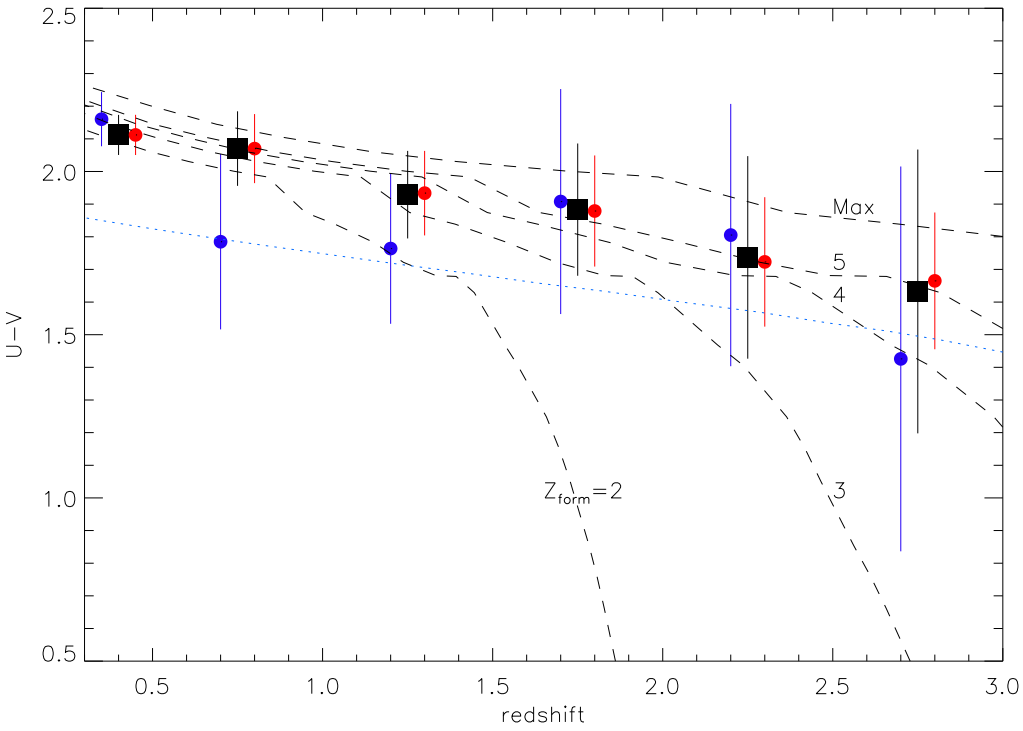

Figure 4.4: Median Rest-frame $U-V$ colour versus redshift of the C-GaND selected sample. The black squares show the evolution of the median $U-V$ colour of the whole progenitor population. The red and the blue circles show the evolution of the median $U-V$ colour of the passive and star forming samples respectively. Also shown is the colour evolution tracks from Bruzual & Charlot (2003) models. The black dashed lines show the colour evolution of a declining star formation history and varying formation redshifts from the beginning of the Universe (Max) to $\mathrm{Z_{form}} = 2$. The light blue dotted line shows the colour evolution of a constant star formation history and $A_{\mathrm{v}} = 2$ mag of dust extinction. This level of dust extinction is equivalent to the average dust correction of the star forming progenitors.

sign. The red points show the quiescent progenitors with the median of this population represented by the black X. The greyscale show the total galaxy population within each redshift interval.

We find that the lowest redshift population of massive galaxy progenitors have very small scatter in both colour (~ 0.08 mag) and stellar mass, with the scatter increasing to higher redshifts. However the median points for both the star forming and passive population do not show a large evolution, with the median $U-V$ colour of the star forming progenitors increasing by 0.7 ± 0.6 mag and the median colour for the passive progenitors increasing by 0.5 ± 0.2 mag. Figure 4.3 demonstrates that the average star forming progenitor has a similar optical colour as a passive progenitor at the same redshift. Figure 4.3 also shows that the average star forming progenitor has not lived in the blue star forming cloud at least since $z = 3.0$.

However, upon examining the population of star forming progenitors in more detail we find, 27% at $z = 3.0$ display blue, $U - V < 1.0$, colours comparable to galaxies living on the $z = 3.0$ blue cloud. Conversely, 24% of the star forming progenitors at $z = 3.0$ also have extreme red, $U - V > 2.0$, colours. Of all the progenitor galaxies $z = 3.0$ that have extreme red colours the star forming progenitor galaxies are more numerous than passive UVJ selected progenitors by a ratio of $3:1$. The larger scatter in $U-V$ colours of the star forming progenitors is more pronounced than in the passive progenitors i.e. 0.6 mag for star forming and 0.2 mag for passive at $z = 3.0$. The evolution in scatter between low and high redshift shows that the local red sequence is in the process of assembly between $0.3 < z < 3.0$.

In Figure 4.4 we show how the median $U-V$ colours for the total (black squares), star forming (blue circles) and, passive (red circles) evolve with redshift. Also plotted are the $U-V$ colour evolution tracks derived from Bruzual & Charlot (2003) SSP models with DSFH as shown in Figure 4.1 plotted in black dashed lines and one with CSFH with $A_{\rm v} = 2$ mag of dust extinction, comparable to the average dust correction of the star forming population, shown by the light blue dotted line. The tracks shown are of varying formation redshift from the beginning of the Universe (Max) to $\rm Z_{form} = 2$. The total population progenitors show a gradual evolution in their $U-V$ colours towards redder colours at lower redshifts, indicative of an ageing stellar population that formed

at, from the evolution tracks, redshifts of $z > 4$. Dividing the population into star forming and passive we find that the passive population follow the passively evolving colour tracks with hints that they may have stopped actively forming stars by $z = 5$. The effect of increasing dust extinction would be to decrease the formation redshift. While the star forming population appears to be following the declining star formation history colour evolution tracks, they are also consistent with the dust reddened constant star formation history colour evolution track. However, from Figure 4.1 we see that they are not consistent with the DSFH when examined in combination with other colours.

This result hints that this population has formed the majority of their $z = 3$ stellar mass (on average $\log M_* = 10.85$) within the first Gyr of cosmic time. Is this plausible given our knowledge of the global cosmic star formation history? If we assume these objects formed their $z = 3$ stellar masses over the redshift range $5 < z < 9$ (~ 0.6 Gyr) via star formation, the average SFR this implies is $114\,\mathrm{M_\odot yr^{-1}}$. Incorporating the number density of the progenitor galaxies, $n = 1 \times 10^{-4}\,\mathrm{Mpc^{-3}}$, gives a SFR density of these objects of $\rho_{\mathrm{SFR,progenitors}} = 0.01\,\mathrm{M_\odot yr^{-1} Mpc^{-3}}$. From various works (e.g. Duncan *et al.* 2014, McLure *et al.* 2013) the global cosmic SFR density over the redshift range $5 < z < 9$ varies from $\rho_{\mathrm{SFR,cosmic}} = 0.05 \pm 0.03\,\mathrm{M_\odot yr^{-1} Mpc^{-3}}$ at $z = 5$ to $\rho_{\mathrm{SFR,cosmic}} = 0.02 \pm 0.06\,\mathrm{M_\odot yr^{-1} Mpc^{-3}}$ at $z = 9$. As the global cosmic SFR density is larger than the SFR density inferred for the progenitor galaxies, it is therefore possible for these objects to form via star formation within the first Gyr of cosmic time.

4.4.3 Star Formation History

Using our knowledge from the previous sections we now examine how and when the progenitors of the local massive galaxies became the quiescent objects we see today.

Figure 4.5 shows the average specific star formation rate (sSFR, SFR/M_*) of the total, star forming and, passive progenitor galaxies have evolved from $z = 3.0$. The blue circles show the median sSFR of the UVJ selected star forming progenitor galaxies, the red circles show the median sSFR of the UVJ selected passive progenitor galaxies and, the black squares show how the median sSFR of the whole population evolves

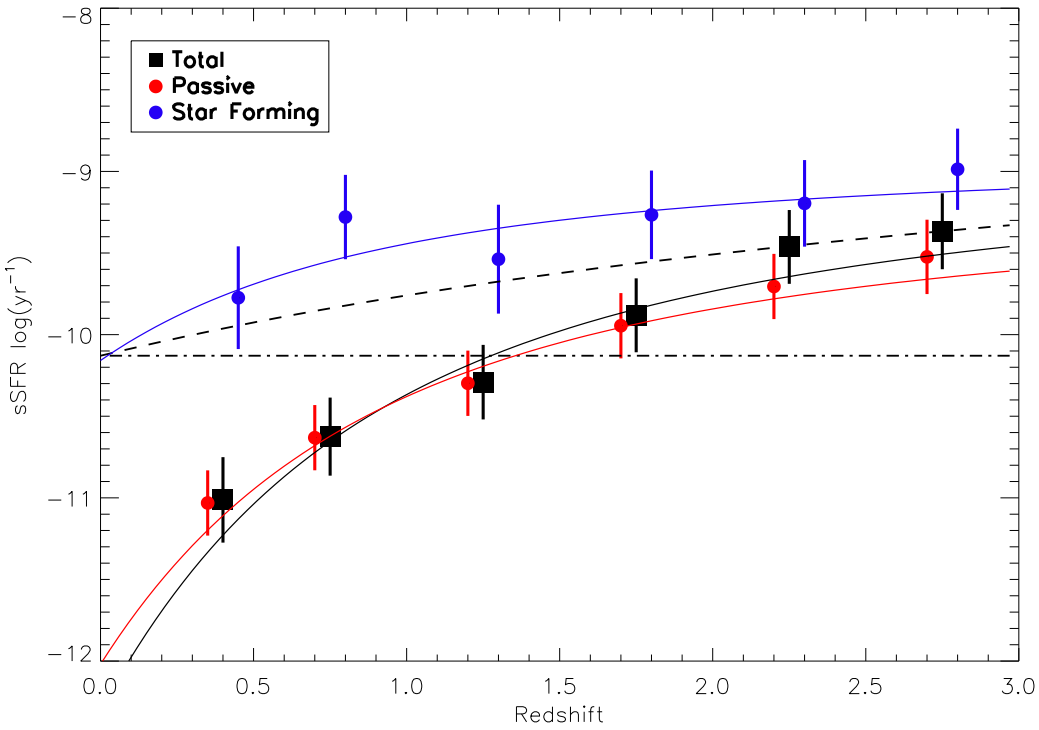

Figure 4.5: sSFR versus redshift for all galaxies selected via the C-GaND selected sample with $n = 1 \times 10^{-4}\mathrm{Mpc}^{-3}$. Black squares show the evolution of the whole population. Red circles show galaxies that are selected as passive via the UVJ method. Blue circles show galaxies that are selected as star forming via the UVJ method. The dot-dashed line represents a stellar mass doubling time equal to the age of the universe at $z = 0$. The dashed line represents a stellar mass doubling time equal to the age of the universe at z. The solid red, blue and black lines show the best fit exponentially declining star formation histories for the passive, star forming and total progenitor population respectively. The errors of the fractions are derived from Monte Carlo analysis.

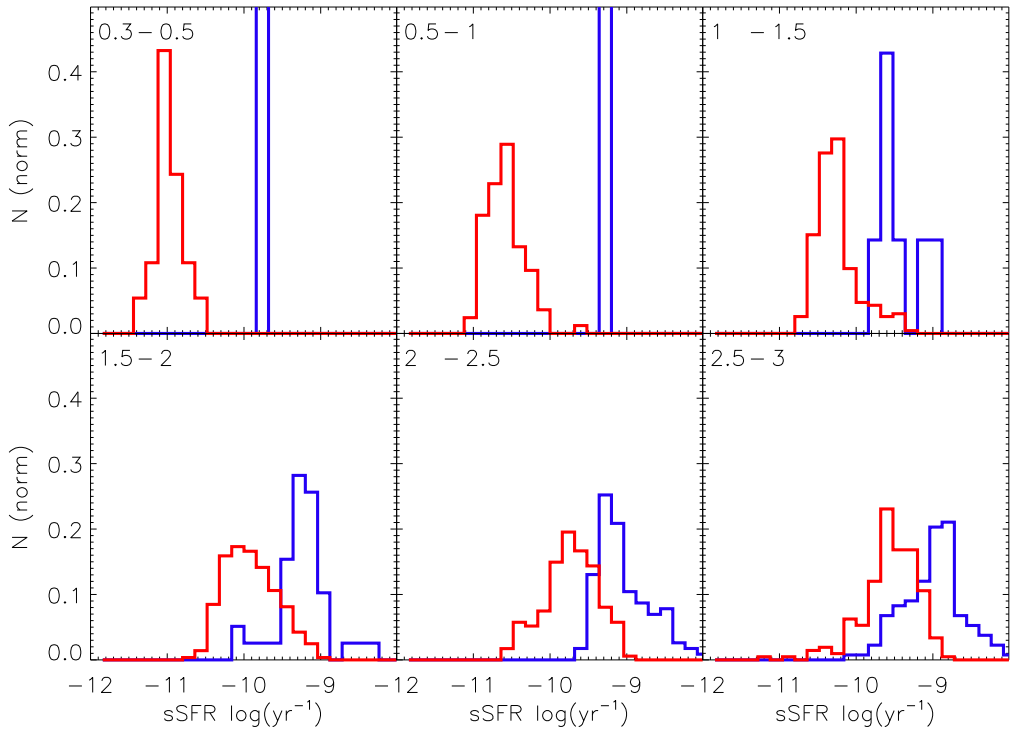

Figure 4.6: Histograms of the sSFRs of the UVJ defined passive and star forming progenitor galaxies over the redshift range $0.3 < z < 3.0$ split into six redshift bins. The red histogram shows the sSFRs of the progenitors of local massive galaxies that are defined as passive via UVJ colour selection and blue shows those that are classified as star forming. Both the passive and star forming histograms are normalised to the number of objects in each selection.

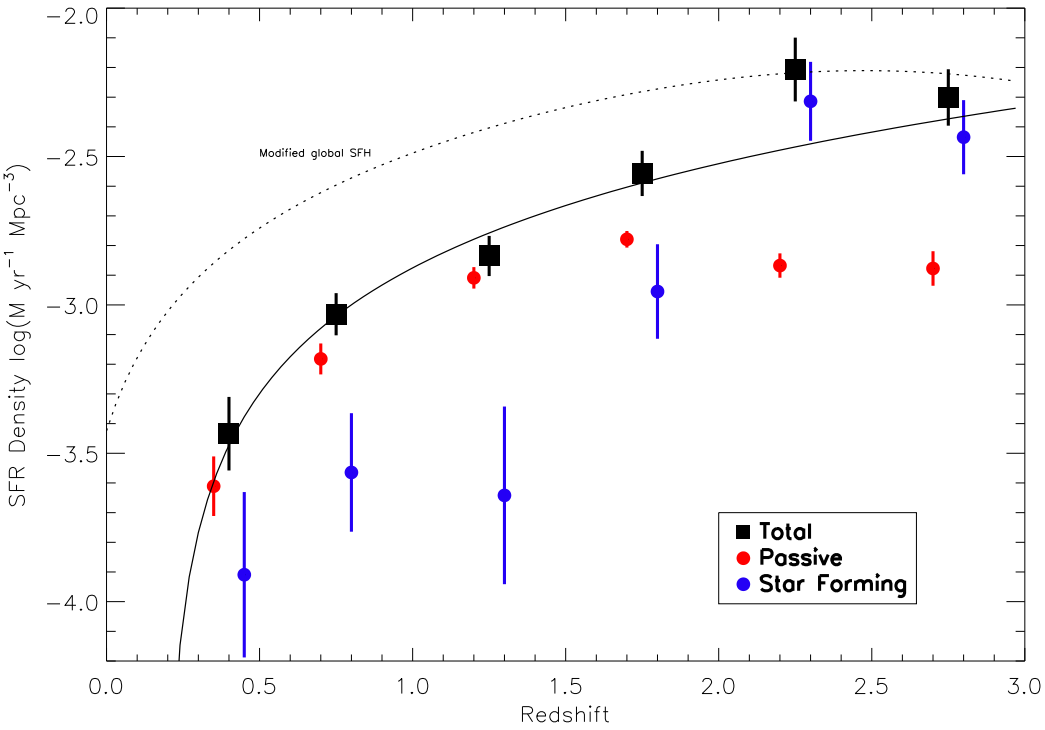

Figure 4.7: Star formation density versus redshift for all galaxies selected via the C-GaND selected sample with $n = 1 \times 10^{-4}\mathrm{Mpc}^{-3}$. The black squares show the evolution of the whole galaxy sample and red and blue circles show the evolution of the star formation density of the passive and star forming populations selected vis UVJ colours. The errors of the densities are derived from Monte Carlo analysis. The dotted line shows the global star formation history from Hopkins & Beacom (2006) modified by -1.5 dex for clarity. The solid black line represents the best fit to the star formation density evolution of the total progenitor galaxy population.

across this redshift range. Also shown in Figure 4.5 are lines denoting different stellar mass doubling times, i.e. the time it to takes for ongoing SFR to double the stellar mass of a given galaxy. The dot-dashed line denotes a doubling time equal to the age of the Universe at $z = 0$, a passivity selection made in the local Universe. The dashed line shows a doubling time equal to the age of the Universe at z. We note that the doubling time equal to the age of the Universe at z appears to be a good dividing line between UVJ passive and star forming systems. We find that the evolution of the sSFRs of the passive progenitor galaxies is more apparent than for star forming systems. The passive progenitor galaxies median sSFR decreases with redshift by 1.5 ± 0.3 dex from $z = 3.0$. The star forming progenitor galaxies median sSFR also decreases over the same time interval by only 0.8 ± 0.4 dex. If we examine the divide between the two populations, at low redshifts the difference in sSFR is more pronounced than at higher redshifts, with $\Delta\mathrm{sSFR} = 1.2 \pm 0.2$ dex at $z = 0.3$ and $\Delta\mathrm{sSFR} = 0.5 \pm 0.4$ dex at $z = 3.0$. We quantify the sSFR histories of the progenitor galaxies by fitting an exponentially declining model of the form:

$$sSFR(t) = sSFR_0 \times \exp(-\mathrm{t}/\tau) \tag{4.1}$$

with $\tau = 1.9 \pm 0.8$ Gyr for the total progenitor galaxy population, $\tau = 2.1 \pm 0.4$ Gyr for the passive objects and $\tau = 4.7 \pm 0.5$ Gyr for the star forming objects. The larger value of τ for the star forming sample, compared to the passive objects, is as expected for a star forming population.

Using our knowledge of the sSFRs of the progenitor galaxies in Figure 4.6 we examine validity of the UVJ colour selection. Figure 4.6 shows the normalised histograms of the passive and star forming populations as defined via the UVJ colour selections across the redshift range we study. We find that both populations appear to be single peaked distributions across the redshift range studied with increasing overlap towards higher redshifts. Therefore, due to the lack of a sSFR bimodality signature in the histograms of both populations at all redshifts the UVJ colour selection appears to be an effective measure in separating the two populations.

We also examine the evolution of the SFR density of the progenitors of local massive galaxies. Figure 4.7 shows the evolution of the SFR density with redshift. The black squares show the evolution of the total progenitor population and the red and blue

circles show the passive and star forming objects respectively. Also shown in Figure 4.7 is the global SFR history (SFH) from Hopkins & Beacom (2006) with the form of Cole *et al.* (2001), $\rho(t) = (a + bz)h/(1 + (z/c)^d)$ with $a = 0.017$, $b = 0.13$, $c = 3.3$, $d = 5.3$. The solid black line shows the best fit to the total progenitor population with the same form as the global SFH. We do not fit the SFR density evolution of the passive and star forming populations as their evolution is driven by their individual abundances as well as their star formation history. Therefore, the evolution of the passive and star forming SFR densities will not trace the same objects at all redshifts. We find that the progenitors of local massive galaxies appear to undergo a sharper decrease in their SFR density than the global galaxy population SFH. They also show evidence that their SFH peaks at a higher redshift than the global galaxy population SFH. Both of theses findings are evidence for the downsizing scenario of galaxy formation.

4.4.4 Passive Fraction Evolution

In Figure 4.8 we show evolution of the UVJ defined passive fraction of the progenitors of local massive galaxies. The black circles shows the fraction of galaxies that are selected as passive via this work. The black dashed line is the best fit to the fraction with the form:

$$F_{passive} = 1.0 - 0.02 \times \mathrm{e}^{1.2\times \mathrm{z}} \tag{4.2}$$

We find that the passive fraction of progenitor galaxies undergoes a significant evolution over the redshift range of $0.3 < z < 3.0$. Within our lowest redshift bin $94 \pm 8\%$ of the progenitor galaxies are passive, much like their local universe descendants. In our highest redshift bin $57 \pm 7\%$ of the progenitor galaxies are passive. This implies that over half of the progenitors of todays massive galaxies had already stopped actively star forming by $z = 3.0$.

The observed weakening of the colour-density relation at $z > 2$ (e.g. Chuter *et al.* 2011, Grützbauch *et al.* 2011) implies that the environments of galaxies have not been fully established at high redshift. Therefore, the role of environmental quenching mechanisms, such as ram pressure stripping, may not play a dominant role in the quenching of the progenitors of local massive galaxies at early cosmic times. The result that we present here shows that a large fraction of galaxies are already passive by

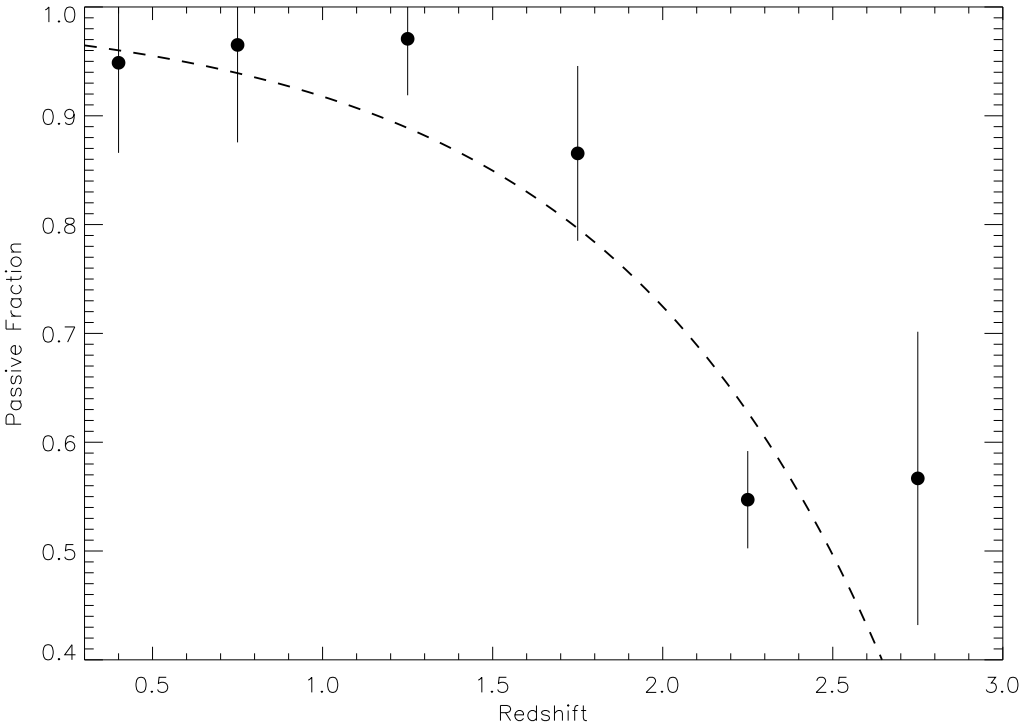

Figure 4.8: Passive fraction of the C-GaND selected sample with $n = 1 \times 10^{-4}\mathrm{Mpc}^{-3}$ vs redshift. Black circles denote the fraction of galaxies selected as passive via the UVJ method. The black dashed line is the best fit to the passive fractions with the equation: $F_{\mathrm{passive}} = 1.0 - 0.025 * \mathrm{EXP}(1.2 * \mathrm{z})$. The errors of the fractions are derived from Monte Carlo analysis.

Table 4.1: C-GaND average galaxy effective radius. Local ETG size derived from Shen et al. (2003) at the same stellar mass.

z	Average size (kpc)	Local ETG size/Average size
$0.3-0.5$	6.7 ± 1.1	$1.2\pm^{+0.2}_{-0.2}$
$0.5-1.0$	5.6 ± 1.0	$1.4\pm^{+0.3}_{-0.2}$
$1.0-1.5$	3.8 ± 0.9	$1.8\pm^{+0.5}_{-0.3}$
$1.5-2.0$	3.2 ± 0.9	$1.7\pm^{+0.7}_{-0.4}$
$2.0-2.5$	2.9 ± 0.9	$1.6\pm^{+0.8}_{-0.4}$
$2.5-3.0$	2.5 ± 0.9	$1.6\pm^{+0.9}_{-0.4}$

$z = 3.0$ and implies that internal quenching mechanisms, such as the hot halo model, could be responsible.

4.4.5 Structural Parameter Evolution

In this section we investigate various structural parameter properties and their evolution over time of the progenitors of local massive galaxies using number density selection techniques.

4.4.5.1 Galaxy Size

Many papers examining the sizes of high redshift massive galaxies have found that on average their sizes are smaller, by a factor of between $2-4$, than present day galaxies of equal mass (e.g.Daddi *et al.* 2005, Trujillo *et al.* 2007, Buitrago *et al.* 2008, Cimatti *et al.* 2008, van Dokkum *et al.* 2008, 2010, Franx *et al.* 2008, van der Wel *et al.* 2008, Damjanov *et al.* 2009, Carrasco, Conselice & Trujillo 2010, Newman *et al.* 2010, Szomoru *et al.* 2011, Weinzirl *et al.* 2011, Lani *et al.* 2013). This size evolution has been found to be most pronounced when linking high redshift passive massive galaxies to the passive massive galaxies in the local universe. This observed size evolution could be produced through various processes such as AGN feedback (e.g. Fan *et al.* 2008), mergers (e.g. Khochfar & Silk 2006), and star formation (e.g. Dekel, Sari & Ceverino 2009, Ownsworth *et al.* 2012, Ownsworth *et al.* 2014). Another possible suggestion is that there is an inherent bias in the selection methods used in previous works that could enhance apparent observable size growth. It has been suggested that number density selection techniques could be a solution to this problem (e.g. Poggianti *et al.*

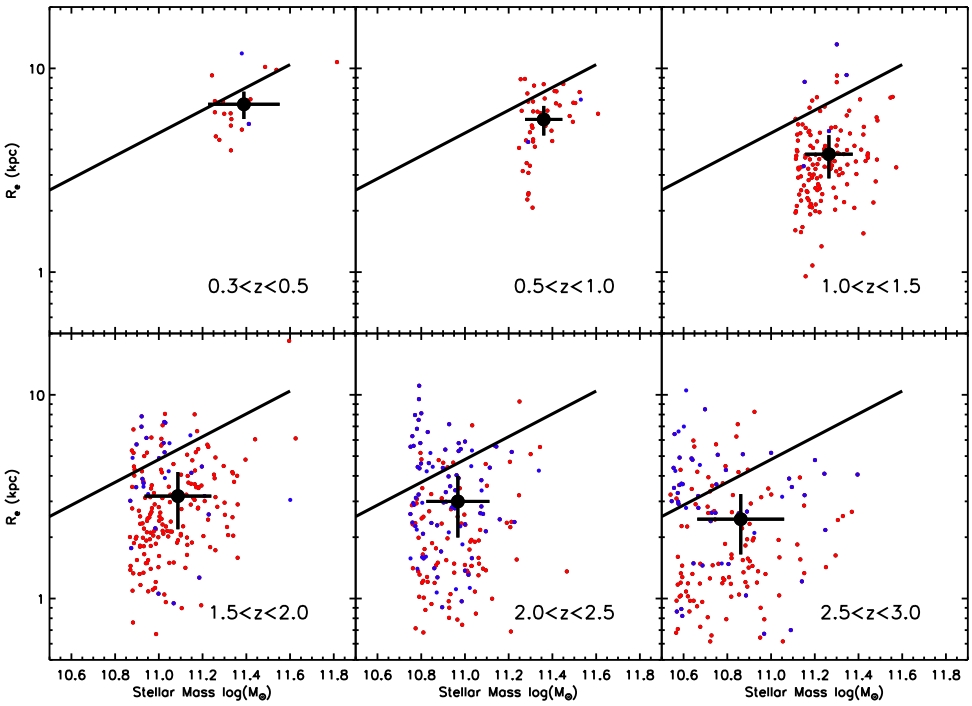

Figure 4.9: Galaxy size (effective radius) versus total stellar mass for the progenitor galaxy sample. The black line denotes the local early type galaxy relation modified from Shen et al. (2003). Within each redshift bin are plotted all the galaxies that reside within that redshift range (small circles) and the average stellar mass and size (large circle) with errors derived from Monte Carlo analysis within each redshift bin.

2013). For example van Dokkum *et al.* (2010) investigated the size evolution within a constant number density selection over the range $0 < z < 2$, finding that the average galaxy size still increases by a factor of four.

Most of these studies have examined size evolution using a cut in galaxy stellar mass in order to link galaxies across redshift. This method does not account for the stellar mass growth of galaxies that are below the stellar mass selection cut at high redshift. The number density selection techniques employed in this chapter compensates for this, and can give us a cleaner sample of the progenitors of local massive galaxies. Using this sample of progenitor galaxies we can examine the size evolution in a more robust way.

Using the direct progenitor galaxy sample we investigate the evolution of the sizes of the progenitors of massive galaxies from $z = 3.0$ to $z = 0.3$. We do this by applying no passivity or morphological selection criteria to the sample and measure the size evolution of all the progenitor galaxies. As shown from this work a large fraction of the progenitors of local massive galaxies are highly star forming at high redshift and also appear to undergo a morphological change from disk-like to spheroid-like systems within the redshift range studied (Buitrago *et al.* 2013, Mortlock *et al.* 2013).

Figure 4.9 shows the effective radius versus total stellar mass of the whole progenitor galaxy sample split up into six redshift bins. In each bin we plot the galaxies that lie within the bin (small circles) and the average of the sample in both stellar mass and size (large circle with error bars). The solid back line denotes the local early type galaxy relation modified from Shen *et al.* (2003). We compare the average galaxy size at each redshift to the local early type galaxy relation. We do this as the majority of the most massive galaxies lie on this relation in the local universe. When we compare the average points in each redshift bin to the local relation we find that all the progenitor galaxies are smaller than equal mass early type galaxies in the local universe, ranging from a factor of 1.8 to 1.2 over the redshift range studied.

Table 4.1 lists the average sizes of the progenitor galaxies and the ratio of the local size of an early type galaxy of the same stellar mass to the average size in each redshift bin. This would seem to be in disagreement with van Dokkum *et al.* (2010), however this could be due to differences between the selection techniques used. We find that the

size evolution of a galaxy sample selected this way is on average slightly lower than the findings of other investigations into the size evolution of massive galaxies which have found that they grow in size by a factor of $2-4$ from redshift $z=3.0$ to the present day.

4.4.5.2 Sérsic Index

The present day massive galaxy population is dominated by objects with early-type morphologies and high Sérsic indices (e.g. Baldry *et al.* 2004, Conselice 2006b, Buitrago *et al.* 2013). Examining similar stellar mass objects at $z>2$ studies have found this not to be the case (Mortlock *et al.* 2013, Buitrago *et al.* 2013, Bruce *et al.* 2014). However, this has not been examined using a number density selected sample.

In Figure 4.10 (a) we show the evolution of the Sérsic indices of the progenitors of local massive galaxies. The progenitor galaxies have been split into high and low Sérsic index systems with a dividing line at $n=2.5$. The value of $n=2.5$ has been used in many studies as a quantitative way to segregate between early and late type galaxies, with early type galaxies having $n>2.5$ (e.g. Shen *et al.* 2003, Barden *et al.* 2005, McIntosh *et al.* 2005, Buitrago *et al.* 2013). The fraction of progenitors with high Sérsic indices is represented by green rectangles and the fraction with low Sérsic indices is represented by black circles. Figure 4.10 (a) clearly indicates that the fraction of the progenitors of local massive galaxies with lower Sérsic indices has greatly increased with redshift, eith $8\pm5\%$ of the progenitor galaxies at $z=0.3$ with low Sérsic indices increasing to $65\pm7\%$ at $z=3$.

If we take the assumption that objects with low Sérsic indices have a disk-like, late-type morphology this result implies that the progenitor galaxies at high redshift are mostly disky galaxies. However, this assumption breaks down if we consider the effect of galaxies with disturbed and irregular morphologies. Both Buitrago *et al.* (2013) and Mortlock *et al.* (2013) showed that galaxies at high redshift with low Sérsic indices also display disturbed morphologies when examined using visual classification. These studies also showed that the number of galaxies with disturbed visual morphologies increases dramatically with redshift, with $\sim 40\%$ of massive galaxies showing a disturbed morphology at $z=3$. This increase in the number of galaxies with disturbed morphologies could be linked to the increase in the importance of major mergers with

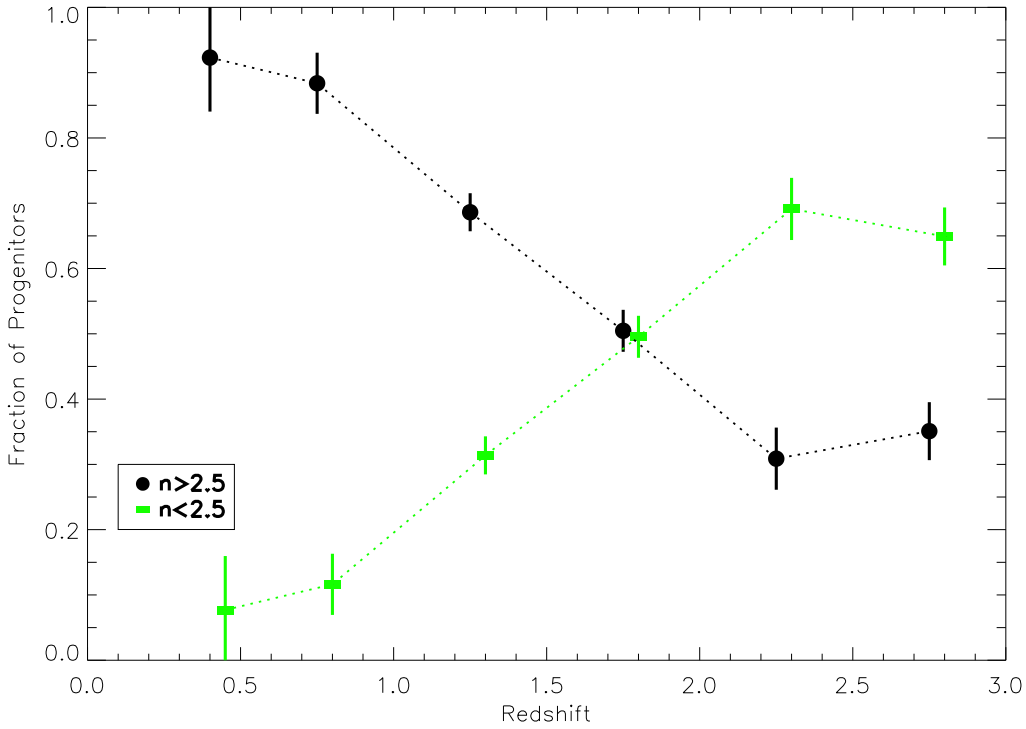

(a)

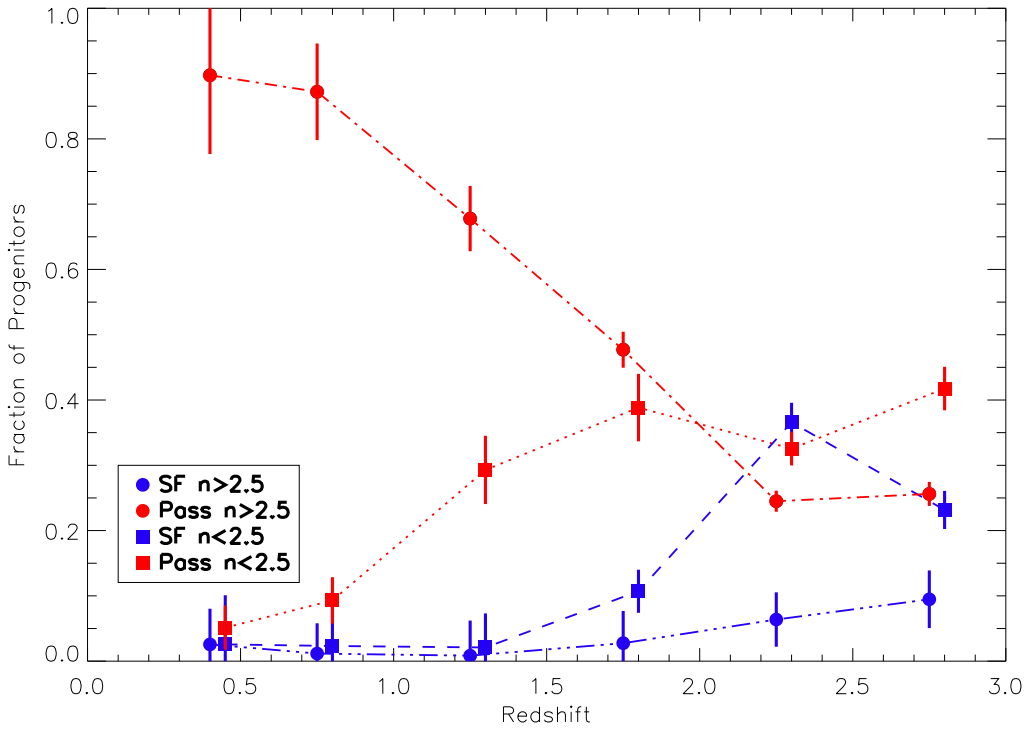

(b)

Figure 4.10: Fraction of the progenitors of local massive galaxies with high ($n > 2.5$) and low ($n < 2.5$) Sérsic indices. Figure (a) show the evolution of the whole progenitor sample with, green rectangles showing the fraction of progenitors with low Sérsic index and, black circles showing progenitors with high Sérsic light profiles as a function of redshift. Error bars are derived using Monte Carlo analysis. Figure (b) shows the high and low Sérsic populations split into star forming and passive systems.

redshift as explored in the previous chapter. Therefore, using just the Sérsic profile information we cannot determine if the progenitor galaxy population we present here are true disk or, disturbed galaxies. Using methods that examine the asymmetry in systems (e.g. CAS Conselice 2006a) could help disentangle disturbed from true disk galaxies at high redshift (see Mortlock *et al.* 2013 for more discussion).

Also from Figure 4.10 (a) we find that the redshift where the progenitor galaxies transition into the high Sérsic index dominated population we see in the local Universe is between $1.5 < z < 2.0$. This is in agreement with previous studies that have examined the morphological change of galaxies with similar stellar masses as our sample (e.g. Mortlock *et al.* 2013).

We further divide the high and low Sérsic progenitor samples into star forming and passive systems using our UVJ selection and present the results in Figure 4.10 (b). This figure shows the clear dominance at $z < 1.7$ of the passive high Sérsic index systems that we associate with massive galaxies in the local Universe. The population of high Sérsic index galaxies is, at all redshifts examined in this study, dominated by the passive population. The star forming high Sérsic index systems are most abundant at $z = 3.0$ however, only constitute $9 \pm 3\%$ of the total progenitor population. Examining the low Sérsic index systems we find that these objects are dominated at almost all redshifts by passive systems much like the high Sérsic index population. At $z = 3.0$, $41 \pm 4\%$ of the progenitor galaxies are passive and have low Sérsic indices and $23 \pm 3\%$ of the progenitor galaxies are star forming and have low Sérsic indices. This result implies that passive low Sérsic index systems out number star forming low Sérsic index systems by nearly a factor of two within the progenitor massive galaxy population. This result is surprising as the morphologies that constitute the low Sérsic index population are generally thought to be star forming. However, this result is in agreement with recent work by Bruce *et al.* (2014) using two component light profile fitting which has shown that a large fraction, $\sim 38\%$ of passive massive galaxies at $z > 1.5$ are disk-like dominated systems.

4.5 Summary

In this chapter we present a study of the evolution of a constant number density selected sample of the progenitors of today's massive galaxies over the redshift range of $0.3 < z < 3.0$. We examine the evolution of the properties of galaxy colour, location on the colour-stellar mass diagram, passivity and, structural parameters. We find the following:

- We find that the average $U - V$ and $V - J$ colours of the progenitors of local massive galaxies have been located within the UVJ defined passive region since at least $z = 3.0$. However the progenitors that are classified as star forming have a large scatter in both colours and in some case show redder colours than the passive galaxies at the same epoch. If we examine these galaxies using the colour-stellar mass diagram we also find that the average progenitor of local massive galaxies has not lived on the blue cloud since $z = 3.0$. Using stellar population models we find that the passive progenitor galaxies have old stellar ages (age > 5 Gyr) and appear to show hints that they have been passively evolving since $z = 5$.

- We examine how the the progenitor population becomes the passive population we see today over this redshift range. We find that the passive fraction of the progenitor galaxies undergoes significant evolution from $z = 3.0$, increasing from $56 \pm 7\%$ at $z = 3.0$ to $94 \pm 8\%$ at $z = 0.3$. This implies that over half of the population of the progenitors of local massive galaxies have already stopped forming stars by $z = 3.0$. Also the star formation density of the progenitors shows signs of galaxy formation downsizing.

- We also investigate the size evolution of the constant number density selected sample using no passivity cuts and find that the sizes of the progenitors of massive galaxies range from a factor of 1.8 to 1.2 smaller than local early type galaxies of similar mass over the redshift range studied. This is smaller than previous studies have found, quoting size evolution factors of two to four.

- The morphological evolution of the progenitor galaxies is also probed using the evolution of the Sérsic indices within the sample. We find that these galaxies

are dominated at high redshifts by low Sérsic index ($n < 2.5$) light profiles and evolve to be come high Sérsic index ($n > 2.5$) dominated objects by $z = 1.7$. We further split the high and low Sérsic populations into star forming and passive systems. We find that passive high Sérsic index systems are the most abundant objects at $z < 1.7$, equivalent to their descendants at low redshift. There exists a small population of star forming high Sérsic index objects at high redshift but they rapidly decrease towards low redshift. We also find that $41 \pm 4\%$ of the population within the highest redshift bin are passive low Sérsic index objects. This could imply that a significant proportion of the progenitor galaxies were passive disk-like systems at early times. However, this low Sérsic index trend could be being driven by the increase in the abundance of morphologically disturbed systems at higher redshifts.

To further this work large surveys such as the Hyper Supreme-Cam survey and future telescopes such as JWST, E-ELT and Euclid will be able to push these trends out to higher redshifts and be able to investigate the full history of local massive galaxies.

Chapter 5

Conclusions

At the beginning of this thesis we highlighted some of the open questions in astronomy. This thesis aimed to address some of these questions. In this chapter, we will summarise and discuss what we can conclude from this work about the evolution of massive galaxies.

5.1 Structural Evolution

In Chapters 2 and 4 we investigate the evolution of the structural parameters of massive galaxies.

5.1.1 Size

We show that the star formation distribution we observe at high redshift within massive galaxies, and its effects on galaxy light profiles, is not large enough to fully explain the observed galaxy size growth. The in-situ star formation distribution observed in these galaxies can only produce a small increase in the average effective radius. This increase can vary by using different evolution mechanisms, but is always insufficient to fully explain the observed evolution.

To further investigate this we explore the effect of stellar migration on the stellar mass profiles of massive galaxies, and find that this effect can increase the total effective

radius growth. However, this result is still unable to account for the total observed size evolution over the same epoch. From this we conclude that, due to the lack of sufficient size growth by star formation and stellar migration, other mechanisms must also be at work to account for the observed structural evolution from $z > 1$ to the present day.

In Chapter 4, we investigate the size evolution of the constant number density selected sample and find that the size evolution of the progenitors of massive galaxies is less pronounced than previous studies have found. This hints that the observed size evolution might not be as extreme as previously reported. Although the size evolution of massive galaxies might be milder, the contribution from star formation and stellar migration is still not large enough to reproduce the result.

5.1.2 Sérsic index

In Chapter 2, we explored the effect in-situ star formation has on the shape of massive galaxy light profiles. We find that the Sérsic index of the galaxy light profiles is marginally affected by the in-situ star formation, and that on average n decreases with redshift. This indicates that the star formation distribution present within massive galaxies at high redshift must follow a similar radial distribution as the stellar mass at high redshift. This also implies that star formation evolution has a minimal effect on structural evolution of massive galaxies between $z = 3$ and the present day. However, in Chapter 4 the full morphological evolution of the progenitors of local massive galaxies is probed using the evolution of the Sérsic indices within a constant number density selected sample. We find that the progenitor galaxies are dominated at high redshifts by low Sérsic index ($n < 2.5$) light profiles and evolve to become high Sérsic index ($n > 2.5$) dominated objects by $z \simeq 1.7$. Therefore, we must conclude similarly to the previous section, that star formation cannot fully reproduce the observed change in the profiles of massive galaxies from $z = 3$ to the local universe.

To further investigate this evolution in Chapter 4 we split the high and low Sérsic populations into star forming and passive systems. We find that passive high Sérsic index systems are the most abundant objects within the progenitor galaxy sample at $z \lesssim 1.7$. This shows that the local massive galaxies already resemble their massive galaxy descendants at low redshift by $z \simeq 1.7$. There also exists a small population

of star forming high Sérsic index objects at high redshift but their number rapidly decrease towards low redshift. We also find that a large fraction of the population within our highest redshift bin are passive low Sérsic index objects. This could imply that a significant proportion of the progenitor galaxies were passive disk-like systems at early times. However, this low Sérsic index trend could be driven by the increase in the abundance of morphologically disturbed systems at higher redshifts as shown by previous studies.

5.2 Stellar Mass Evolution

In Chapter 3 we investigate the roles of star formation, major, and minor mergers in relation to the total stellar mass growth of a constant number density selected galaxy sample within the redshift range of $0.3 < z < 3.0$.

We find that massive galaxies in the local universe assemble the majority of their total present day stellar mass between $0.3 < z < 3.0$. This stellar mass is built up mainly through merger events. More precisely, over half of the total stellar mass of massive galaxies at $z = 0.3$ arises from merger events and a quarter arises from star formation between $0.3 < z < 3.0$. This result implies that at least half of the total stellar mass of local massive galaxies is formed externally and then accreted at later times.

5.2.1 Merger Rates

Using previous research in the major merger rates of massive galaxies in the high redshift universe, we disentangle the two merger processes of major and minor mergers to the total stellar mass growth. From this we find that the minor merger rate of the progenitors of local massive galaxies has been increasing with time since $z = 3.0$. Minor mergers from $z = 3.0$ contribute 34% of the total stellar mass of local massive galaxies whereas, major mergers only contribute 17%. This is converse to what other studies have implied, finding that major mergers could be the main contributor to the stellar mass growth of massive galaxies over this redshift range. We examine the two merger rates across the redshift range of $0.3 < z < 3.0$. We find that minor mergers are

the dominant form of stellar mass growth at $z < 1.0$ and, major mergers are at no point the dominant form of stellar mass growth between $0.3 < z < 3.0$. This is due to the increasing importance of the stellar mass added via star formation as we look back in time, which is the dominant form of stellar mass growth for the progenitors of massive galaxies at $z > 2$. This is important from the perspective of the size growth examined earlier as minor mergers are the current favoured mechanism to explain galaxy size evolution.

From these results we explored the implications of the stellar mass growth on the cold gas accretion rate. We use the global Schimidt-Kennicutt relation to show that the cold gas accretion history of the progenitor galaxies decreases with cosmic time from an high average cold gas accretion rate of at $z = 3.0$ to negative accretion rates in the lowest redshifts investigated. This negative accretion is consistent with zero cold gas accretion, however negative cold gas accretion rates could due to processes actively expelling gas from the host galaxy such as AGN.

5.3 Colour Evolution

In Chapter 4 we explore the evolution of the properties of a constant number density selected sample of the progenitors of today's massive galaxies over the redshift range of $0.3 < z < 3.0$.

We find that the average progenitor of local massive galaxies have $U - V$ and $V - J$ colours consistent with them being passive since at least $z = 3.0$. This result can also be seen if we examine the passive fraction of the sample and find over half are passive at $z = 3.0$, increasing towards lower redshifts. Therefore, the majority of the progenitors of local massive galaxies must have undergone some form of quenching at $z > 3.0$. If we examine the progenitor galaxies using the colour-stellar mass diagram we also find that the average progenitor of local massive galaxies has not lived on the blue cloud since $z = 3.0$. This suggests that massive galaxies must form quickly in the early Universe. With the observed weakening of environmental signatures towards higher redshifts, this result could imply that that internal quenching mechanisms, such as the hot halo model or AGN feedback, could be responsible for quenching the progenitors

of local massive galaxies at early cosmic times.

Splitting the progenitor galaxy sample into passive and star forming using their UVJ colours we still find the same results with both populations. However, a small fraction of the star forming progenitors do show colours consistent with objects on the blue cloud within the same redshift interval. There also exists a population of star forming progenitors that exhibit redder $U - V$ colours than the passive progenitor population. This hints that the star forming progenitors of local massive galaxies at high redshift have a wide range of dust, star formation and stellar population properties, unlike their low redshift descendants. This indicates that a wide range of the properties of local massive galaxies must under go drastic evolution over the last 11 billion years.

5.4 Future Work

Needless to say, this work needs to be extended to earlier cosmic times to investigate the properties of the progenitors at $z > 3$. With astronomy entering an era where deep, large volume extragalactic surveys are routinely obtained, these trends can begin to be probed at even earlier cosmic times. Several studies have already given us hints at how galaxies form and evolve in the early universe (e.g. Papovich *et al.* 2011, McLure *et al.* 2013, Bowler *et al.* 2014, Duncan et al. 2014 Submitted) allowing us to begin to explore the stellar mass growth and star formation rates of massive galaxies at early cosmic times. With these and future studies the galaxy number statistics at high redshift are constantly increasing thus making it possible to further examine and constrain the galaxy evolutionary paths. This will be greatly enhanced by the next generation of ground and space based telescopes, such as the JWST.

With the advent of Integral Field Units (IFUs) and adaptive optics on large ground based telescopes we can begin to observe the internal kinematics of galaxies. The data IFUs provide can measure the rotational and the velocity dispersion support for a galaxy, and thus provide us information on both baryonic and dark matter components, as well as the presence of rotation. This allows us to address the question of how morphology and galaxy assembly are linked. In the low redshift universe large IFU surveys such as the SAURON survey (de Zeeuw *et al.* 2002) and the ATLAS 3D

survey (Cappellari *et al.* 2011) have opened a new perspective on the kinematics of local massive galaxies, with a significant fraction of early-type galaxies found to host large angular momentum supported disk-like components (e.g. Krajnović *et al.* 2013). Could this be a link to their high redshift progenitors that, in Chapter 4, we find appear to have low Sérsic indices? The future of IFUs on large current and future telescopes, such as HARMONI on the E-ELT, will allow for deep observations of multiple high redshift objects and begin to answer these questions.

Bibliography

Ade P. A. R., Aghanim N., Armitage-Caplan C., Arnaud M., Ashdown M., Atrio-Barandela F., Aumont J., Baccigalupi C., Banday A. J., et al., 2013. *ArXiv e-prints*. *Planck 2013 results. XVI. Cosmological parameters*.

Baldry I. K., Glazebrook K., 2003. *ApJ*, **593**, 258. *Constraints on a Universal Stellar Initial Mass Function from Ultraviolet to Near-Infrared Galaxy Luminosity Densities*.

Baldry I. K., Glazebrook K., Brinkmann J., Ivezić Ž., Lupton R. H., Nichol R. C., Szalay A. S., 2004. *ApJ*, **600**, 681. *Quantifying the Bimodal Color-Magnitude Distribution of Galaxies*.

Baldry I. K., Balogh M. L., Bower R. G., Glazebrook K., Nichol R. C., Bamford S. P., Budavari T., 2006. *MNRAS*, **373**, 469. *Galaxy bimodality versus stellar mass and environment*.

Barden M., Rix H.-W., Somerville R. S., Bell E. F., Häußler B., Peng C. Y., Borch A., Beckwith S. V. W., Caldwell J. A. R., Heymans C., Jahnke K., Jogee S., McIntosh D. H., Meisenheimer K., Sánchez S. F., Wisotzki L., Wolf C., 2005. *ApJ*, **635**, 959. *GEMS: The Surface Brightness and Surface Mass Density Evolution of Disk Galaxies*.

Barden M., Häußler B., Peng C. Y., McIntosh D. H., Guo Y., 2012. *MNRAS*, **422**, 449. *GALAPAGOS: from pixels to parameters*.

Barger A. J., Cowie L. L., Wang W.-H., 2008. *ApJ*, **689**, 687. *A Highly Complete Spectroscopic Survey of the GOODS-N Field1,*.

Bauer A. E., Conselice C. J., Pérez-González P. G., Grützbauch R., Bluck A. F. L., Buitrago F., Mortlock A., 2011. *MNRAS*, **417**, 289. *Star formation in a stellar mass-selected sample of galaxies to z= 3 from the GOODS-NICMOS Survey*.

Behroozi P. S., Marchesini D., Wechsler R. H., Muzzin A., Papovich C., Stefanon M., 2013. *ApJL*, **777**, L10. *Using Cumulative Number Densities to Compare Galaxies across Cosmic Time*.

Behroozi P. S., Wechsler R. H., Conroy C., 2013. *ApJ*, **770**, 57. *The Average Star Formation Histories of Galaxies in Dark Matter Halos from z = 0-8*.

Bell E. F., McIntosh D. H., Katz N., Weinberg M. D., 2003. *ApJS*, **149**, 289. *The Optical and Near-Infrared Properties of Galaxies. I. Luminosity and Stellar Mass Functions*.

Bell E. F., McIntosh D. H., Barden M., Wolf C., Caldwell J. A. R., Rix H.-W., Beckwith S. V. W., Borch A., Häussler B., Jahnke K., Jogee S., Meisenheimer K., Peng C., Sanchez S. F., Somerville R. S., Wisotzki L., 2004. *ApJL*, **600**, L11. *GEMS Imaging of Red-Sequence Galaxies at z∼0.7: Dusty or Old?*

Bertin E., Arnouts S., 1996. *A&AS*, **117**, 393. *SExtractor: Software for source extraction.*

Bertone S., De Lucia G., Thomas P. A., 2007. *MNRAS*, **379**, 1143. *The recycling of gas and metals in galaxy formation: predictions of a dynamical feedback model.*

Binney J., Tremaine S., 1987. *Galactic dynamics.*

Blanton M. R., Roweis S., 2007. *AJ*, **133**, 734. *K-Corrections and Filter Transformations in the Ultraviolet, Optical, and Near-Infrared.*

Blanton M. R., Hogg D. W., Bahcall N. A., Baldry I. K., Brinkmann J., Csabai I., Eisenstein D., Fukugita M., Gunn J. E., Ivezić Ž., Lamb D. Q., Lupton R. H., Loveday J., Munn J. A., Nichol R. C., Okamura S., Schlegel D. J., Shimasaku K., Strauss M. A., Vogeley M. S., Weinberg D. H., 2003. *ApJ*, **594**, 186. *The Broadband Optical Properties of Galaxies with Redshifts 0.02<z<0.22.*

Bluck A. F. L., Conselice C. J., Bouwens R. J., Daddi E., Dickinson M., Papovich C., Yan H., 2009. *MNRAS*, **394**, L51. *A surprisingly high pair fraction for extremely massive galaxies at z ∼ 3 in the GOODS NICMOS survey.*

Bluck A. F. L., Conselice C. J., Almaini O., Laird E. S., Nandra K., Grützbauch R., 2011. *MNRAS*, **410**, 1174. *On the co-evolution of supermassive black holes and their host galaxies since z= 3.*

Bluck A. F. L., Conselice C. J., Buitrago F., Grützbauch R., Hoyos C., Mortlock A., Bauer A. E., 2012. *ApJ*, **747**, 34. *The Structures and Total (Minor + Major) Merger Histories of Massive Galaxies up to z ∼ 3 in the HST GOODS NICMOS Survey: A Possible Solution to the Size Evolution Problem.*

Bolzonella M., Miralles J.-M., Pelló R., 2000. *A&A*, **363**, 476. *Photometric redshifts based on standard SED fitting procedures.*

Boquien M., Calzetti D., Combes F., Henkel C., Israel F., Kramer C., Relaño M., Verley S., van der Werf P., Xilouris E. M., HERM33ES Team, 2011. *AJ*, **142**, 111. *Dust Heating Sources in Galaxies: The Case of M33 (HERM33ES).*

Bournaud F., Chapon D., Teyssier R., Powell L. C., Elmegreen B. G., Elmegreen D. M., Duc P.-A., Contini T., Epinat B., Shapiro K. L., 2011. *ApJ*, **730**, 4. *Hydrodynamics of High-redshift Galaxy Collisions: From Gas-rich Disks to Dispersion-dominated Mergers and Compact Spheroids.*

Bourne N., Maddox S. J., Dunne L., Auld R., Baes M., Baldry I. K., Bonfield D. G., Cooray A., Croom S. M., Dariush A., de Zotti G., Driver S. P., Dye S., Eales S., Gomez H. L., González-Nuevo J., Hopkins A. M., Ibar E., Jarvis M. J., Lapi A., Madore B., Michałowski M. J., Pohlen M., Popescu C. C., Rigby E. E., Seibert M., Smith D. J. B., Tuffs R. J., Werf P. v. d., Brough S., Buttiglione S., Cava A., Clements

D. L., Conselice C. J., Fritz J., Hopwood R., Ivison R. J., Jones D. H., Kelvin L. S., Liske J., Loveday J., Norberg P., Robotham A. S. G., Rodighiero G., Temi P., 2012. *MNRAS*, **421**, 3027. *Herschel-ATLAS/GAMA: a census of dust in optically selected galaxies from stacking at submillimetre wavelengths*.

Bower R. G., Lucey J. R., Ellis R. S., 1992. *MNRAS*, **254**, 601. *Precision Photometry of Early Type Galaxies in the Coma and Virgo Clusters - a Test of the Universality of the Colour / Magnitude Relation - Part Two - Analysis*.

Bowler R. A. A., Dunlop J. S., McLure R. J., Rogers A. B., McCracken H. J., Milvang-Jensen B., Furusawa H., Fynbo J. P. U., Taniguchi Y., Afonso J., Bremer M. N., Le Fèvre O., 2014. *MNRAS*, **440**, 2810. *The bright end of the galaxy luminosity function at z=7: before the onset of mass quenching?*

Bradshaw E. J., Almaini O., Hartley W. G., Smith K. T., Conselice C. J., Dunlop J. S., Simpson C., Chuter R. W., Cirasuolo M., Foucaud S., McLure R. J., Mortlock A., Pearce H., 2013. *MNRAS*, **433**, 194. *High-velocity outflows from young star-forming galaxies in the UKIDSS Ultra-Deep Survey*.

Brammer G. B., Whitaker K. E., van Dokkum P. G., Marchesini D., Franx M., Kriek M., Labbé I., Lee K.-S., Muzzin A., Quadri R. F., Rudnick G., Williams R., 2011. *ApJ*, **739**, 24. *The Number Density and Mass Density of Star-forming and Quiescent Galaxies at 0.4 <= z <= 2.2*.

Brammer G. B., van Dokkum P. G., Coppi P., 2008. *ApJ*, **686**, 1503. *EAZY: A Fast, Public Photometric Redshift Code*.

Bridge C. R., Carlberg R. G., Sullivan M., 2010. *ApJ*, **709**, 1067. *The CFHTLS-Deep Catalog of Interacting Galaxies. I. Merger Rate Evolution to z = 1.2*.

Brinchmann J., Ellis R. S., 2000. *ApJL*, **536**, L77. *The Mass Assembly and Star Formation Characteristics of Field Galaxies of Known Morphology*.

Bruce V. A., Dunlop J. S., McLure R. J., Cirasuolo M., Buitrago F., Bowler R. A. A., Targett T. A., Bell E. F., McIntosh D. H., Dekel A., Faber S. M., Ferguson H. C., Grogin N. A., Hartley W., Kocevski D. D., Koekemoer A. M., Koo D. C., McGrath E. J., 2014. *ArXiv e-prints*. *The Bulge-Disk Decomposed Evolution of Massive Galaxies at 1<z<3 in CANDELS*.

Bruzual G., Charlot S., 2003. *MNRAS*, **344**, 1000. *Stellar population synthesis at the resolution of 2003*.

Bruzual A. G., Charlot S., 1993. *ApJ*, **405**, 538. *Spectral evolution of stellar populations using isochrone synthesis*.

Buat V., Iglesias-Páramo J., Seibert M., Burgarella D., Charlot S., Martin D. C., Xu C. K., Heckman T. M., Boissier S., Boselli A., Barlow T., Bianchi L., Byun Y.-I., Donas J., Forster K., Friedman P. G., Jelinski P., Lee Y.-W., Madore B. F., Malina R., Milliard B., Morissey P., Neff S., Rich M., Schiminovitch D., Siegmund O., Small T., Szalay A. S., Welsh B., Wyder T. K., 2005. *ApJL*, **619**, L51. *Dust Attenuation in the Nearby Universe: A Comparison between Galaxies Selected in the Ultraviolet and in the Far-Infrared*.

Buitrago F., Trujillo I., Conselice C. J., Bouwens R. J., Dickinson M., Yan H., 2008. *ApJL*, **687**, L61. *Size Evolution of the Most Massive Galaxies at 1.7 $<$ z $<$ 3 from GOODS NICMOS Survey Imaging*.

Buitrago F., Trujillo I., Conselice C. J., Häußler B., 2013. *MNRAS*, **428**, 1460. *Early-type galaxies have been the predominant morphological class for massive galaxies since only z 1*.

Bundy K., Ellis R. S., Conselice C. J., Taylor J. E., Cooper M. C., Willmer C. N. A., Weiner B. J., Coil A. L., Noeske K. G., Eisenhardt P. R. M., 2006. *ApJ*, **651**, 120. *The Mass Assembly History of Field Galaxies: Detection of an Evolving Mass Limit for Star-Forming Galaxies*.

Bundy K., Fukugita M., Ellis R. S., Targett T. A., Belli S., Kodama T., 2009. *ApJ*, **697**, 1369. *The Greater Impact of Mergers on the Growth of Massive Galaxies: Implications for Mass Assembly and Evolution since z sime 1*.

Calzetti D., Armus L., Bohlin R. C., Kinney A. L., Koornneef J., Storchi-Bergmann T., 2000. *ApJ*, **533**, 682. *The Dust Content and Opacity of Actively Star-forming Galaxies*.

Calzetti D., Kinney A. L., Storchi-Bergmann T., 1994. *ApJ*, **429**, 582. *Dust extinction of the stellar continua in starburst galaxies: The ultraviolet and optical extinction law*.

Calzetti D., 2001. *PASP*, **113**, 1449. *The Dust Opacity of Star-forming Galaxies*.

Cameron E., Carollo C. M., Oesch P. A., Bouwens R. J., Illingworth G. D., Trenti M., Labbé I., Magee D., 2011. *ApJ*, **743**, 146. *Active and Passive Galaxies at z $\sim$ 2: Rest-frame Optical Morphologies with WFC3*.

Cappellari M., Emsellem E., Krajnović D., McDermid R. M., Serra P., Alatalo K., Blitz L., Bois M., Bournaud F., Bureau M., Davies R. L., Davis T. A., de Zeeuw P. T., Khochfar S., Kuntschner H., Lablanche P.-Y., Morganti R., Naab T., Oosterloo T., Sarzi M., Scott N., Weijmans A.-M., Young L. M., 2011. *MNRAS*, **416**, 1680. *The ATLAS^{3D} project - VII. A new look at the morphology of nearby galaxies: the kinematic morphology-density relation*.

Carrasco E. R., Conselice C. J., Trujillo I., 2010. *MNRAS*, **405**, 2253. *Gemini K-band NIRI Adaptive Optics Observations of massive galaxies at 1 $<$ z $<$ 2*.

Cassata P., Giavalisco M., Guo Y., Ferguson H., Koekemoer A. M., Renzini A., Fontana A., Salimbeni S., Dickinson M., Casertano S., Conselice C. J., Grogin N., Lotz J. M., Papovich C., Lucas R. A., Straughn A., Gardner J. P., Moustakas L., 2010. *ApJL*, **714**, L79. *The Morphology of Passively Evolving Galaxies at z $\sim$ 2 from Hubble Space Telescope/WFC3 Deep Imaging in the Hubble Ultra Deep Field*.

Cassata P., Le Fèvre O., Garilli B., Maccagni D., Le Brun V., Scodeggio M., Tresse L., Ilbert O., Zamorani G., Cucciati O., Contini T., Bielby R., Mellier Y., McCracken H. J., Pollo A., Zanichelli A., Bardelli S., Cappi A., Pozzetti L., Vergani D., Zucca E., 2011. *A&A*, **525**, A143. *The VIMOS VLT Deep Survey: star formation rate density*

of Lyα emitters from a sample of 217 galaxies with spectroscopic redshifts $2 < z < 6.6$.

Cava A., Rodighiero G., Pérez-Fournon I., Buitrago F., Trujillo I., Altieri B., Amblard A., Auld R., Bock J., Brisbin D., Burgarella D., Castro-Rodríguez N., Chanial P., Cirasuolo M., Clements D. L., Conselice C. J., Cooray A., Eales S., Elbaz D., Ferrero P., Franceschini A., Glenn J., Solares E. A. G., Griffin M., Ibar E., Ivison R. J., Marchetti L., Morrison G. E., Mortier A. M. J., Oliver S. J., Page M. J., Papageorgiou A., Pearson C. P., Pohlen M., Rawlings J. I., Raymond G., Rigopoulou D., Roseboom I. G., Rowan-Robinson M., Scott D., Seymour N., Smith A. J., Symeonidis M., Tugwell K. E., Vaccari M., Valtchanov I., Vieira J. D., Vigroux L., Wang L., Wright G., 2010. *MNRAS*, **409**, L19. *HerMES: SPIRE detection of high-redshift massive compact galaxies in GOODS-N field*.

Chabrier G., 2003. PASP, **115**, 763. *Galactic Stellar and Substellar Initial Mass Function*.

Charlot S., Fall S. M., 2000. *ApJ*, **539**, 718. *A Simple Model for the Absorption of Starlight by Dust in Galaxies*.

Chuter R. W., Almaini O., Hartley W. G., McLure R. J., Dunlop J. S., Foucaud S., Conselice C. J., Simpson C., Cirasuolo M., Bradshaw E. J., 2011. *MNRAS*, **413**, 1678. *Galaxy environments in the UKIDSS Ultra Deep Survey*.

Cimatti A., Cassata P., Pozzetti L., Kurk J., Mignoli M., Renzini A., Daddi E., Bolzonella M., Brusa M., Rodighiero G., Dickinson M., Franceschini A., Zamorani G., Berta S., Rosati P., Halliday C., 2008. *A&A*, **482**, 21. *GMASS ultradeep spectroscopy of galaxies at $z \sim 2$. II. Superdense passive galaxies: how did they form and evolve?*

Cole S., Norberg P., Baugh C. M., Frenk C. S., Bland-Hawthorn J., Bridges T., Cannon R., Colless M., Collins C., Couch W., Cross N., Dalton G., De Propris R., Driver S. P., Efstathiou G., Ellis R. S., Glazebrook K., Jackson C., Lahav O., Lewis I., Lumsden S., Maddox S., Madgwick D., Peacock J. A., Peterson B. A., Sutherland W., Taylor K., 2001. *MNRAS*, **326**, 255. *The 2dF galaxy redshift survey: near-infrared galaxy luminosity functions*.

Conselice C. J., Newman J. A., Georgakakis A., Almaini O., Coil A. L., Cooper M. C., Eisenhardt P., Foucaud S., Koekemoer A., Lotz J., Noeske K., Weiner B., Willmer C. N. A., 2007. *ApJL*, **660**, L55. *AEGIS: The Diversity of Bright Near-IR-selected Distant Red Galaxies*.

Conselice C. J., Bluck A. F. L., Buitrago F., Bauer A. E., Grützbauch R., Bouwens R. J., Bevan S., Mortlock A., Dickinson M., Daddi E., Yan H., Scott D., Chapman S. C., Chary R.-R., Ferguson H. C., Giavalisco M., Grogin N., Illingworth G., Jogee S., Koekemoer A. M., Lucas R. A., Mobasher B., Moustakas L., Papovich C., Ravindranath S., Siana B., Teplitz H., Trujillo I., Urry M., Weinzirl T., 2011. *MNRAS*, **413**, 80. *The Hubble Space Telescope GOODS NICMOS Survey: overview and the evolution of massive galaxies at $1.5 < z < 3$*.

Conselice C. J., Mortlock A., Bluck A. F. L., Grützbauch R., Duncan K., 2013. *MNRAS*, **430**, 1051. *Gas accretion as a dominant formation mode in massive galaxies from the GOODS NICMOS Survey*.

Conselice C. J., 2006a. *MNRAS*, **373**, 1389. *The fundamental properties of galaxies and a new galaxy classification system*.

Conselice C. J., 2006b. *ApJ*, **638**, 686. *Early and Rapid Merging as a Formation Mechanism of Massive Galaxies: Empirical Constraints*.

Cowie L. L., Songaila A., 1977. *Nature*, **266**, 501. *Thermal evaporation of gas within galaxies by a hot intergalactic medium*.

Cowie L. L., Songaila A., Hu E. M., Cohen J. G., 1996. *AJ*, **112**, 839. *New Insight on Galaxy Formation and Evolution From Keck Spectroscopy of the Hawaii Deep Fields*.

Crocker A. F., Calzetti D., Thilker D. A., Aniano G., Draine B. T., Hunt L. K., Kennicutt R. C., Sandstrom K., Smith J. D. T., 2013. *ApJ*, **762**, 79. *Quantifying Non-star-formation-associated 8 μm Dust Emission in NGC 628*.

Croton D. J., Springel V., White S. D. M., De Lucia G., Frenk C. S., Gao L., Jenkins A., Kauffmann G., Navarro J. F., Yoshida N., 2006. *MNRAS*, **365**, 11. *The many lives of active galactic nuclei: cooling flows, black holes and the luminosities and colours of galaxies*.

Daddi E., Cimatti A., Renzini A., Fontana A., Mignoli M., Pozzetti L., Tozzi P., Zamorani G., 2004. *ApJ*, **617**, 746. *A New Photometric Technique for the Joint Selection of Star-forming and Passive Galaxies at 1.4 ¡ z ¡ 2.5*.

Daddi E., Renzini A., Pirzkal N., Cimatti A., Malhotra S., Stiavelli M., Xu C., Pasquali A., Rhoads J. E., Brusa M., di Serego Alighieri S., Ferguson H. C., Koekemoer A. M., Moustakas L. A., Panagia N., Windhorst R. A., 2005. *ApJ*, **626**, 680. *Passively Evolving Early-Type Galaxies at 1.4 $<$ z $<$ 2.5 in the Hubble Ultra Deep Field*.

Daddi E., Dickinson M., Morrison G., Chary R., Cimatti A., Elbaz D., Frayer D., Renzini A., Pope A., Alexander D. M., Bauer F. E., Giavalisco M., Huynh M., Kurk J., Mignoli M., 2007. *ApJ*, **670**, 156. *Multiwavelength Study of Massive Galaxies at z$\sim$2. I. Star Formation and Galaxy Growth*.

Damjanov I., McCarthy P. J., Abraham R. G., Glazebrook K., Yan H., Mentuch E., Le Borgne D., Savaglio S., Crampton D., Murowinski R., Juneau S., Carlberg R. G., Jørgensen I., Roth K., Chen H.-W., Marzke R. O., 2009. *ApJ*, **695**, 101. *Red Nuggets at z $\sim$ 1.5: Compact Passive Galaxies and the Formation of the Kormendy Relation*.

de Ravel L., Kampczyk P., Le Fèvre O., Lilly S. J., Tasca L., Tresse L., Lopez-Sanjuan C., Bolzonella M., Kovac K., Abbas U., Bardelli S., Bongiorno A., Caputi K., Contini T., Coppa G., Cucciati O., de la Torre S., Dunlop J. S., Franzetti P., Garilli B., Iovino A., Kneib J. ., Koekemoer A. M., Knobel C., Lamareille F., Le Borgne J. ., Le Brun V., Leauthaud A., Maier C., Mainieri V., Mignoli M., Pello R., Peng Y., Perez Montero E., Ricciardelli E., Scodeggio M., Silverman J. D., Tanaka M., Vergani D., Zamorani G., Zucca E., Bottini D., Cappi A., Carollo C. M., Cassata P., Cimatti A., Fumana M., Guzzo L., Maccagni D., Marinoni C., McCracken H. J., Memeo P., Meneux B., Oesch P., Porciani C., Pozzetti L., Renzini A., Scaramella R., Scarlata C., 2011. *ArXiv e-prints*. *The zCOSMOS redshift survey : Influence of luminosity, mass and environment on the galaxy merger rate*.

de Zeeuw P. T., Bureau M., Emsellem E., Bacon R., Carollo C. M., Copin Y., Davies R. L., Kuntschner H., Miller B. W., Monnet G., Peletier R. F., Verolme E. K., 2002. *MNRAS*, **329**, 513. *The SAURON project - II. Sample and early results*.

Dekel A., Sari R., Ceverino D., 2009. *ApJ*, **703**, 785. *Formation of Massive Galaxies at High Redshift: Cold Streams, Clumpy Disks, and Compact Spheroids*.

Drory N., Bender R., Feulner G., Hopp U., Maraston C., Snigula J., Hill G. J., 2004. *ApJ*, **608**, 742. *The Munich Near-Infrared Cluster Survey (MUNICS). VI. The Stellar Masses of K-Band-selected Field Galaxies to z∼1.2*.

Duncan K., Conselice C. J., Mortlock A., Hartley W. G., Guo Y., Ferguson H. C., Davé R., Lu Y., Ownsworth J., Ashby M. L. N., Dekel A., Dickinson M., Faber S., Giavalisco M., Grogin N., Kocevski D., Koekemoer A., Somerville R. S., White C. E., 2014. *MNRAS*, **444**, 2960. *The mass evolution of the first galaxies: stellar mass functions and star formation rates at 4 ¡ z ¡ 7 in the CANDELS GOODS-South field*.

Ebeling H., Stephenson L. N., Edge A. C., 2014. *The Astrophysical Journal Letters*, **781(2)**, L40. *Jellyfish: Evidence of Extreme Ram-pressure Stripping in Massive Galaxy Clusters*.

Elbaz D., Daddi E., Le Borgne D., Dickinson M., Alexander D. M., Chary R.-R., Starck J.-L., Brandt W. N., Kitzbichler M., MacDonald E., Nonino M., Popesso P., Stern D., Vanzella E., 2007. *A&A*, **468**, 33. *The reversal of the star formation-density relation in the distant universe*.

Elbaz D., Hwang H. S., Magnelli B., Daddi E., Aussel H., Altieri B., Amblard A., Andreani P., Arumugam V., Auld R., Babbedge T., Berta S., Blain A., Bock J., Bongiovanni A., Boselli A., Buat V., Burgarella D., Castro-Rodriguez N., Cava A., Cepa J., Chanial P., Chary R.-R., Cimatti A., Clements D. L., Conley A., Conversi L., Cooray A., Dickinson M., Dominguez H., Dowell C. D., Dunlop J. S., Dwek E., Eales S., Farrah D., Förster Schreiber N., Fox M., Franceschini A., Gear W., Genzel R., Glenn J., Griffin M., Gruppioni C., Halpern M., Hatziminaoglou E., Ibar E., Isaak K., Ivison R. J., Lagache G., Le Borgne D., Le Floc'h E., Levenson L., Lu N., Lutz D., Madden S., Maffei B., Magdis G., Mainetti G., Maiolino R., Marchetti L., Mortier A. M. J., Nguyen H. T., Nordon R., O'Halloran B., Okumura K., Oliver S. J., Omont A., Page M. J., Panuzzo P., Papageorgiou A., Pearson C. P., Perez Fournon I., Pérez García A. M., Poglitsch A., Pohlen M., Popesso P., Pozzi F., Rawlings J. I., Rigopoulou D., Riguccini L., Rizzo D., Rodighiero G., Roseboom I. G., Rowan-Robinson M., Saintonge A., Sanchez Portal M., Santini P., Sauvage M., Schulz B., Scott D., Seymour N., Shao L., Shupe D. L., Smith A. J., Stevens J. A., Sturm E., Symeonidis M., Tacconi L., Trichas M., Tugwell K. E., Vaccari M., Valtchanov I., Vieira J., Vigroux L., Wang L., Ward R., Wright G., Xu C. K., Zemcov M., 2010. *A&A*, **518**, L29. *Herschel unveils a puzzling uniformity of distant dusty galaxies*.

Erb D. K., 2008. *ApJ*, **674**, 151. *A Model for Star Formation, Gas Flows, and Chemical Evolution in Galaxies at High Redshifts*.

Faber S. M., Willmer C. N. A., Wolf C., Koo D. C., Weiner B. J., Newman J. A., Im M., Coil A. L., Conroy C., Cooper M. C., Davis M., Finkbeiner D. P., Gerke B. F.,

Gebhardt K., Groth E. J., Guhathakurta P., Harker J., Kaiser N., Kassin S., Kleinheinrich M., Konidaris N. P., Kron R. G., Lin L., Luppino G., Madgwick D. S., Meisenheimer K., Noeske K. G., Phillips A. C., Sarajedini V. L., Schiavon R. P., Simard L., Szalay A. S., Vogt N. P., Yan R., 2007. *ApJ*, **665**, 265. *Galaxy Luminosity Functions to z∼1 from DEEP2 and COMBO-17: Implications for Red Galaxy Formation*.

Fabian A. C., Sanders J. S., Taylor G. B., Allen S. W., Crawford C. S., Johnstone R. M., Iwasawa K., 2006. *MNRAS*, **366**, 417. *A very deep Chandra observation of the Perseus cluster: shocks, ripples and conduction*.

Fabian A. C., 1999. *MNRAS*, **308**, L39. *The obscured growth of massive black holes*.

Fan L., Lapi A., De Zotti G., Danese L., 2008. *ApJL*, **689**, L101. *The Dramatic Size Evolution of Elliptical Galaxies and the Quasar Feedback.*

Fan L., Lapi A., Bressan A., Bernardi M., De Zotti G., Danese L., 2010. *ApJ*, **718**, 1460. *Cosmic Evolution of Size and Velocity Dispersion for Early-type Galaxies*.

Feldmann R., Carollo C. M., Mayer L., Renzini A., Lake G., Quinn T., Stinson G. S., Yepes G., 2010. *ApJ*, **709**, 218. *The Evolution of Central Group Galaxies in Hydrodynamical Simulations*.

Ferreras I., Trujillo I., Mármol-Queraltó E., Pérez-González P., Cava A., Barro G., Cenarro J., Hernán-Caballero A., Cardiel N., 2013. *ArXiv e-prints*. *Constraints on the merging channel of massive galaxies since z∼1*.

Fischera J., Dopita M., 2005. *ApJ*, **619**, 340. *Attenuation Caused by a Distant Isothermal Turbulent Screen*.

Fontanot F., De Lucia G., Monaco P., Somerville R. S., Santini P., 2009. *MNRAS*, **397**, 1776. *The many manifestations of downsizing: hierarchical galaxy formation models confront observations*.

Franx M., van Dokkum P. G., Schreiber N. M. F., Wuyts S., Labbé I., Toft S., 2008. *ApJ*, **688**, 770. *Structure and Star Formation in Galaxies out to z = 3: Evidence for Surface Density Dependent Evolution and Upsizing*.

Fujita Y., 1998. *ApJ*, **509**, 587. *Quantitative Estimates of Environmental Effects on the Star Formation Rate of Disk Galaxies in Clusters of Galaxies*.

Furusawa H., Kosugi G., Akiyama M., Takata T., Sekiguchi K., Furusawa J., 2008. *Subaru/XMM-Newton Deep Survey (SXDS) - Optical Imaging Survey and Photometric Catalogs*, In: *Panoramic Views of Galaxy Formation and Evolution*, 131, eds Kodama T., Yamada T., Aoki K.

Gallazzi A., Charlot S., Brinchmann J., White S. D. M., Tremonti C. A., 2005. *MNRAS*, **362**, 41. *The ages and metallicities of galaxies in the local universe*.

Gallazzi A., Charlot S., Brinchmann J., White S. D. M., 2006. *MNRAS*, **370**, 1106. *Ages and metallicities of early-type galaxies in the Sloan Digital Sky Survey: new insight into the physical origin of the colour-magnitude and the Mg_2-σ_V relations*.

Giavalisco M., Ferguson H. C., Koekemoer A. M., Dickinson M., Alexander D. M., Bauer F. E., Bergeron J., Biagetti C., Brandt W. N., Casertano S., Cesarsky C., Chatzichristou E., Conselice C., Cristiani S., Da Costa L., Dahlen T., de Mello D., Eisenhardt P., Erben T., Fall S. M., Fassnacht C., Fosbury R., Fruchter A., Gardner J. P., Grogin N., Hook R. N., Hornschemeier A. E., Idzi R., Jogee S., Kretchmer C., Laidler V., Lee K. S., Livio M., Lucas R., Madau P., Mobasher B., Moustakas L. A., Nonino M., Padovani P., Papovich C., Park Y., Ravindranath S., Renzini A., Richardson M., Riess A., Rosati P., Schirmer M., Schreier E., Somerville R. S., Spinrad H., Stern D., Stiavelli M., Strolger L., Urry C. M., Vandame B., Williams R., Wolf C., 2004. *ApJL*, **600**, L93. *The Great Observatories Origins Deep Survey: Initial Results from Optical and Near-Infrared Imaging*.

Grogin N. A., Kocevski D. D., Faber S. M., Ferguson H. C., Koekemoer A. M., Riess A. G., Acquaviva V., Alexander D. M., Almaini O., Ashby M. L. N., Barden M., Bell E. F., Bournaud F., Brown T. M., Caputi K. I., Casertano S., Cassata P., Castellano M., Challis P., Chary R.-R., Cheung E., Cirasuolo M., Conselice C. J., Roshan Cooray A., Croton D. J., Daddi E., Dahlen T., Davé R., de Mello D. F., Dekel A., Dickinson M., Dolch T., Donley J. L., Dunlop J. S., Dutton A. A., Elbaz D., Fazio G. G., Filippenko A. V., Finkelstein S. L., Fontana A., Gardner J. P., Garnavich P. M., Gawiser E., Giavalisco M., Grazian A., Guo Y., Hathi N. P., Häussler B., Hopkins P. F., Huang J.-S., Huang K.-H., Jha S. W., Kartaltepe J. S., Kirshner R. P., Koo D. C., Lai K., Lee K.-S., Li W., Lotz J. M., Lucas R. A., Madau P., McCarthy P. J., McGrath E. J., McIntosh D. H., McLure R. J., Mobasher B., Moustakas L. A., Mozena M., Nandra K., Newman J. A., Niemi S.-M., Noeske K. G., Papovich C. J., Pentericci L., Pope A., Primack J. R., Rajan A., Ravindranath S., Reddy N. A., Renzini A., Rix H.-W., Robaina A. R., Rodney S. A., Rosario D. J., Rosati P., Salimbeni S., Scarlata C., Siana B., Simard L., Smidt J., Somerville R. S., Spinrad H., Straughn A. N., Strolger L.-G., Telford O., Teplitz H. I., Trump J. R., van der Wel A., Villforth C., Wechsler R. H., Weiner B. J., Wiklind T., Wild V., Wilson G., Wuyts S., Yan H.-J., Yun M. S., 2011. *ApJS*, **197**, 35. *CANDELS: The Cosmic Assembly Near-infrared Deep Extragalactic Legacy Survey*.

Grützbauch R., Conselice C. J., Bauer A. E., Bluck A. F. L., Chuter R. W., Buitrago F., Mortlock A., Weinzirl T., Jogee S., 2011. *MNRAS*, **418**, 938. *The relationship between star formation rates, local density and stellar mass up to z 3 in the GOODS NICMOS Survey*.

Gunn J. E., Gott, III J. R., 1972. *ApJ*, **176**, 1. *On the Infall of Matter Into Clusters of Galaxies and Some Effects on Their Evolution*.

Hartley W. G., Almaini O., Mortlock A., Conselice C. J., Grützbauch R., Simpson C., Bradshaw E. J., Chuter R. W., Foucaud S., Cirasuolo M., Dunlop J. S., McLure R. J., Pearce H. J., 2013. *MNRAS*, **431**, 3045. *Studying the emergence of the red sequence through galaxy clustering: host halo masses at $z > 2$.*

Heavens A., Panter B., Jimenez R., Dunlop J., 2004. *Nature*, **428**, 625. *The star-formation history of the Universe from the stellar populations of nearby galaxies*.

Helou G., 1986. *ApJL*, **311**, L33. *The IRAS colors of normal galaxies*.

Hickox R. C., Jones C., Forman W. R., Murray S. S., Kochanek C. S., Eisenstein D., Jannuzi B. T., Dey A., Brown M. J. I., Stern D., Eisenhardt P. R., Gorjian V., Brodwin M., Narayan R., Cool R. J., Kenter A., Caldwell N., Anderson M. E., 2009. *ApJ*, **696**, 891. *Host Galaxies, Clustering, Eddington Ratios, and Evolution of Radio, X-Ray, and Infrared-Selected AGNs*.

Hilton M., Conselice C. J., Roseboom I. G., Burgarella D., Buat V., Berta S., Béthermin M., Bock J., Chapman S. C., Clements D. L., Conley A., Conversi L., Cooray A., Farrah D., Ibar E., Magdis G., Magnelli B., Marsden G., Nordon R., Oliver S. J., Page M. J., Popesso P., Pozzi F., Schulz B., Scott D., Smith A. J., Symeonidis M., Valtchanov I., Viero M., Wang L., Zemcov M., 2012. *MNRAS*, **425**, 540. *Herschel observations of a z 2 stellar mass selected galaxy sample drawn from the GOODS NICMOS Survey*.

Hopkins A. M., Beacom J. F., 2006. *ApJ*, **651**, 142. *On the Normalization of the Cosmic Star Formation History*.

Hopkins P. F., Hernquist L., Cox T. J., Kereš D., 2008. *ApJS*, **175**, 356. *A Cosmological Framework for the Co-Evolution of Quasars, Supermassive Black Holes, and Elliptical Galaxies. I. Galaxy Mergers and Quasar Activity*.

Hopkins P. F., Somerville R. S., Cox T. J., Hernquist L., Jogee S., Kereš D., Ma C.-P., Robertson B., Stewart K., 2009. *MNRAS*, **397**, 802. *The effects of gas on morphological transformation in mergers: implications for bulge and disc demographics*.

Hopkins P. F., Croton D., Bundy K., Khochfar S., van den Bosch F., Somerville R. S., Wetzel A., Keres D., Hernquist L., Stewart K., Younger J. D., Genel S., Ma C.-P., 2010. *ApJ*, **724**, 915. *Mergers in ΛCDM: Uncertainties in Theoretical Predictions and Interpretations of the Merger Rate*.

Hubble E. P., 1925a. *Popular Astronomy*, **33**, 252. *Cepheids in Spiral Nebulae*.

Hubble E. P., 1925b. *ApJ*, **62**, 409. *NGC 6822, a remote stellar system.*

Ilbert O., Salvato M., Le Floc'h E., Aussel H., Capak P., McCracken H. J., Mobasher B., Kartaltepe J., Scoville N., Sanders D. B., Arnouts S., Bundy K., Cassata P., Kneib J.-P., Koekemoer A., Le Fèvre O., Lilly S., Surace J., Taniguchi Y., Tasca L., Thompson D., Tresse L., Zamojski M., Zamorani G., Zucca E., 2010. *ApJ*, **709**, 644. *Galaxy Stellar Mass Assembly Between 0.2 $<$ z $<$ 2 from the S-COSMOS Survey*.

Juneau S., Glazebrook K., Crampton D., McCarthy P. J., Savaglio S., Abraham R., Carlberg R. G., Chen H.-W., Le Borgne D., Marzke R. O., Roth K., Jørgensen I., Hook I., Murowinski R., 2005. *ApJL*, **619**, L135. *Cosmic Star Formation History and Its Dependence on Galaxy Stellar Mass*.

Kauffmann G., Heckman T. M., White S. D. M., Charlot S., Tremonti C., Peng E. W., Seibert M., Brinkmann J., Nichol R. C., SubbaRao M., York D., 2003. *MNRAS*, **341**, 54. *The dependence of star formation history and internal structure on stellar mass for 10^5 low-redshift galaxies*.

Kauffmann G., White S. D. M., Heckman T. M., Ménard B., Brinchmann J., Charlot S., Tremonti C., Brinkmann J., 2004. *MNRAS*, **353**, 713. *The environmental dependence of the relations between stellar mass, structure, star formation and nuclear activity in galaxies*.

Kaviraj S., Cohen S., Ellis R. S., Peirani S., Windhorst R. A., O'Connell R. W., Silk J., Whitmore B. C., Hathi N. P., Ryan R. E., Dopita M. A., Frogel J. A., Dekel A., 2013. *MNRAS*, **428**, 925. *Newborn spheroids at high redshift: when and how did the dominant, old stars in today's massive galaxies form?*

Kennicutt, Jr. R. C., 1983. *ApJ*, **272**, 54. *The rate of star formation in normal disk galaxies*.

Kennicutt, Jr. R. C., 1998a. *ARA&A*, **36**, 189. *Star Formation in Galaxies Along the Hubble Sequence*.

Kennicutt, Jr. R. C., 1998b. *ApJ*, **498**, 541. *The Global Schmidt Law in Star-forming Galaxies*.

Kereš D., Katz N., Weinberg D. H., Davé R., 2005. *MNRAS*, **363**, 2. *How do galaxies get their gas?*

Khochfar S., Silk J., 2006. *ApJL*, **648**, L21. *A Simple Model for the Size Evolution of Elliptical Galaxies*.

Koekemoer A. M., Faber S. M., Ferguson H. C., Grogin N. A., Kocevski D. D., Koo D. C., Lai K., Lotz J. M., Lucas R. A., McGrath E. J., Ogaz S., Rajan A., Riess A. G., Rodney S. A., Strolger L., Casertano S., Castellano M., Dahlen T., Dickinson M., Dolch T., Fontana A., Giavalisco M., Grazian A., Guo Y., Hathi N. P., Huang K.-H., van der Wel A., Yan H.-J., Acquaviva V., Alexander D. M., Almaini O., Ashby M. L. N., Barden M., Bell E. F., Bournaud F., Brown T. M., Caputi K. I., Cassata P., Challis P. J., Chary R.-R., Cheung E., Cirasuolo M., Conselice C. J., Roshan Cooray A., Croton D. J., Daddi E., Davé R., de Mello D. F., de Ravel L., Dekel A., Donley J. L., Dunlop J. S., Dutton A. A., Elbaz D., Fazio G. G., Filippenko A. V., Finkelstein S. L., Frazer C., Gardner J. P., Garnavich P. M., Gawiser E., Gruetzbauch R., Hartley W. G., Häussler B., Herrington J., Hopkins P. F., Huang J.-S., Jha S. W., Johnson A., Kartaltepe J. S., Khostovan A. A., Kirshner R. P., Lani C., Lee K.-S., Li W., Madau P., McCarthy P. J., McIntosh D. H., McLure R. J., McPartland C., Mobasher B., Moreira H., Mortlock A., Moustakas L. A., Mozena M., Nandra K., Newman J. A., Nielsen J. L., Niemi S., Noeske K. G., Papovich C. J., Pentericci L., Pope A., Primack J. R., Ravindranath S., Reddy N. A., Renzini A., Rix H.-W., Robaina A. R., Rosario D. J., Rosati P., Salimbeni S., Scarlata C., Siana B., Simard L., Smidt J., Snyder D., Somerville R. S., Spinrad H., Straughn A. N., Telford O., Teplitz H. I., Trump J. R., Vargas C., Villforth C., Wagner C. R., Wandro P., Wechsler R. H., Weiner B. J., Wiklind T., Wild V., Wilson G., Wuyts S., Yun M. S., 2011. *ApJS*, **197**, 36. *CANDELS: The Cosmic Assembly Near-infrared Deep Extragalactic Legacy Survey The Hubble Space Telescope Observations, Imaging Data Products, and Mosaics*.

Krajnović D., Karick A. M., Davies R. L., Naab T., Sarzi M., Emsellem E., Cappellari M., Serra P., de Zeeuw P. T., Scott N., McDermid R. M., Weijmans A.-M., Davis T. A., Alatalo K., Blitz L., Bois M., Bureau M., Bournaud F., Crocker A., Duc P.-A.,

Khochfar S., Kuntschner H., Morganti R., Oosterloo T., Young L. M., 2013. *MNRAS*, **433**, 2812. *The ATLAS^{3D} Project - XXIII. Angular momentum and nuclear surface brightness profiles*.

Kroupa P., Tout C. A., Gilmore G., 1993. *MNRAS*, **262**, 545. *The distribution of low-mass stars in the Galactic disc*.

Kroupa P., 2001. *MNRAS*, **322**, 231. *On the variation of the initial mass function*.

Labbé I., Bouwens R., Illingworth G. D., Franx M., 2006. *ApJL*, **649**, L67. *Spitzer IRAC Confirmation of z_{850}-Dropout Galaxies in the Hubble Ultra Deep Field: Stellar Masses and Ages at $z \sim 7$*.

Lacey C., Cole S., 1993a. *MNRAS*, **262**, 627. *Merger rates in hierarchical models of galaxy formation*.

Lacey C., Cole S., 1993b. *MNRAS*, **262**, 627. *Merger rates in hierarchical models of galaxy formation*.

Lani C., Almaini O., Hartley W. G., Mortlock A., Häußler B., Chuter R. W., Simpson C., van der Wel A., Grützbauch R., Conselice C. J., Bradshaw E. J., Cooper M. C., Faber S. M., Grogin N. A., Kocevski D. D., Koekemoer A. M., Lai K., 2013. *MNRAS*, **435**, 207. *Evidence for a correlation between the sizes of quiescent galaxies and local environment to z 2*.

Lawrence A., Warren S. J., Almaini O., Edge A. C., Hambly N. C., Jameson R. F., Lucas P., Casali M., Adamson A., Dye S., Emerson J. P., Foucaud S., Hewett P., Hirst P., Hodgkin S. T., Irwin M. J., Lodieu N., McMahon R. G., Simpson C., Smail I., Mortlock D., Folger M., 2007. *MNRAS*, **379**, 1599. *The UKIRT Infrared Deep Sky Survey (UKIDSS)*.

Lee J., Yi S. K., 2013. *ApJ*, **766**, 38. *On the Assembly History of Stellar Components in Massive Galaxies*.

Leja J., van Dokkum P., Franx M., 2013. *ApJ*, **766**, 33. *Tracing Galaxies through Cosmic Time with Number Density Selection*.

Lintott C. J., Schawinski K., Slosar A., Land K., Bamford S., Thomas D., Raddick M. J., Nichol R. C., Szalay A., Andreescu D., Murray P., Vandenberg J., 2008. *MNRAS*, **389**, 1179. *Galaxy Zoo: morphologies derived from visual inspection of galaxies from the Sloan Digital Sky Survey*.

López-Sanjuan C., Le Fèvre O., Ilbert O., Tasca L. A. M., Bridge C., Cucciati O., Kampczyk P., Pozzetti L., Xu C. K., Carollo C. M., Contini T., Kneib J.-P., Lilly S. J., Mainieri V., Renzini A., Sanders D., Scodeggio M., Scoville N. Z., Taniguchi Y., Zamorani G., Aussel H., Bardelli S., Bolzonella M., Bongiorno A., Capak P., Caputi K., de la Torre S., de Ravel L., Franzetti P., Garilli B., Iovino A., Knobel C., Kovač K., Lamareille F., Le Borgne J.-F., Le Brun V., Le Floc'h E., Maier C., McCracken H. J., Mignoli M., Pelló R., Peng Y., Pérez-Montero E., Presotto V., Ricciardelli E., Salvato M., Silverman J. D., Tanaka M., Tresse L., Vergani D., Zucca E., Barnes L., Bordoloi R., Cappi A., Cimatti A., Coppa G., Koekemoer A., Liu C. T., Moresco M.,

Nair P., Oesch P., Schawinski K., Welikala N., 2012. *A&A*, **548**, A7. *The dominant role of mergers in the size evolution of massive early-type galaxies since z ∼ 1*.

Lotz J. M., Jonsson P., Cox T. J., Primack J. R., 2008. *MNRAS*, **391**, 1137. *Galaxy merger morphologies and time-scales from simulations of equal-mass gas-rich disc mergers*.

Lundgren B. F., van Dokkum P., Franx M., Labbe I., Trenti M., Bouwens R., Gonzalez V., Illingworth G., Magee D., Oesch P., Stiavelli M., 2014. *ApJ*, **780**, 34. *Tracing the Mass Growth and Star Formation Rate Evolution of Massive Galaxies from z ∼ 6 to z ∼ 1 in the Hubble Ultra-Deep Field*.

Madau P., Ferguson H. C., Dickinson M. E., Giavalisco M., Steidel C. C., Fruchter A., 1996. *MNRAS*, **283**, 1388. *High-redshift galaxies in the Hubble Deep Field: colour selection and star formation history to z∼4*.

Magdis G. E., Elbaz D., Hwang H. S., Daddi E., Rigopoulou D., Altieri B., Andreani P., Aussel H., Berta S., Cava A., Bongiovanni A., Cepa J., Cimatti A., Dickinson M., Dominguez H., Förster Schreiber N., Genzel R., Huang J.-S., Lutz D., Maiolino R., Magnelli B., Morrison G. E., Nordon R., Pérez García A. M., Poglitsch A., Popesso P., Pozzi F., Riguccini L., Rodighiero G., Saintonge A., Santini P., Sanchez-Portal M., Shao L., Sturm E., Tacconi L., Valtchanov I., 2010. *ApJL*, **720**, L185. *A First Glimpse Into the Far-IR Properties of High-z UV-selected galaxies: Herschel/PACS Observations of z ∼ 3 LBGs*.

Marble A. R., Engelbracht C. W., van Zee L., Dale D. A., Smith J. D. T., Gordon K. D., Wu Y., Lee J. C., Kennicutt R. C., Skillman E. D., Johnson L. C., Block M., Calzetti D., Cohen S. A., Lee H., Schuster M. D., 2010. *ApJ*, **715**, 506. *An Aromatic Inventory of the Local Volume*.

Marchesini D., Muzzin A., Stefanon M., Franx M., Brammer G. G., Marsan C. Z., Vulcani B., Fynbo J. P. U., Milvang-Jensen B., Dunlop J. S., Buitrago F., 2014. *ArXiv e-prints*. *The Progenitors of Local Ultra-massive Galaxies Across Cosmic Time: from Dusty Star-bursting to Quiescent Stellar Populations*.

McCarthy P. J., Le Borgne D., Crampton D., Chen H.-W., Abraham R. G., Glazebrook K., Savaglio S., Carlberg R. G., Marzke R. O., Roth K., Jørgensen I., Hook I., Murowinski R., Juneau S., 2004. *ApJL*, **614**, L9. *Evolved Galaxies at z>1.5 from the Gemini Deep Deep Survey: The Formation Epoch of Massive Stellar Systems*.

McIntosh D. H., Bell E. F., Rix H.-W., Wolf C., Heymans C., Peng C. Y., Somerville R. S., Barden M., Beckwith S. V. W., Borch A., Caldwell J. A. R., Häußler B., Jahnke K., Jogee S., Meisenheimer K., Sánchez S. F., Wisotzki L., 2005. *ApJ*, **632**, 191. *The Evolution of Early-Type Red Galaxies with the GEMS Survey: Luminosity-Size and Stellar Mass-Size Relations Since z=1*.

McLure R. J., Dunlop J. S., Bowler R. A. A., Curtis-Lake E., Schenker M., Ellis R. S., Robertson B. E., Koekemoer A. M., Rogers A. B., Ono Y., Ouchi M., Charlot S., Wild V., Stark D. P., Furlanetto S. R., Cirasuolo M., Targett T. A., 2013. *MNRAS*, **432**, 2696. *A new multifield determination of the galaxy luminosity function at z = 7-9 incorporating the 2012 Hubble Ultra-Deep Field imaging*.

Meurer G. R., Heckman T. M., Calzetti D., 1999. *ApJ*, **521**, 64. *Dust Absorption and the Ultraviolet Luminosity Density at Z∼3 as Calibrated by Local Starburst Galaxies*.

Miller G. E., Scalo J. M., 1979. *ApJS*, **41**, 513. *The initial mass function and stellar birthrate in the solar neighborhood*.

Mineo S., Gilfanov M., Sunyaev R., 2012. *MNRAS*, **419**, 2095. *X-ray emission from star-forming galaxies - I. High-mass X-ray binaries*.

Mortlock A., Conselice C. J., Bluck A. F. L., Bauer A. E., Grützbauch R., Buitrago F., Ownsworth J., 2011. *MNRAS*, **413**, 2845. *A deep probe of the galaxy stellar mass functions at z 1-3 with the GOODS NICMOS Survey*.

Mortlock A., Conselice C. J., Hartley W. G., Ownsworth J. R., Lani C., Bluck A. F. L., Almaini O., Duncan K., Wel A. v. d., Koekemoer A. M., Dekel A., Davé R., Ferguson H. C., de Mello D. F., Newman J. A., Faber S. M., Grogin N. A., Kocevski D. D., Lai K., 2013. *MNRAS*, **433**, 1185. *The redshift and mass dependence on the formation of the Hubble sequence at $z > 1$ from CANDELS/UDS*.

Murphy E. J., Condon J. J., Schinnerer E., Kennicutt R. C., Calzetti D., Armus L., Helou G., Turner J. L., Aniano G., Beirão P., Bolatto A. D., Brandl B. R., Croxall K. V., Dale D. A., Donovan Meyer J. L., Draine B. T., Engelbracht C., Hunt L. K., Hao C.-N., Koda J., Roussel H., Skibba R., Smith J.-D. T., 2011. *ApJ*, **737**, 67. *Calibrating Extinction-free Star Formation Rate Diagnostics with 33 GHz Free-free Emission in NGC 6946*.

Muzzin A., Marchesini D., Stefanon M., Franx M., McCracken H. J., Milvang-Jensen B., Dunlop J. S., Fynbo J. P. U., Brammer G., Labbé I., van Dokkum P. G., 2013. *ApJ*, **777**, 18. *The Evolution of the Stellar Mass Functions of Star-forming and Quiescent Galaxies to z = 4 from the COSMOS/UltraVISTA Survey*.

Naab T., Johansson P. H., Ostriker J. P., 2009. *ApJL*, **699**, L178. *Minor Mergers and the Size Evolution of Elliptical Galaxies*.

Nair P. B., Abraham R. G., 2010. *ApJS*, **186**, 427. *A Catalog of Detailed Visual Morphological Classifications for 14,034 Galaxies in the Sloan Digital Sky Survey*.

Nelan J. E., Smith R. J., Hudson M. J., Wegner G. A., Lucey J. R., Moore S. A. W., Quinney S. J., Suntzeff N. B., 2005. *ApJ*, **632**, 137. *NOAO Fundamental Plane Survey. II. Age and Metallicity along the Red Sequence from Line-Strength Data*.

Newman A. B., Ellis R. S., Treu T., Bundy K., 2010. *ApJL*, **717**, L103. *Keck Spectroscopy of $z > 1$ Field Spheroidals: Dynamical Constraints on the Growth Rate of Red "Nuggets"*.

Noeske K. G., Weiner B. J., Faber S. M., Papovich C., Koo D. C., Somerville R. S., Bundy K., Conselice C. J., Newman J. A., Schiminovich D., Le Floc'h E., Coil A. L., Rieke G. H., Lotz J. M., Primack J. R., Barmby P., Cooper M. C., Davis M., Ellis R. S., Fazio G. G., Guhathakurta P., Huang J., Kassin S. A., Martin D. C., Phillips A. C., Rich R. M., Small T. A., Willmer C. N. A., Wilson G., 2007. *ApJL*, **660**, L43. *Star Formation in AEGIS Field Galaxies since z=1.1: The Dominance of Gradually Declining Star Formation, and the Main Sequence of Star-forming Galaxies*.

Nordon R., Lutz D., Shao L., Magnelli B., Berta S., Altieri B., Andreani P., Aussel H., Bongiovanni A., Cava A., Cepa J., Cimatti A., Daddi E., Dominguez H., Elbaz D., Förster Schreiber N. M., Genzel R., Grazian A., Magdis G., Maiolino R., Pérez García A. M., Poglitsch A., Popesso P., Pozzi F., Riguccini L., Rodighiero G., Saintonge A., Sanchez-Portal M., Santini P., Sturm E., Tacconi L., Valtchanov I., Wetzstein M., Wieprecht E., 2010. *A&A*, **518**, L24. *The star-formation rates of $1.5 < z < 2.5$ massive galaxies*.

Oser L., Ostriker J. P., Naab T., Johansson P. H., Burkert A., 2010. *ApJ*, **725**, 2312. *The Two Phases of Galaxy Formation*.

Osterbrock D. E., Ferland G. J., 2006. *Astrophysics of gaseous nebulae and active galactic nuclei*.

Ownsworth J. R., Conselice C. J., Mortlock A., Hartley W. G., Buitrago F., 2012. *MNRAS*, **426**, 764. *Evolution of massive galaxy structural properties and sizes via star formation in the GOODS NICMOS Survey*.

Ownsworth J. R., Conselice C. J., Mortlock A., Hartley W. G., Almaini O., Duncan K., Mundy C. J., 2014. *ArXiv e-prints*. *Minor vs Major Mergers: The Stellar Mass Growth of Massive Galaxies from z=3 using Number Density Selection Techniques*.

Pannella M., Gabasch A., Goranova Y., Drory N., Hopp U., Noll S., Saglia R. P., Strazzullo V., Bender R., 2009. *ApJ*, **701**, 787. *The Evolution of Early- and Late-type Galaxies in the Cosmic Evolution Survey up to z = 1.2*.

Papovich C., Rudnick G., Le Floc'h E., van Dokkum P. G., Rieke G. H., Taylor E. N., Armus L., Gawiser E., Huang J., Marcillac D., Franx M., 2007. *ApJ*, **668**, 45. *Spitzer Mid- to Far-Infrared Flux Densities of Distant Galaxies*.

Papovich C., Finkelstein S. L., Ferguson H. C., Lotz J. M., Giavalisco M., 2011. *MNRAS*, **412**, 1123. *The rising star formation histories of distant galaxies and implications for gas accretion with time*.

Patel S. G., van Dokkum P. G., Franx M., Quadri R. F., Muzzin A., Marchesini D., Williams R. J., Holden B. P., Stefanon M., 2013. *ApJ*, **766**, 15. *HST/WFC3 Confirmation of the Inside-out Growth of Massive Galaxies at $0 < z < 2$ and Identification of Their Star-forming Progenitors at $z \sim 3$*.

Peebles P. J. E., 1980. *The large-scale structure of the universe*.

Peeters E., Mattioda A. L., Hudgins D. M., Allamandola L. J., 2004. *ApJL*, **617**, L65. *Polycyclic Aromatic Hydrocarbon Emission in the 15-21 Micron Region*.

Peng C. Y., Ho L. C., Impey C. D., Rix H.-W., 2002. *AJ*, **124**, 266. *Detailed Structural Decomposition of Galaxy Images*.

Peng C., 2010. *Using GALFIT to Classify Galaxies at High-z: Measuring Asymmetry Parametrically*, In: *American Astronomical Society Meeting Abstracts #215*, 229.09.

Pérez-González P. G., Rieke G. H., Villar V., Barro G., Blaylock M., Egami E., Gallego J., Gil de Paz A., Pascual S., Zamorano J., Donley J. L., 2008a. *ApJ*, **675**, 234. *The Stellar Mass Assembly of Galaxies from z = 0 to z = 4: Analysis of a Sample Selected in the Rest-Frame Near-Infrared with Spitzer*.

Pérez-González P. G., Rieke G. H., Villar V., Barro G., Blaylock M., Egami E., Gallego J., Gil de Paz A., Pascual S., Zamorano J., Donley J. L., 2008b. *ApJ*, **675**, 234. *The Stellar Mass Assembly of Galaxies from z = 0 to z = 4: Analysis of a Sample Selected in the Rest-Frame Near-Infrared with Spitzer*.

Pigott E., 1784. *Royal Society of London Philosophical Transactions Series I*, **75**, 127. *Observations of a New Variable Star. In a Letter from Edward Pigott, Esq. to Sir H. C. Englefield, Bart. F. R. S. and A. S.*

Poggianti B. M., Calvi R., Bindoni D., D'Onofrio M., Moretti A., Valentinuzzi T., Fasano G., Fritz J., De Lucia G., Vulcani B., Bettoni D., Gullieuszik M., Omizzolo A., 2013. *ApJ*, **762**, 77. *Superdense Galaxies and the Mass-Size Relation at Low Redshift*.

Pozzetti L., Bolzonella M., Zucca E., Zamorani G., Lilly S., Renzini A., Moresco M., Mignoli M., Cassata P., Tasca L., Lamareille F., Maier C., Meneux B., Halliday C., Oesch P., Vergani D., Caputi K., Kovač K., Cimatti A., Cucciati O., Iovino A., Peng Y., Carollo M., Contini T., Kneib J.-P., Le Févre O., Mainieri V., Scodeggio M., Bardelli S., Bongiorno A., Coppa G., de la Torre S., de Ravel L., Franzetti P., Garilli B., Kampczyk P., Knobel C., Le Borgne J.-F., Le Brun V., Pellò R., Perez Montero E., Ricciardelli E., Silverman J. D., Tanaka M., Tresse L., Abbas U., Bottini D., Cappi A., Guzzo L., Koekemoer A. M., Leauthaud A., Maccagni D., Marinoni C., McCracken H. J., Memeo P., Porciani C., Scaramella R., Scarlata C., Scoville N., 2010. *A&A*, **523**, A13. *zCOSMOS - 10k-bright spectroscopic sample. The bimodality in the galaxy stellar mass function: exploring its evolution with redshift.*

Prevot M. L., Lequeux J., Prevot L., Maurice E., Rocca-Volmerange B., 1984. *A&A*, **132**, 389. *The typical interstellar extinction in the Small Magellanic Cloud*.

Quadri R., van Dokkum P., Gawiser E., Franx M., Marchesini D., Lira P., Rudnick G., Herrera D., Maza J., Kriek M., Labbé I., Francke H., 2007. *ApJ*, **654**, 138. *Clustering of K-selected Galaxies at $2 < z < 3.5$: Evidence for a Color-Density Relation.*

Ravindranath S., Ferguson H. C., Conselice C., Giavalisco M., Dickinson M., Chatzichristou E., de Mello D., Fall S. M., Gardner J. P., Grogin N. A., Hornschemeier A., Jogee S., Koekemoer A., Kretchmer C., Livio M., Mobasher B., Somerville R., 2004. *ApJL*, **604**, L9. *The Evolution of Disk Galaxies in the GOODS-South Field: Number Densities and Size Distribution.*

Reddy N. A., Steidel C. C., 2009. *ApJ*, **692**, 778. *A Steep Faint-End Slope of the UV Luminosity Function at $z \sim$ 2-3: Implications for the Global Stellar Mass Density and Star Formation in Low-Mass Halos*.

Reddy N. A., Erb D. K., Pettini M., Steidel C. C., Shapley A. E., 2010. *ApJ*, **712**, 1070. *Dust Obscuration and Metallicity at High Redshift: New Inferences from UV, Hα, and 8 μm Observations of $z \sim$ 2 Star-forming Galaxies*.

Reddy N. A., Pettini M., Steidel C. C., Shapley A. E., Erb D. K., Law D. R., 2012. *ApJ*, **754**, 25. *The Characteristic Star Formation Histories of Galaxies at Redshifts z ∼ 2-7*.

Renzini A., 2006. *ARA&A*, **44**, 141. *Stellar Population Diagnostics of Elliptical Galaxy Formation*.

Retzlaff J., Rosati P., Dickinson M., Vandame B., Rité C., Nonino M., Cesarsky C., GOODS Team, 2010. *A&A*, **511**, A50. *The Great Observatories Origins Deep Survey. VLT/ISAAC near-infrared imaging of the GOODS-South field*.

Ricciardelli E., Trujillo I., Buitrago F., Conselice C. J., 2010. *MNRAS*, **406**, 230. *The evolutionary sequence of submillimetre galaxies: from diffuse discs to massive compact ellipticals?*

Roškar R., Debattista V. P., Quinn T. R., Stinson G. S., Wadsley J., 2008. *ApJL*, **684**, L79. *Riding the Spiral Waves: Implications of Stellar Migration for the Properties of Galactic Disks*.

Roškar R., Debattista V. P., Loebman S. R., Ivezić Z., Quinn T. R., 2011. *Implications of Radial Migration for Stellar Population Studies*, In: *16th Cambridge Workshop on Cool Stars, Stellar Systems, and the Sun*, 371, eds Johns-Krull C., Browning M. K., West A. A.

Rubin V. C., Thonnard N., Ford, Jr. W. K., 1978. *ApJL*, **225**, L107. *Extended rotation curves of high-luminosity spiral galaxies. IV - Systematic dynamical properties, SA through SC*.

Ruiz P., Trujillo I., Mármol-Queraltó E., 2013. *ArXiv e-prints*. *Satellite galaxies around present-day massive ellipticals*.

Rybicki B. G., Lightman P. A., 2004. *Radiative Processes in Astrophysics*, Wiley.

Salpeter E. E., 1955. *ApJ*, **121**, 161. *The Luminosity Function and Stellar Evolution.*

Saracco P., Longhetti M., Severgnini P., Della Ceca R., Braito V., Mannucci F., Bender R., Drory N., Feulner G., Hopp U., Maraston C., 2005. *MNRAS*, **357**, L40. *The density of very massive evolved galaxies to z∼= 1.7*.

Scalo J. M., 1986. Fund. Cosmic Phys., **11**, 1. *The stellar initial mass function*.

Schawinski K., Khochfar S., Kaviraj S., Yi S. K., Boselli A., Barlow T., Conrow T., Forster K., Friedman P. G., Martin D. C., Morrissey P., Neff S., Schiminovich D., Seibert M., Small T., Wyder T. K., Bianchi L., Donas J., Heckman T., Lee Y.-W., Madore B., Milliard B., Rich R. M., Szalay A., 2006. *Nature*, **442**, 888. *Suppression of star formation in early-type galaxies by feedback from supermassive black holes*.

Schmidt M., 1959. *ApJ*, **129**, 243. *The Rate of Star Formation.*

Seibert M., Martin D. C., Heckman T. M., Buat V., Hoopes C., Barlow T., Bianchi L., Byun Y.-I., Donas J., Forster K., Friedman P. G., Jelinsky P., Lee Y.-W., Madore B. F., Malina R., Milliard B., Morrissey P., Neff S., Rich R. M., Schiminovich D.,

Siegmund O., Small T., Szalay A. S., Welsh B., Wyder T. K., 2005. *ApJL*, **619**, L55. *Testing the Empirical Relation between Ultraviolet Color and Attenuation of Galaxies*.

Sellwood J. A., Binney J. J., 2002. *MNRAS*, **336**, 785. *Radial mixing in galactic discs*.

Sérsic J. L., 1968. *Atlas de galaxias australes*.

Shen S., Mo H. J., White S. D. M., Blanton M. R., Kauffmann G., Voges W., Brinkmann J., Csabai I., 2003. *MNRAS*, **343**, 978. *The size distribution of galaxies in the Sloan Digital Sky Survey*.

Silk J., Rees M. J., 1998. *A&A*, **331**, L1. *Quasars and galaxy formation*.

Simpson C., Martínez-Sansigre A., Rawlings S., Ivison R., Akiyama M., Sekiguchi K., Takata T., Ueda Y., Watson M., 2006. *MNRAS*, **372**, 741. *Radio imaging of the Subaru/XMM-Newton Deep Field - I. The 100-μJy catalogue, optical identifications, and the nature of the faint radio source population*.

Smith M. W. L., Eales S. A., Gomez H. L., Roman-Duval J., Fritz J., Braun R., Baes M., Bendo G. J., Blommaert J. A. D. L., Boquien M., Boselli A., Clements D. L., Cooray A. R., Cortese L., de Looze I., Ford G. P., Gear W. K., Gentile G., Gordon K. D., Kirk J., Lebouteiller V., Madden S., Mentuch E., O'Halloran B., Page M. J., Schulz B., Spinoglio L., Verstappen J., Wilson C. D., Thilker D. A., 2012. *ApJ*, **756**, 40. *The Herschel Exploitation of Local Galaxy Andromeda (HELGA). II. Dust and Gas in Andromeda*.

Springel V., White S. D. M., Jenkins A., Frenk C. S., Yoshida N., Gao L., Navarro J., Thacker R., Croton D., Helly J., Peacock J. A., Cole S., Thomas P., Couchman H., Evrard A., Colberg J., Pearce F., 2005. *Nature*, **435**, 629. *Simulations of the formation, evolution and clustering of galaxies and quasars*.

Strateva I., Ivezić Ž., Knapp G. R., Narayanan V. K., Strauss M. A., Gunn J. E., Lupton R. H., Schlegel D., Bahcall N. A., Brinkmann J., Brunner R. J., Budavári T., Csabai I., Castander F. J., Doi M., Fukugita M., Győry Z., Hamabe M., Hennessy G., Ichikawa T., Kunszt P. Z., Lamb D. Q., McKay T. A., Okamura S., Racusin J., Sekiguchi M., Schneider D. P., Shimasaku K., York D., 2001. *AJ*, **122**, 1861. *Color Separation of Galaxy Types in the Sloan Digital Sky Survey Imaging Data*.

Szomoru D., Franx M., Bouwens R. J., van Dokkum P. G., Labbé I., Illingworth G. D., Trenti M., 2011. *ApJL*, **735**, L22. *Morphological Evolution of Galaxies from Ultra-deep Hubble Space Telescope Wide Field Camera 3 Imaging: The Hubble Sequence at $z \sim 2$*.

Tacconi L. J., Genzel R., Neri R., Cox P., Cooper M. C., Shapiro K., Bolatto A., Bouché N., Bournaud F., Burkert A., Combes F., Comerford J., Davis M., Schreiber N. M. F., Garcia-Burillo S., Gracia-Carpio J., Lutz D., Naab T., Omont A., Shapley A., Sternberg A., Weiner B., 2010. *Nature*, **463**, 781. *High molecular gas fractions in normal massive star-forming galaxies in the young Universe*.

Taylor E. N., Hopkins A. M., Baldry I. K., Bland-Hawthorn J., Brown M. J. I., Colless M., Driver S., Norberg P., Robotham A. S. G., Alpaslan M., Brough S., Cluver M. E., Gunawhardhana M., Kelvin L. S., Liske J., Conselice C. J., Croom S., Foster C., Jarrett T. H., Lopez M. L., Loveday J., 2014. *ArXiv e-prints*. *Galaxy And Mass Assembly: Deconstructing Bimodality - I. Red ones and blue ones*.

Tremonti C. A., Moustakas J., Diamond-Stanic A. M., 2007. *ApJL*, **663**, L77. *The Discovery of 1000 km s^{-1} Outflows in Massive Poststarburst Galaxies at z=0.6*.

Tresse L., Ilbert O., Zucca E., Zamorani G., Bardelli S., Arnouts S., Paltani S., Pozzetti L., Bottini D., Garilli B., Le Brun V., Le Fèvre O., Maccagni D., Picat J.-P., Scaramella R., Scodeggio M., Vettolani G., Zanichelli A., Adami C., Arnaboldi M., Bolzonella M., Cappi A., Charlot S., Ciliegi P., Contini T., Foucaud S., Franzetti P., Gavignaud I., Guzzo L., Iovino A., McCracken H. J., Marano B., Marinoni C., Mazure A., Meneux B., Merighi R., Pellò R., Pollo A., Radovich M., Bondi M., Bongiorno A., Busarello G., Cucciati O., Lamareille F., Mathez G., Mellier Y., Merluzzi P., Ripepi V., 2007. *A&A*, **472**, 403. *The cosmic star formation rate evolution from z = 5 to z = 0 from the VIMOS VLT deep survey*.

Trujillo I., Feulner G., Goranova Y., Hopp U., Longhetti M., Saracco P., Bender R., Braito V., Della Ceca R., Drory N., Mannucci F., Severgnini P., 2006a. *MNRAS*, **373**, L36. *Extremely compact massive galaxies at z $\sim$ 1.4*.

Trujillo I., Förster Schreiber N. M., Rudnick G., Barden M., Franx M., Rix H.-W., Caldwell J. A. R., McIntosh D. H., Toft S., Häussler B., Zirm A., van Dokkum P. G., Labbé I., Moorwood A., Röttgering H., van der Wel A., van der Werf P., van Starkenburg L., 2006b. *ApJ*, **650**, 18. *The Size Evolution of Galaxies since z$\sim$3: Combining SDSS, GEMS, and FIRES*.

Trujillo I., Conselice C. J., Bundy K., Cooper M. C., Eisenhardt P., Ellis R. S., 2007. *MNRAS*, **382**, 109. *Strong size evolution of the most massive galaxies since z $\sim$ 2*.

Trujillo I., Ferreras I., de La Rosa I. G., 2011. *MNRAS*, **415**, 3903. *Dissecting the size evolution of elliptical galaxies since z 1: puffing-up versus minor-merging scenarios*.

Ueda Y., Watson M. G., Stewart I. M., Akiyama M., Schwope A. D., Lamer G., Ebrero J., Carrera F. J., Sekiguchi K., Yamada T., Simpson C., Hasinger G., Mateos S., 2008. *ApJS*, **179**, 124. *The Subaru/XMM-Newton Deep Survey (SXDS). III. X-Ray Data*.

van der Wel A., Holden B. P., Zirm A. W., Franx M., Rettura A., Illingworth G. D., Ford H. C., 2008. *ApJ*, **688**, 48. *Recent Structural Evolution of Early-Type Galaxies: Size Growth from z = 1 to z = 0*.

van der Wel A., Rix H.-W., Wuyts S., McGrath E. J., Koekemoer A. M., Bell E. F., Holden B. P., Robaina A. R., McIntosh D. H., 2011. *ApJ*, **730**, 38. *The Majority of Compact Massive Galaxies at z $\sim$ 2 are Disk Dominated*.

van der Wel A., Bell E. F., Häussler B., McGrath E. J., Chang Y.-Y., Guo Y., McIntosh D. H., Rix H.-W., Barden M., Cheung E., Faber S. M., Ferguson H. C., Galametz A., Grogin N. A., Hartley W., Kartaltepe J. S., Kocevski D. D., Koekemoer A. M., Lotz

J., Mozena M., Peth M. A., Peng C. Y., 2012. *ApJS*, **203**, 24. *Structural Parameters of Galaxies in CANDELS*.

van der Wel A., Franx M., van Dokkum P. G., Skelton R. E., Momcheva I. G., Whitaker K. E., Brammer G. B., Bell E. F., Rix H.-W., Wuyts S., Ferguson H. C., Holden B. P., Barro G., Koekemoer A. M., Chang Y.-Y., McGrath E. J., Häussler B., Dekel A., Behroozi P., Fumagalli M., Leja J., Lundgren B. F., Maseda M. V., Nelson E. J., Wake D. A., Patel S. G., Labbé I., Faber S. M., Grogin N. A., Kocevski D. D., 2014. *ApJ*, **788**, 28. *3D-HST+CANDELS: The Evolution of the Galaxy Size-Mass Distribution since z = 3*.

van Dokkum P. G., Franx M., Kriek M., Holden B., Illingworth G. D., Magee D., Bouwens R., Marchesini D., Quadri R., Rudnick G., Taylor E. N., Toft S., 2008. *ApJL*, **677**, L5. *Confirmation of the Remarkable Compactness of Massive Quiescent Galaxies at z ∼ 2.3: Early-Type Galaxies Did not Form in a Simple Monolithic Collapse*.

van Dokkum P. G., Whitaker K. E., Brammer G., Franx M., Kriek M., Labbé I., Marchesini D., Quadri R., Bezanson R., Illingworth G. D., Muzzin A., Rudnick G., Tal T., Wake D., 2010. *ApJ*, **709**, 1018. *The Growth of Massive Galaxies Since z = 2*.

van Dokkum P. G., Leja J., Nelson E. J., Patel S., Skelton R. E., Momcheva I., Brammer G., Whitaker K. E., Lundgren B., Fumagalli M., Conroy C., Förster Schreiber N., Franx M., Kriek M., Labbé I., Marchesini D., Rix H.-W., van der Wel A., Wuyts S., 2013. *ApJL*, **771**, L35. *The Assembly of Milky-Way-like Galaxies Since z ∼ 2.5*.

Wake D. A., Nichol R. C., Eisenstein D. J., Loveday J., Edge A. C., Cannon R., Smail I., Schneider D. P., Scranton R., Carson D., Ross N. P., Brunner R. J., Colless M., Couch W. J., Croom S. M., Driver S. P., da Ângela J., Jester S., de Propris R., Drinkwater M. J., Bland-Hawthorn J., Pimbblet K. A., Roseboom I. G., Shanks T., Sharp R. G., Brinkmann J., 2006. *MNRAS*, **372**, 537. *The 2df SDSS LRG and QSO survey: evolution of the luminosity function of luminous red galaxies to z = 0.6*.

Weiner B. J., Coil A. L., Prochaska J. X., Newman J. A., Cooper M. C., Bundy K., Conselice C. J., Dutton A. A., Faber S. M., Koo D. C., Lotz J. M., Rieke G. H., Rubin K. H. R., 2009. *ApJ*, **692**, 187. *Ubiquitous Outflows in DEEP2 Spectra of Star-Forming Galaxies at z = 1.4*.

Weinzirl T., Jogee S., Conselice C. J., Papovich C., Chary R.-R., Bluck A., Grützbauch R., Buitrago F., Mobasher B., Lucas R. A., Dickinson M., Bauer A. E., 2011. *ApJ*, **743**, 87. *Insights on the Formation, Evolution, and Activity of Massive Galaxies from Ultracompact and Disky Galaxies at z = 2-3*.

Wetzel A. R., Schulz A. E., Holz D. E., Warren M. S., 2008. *ApJ*, **683**, 1. *Close Pairs as Proxies for Galaxy Cluster Mergers*.

Whitaker K. E., Kriek M., van Dokkum P. G., Bezanson R., Brammer G., Franx M., Labbé I., 2012a. *ApJ*, **745**, 179. *A Large Population of Massive Compact Post-starburst Galaxies at z ¿ 1: Implications for the Size Evolution and Quenching Mechanism of Quiescent Galaxies*.

Whitaker K. E., van Dokkum P. G., Brammer G., Franx M., 2012b. *ApJL*, **754**, L29. *The Star Formation Mass Sequence Out to z = 2.5*.

White S. D. M., Rees M. J., 1978. *MNRAS*, **183**, 341. *Core condensation in heavy halos - A two-stage theory for galaxy formation and clustering*.

Wijesinghe D. B., Hopkins A. M., Kelly B. C., Welikala N., Connolly A. J., 2010. *MNRAS*, **404**, 2077. *Morphological classification of galaxies and its relation to physical properties*.

Wijesinghe D. B., Hopkins A. M., Brough S., Taylor E. N., Norberg P., Bauer A., Brown M. J. I., Cameron E., Conselice C. J., Croom S., Driver S., Grootes M. W., Jones D. H., Kelvin L., Loveday J., Pimbblet K. A., Popescu C. C., Prescott M., Sharp R., Baldry I., Sadler E. M., Liske J., Robotham A. S. G., Bamford S., Bland-Hawthorn J., Gunawardhana M., Meyer M., Parkinson H., Drinkwater M. J., Peacock J., Tuffs R., 2012. *MNRAS*, **423**, 3679. *Galaxy And Mass Assembly (GAMA): galaxy environments and star formation rate variations*.

Wilkins S. M., Trentham N., Hopkins A. M., 2008. *MNRAS*, **385**, 687. *The evolution of stellar mass and the implied star formation history*.

Williams R. J., Quadri R. F., Franx M., van Dokkum P., Labbé I., 2009. *ApJ*, **691**, 1879. *Detection of Quiescent Galaxies in a Bicolor Sequence from Z = 0-2*.

Wolf C., Gray M. E., Meisenheimer K., 2005. *A&A*, **443**, 435. *Red-sequence galaxies with young stars and dust: the cluster Abell 901/902 seen with COMBO-17*.

Wuyts S., Labbé I., Schreiber N. M. F., Franx M., Rudnick G., Brammer G. B., van Dokkum P. G., 2008. *ApJ*, **682**, 985. *FIREWORKS U_{38}-to-24 μm Photometry of the GOODS Chandra Deep Field-South: Multiwavelength Catalog and Total Infrared Properties of Distant K_s-selected Galaxies*.

Wuyts S., Cox T. J., Hayward C. C., Franx M., Hernquist L., Hopkins P. F., Jonsson P., van Dokkum P. G., 2010. *ApJ*, **722**, 1666. *On Sizes, Kinematics, M/L Gradients, and Light Profiles of Massive Compact Galaxies at z $\sim$ 2*.

Xu C. K., Zhao Y., Scoville N., Capak P., Drory N., Gao Y., 2012. *ApJ*, **747**, 85. *Major-merger Galaxy Pairs in the COSMOS Field Mass-dependent Merger Rate Evolution since z = 1*.

York D. G., Adelman J., Anderson, Jr. J. E., Anderson S. F., Annis J., Bahcall N. A., Bakken J. A., Barkhouser R., Bastian S., Berman E., Boroski W. N., Bracker S., Briegel C., Briggs J. W., Brinkmann J., Brunner R., Burles S., Carey L., Carr M. A., Castander F. J., Chen B., Colestock P. L., Connolly A. J., Crocker J. H., Csabai I., Czarapata P. C., Davis J. E., Doi M., Dombeck T., Eisenstein D., Ellman N., Elms B. R., Evans M. L., Fan X., Federwitz G. R., Fiscelli L., Friedman S., Frieman J. A., Fukugita M., Gillespie B., Gunn J. E., Gurbani V. K., de Haas E., Haldeman M., Harris F. H., Hayes J., Heckman T. M., Hennessy G. S., Hindsley R. B., Holm S., Holmgren D. J., Huang C.-h., Hull C., Husby D., Ichikawa S.-I., Ichikawa T., Ivezić Ž., Kent S., Kim R. S. J., Kinney E., Klaene M., Kleinman A. N., Kleinman S., Knapp G. R., Korienek J., Kron R. G., Kunszt P. Z., Lamb D. Q., Lee B., Leger R. F.,

Limmongkol S., Lindenmeyer C., Long D. C., Loomis C., Loveday J., Lucinio R., Lupton R. H., MacKinnon B., Mannery E. J., Mantsch P. M., Margon B., McGehee P., McKay T. A., Meiksin A., Merelli A., Monet D. G., Munn J. A., Narayanan V. K., Nash T., Neilsen E., Neswold R., Newberg H. J., Nichol R. C., Nicinski T., Nonino M., Okada N., Okamura S., Ostriker J. P., Owen R., Pauls A. G., Peoples J., Peterson R. L., Petravick D., Pier J. R., Pope A., Pordes R., Prosapio A., Rechenmacher R., Quinn T. R., Richards G. T., Richmond M. W., Rivetta C. H., Rockosi C. M., Ruthmansdorfer K., Sandford D., Schlegel D. J., Schneider D. P., Sekiguchi M., Sergey G., Shimasaku K., Siegmund W. A., Smee S., Smith J. A., Snedden S., Stone R., Stoughton C., Strauss M. A., Stubbs C., SubbaRao M., Szalay A. S., Szapudi I., Szokoly G. P., Thakar A. R., Tremonti C., Tucker D. L., Uomoto A., Vanden Berk D., Vogeley M. S., Waddell P., Wang S.-i., Watanabe M., Weinberg D. H., Yanny B., Yasuda N., SDSS Collaboration, 2000. *AJ*, **120**, 1579. *The Sloan Digital Sky Survey: Technical Summary*.

Yun M. S., Reddy N. A., Condon J. J., 2001. *ApJ*, **554**, 803. *Radio Properties of Infrared-selected Galaxies in the IRAS 2 Jy Sample*.

Zwicky F., 1933. *Helvetica Physica Acta*, **6**, 110. *Die Rotverschiebung von extragalaktischen Nebeln*.